Docket Nos. 50-282
and 50-306

February 11, 1985

DL 016

Mr. D. M. Musolf
Nuclear Support Services Department
Northern States Power Company
414 Nicollet Mall
Midland Square - 4th Floor
Minneapolis, Minnesota 55401

Dear Mr. Musolf:

Subject: TRANSMITTAL OF TEST DATA ON UPPER PLENUM INJECTION (UPI) AND A TWO-DAY UPI MEETING ABOUT MARCH 12-14, 1985.

At the January 10, 1985 meeting at NRC to discuss upper plenum injection (UPI), we were asked to provide additional UPI test data as soon as it could be made available. Accordingly, I am providing herewith three copies of "JAERI-M-84-221, Effects of Upper Plenum Injection on Thermo-Hydrodynamic Behavior Under Refill and Reflood Phases," December 1984.

This report describes the effects of UPI as measured on the Slab Core Test Facility (SCTF) operated by the Japan Atomic Energy Research Institute (JAERI). It contains SCTF test data which show that (1) adding UPI to a cold leg injection (CLI) system caused the post-LOCA maximum core temperature to decrease from 1195°K to 1158°K, and (2) subcooling of the UPI water caused a further decrease to 1119°K (per pages 24-27). However, (3) the corresponding time to bottom of core recovery (BOCREC) (equivalent to the beginning of reflood) increased substantially from 19 seconds to 80 and 81 seconds (per pages 47 and 30) and (4) downward flow of subcooled UPI liquid into the core was apparently intermittent (per pages 6, 37 and 47).

The SCTF-UPI data is not directly applicable to the existing Westinghouse two loop UPI plants because the SCTF-UPI test used both accumulators and pumps to provide both UPI and CLI, with the UPI flow about equal to the CLI flow (per page 24). Additionally, the UPI nozzle was at the bottom of the upper plenum (per page 24) rather than the level of the hot legs. Nevertheless, the SCTF tests had important features representative of a full size 1100 MWe Westinghouse PWR, e.g., full height heater rods and full radial width of a core. Also, the tests document phenomena which can be used to develop and/or test a UPI model, e.g., hot leg flow reversal (pages 15 and 53-54), fluid temperature variations in the upper plenum and upper core (pages 38-40) and horizontal pressure variations at three heights inside the core (pages 42-43).

Besides providing JAERI-M-84-221, we will provide proprietary "Quick Look" Reports (QLRs) on UPI tests at JAERI's Cylindrical Core Test Facility (CCTF) as follows: (1) QLRs on CCTF UPI tests 57 and 59 were provided previously; (2) a QLR on the no-single failure UPI test 72 will probably be available in February or March; and (3) draft QLRs on asymmetric UPI tests 76 and 78 will probably be available in March. We suggest you provide copies of the enclosure and of the QLRs to those fuel vendors assisting you in UPI model development.

An NRC-JAERI discussion of the UPI tests will be held in the Bethesda, MD. area for two days about March 12-14, 1985. The NRC Office of Nuclear Regulatory Research (RES) expects to arrange for UPI licensees and their designated fuel vendor representatives to observe those discussions and to participate with JAERI representatives in round-table technical discussions of UPI phenomena. We anticipate that we will be able to keep the discussions from becoming unwieldy if we limit each UPI licensee to designating one employee observer, one employee participant, one vendor observer and one vendor participant, with a maximum of one observer and one participant present from any given fuel vendor.

Please let me know if you intend to send an employee observer, an employee technical participant, a vendor observer and/or a vendor technical participant so that we can set up the meeting with JAERI and the NRC. Please respond by phone by February 20, 1985 to Dr. David Langford, at 301-492-9403.

Sincerely,

James R. Miller, Chief
Operating Reactors Branch No. 3
Division of Licensing

Enclosures:
As stated

cc w/enclosures:
See next page

Distribution:
Docket File
NRC & L PDRs
Branch Files
OELD
FMiraglia
PKreutzer
DDiIanni
DLangford
EJordan
JPartlow
PMcKee
ACRS 10

DC8

ORB#3:DL	ORB#3:DL	ORB#3:DL
PKreutzer	DDiIanni;ef	JRMiller
2/7/85	2/7/85	2/11/85

Northern States Power Company

cc:
Gerald Charnoff, Esquire
Shaw, Pittman, Potts and Trowbridge
1800 M Street, NW
Washington, DC 20036

Ms. Sandra Gardebring
Executive Director
Minnesota Pollution Control Agency
1935 W. County Road, B2
Roseville, Minnesota 55113

Mr. E. L. Watzl, Plant Manager
Prairie Island Nuclear Generating Plant
Northern State Power Company
Route 2
Welch, Minnesota 55089

Jocelyn F. Olson, Esquire
Special Assistant Attorney General
Minnesota Pollution Control Agency
1935 W. County Road, B2
Roseville, Minnesota 55113

U.S. Nuclear Regulatory Commission
Resident Inspectors Office
Route #2, Box 500A
Welch, Minnesota 55089

Regional Administrator
Nuclear Regulatory Commission
Region III
Office of Executive Director for Operations
799 Roosevelt Road
Glen Ellyn, Illinois 60137

Mr. William Miller
Goodhue County Auditor
Red Wing, Minnesota 55066

U.S. Environmental Protection Agency
Federal Activities Branch
Region V Office
ATTN: Regional Radiation Representative
230 South Dearborn Street
Chicago, Illinois 60604

JAERI-M
84-221

EFFECTS OF UPPER PLENUM INJECTION ON THERMO-HYDRODYNAMIC BEHAVIOR UNDER REFILL AND REFLOOD PHASES

December 1984

Takamichi IWAMURA, Makoto SOBAJIMA
Yutaka ABE, Hiromichi ADACHI,
Akira OHNUKI and Masahiro OSAKABE

日本原子力研究所
Japan Atomic Energy Research Institute

Effects of Upper Plenum Injection on Thermo-Hydrodynamic Behavior Under Refill and Reflood Phases

Takamichi IWAMURA, Makoto SOBAJIMA,
Yutaka ABE, Hiromichi ADACHI
Akira OHNUKI and Masahiro OSAKABE

Department of Nuclear Safety Research,
Tokai Research Establishment, JAERI

(Received November 7, 1984)

In order to investigate the thermo-hydrodynamic behavior in core under simultaneous ECC water injection into the upper plenum and the intact cold leg during the refill and reflood phases of a PWR-LOCA, Tests S1-SH3 and S1-SH4 were performed by using Slab Core Test Facility (SCTF) with the injection of saturated and 67K subcooled water into the upper plenum, respectively, under the same cold leg injection condition.

The following major findings were obtained by examining these test results.

(1) Although the core was cooled by the fall back water from the upper plenum into the core during the period of high injection rate into the upper plenum, the core was cooled mainly by the bottom flooding after the BOCREC (Bottom of core recovery).
(2) The possible fall back flow rate estimated with a CCFL correlation rapidly decreased after the BOCREC because of the increase of steam generation rate in core.
(3) Continuous fall back of subcooled water was not observed even under the condition with large upper plenum injection rate of subcooled water and with steam outflow through the lower plenum into the downcomer. The fall back was intermittently limited by the rapid increase of upward steam flow which was generated in the core due to the evaporation of the fall back water.
(4) The rising of liquid level in the lower plenum was suppressed by

---

The work was performed under contract with the Atomic Energy Bureau of Science and Technology Agency of Japan

the pressurization in core due to the evaporation of fall back water before the BOCREC and therefore the beginning of bottom reflood was delayed.

Some selected data from Tests S1-SH3 and S1-SH4 are also included in this report.

Keywords: Reflood, Refill, LOCA, ECCS, PWR, Combined Injection, Water Fall Back, Heat Transfer, Quench, Carryover, Two-phase Flow, SCTF, Thermo-hydrodynamic Behavior, Reactor Safety

上部プレナム注水かリフィルおよび再冠水時の熱水力現象に及ぼす影響

日本原子力研究所東海研究所安全工学部

岩村公道・傍島　真・阿部　豊

安達公道・大貫　晃・前部真弘

（1984年11月7日受理）

PWR-LOCA時再冠水過程において，ECC水を健全コールドレグと上部プレナムに同時に注入した場合の炉心熱水力挙動を調べるため，平板炉心試験装置（SCTF）を用いて，同一コールドレグ注入条件下で飽和水および67Kサブクール水を上部プレナムに注入する試験SI-SH3およびSI-SH4を実施した。

両試験結果の検討を行い，以下の知見を得た。

(1) 上部プレナム注入量が多い期間中は，上部プレナムから炉心への水の落下により，炉心が冷却されたか，本格的な炉心冷却は下部からの冠水開始後に行われた。

(2) CCFL実験式により推定された落下可能流量は，再冠水開始後は炉心で発生する蒸気量の増加により急減した。

(3) 上部プレナムにサブクール水を大量に注入し，かつ下部プレナムからダウンカマに蒸気が流出できる条件下でも，サブクール水の連続的な落下は起らず，落下水の蒸発による上向き蒸気流量の急増により落下が制限された。

(4) 炉心下端再冠水開始前には，落下水の蒸発により発生する蒸気の圧力上昇効果のため，下部プレナム水位の上昇がおさえられ，下からの炉心冠水が遅れる現象が認められる。

なお，試験SI-SH3とSI-SH4のデータの一部も本報告書に収録した。

本報告は，電源開発促進対策特別会計法に基づき，科学技術庁からの受託によって行なった研究の成果である。

Contents

目　　次

List of Tables

List of Figures

1. Introduction

The thermal-hydraulic behavior during the refill and reflood phases of a postulated loss of coolant accident (LOCA) in a pressurized water reactor (PWR) has been investigated by using the Slab Core Test Facility (SCTF) which has an electrically heated core with a full height, full radial width and azimuthal single-bundle depth. The SCTF program is a part of the large scale reflood test program under contract with the Atomic Energy Bureau of Science and Technology Agency of Japan together with the Cylindrical Core Test Facility (CCTF) program.

As an alternative Emergency Core Cooling System (ECCS), the combined injection mode in which the ECC water is simultaneously injected into both the hot leg and the cold leg is proposed in order to improve the core cooling by a large amount of fall back water into the core.

The thermal-hydraulic behavior during the initial period of the combined injection mode was investigated in the present two preliminary tests: Tests S1-SH3 and S1-SH4, by injecting the ECC water into the upper plenum instead of the hot legs and into the cold leg in the SCTF Core-I test series. These two tests were performed with saturated and subcooled water injection into the upper plenum and therefore the effects of injection water temperature can be investigated by comparing the results of these two tests.

Since included in the purposes of these two tests were to confirm the performance of the upper plenum injection and extraction system and to establish the technical method of the combined injection tests planned in the SCTF Core-III test series, the test conditions were not necessarily appropriate for the simulation of the typical combined injection mode for a PWR. However, qualitatively useful information was obtained on the initial thermal-hydraulic behavior in core particular to the combined injection mode.

The present report describes the fall back behavior from the upper plenum into the core, the water accumulation behavior in the core, the lower plenum and the downcomer, the fluid behavior in the primary loops and the core cooling behavior.

Presented in Appendix A are the brief description of SCTF and measurement locations.

The selected data obtained in Tests S1-SH3 and S1-SH4 are presented in Appendixes B and C, respectively.

2. Experiment

2.1 Test Facility

The schematic diagram of SCTF and the comparison of dimensions between the SCTF and a 1,100 MWe PWR are shown in Fig. 2-1 and Table 2-1, respectively.

The primary coolant loops consist of a hot leg equivalent to the four actual hot legs, a steam/water separator corresponding to the four actual steam generators, an intact cold leg equivalent to the three actual intact cold legs, a broken cold leg on the pressure vessel side, and a broken cold leg on the steam/water separator side. These two broken cold legs are connected to two different containment tanks.

The flow area scaling ratio is 1/21 to a 1,100 MWe PWR, whereas the height of each component simulates the actual PWR.

The emergency core cooling system (ECCS) consists of an accumulator (Acc) system, a low pressure coolant injection (LPCI) system, and an upper core suport plate (UCSP) water injection system. All of these three injection systems were used for the combined injection pre-tests. The injection port for the Acc and LPCI systems is located on the intact cold leg and that for the UCSP water injection system is the eight injection nozzles located just above the UCSP for each bundle. The schematic of the UCSP water injection system is shown in Fig. 2-2. As adjacent two nozzles are connected into one at the outside of the pressure vessel, four lines in total are provided for giving the specified flow and fluid temperature transients independently.

Figure 2-3 shows the vertical cross section of the pressure vessel. The pressure vessel includes a simulated core, an upper plenum with internals, a lower plenum, a core baffle and a downcomer.

The simulated core consists of 8 bundles arranged in a row with full radial width. Each bundle consists of 234 heater rods and 22 non-heated rods arranged in 16×16 array. The outer diameter and the heated length of the heater rod are 10.7 mm and 3660 mm, respectively. The dimensions of rod bundle, such as the rod pitch, the spacers, the end box tie plate etc., are based on those for a 15×15 fuel rod bundle of a PWR.

The core and the upper plenum are enveloped by honeycomb thermal insulators to minimize the wall effects.

More detailed inrormation on the SCTF is available in reference (1)

and brief description is presented in Appendix A.

2.2 Test Conditions

In the combined injection mode of an actual reactor, the subcooled water injected into the hot leg flows into the upper plenum and then falls on to the UCSP after hitting the upper plenum internals. In the present combined injection pre-tests: Test S1-SH3 (Run 528) and Test S1-SH4 (Run 529), the fluid characteristics in the upper plenum was simulated by horizontally injecting the ECC water through the side nozzles and extracting from the other side nozzles located just above the UCSP as shown in Fig. 2-2.

The water subcooling in the upper plenum is estimated to be in the range of 20 to 40 K according to the calculated results for a reference PWR. Since the water subcooling in the upper plenum is considered to affect the fall back characteristics, the temperature of upper plenum injection water was selected as a test parameter. That was almost saturated in Test S1-SH3 and subcooled of about 67 K with respect to the saturation temperature at 0.25 MPa in Test S1-SH4 so as to include the calculated range of a reference PWR.

These two tests were performed under refill and reflood simulation condition. The refill simulation test: Test S1-19 (Run 525), is referred as a counterpart test with cold leg injection mode. Major test conditions for Tests S1-SH3, S1-SH4 and S1-19 and the calculated results for a reference PWR are listed in Table 2-2. Chronologies of events for these three tests are listed in Table 2-3. The BOCREC in Tables 2-2 and 2-3 represents the time at the bottom of core recovery when the ECC water reaches the bottom of heated part.

Tests S1-SH3 and S1-SH4 were performed under almost the same conditions except the water temperature of UCSP injection system. The test conditions for Test S1-19 were almost the same as those for Tests S1-SH3 and S1-SH4 except that no UCSP injection system was used and the vent line connecting the upper plenum and the downcomer was open in Test S1-19 while it was closed in Tests S1-SH3 and S1-SH4.

As indicated in Table 2-2, the scaled upper plenum injection rate and cold leg injection rate are larger in the present tests than in the calculated results during the Acc period. However, the Acc injection time is much shorter and the LPCI flow rate is much lower in these two

tests as compared with the calculated results because one of the objectives of the present tests is to confirm the flow rate control function of the UCSP injection system under the lower flow rate condition. Therefore it should be noted that the thermal-hydraulic behavior after 28 s from the initiation of upper plenum injection does not well simulate the thermal-hydraulic behavior under the typical combined injection mode.

2.3 Test Procedure

The test procedure for the combined injection pre-tests is as follows.

After setting the initial conditions, core heating was initiated. At 100 s after the core power on, the break valves were opened and the core power decay simulation started with the initiation of UCSP water injection and extraction system. The maximum cladding temperature at this time was intended to be 995 K. The decay curve is simulated from 21 s after the shutdown of a Westinghouse type PWR. The decay curve is based on the "ANS Standard + Actinides + Delayed Neutron Effect for voided Core".

At 105 s (Test S1-SH3) or 103 s (Test S1-SH4) after the core power on, Acc injection was initiated into the intact cold leg. After 23 s (Test S1-SH3) or 21 s (Test S1-SH4) from Acc injection, the Acc injection was switched to LPCI. The maximum Acc and LPCI flow rate were about 84 kg/s and 8 kg/s, respectively.

The total UCSP water injection rate was intended to be about 100 kg/s during the first 28 s and about 11 kg/s thereafter with equal flow rate for each of eight UCSP injection nozzles. However, the UCSP injection line connecting to the upper plenum above Bundles 1 and 2 did not open during the first 60 s for Test S1-SH3 accidently.

The test was finished after 900 s from LPCI initiation.

3. Test Results and Discussions

3.1 Boundary Conditions

Figure 3-1 shows the comparison of ECC water injection rates into the cold leg between Tests S1-SH3, S1-SH4 and S1-19. The Acc flow rate and injection period and the LPCI flow rate are almost identical for these three tests.

Figure 3-2 shows the UCSP water injection rates into the upper plenum in Tests S1-SH3 and S1-SH4. As shown in Fig. 3-2(1), the UCSP water injection system above bundles 1 and 2 in Test S1-SH3 did not work well. Through the nozzles above bundles 1 and 2 in Test S1-SH3, no water was injected until 60 s after the break valves open and then the UCSP injection started at very high flow rate up to 0.044 m^3/s. About 20 s later, the UCSP injection rate through these nozzles approached the nominal injection rate. In Test S1-SH4, on the other hand, the same amount of water was injected into the upper plenum through all nozzles as shown in Fig. 3-2(2).

The upper plenum water was extracted through the UCSP extraction nozzles above each bundle at the opposite side of the injection nozzles. In these two tests, however, the UCSP water extraction system did not work well and the accuracy of the extracted water flow rate is doubtful. The UCSP extraction system will be improved in the later part of SCTF Core-II test series.

Figure 3-3 shows the temperatures of water injected into the upper plenum in Tests S1-SH3 and S1-SH4. The saturation temperatures corresponding to the pressure at the top of upper plenum are also shown in Fig. 3-3 for these two tests. The UCSP injection water temperature in Test S1-SH3 is about 405 K which is almost in agreement with the saturation temperature at the pressure in the upper plenum. The UCSP injection water temperature in Test S1-SH4 is about 333 K above bundles 1, 2, 5 and 6, and about 344 K above bundles 3, 4, 7 and 8. The average subcoolings with respect to the saturation temperature at the pressure in the upper plenum are about 67 K and 56 K, respectively.

The temperature of cold leg injection water is about 335 K in Tests S1-SH3, S1-SH4 and S1-19.

The comparisons of pressure transients at the center of core and

at the top of containment tank I are shown in Figs. 3-4 and 3-5, respectively.

Although both of Tests S1-SH3 and S1-SH4 are the refill simulation tests with the same initial pressure of 0.54 MPa, the pressure at the center of core is higher in Test S1-SH3 than in Test S1-SH4 after the break valves open, indicating the condensation of steam in Test S1-SH4 due to the higher subcooling of UCSP injection water in this test.

Core heating power transients are identical for these three tests as shown in Fig. 3-6.

3.2 Fall Back Characteristics

3.2.1 Occurrence of Fall Back at End Box Tie Plate

Figure 3-7 shows the differential pressure across the end box tie plate, the fluid temperature just below the end box tie plate and the saturation temperature above bundle 4 in Test S1-SH4. The saturation temperature was obtained from the average of two pressures measured at the top of upper plenum and at the center of core. As shown in this figure, subcooled water is intermittently observed just below the end box tie plate before the BOCREC, indicating that the subcooled water injected into the upper plenum intermittently penetrates into the core through the end box tie plate before the BOCREC. The intermittent and rapid decreases in fluid temperature are in many cases accompanied by the significant decreases of differential pressure across the end box tie plate.

As shown in Fig. 3-8, the water in the upper plenum is subcooled during the high flow rate period of UCSP injection and after that period the water temperature becomes almost saturated for Test S1-SH4. The maximum subcooling on UCSP is 59 K at 15 s after the break valves open. As listed in Table 2-2, during the initial 28 s, the upper plenum injection rate is higher than the calculated hot leg injection rate in th typical combined injection mode for a reference PWR. In addition, the lower plenum water level is below the bottom of core barrel during this period as shown in Fig. 3-18. Therefore it is noted that even when the upper plenum injection rate and subcooling are large enough and the steam generated in core can flow into the downcomer through the lower plenum, the fall back of subcooled water does not continue for more than 5 s and the saturated CCFL condition is established again.

The reason why the continuous fall back does not occur is considered that a part of fall back water is evaporated in core and the generated steam up-flow supports the weight of subcooled water. When the fall back is stopped, the steam generation rate in the core decreases and therefore the steam up-flow rate becomes lower than that corresponding to the CCFL break condition. The intermittent fall back behavior shown in Fig. 3-7 is probably attributed to the time lag between the fall back and the steam generation.

3.2.2 Two-Dimensional Fall Back Behavior

Figures 3-9 and 3-10 show the comparisons of the fluid temperatures just below the end box tie plate, the saturation temperature, and the differential pressures across the end box tie plate above Bundles 1 through 8 in Tests S1-SH3 and S1-SH4, respectively.

As shown in Fig. 3-9, the differential pressures across the end box tie plate in Test S1-SH3 intermittently show negative values during the initial 30 s except above Bundles 1, 2 and 3, while the differential pressures in Test S1-SH4 almost always show the positive values, suggesting that the amount of fall back water during this period is larger in Test S1-SH3 than in Test S1-SH4. The fall back water during this period promotes the cooling of upper core as will be discussed in Section 3.7.1. The relatively larger possitive differential pressure across the end box tie plate above Bundle 1 side in Test S1-SH3 is due to the 60 s delay of the UCSP injection above Bundles 1 and 2 as described in section 2.3.

It is suggested from Fig. 3-10 that the intermittent fall back of subcooled water through the end box tie plate during the initial 40 s occurs nonuniformly over the eight bundles and simultaneous CCFL break all over the eight bundles is not observed.

Figure 3-11 shows the comparisons of void fractions in Bundles 2, 4 and 8 at the upper part of core in these two tests. These void fractions are calculated from the measured vertical differential pressures between core spacers by neglecting the effects of frictional and accelerational pressure drops. During the period from about 20 to 30 s, the void fraction is the lowest in Bundle 8 in Test S1-SH3 and the void fraction is the highest in Bundle 8 in Test S1-SH4. These radial distributions in the void fractions are corresponding to those

in the differential pressures across the end box tie plate shown in Figs. 3-9 and 3-10 and then to the radial distribution in the fall back flow rates.

Figures 3-12 and 3-13 show the comparisons of horizontal differential pressures between Bundles 5 and 8 and between Bundles 1 and 8, respectively, at the elevations of 1.905 m, 3.235 m and 3.821 m (just below the end box tie plate) from the bottom of heated length in these two tests. The positive differential pressure in these figures means that the pressure in Bundle 5 or Bundle 1 is higher than the pressure in Bundle 8.

Before the BOCREC, the pressure in Bundle 8 is much higher than the pressures in Bundles 1 and 5 at the elevations of 3.235 and 3.821 m and the differential pressures between Bundles 5 and 8 and between Bundles 1 and 8 are relatively small at the elevation of 1.905 m in Test S1-SH3. In Test S1-SH4, on the other hand, during the initial 40 s from the break valves open, the pressure in Bundle 8 is much lower than the pressures in Bundles 1 and 5 at the elevations of 1.905 and 3.235 m.

The above-mentioned characteristics of horizontal differential pressures before the BOCREC indicate that the amount of fall back water is larger in Bundle 8 side in Test S1-SH3 and is larger in Bundle 1 side in Test S1-SH4. This is consistent with the radial distribution of the subcool time indication in fluid temperatures below the end box tie plate and the differential pressures across the end box tie plate shown in Figs. 3-9 and 3-10 and also with the void fractions in the upper part of core shown in Fig. 3-11. The negative differential pressures between Bundles 1 and 8 and between Bundles 5 and 8 below the end box tie plate in Test S1-SH4 indicate that the direction of steam horizontal flow is from Bundle 8 to Bundle 1 even when the amount of fall back water is larger in Bundle 1 side.

3.2.3 Estimation of Fall Back Flow Rate

The fall back water from the upper plenum into the core is considered to enhance the core cooling especially for the combined injection tests. In the present combined injection pre-tests, however, the fall back flow rate was not measured directly and was not estimated by the mass balance method because the extraction flow rate from the upper plenum could not be measured correctly. Therefore, an empirical

CCFL correlation is used for the estimation of possible fall back flow rate.

The CCFL correlation is derived from the experimental data based on the end box tie plate which has the same vertical configuration as that in the SCTF-I with 1/72 scaled to the SCTF-I.

The CCFL correlation for the SCTF-I tie plate is given by

$$j_g^{*1/2} + j_f^{*1/2} = 1.25 \qquad (1)$$

where

$$j_g^* = \frac{W_g}{\rho_g A}\left[\rho_g / gD(\rho_f - \rho_g)\right]^{1/2}$$

$$j_f^* = \frac{W_f}{\rho_f A}\left[\rho_f / gD(\rho_f - \rho_g)\right]^{1/2}$$

W_g = Steam up flow rate

W_f = Water down flow rate (Fall back flow rate)

ρ_g = Steam density

ρ_f = Water density

D = Tie plate hole diameter (0.012 m)

A = Total flow area in the plate (0.2036 m^2)

g = Acceleration due to gravity (9.80665 m/s^2)

The steam up flow rate, W_g, is assumed to be the summation of the steam generation rate calculated by the heat balance method and the flashing rate in the lower plenum. The steam generation rate and the lower plenum flashing rate are shown in Figs. 3-28 and 3-22, respectively and the total steam generation rate is shown in Fig. 3-29.

Figure 3-14 shows the estimated fall back flow rates in Tests S1-SH3 and S1-SH4. As shown in this figure, the maximum calculated fall back flow rate is seen before the BOCREC and after that time the fall back flow rate is significantly reduced due to the increase of steam generation rate in the core.

It should be noted here that the following assumptions are made for the estimation of fall back flow rates shown in Fig. 3-14.

(1) Saturated CCFL is assumed even for Test S1-SH4 in which subcooled

water is observed below the end box tie plate as shown in Fig. 3-7.

(2) The fall back is assumed to occur uniformly over all bundles though there exists radial distribution in the fall back distribution as indicated in Figs. 3-9 and 3-10.

(3) The steam bypass flow from the core into the downcomer through the lower plenum is neglected though the steam bypass flow is observed before the water level in lower plenum reaches the bottom of core barrel as will be discussed in section 3.4.1.

(4) The fall back flow rate is estimated regardless of the existence of water in the upper plenum.

The assumptions (1) through (3) may result in underestimation of the fall back flow rate. As shown in Fig. 3-15, on the other hand, the collapsed liquid level in the upper plenum is reduced to very low level from 40 to 120 s, indicating that the amount of water in the upper plenum is not enough to fall back into the core during this period. Therefore, the fall back flow rate is considerably overestimated after about 40 s in Fig. 3-14.

Although the estimated fall back flow rate in Fig. 3-14 is not quantitatively reliable due to the above-mentioned reasons, it is qualitatively concluded that the fall back flow rate is negligibly small after the initiation of bottom reflood.

3.3 Water Accumulation Behavior in Core

Figure 3-16 shows the comparison of vertical differential pressure across the core full height between Tests S1-SH3 and S1-SH4. The differential pressures in these tests increase temporarily just after the intiation of ECC injection and then increase again after the BOCREC. The comparison between these two tests indicates that the higher subcooling of the UCSP injection water results in the higher water accumulation rate in the core after the BOCREC.

Figure 3-17 shows the comparison of void fractions at six elevations in the core. In general, the void fractions in Test S1-SH3 are higher than those in Test S1-SH4 except during the period from 40 to 80 s above the elevation of 1.365 m. Below the elevation of 1.24 m, no water accumulation is observed before the BOCREC. After the BOCREC, the void fraction is higher in Test S1-SH3 than in Test S1-SH4 at all elevations.

The occurrence of fall back during the period from about 10 to 40 s is also indicated in Fig. 3-17 by the rapid decrease of void fraction at the upper part of core.

Although the amount of fall back water is negligibly small in these two tests during the period between 120 and 200 s as shown in Fig. 3-14, the void fraction in the core is lower in Test S1-SH4 than in Test S1-SH3 during this period especially at the upper half of core as shown in Fig. 3-17. In addition, the generated steam is condensed in the upper plenum at almost constant rate of about 1.4 kg/s during this period as shown in Fig. 3-29. Therefore, it is suggested that the higher water accumulation rate in the core in Test S1-SH4 is not caused by the fall back water but caused by the following reason: Since the steam out flow rate is much lower in Test S1-SH4 than in Test S1-SH3 due to the steam condensation in the upper plenum as shown in Fig. 3-26, the steam binding effect is also weaker in Test S1-SH4. The weaker steam binding effect results in the higher water accumulation rate in the core in Test S1-SH4.

The higher water accumulation rate in the core in Test S1-SH4 results in the higher heat transfer coefficient and the lower cladding surface temperature at the upper half of core as will be discussed in Section 3.7.

3.4 Fluid Behavior in Lower Plenum and Downcomer

3.4.1 Water Accumulation Behavior in Lower Plenum

Figure 3-18 shows the liquid levels in the lower plenum in Tests S1-SH3, S1-SH4 and S1-19.

The liquid levels in the lower plenum in these three tests decrease just after the break valves open due to the water flashing caused by the rapid depressurization. The amount of flashing mass is estimated in the next section.

The liquid level in the lower plenum reaches the bottom of core heating part at 80 s in Tests S1-SH3 and S1-SH4 and at 19 s in Test S1-19. It is estimated that the beginning of bottom reflood is promoted by at most 2.5 s by the effect of open vent line for Test S1-19 and therefore the trend of earlier reflood for this test is not much affected by this difference in condition.

The water accumulation behavior in the lower plenum in Tests S1-SH3 and S1-SH4 is different with each other. The liquid level in the lower plenum in Test S1-SH3 increases gradually even after the liquid level reaches the bottom of core barrel at 50 s, suggesting that the driving force for the bottom flooding given by the downcomer water head is reduced by the pressurization in core due to the evaporation of fall back water. On the other hand, the liquid level in the lower plenum for Test S1-SH4 remains at 0.1 m below the bottom of core barrel until about 76 s and then increases rapidly.

As shown in Fig. 3-19, the fluid velocity data obtained from drag disk flow meter located below the core barrel indicate that the direction of fluid flow is from the lower plenum to the downcomer before the water level reaches the bottom of core barrel and after that time the direction is reversed. The other evidences which indicate the outflow of water and steam from the lower plenum into the downcomer are presented below.

A part of the fall back water is expected to penetrate through the core and reach the lower plenum. The penetration water mass flow rate is obtained by subtracting the steam generation rate in the core from the fall back flow rate. Figure 3-20 shows the estimated fall back flow rate, the steam generation rate and the penetration rate in Test S1-SH4. It is found from Figs. 3-18 and 3-20 that most of the fall back water penetrates into the lower plenum while the water level in the lower plenum gradually increases until the water level reaches the bottom of core barrel, indicating that the penetrated water flows out into the downcomer during this period.

A part of the steam generated in the core and the lower plenum is also expected to flow through the bottom of core barrel into the downcomer before the water level reaches the bottom of core barrel. As shown in Fig. 3-21, the void fraction in the pressure vessel side broken cold leg indicates that the ECC water bypass occurs only before the biginning of bottom reflood. Since the ECC water bypass is caused by the steam up flow in the downcomer, it is evident that the steam also flows from the core into the downcomer before the beginning of bottom reflood.

The steam generation rate in the core is reduced after about 25 s as shown in Fig. 3-27 and the average water head in downcomer increases as shown in Fig. 3-23. At 76 s in Test S1-SH4, the pressure balance between the core and the downcomer breaks and the liquid level in the

lower plenum rapidly increases up to the bottom of core level.

From the view point of reactor safety, it is supposed that the upper plenum injection induces the fall back of water into the core before the BOCREC and the generated steam tends to prevent the reflooding from the bottom, though the initial cooling is promoted by the upper plenum injection as will be discussed in section 3.7.1. Therefore, the upper plenum injection has two opposite effects on the core cooling.

3.4.2 Estimation of Lower Plenum Flashing Rate

Since the combined injection pre-tests were performed under the refill simulation condition, the rapid decrease of system pressure induced the flashing of water in the lower plenum because the initial water temperature in the lower plenum was the saturation temperature at the initial pressure of 0.54 MPa.

The lower plenum flashing rate is calculated from the existing water and steam mass in the lower plenum and the depressurization rate by using the assumption of constant entropy process as follows:

$$\left[M_g \left(\frac{dS_g}{dP} \right)_{sat} + M_\ell \left(\frac{dS_\ell}{dP} \right)_{sat} + (S_{\ell g})_{sat} \frac{dM_{\ell g}}{dP} \right] \frac{dP}{dt} = 0$$

The flashing rate, $\frac{dM_{\ell g}}{dt}$, is obtained by the following equation.

$$\frac{dM_{\ell g}}{dt} = - \frac{1}{(S_{\ell g})_{sat}} \left[M_g \left(\frac{dS_g}{dP} \right)_{sat} + M_\ell \left(\frac{dS_\ell}{dP} \right)_{sat} \right] \frac{dP}{dt} \qquad (2)$$

where $(S_{\ell g})_{sat}$ = Specific entropy change due to evaporation,

S_g = Specific entropy of saturated steam,

S_ℓ = Specific entropy of saturated water,

P = Pressure,

M_g = Mass of steam in lower plenum,

M_ℓ = Mass of water in lower plenum,

$\frac{dP}{dt}$ = Depressurization rate.

The lower plenum flashing rates obtained by equation (2) for Tests S1-SH3 and S1-SH4 are shown in Fig. 3-22. The flashing rate is the highest just after the break balves open and then decreases. After the BOCREC, the average flashing rate is less than 0.1 kg/s and negligibly small as compared with the steam generation rate shown in Fig. 3-27.

The lower plenum flashing rate is larger in Test S1-SH4 than in Test S1-SH3 just after the break valves open because the depressurization rate is larger in Test S1-SH4 as shown in Fig. 3-4. During about 30 s before the BOCREC, however, the flashing rate is larger in Test S1-SH3 because the water inventory in the lower plenum is larger in Test S1-SH3 as shown in Fig. 3-18 and the depressurization rate is also larger in Test S1-SH3 during this period as shown in Fig. 3-4.

3.4.3 Water Accumulation Behavior in Downcomer

As shown in Fig. 3-23, the collapsed water levels in the downcomer in Tests S1-SH3 and S1-SH4 increase gradually up to the final level of about 5.7 m and then remain at the same elevation during the tests. The final level is considered to be corresponding to the overflow level because the liquid level in containment tank-I continues to increase during the test. The higher liquid level in Test S1-SH3 after about 50 s is attributed to the stronger steam binding effect as suggested from the higher steam outflow rate shown in Fig. 3-26.

On the other hand, the collapsed water level in the downcomer in Test S1-19 increases rapidly and after reaching the peak of about 5.6 m the water level decreases and remains at 3.8 m for about 250 s, though the ECC water injection rates into the intact cold leg are almost the same for these three tests.

3.5 Fluid Behavior in Hot Leg

Figures 3-24 and 3-25 show the comparisons of mass flow rates and void fractions, respectively, at four vertical regions in the hot leg spool piece. Region I comprises the upper 31 % of the pipe cross-sectional area, Region 2 comprises the next lower 27 %, Region 3 comprises the next lower 26 %, and Region 4 comprises the bottom 16 %. These mass flow rates are calculated from the measured densities and drag forces at each region by using the homogeneous model.

The flow direction through the hot leg in Test S1-SH3 is positive and no flow reversal is observed. On the other hand, the flow reversal at Regions 3 and 4 is clearly observed in Test S1-SH4 just before the BOCREC and at the later period of the test. The times when the void fractions in regions 3 and 4 decrease to almost 0.0 in Test S1-SH4 are in good agreement with the times when the flow reversal is observed in Fig. 3-24.

The occurrence of hot leg flow reversal is confirmed by the flow observation through the view window at the lower part of hot leg. No flow reversal in Test S1-SH3 is due to the higher steam flow rate as shown in Fig. 3-26.

3.6 Evaluation of Steam Outflow Rate, Steam Generation Rate in Core and Steam Condensation Rate in Upper Plenum

The steam outflow rate through the hot leg is obtained by subtracting the flashing rate in the steam/water separator from the summation of the steam mass flow rate from the steam/water separator to the containment tank-II and the steam mass flow rate from the steam/water separator to the downcomer through the intact cold leg. The flashing rate in the steam/water separator obtained by the same method as described in section 3.4.2 is negligibly small as compared with the total steam outflow

As shown in Fig. 3-26, the steam outflow rate through the hot leg is significantly higher in Test S1-SH3 than in Test S1-SH4, suggesting that considerable amount of steam is condensed in the upper plenum in Test S1-SH4 due to the subcooled water injection into the upper plenum.

Figure 3-27 shows the steam generation rates in the core in these two tests. The steam generation rate was obtained from the heat balance calculation in the whole core. Additional steam is generated by the lower plenum flashing during the depressurization period as shown in Fig. 3-22. Figure 3-28 shows the total steam generation rates obtained by the summation of these two steam generation rates. As shown in this figure, the total steam generation rate after the BOCREC is slightly larger in Test S1-SH4 than in Test S1-SH3, whereas the total steam mass outflow rate is much larger in Test S1-SH3 than in Test S1-SH4 as shown in Fig. 3-26 because a part of the generated steam is condensed in the upper plenum in Test S1-SH4 due to the higher subcooling of UCSP injection water. In addition, during the first 50 s in Test S1-SH3 and

the first 80 s in Test S1-SH4, some amount of the generated steam flows directly into the downcomer through the bottom of core barrel as indicated in Fig. 3-18.

Figure 3-29 compares the two steam condensation rate in the upper plenum in Test S1-SH4 estimated by the difference between the total steam generation rate in the core and the steam outflow rate through the hot leg and estimated by the following equation:

$$W_{gc} = \frac{W_{inj\cdot up}\, C_p\, \Delta T_{sub}}{H_{fg}} \qquad (3)$$

where, W_{gc} = Steam condensation rate,

$W_{inj\cdot up}$ = Upper plenum injection rate,

C_p = Specific heat of water,

ΔT_{sub} = Subcooling of the injected water,

H_{fg} = Latent heat of evaporation.

Equation (3) is derived from the assumption that the whole amount of injected water into the upper plenum becomes saturated due to the condensation of steam. Since the fluid temperatures in the upper plenum are almost saturated except during the first 28 s as shown in Fig. 3-8, the calculated steam condensation rate is plausible after about 30 s from the break valves open.

As shown in Fig. 3-29, the difference between the total steam generation rate and the steam outflow rate agrees well with the calculated steam condensation rate with Eq. (3) after 120 s. The condensation rate in the upper plenum is about 1.4 kg/s after the BOCREC.

The steam condensation in the upper plenum results in the higher water accumulation rate in the core for Test S1-SH4 as discussed in section 3.3.

3.7 Core Thermal Behavior

3.7.1 Heater Rod Surface Temperature

Figure 3-30 shows the comparisons of heater rod surface temperatures at the elevations of 3.19, 1.905 and 0.95 m from the bottom of heated

length between Tests S1-SH3 and S1-SH4. These temperatures are measured at the center rods of Bundle 4 which are not adjacent to non-heated rods.

During the first 30 s, the heater rod is cooled especially at the upper part of core in these two tests by the fall back water during this period. The initial cooling of heater rod is slightly larger in Test S1-SH3, indicating that the initial fall back flow rate is larger in this test during the first 30 s. However, the core cooling is more enhanced in Test S1-SH4 than in Test S1-SH3 except the initial period. Consequently, the turnaround temperatures are lower and the quench times are shorter in Test S1-SH4. The cooling enhancement in this test is attributed to the higher water accumulation rate in the core as discussed in section 3.3.

It is observed in Fig. 3-30 that the heater rod at 3.19 m in Test S1-SH4 is quenched at about 20 s and then increases again. The same temperature behavior is observed in 11 rods out of 57 instrumented heater rods as shown in Fig. 3-36.

Figure 3-30 also indicates that although the upper part of core is cooled by the fall back water during the first 30 s, the core is mainly cooled by the bottom reflood after the BOCREC.

In order to investigate the two-dimensional effects on core thermal behavior, the horizontal distributions of turnaround temperatures at the elevations of 2.76, 1.735 and 0.52 m are compared in Fig. 3-31 for these two tests. At the lowest power bundles, Bundle 7 and 8, the turnaround temperatures are lower in comparison to those at the other bundles for these two tests in accordance with the radial power profile. The relatively higher turnaround temperatures in Bundles 1 and 2 in Test S1-SH3 are due to the delayed injection into the upper plenum above these bundles as mentioned in section 3.1. In Bundles 6, 7 and 8, the turnaround temperatures in Test S1-SH3 are lower than those in Test S1-SH4, while those in Test S1-SH3 are higher than those in Test S1-SH4 in the other bundles, indicating that the amount of initial fall back water into the core is relatively large at the Bundle 8 side in Test S1-SH3 due to the non-uniform UCSP injection during the first 60 s.

The maximum turnaround temperature is 1158 K at 1.735 m in Bundle 1 in Test S1-SH3 and 1119K at 1.735 m in Bundle 6 in Test S1-SH4.

3.7.2 Quench Characteristics

The quench envelopes at the central rods in Bundle 4 are compared in Fig. 3-32 among Tests S1-SH3, S1-SH4 and S1-19 with respect to time after the BOCREC.

At the upper half of core, the quench occurs earlier in Test S1-SH4 than in Test S1-SH3 while no difference is observed in the quench times at the lower half of core between these two tests. The quench times after the BOCREC in Test S1-19 at the lower half of core are in good agreement with those in the combined injection pre-tests. At the upper half of core, on the other hand, the quench times in Test S1-19 are later than those in Tests S1-SH3 and S1-SH4.

Figure 3-33 shows the comparisons of quench envelopes at the central rods in all bundles in these three tests. As shown in this figure, the quench front proceeds upward from the bottom of core up to the elevation of 3.19 m and the downward propagation of quench front from the top of core is limitted above this elevation in most bundles in these tests. The upward quench propagation is approximately one-dimensional in spite of the radial power distribution, whereas the downward quench proceeds often nonuniformly.

Figure 3-34 and 3-35 show the comparisons of radial and azimuthal distributions of the quench times after the break valves open, respectively. As shown in these figures, early quenches at the elevation of 2.76 m are more often observed in Bundles 1 and 8, or at the locations adjacent to the side walls.

In addition, the effect of radial power profile on the quench times is slightly observed in Fig. 3-34 except at the elevation of 2.76 m in Test S1-SH4. Therefore, it is suggested that the distribution of water fall back is much affected by the existance of side walls than by the radial power profile itself.

Figure 3-36 shows the horizontal distributions of earlier quenched rods at the elevation of 3.19 m in Tests S1-SH3 and S1-SH4. The earlier quenched rod is defined as the rod which experienced the quench before the BOCREC. Some thermocouples at this elevation indicate the earlier quench and dry out. Those rods are also shown in Fig. 3-36. As shown in this figure, the earlier quench tends to occur at the locations adjacent to the side walls and the earlier quench also tends to occur more easily at the UCSP injection side than at the UCSP

extraction side. However, the effect of radial power profile is not recognized in the distribution of earlier quenched rods.

It is concluded from the above-mentioned quench characteristics that the upper plenum injection promotes the quench at the upper part of core and especially at the locations adjacent to the walls. And furthermore, the higher subcooling of the UCSP injection water promotes the earlier quench at the upper half of core.

3.7.3 Heat Transfer Characteristics

Figure 3-37 shows the transients of heat transfer coefficients at the elevation of 2.33 m in bundle 4 in Tests S1-SH3, S1-SH4 and S1-19. The heat transfer coefficients are calculated with a heat transfer calculation code "HEATT"[2] developed for the SCTF test analysis. The heat transfer coefficients in Tests S1-SH3 and S1-SH4 temporally increase during the higher upper plenum injection period due to the initial fall back as already mentioned and then remain at low values until the beginning of bottom reflood at 80 s. After that time, the heat transfer coefficients increase again due to the water splahsed up from the bottom quench front.

In order to make clear the heat transfer characteristics, the heat transfer coefficients at the elevation of 2.76, 2.33, 1.905 and 1.38 m in bundle 4 are plotted against the distance from bottom quench front in Fig. 3-38. At the upper half of core, the heat transfer coefficient is higher in Test S1-SH4 than in Test S1-SH3 when the distance from bottom quench front is more than about 0.5 to 0.8 m while no difference is observed within 0.5 m from the quench front. At the elevation of 1.38 m, on the other hand, the heat transfer coefficient is higher in Test S1-SH3 than in Test S1-SH4 within about 0.6 m from the bottom quench front while it is higher in Test S1-SH4 above 0.6 m from the bottom quench front.

The heat transfer coefficient in Test S1-19 is lower than both in Tests S1-SH3 and S1-SH4 except the initial peak caused by the oscillation of water level. The initial peaks of heat transfer coefficients observed in Tests S1-SH3 and S1-SH4 in Fig. 3-37 are not seen in Fig. 3-38 because the bottom quench fronts are not established until 80 s. The difference of heat transfer coefficient between the cold leg and combined injection tests becomes smaller with approaching the quench

front. At the elevation of 1.38 m, the heat transfer coefficient is higher in Test S1-19 than in Tests S1-SH3 and S1-SH4 when the distance from bottom quench front is more than 0.6 m.

The local water fractions at the elevations of 2.76, 2.33, 1.905 and 1.38 m in these three tests are plotted against the distance from bottom quench front in Fig. 3-39. The local water fractions are obtained by the interpolation of the water fractions calculated from the vertical differential pressures measured between core spacers. As shown in this figure, the local water fraction is much higher in Test S1-SH4 than in both Tests S1-SH3 and S1-19 at each elevation with respect to the distance from bottom quench front except the inital peak observed in Test S1-19 which is caused by the initial oscillation of liquid level in core. The local water fractions in Test S1-SH3 almost agree with those in Test S1-19 at the same distance from bottom quench front especially at the lower half of core.

Figure 3-40 shows the relation between the heat transfer coefficient and the local water fraction at the elevations of 2.76, 2.33, 1.905 and 1.38 m in these three tests. As shown in this figure, the heat transfer coefficient in Test S1-19 is rather close to that in Test S1-SH3 if the local water fraction is the same especially at the elevations of 2.76 and 2.33 m, though the heat transfer coefficient in Test S1-SH3 is higher than that in Test S1-19 if the distance from quench front is the same as shown in Fig. 3-38. On the other hand, the heat transfer coefficient in Test S1-SH4 is lower than those in Tests S1-SH3 and S1-19 at the higher water fraction. The water fractions at the quench front are about 0.25 in Tests S1-SH3 and S1-19 and about 0.3 in Test S1-SH4 at the elevations of 2.33 and 2.76 m.

It is therefore suggested that the heat transfer characteristics for the combined injection pre-tests are similar to those for the cold leg injection test with respect to the local water fraction when the temperature of water injected into the upper plenum is nearly saturated. When the upper plenum injection water has large subcooling, however, the heat transfer characteristics in the core are different from those for the cold leg injection test.

4. Conclusions

Test results obtained from the combined injection pre-tests: S1-SH3 (saturated water injection into the upper plenum) and S1-SH4 (subcooled water injection into the upper plenum), were evaluated and the following results were obtained.

(1) Continuous fall back of subcooled water was not observed even under the condition with large injection rate of subcooled water into the upper plenum and with steam outflow through the lower plenum into the downcomer. The fall back was intermittently limited by the rapid increase of upward steam flow which was generated in the core due to the evaporation of the fall back water.

(2) The fall back occurred nonuniformly over the eight bundles.

(3) The possible fall back flow rate estimated with a CCFL correlation rapidly decreased after the BOCREC because of the increase of steam generation rate in the core.

(4) The higher subcooling of the upper plenum injection water resulted in the cooling enhancement especially at the upper part of core due to the following reason: Since the steam out flow rate was much lower due to the steam condensation in the upper plenum in the test with higher subcooling of upper plenum injection water, the steam binding effect was weaker and therefore the water accumulation rate in the core was higher in this test.

(5) The rising of liquid level in the lower plenum was suppressed by the pressurization in the core due to the evaporation of fall back water before the BOCREC and therefore the beginning of bottom reflood was delayed.

(6) The mass outflow through the hot leg was larger in the test with saturated upper plenum injection water and no flow reversal in the hot leg was observed in this test, while significant hot leg flow reversal was observed in the test with subcooled upper plenum injection water.

(7) Although the core was cooled by the fall back water during the period of high injection rate into the upper plenum, the core was mainly cooled by the bottom reflood after the BOCREC.

(8) No significant effect of radial power profile was recognized on the core cooling behavior before the BOCREC, but the core cooling was clearly promoted in the rods adjacent to walls.

Acknowledgement

The authors are much indebted to Dr. M. Nozawa, Dr. K. Hirano and Dr. Y. Murao for their guidance and encouragement for this program.

They would like to express their appreciation to Mr. T. Iguchi, Mr. K. Okabe, Mr. J. Sugimoto, Dr. H. Akimoto, and Mr. T. Okubo of CCTF analysis group for their useful discussions.

References

(1) H. Adachi, et al., Design of Slab Core Test Facility (SCTF) in Large Scale Reflood Test Program, Part I: Core-I, JAERI-M 83-080 (1983).

(2) M. Osakabe and Y. Sudo., Heat Transfer Calculation of Simulated Heater Rods throughout Reflood Phase in Postulated PWR-LOCA Experiments, J. of Nucl. and Tech., Vol. 20, No. 7, pp. 559 ~ 570, (1983).

(3) H. Adachi, et al., Cold Leg Injection Reflood Test Redults obtained in SCTF Core-I under Constant System Pressure, to be published

Table 2-1 Comparison of dimensions between SCTF and 1,100 MWe PWR

Item	SCTF	PWR	Ratio (SCTF/PWR)
Quantity of Bundle	8	193	1/24.1
Number of Heater Rod	1872	39372	1/21.0
Number of Rods	2048	43425	1/21.2
Effective Length of Heater Rod (mm)	3660	3660	1/1
Rod Pitch (mm)	14.30	14.30	1/1
Diameter of Heater Rod (mm)	10.70	10.72	1/1
Diameter of Unheated Rod (mm)	13.80	13.87	1/1
Flow Area of Core (m^2)	0.259	4.76	1/17.7
Effective Core Flow Area Based on the Measured Level-Volume Relationship(m^2)	0.35	4.76	1/13.6
Fluid Volume of Core Enveloped by Honeycomb Insulators*	0.92	17.95	1/19.5
Fluid Volume of Lower Plenum (m^3)	1.305	29.62	1/22.7
Fluid Volume of Upper Head (m^3)	0.86	19.8	1/23.0
Baffle Region Flow Area (m^2)	0.10	1.76	1/17.6
Upper Plenum Fluid Volume (m^3)	1.16	23.8	1/20.5
Downcomer Flow Area (m^2)	0.121	2.47	1/20.4
UCSP Thickness (m)	76	76	1/1
Steam Generator Inlet Plenum Simulator Volume (m^3)	0.931	4.25 × 4	1/18.3
Height of Steam Generator Inlet Plenum Simulator (m)	1.595	1.595	1/1
Flow Area at the Top Plate of Steam Generator Inlet Plenum Simulator (m^2)	0.19	4.0	1/21.2
Major Axis Length of Hot Leg Cross Section	737	736.6	1/1
Flow Area of Hot Leg (4 Loops)	0.0826	1.704	1/20.6
Flow Area of Intact Loop (3 Loops)	0.0696	1.149	1/16.5
Flow Area of Broken Cold Leg (m^2)	0.0179	0.383	1/21.4
* Fluid Volume of Core Including Gaps between Core Barrel and Pressure Vessel Wall	1.74		

Table 2-2 Test conditions for Tests S1-SH3, S1-SH4 and S1-19 and calculated results for combined injection mode for a reference PWR

	Test S1-SH3 (Run 528)	Test S1-SH4 (Run 529)	Test S1-19 (Run 525)	Calculated results for a reference combined injection
Initial pressure				
Core center	0.54 MPa	0.54 MPa	0.59 MPa	—
Containment-I	0.21 MPa	0.21 MPa	0.22 MPa	0.4 MPa
Upper plenum or hot leg injection condition				
Injection rate (Acc)	81 kg/s	97 kg/s*	—	2000-1200 kg/s
Injection time (Acc)	28 s	28 s	—	about 150 s
Injection rate (LPCI)	11 kg/s	11 kg/s	—	—
Subcooling	about 0 K	67 K	—	20-40 K
Cold leg injection condition				
Injection rate (Acc)	84 kg/s	84.5 kg/s**	87.5 kg/s	1500-900 kg/s
Injection rate (LPCI)	8.2 kg/s	8.2 kg/s	7.8 kg/s	—
Acc Injection time	27 s	24 s	24 s	about 150 s
Water temperature (Acc)	335 K	334 K	339 K	303 K
Water temperature (LPCI)	335 K	337 K	337 K	—

Equivalent value for a reference PWR

* Upper plenum injection rate during Acc period

2076 kg/s

*** Cold leg injection rate during Acc period

1816 kg/s

Table 2-3 Chronologies of events for Tests S1-SH3, S1-SH4 and S1-19

(1) Test S1-SH3

	Time after core power "ON"	Time after break valves open
Core power "ON"	0 sec	-101 sec
Core power decay initiation and break valves open	101	0
USCP injection and extraction initiation	101	0
Acc injection initiation	105	4
Maximum ECC injection rate (84 kg/s)	120	19
Switch Acc to LPCI	128	27
BOCREC	181	80
Maximum core temp. (1158 k)	208	107
Whole core quenched	532	431

(2) Test S1-SH4

	Time after core power "ON"	Time after break valves open
Core power "ON"	0 sec	-100 sec
Core power decay initiation and break valves open	100	0
USCP injection and extraction initiation	100	0
Acc injection initiation	103	3
Maximum ECC injection rate (83 kg/s)	124	24
Switch Acc to LPCI	124	24
BOCREC	181	81
Maximum core temp. (1119 k)	190.5	90.5
Whole core quenched	489	389

(3) Test S1-19

	Time after core power "ON"	Time after break valves open
Core power "ON"	0 sec	-138 sec
Core power decay initiation and break valves open	138	0
Acc injection initiation	142	4
Maximum ECC injection rate (87.5 kg/s)	156	18
BOCREC	157	19
Maximum core temp. (1195 k)	160	22
Switch Acc to LPCI	163	25
Whole core quenched	578	440

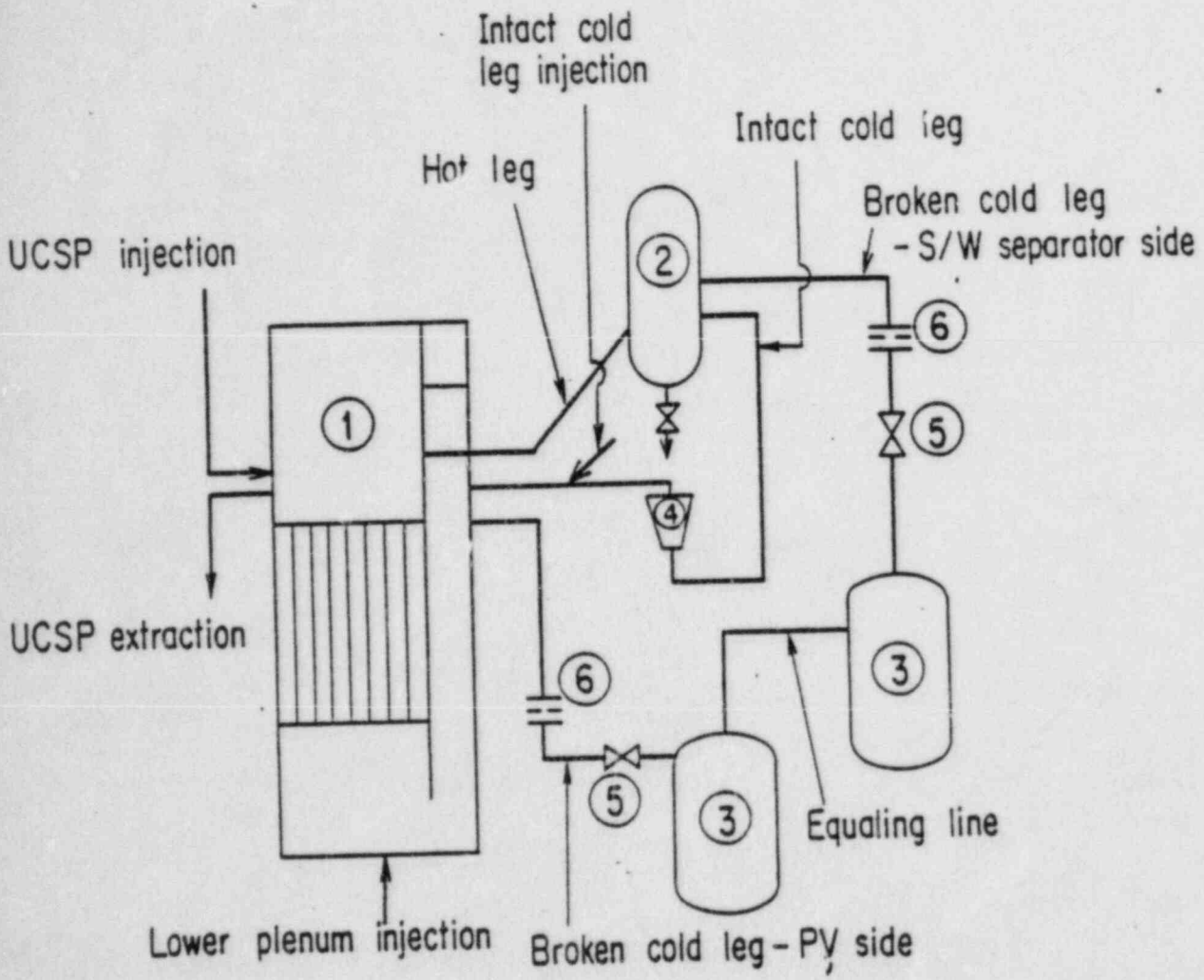

① Pressure vesel
② Steam / water separator
③ Containment tanks
④ Pump simulator
⑤ Break valves
⑥ Flow resistance simulators

Fig. 2-1 Schematic diagram of Slab Core Test Facility

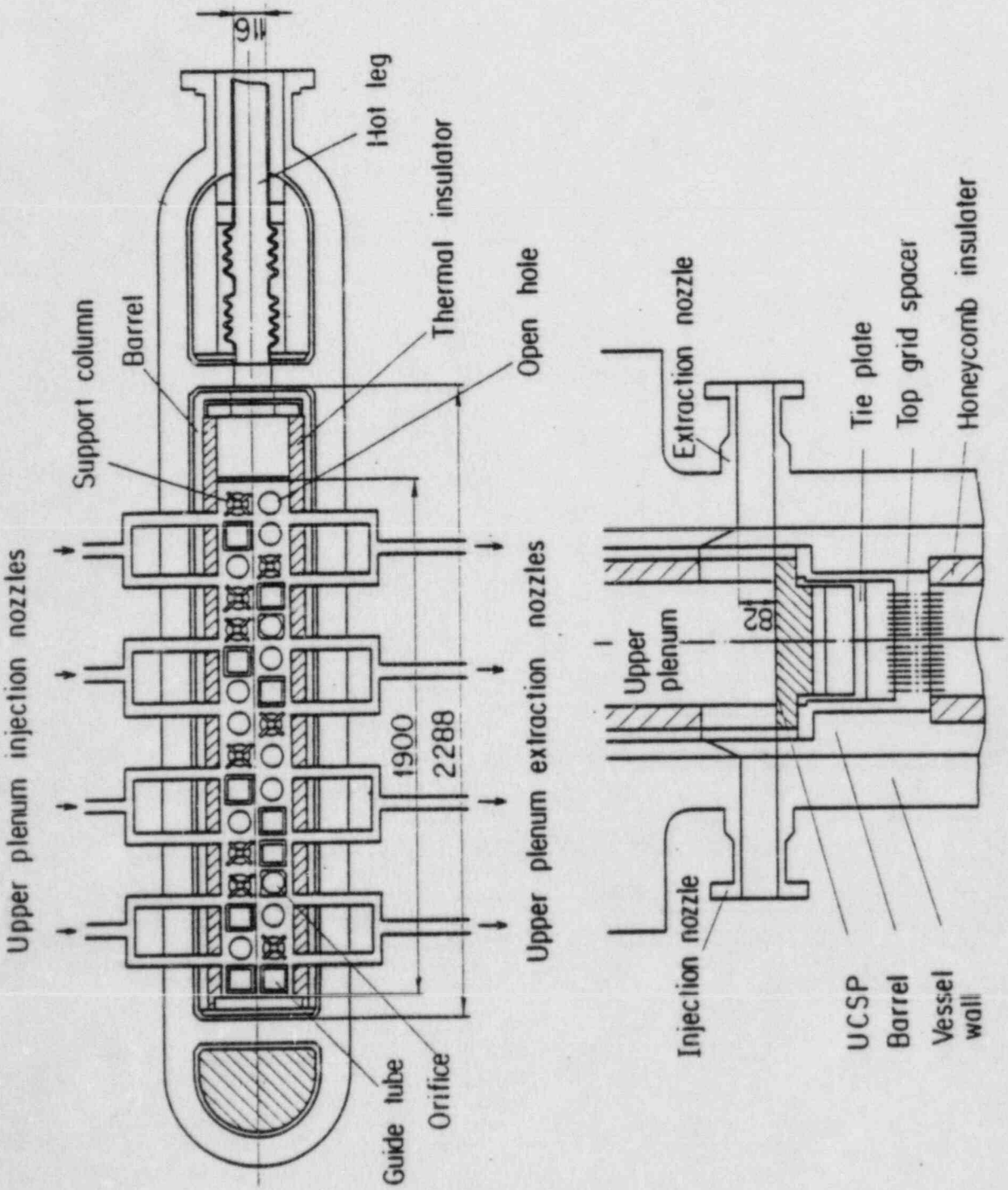

Fig. 2-2 Arrangement and dimension of UCSP water injection and extraction nozzles

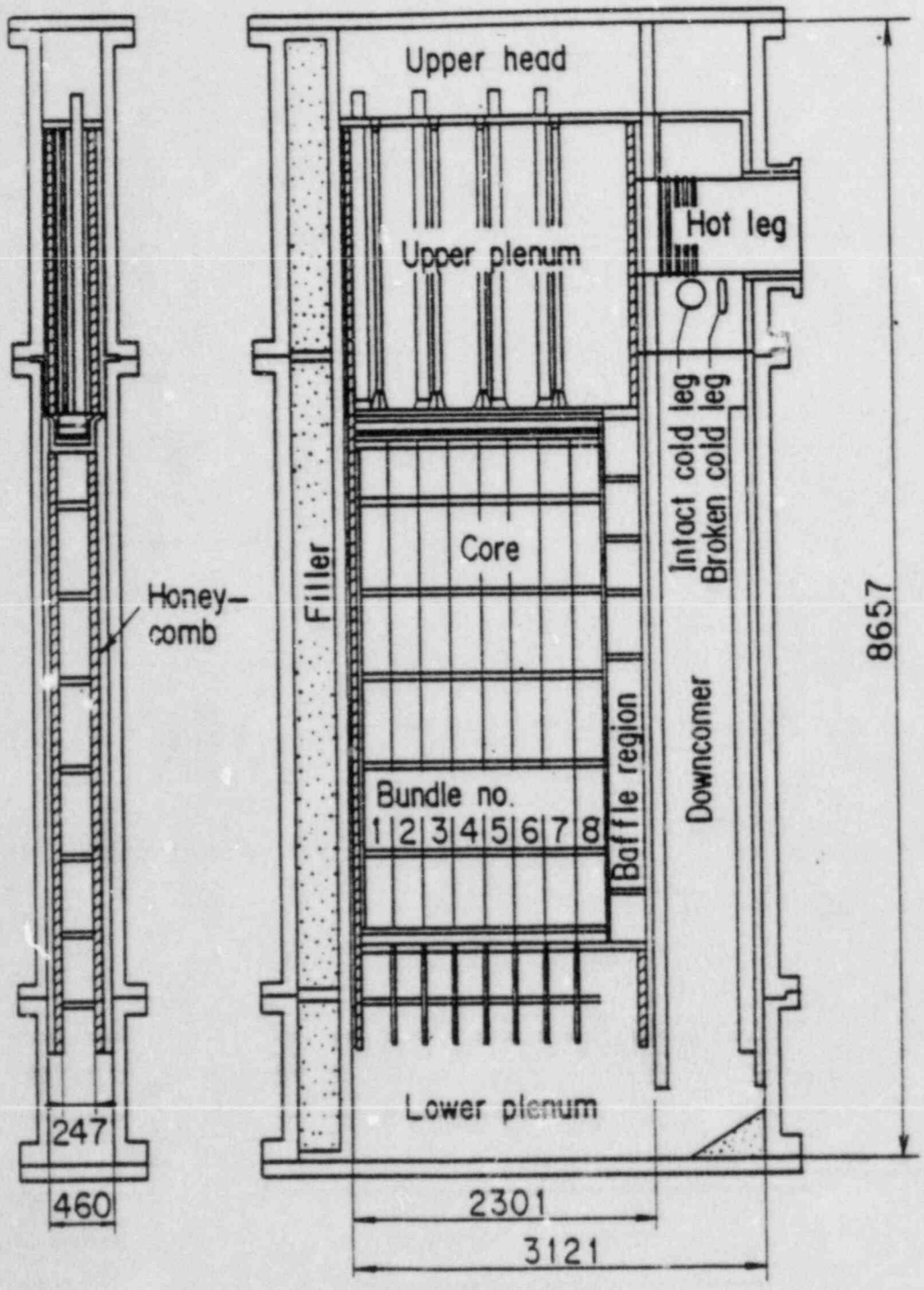

Fig. 2-3 Pressure vessel of Slab Core Test Facility

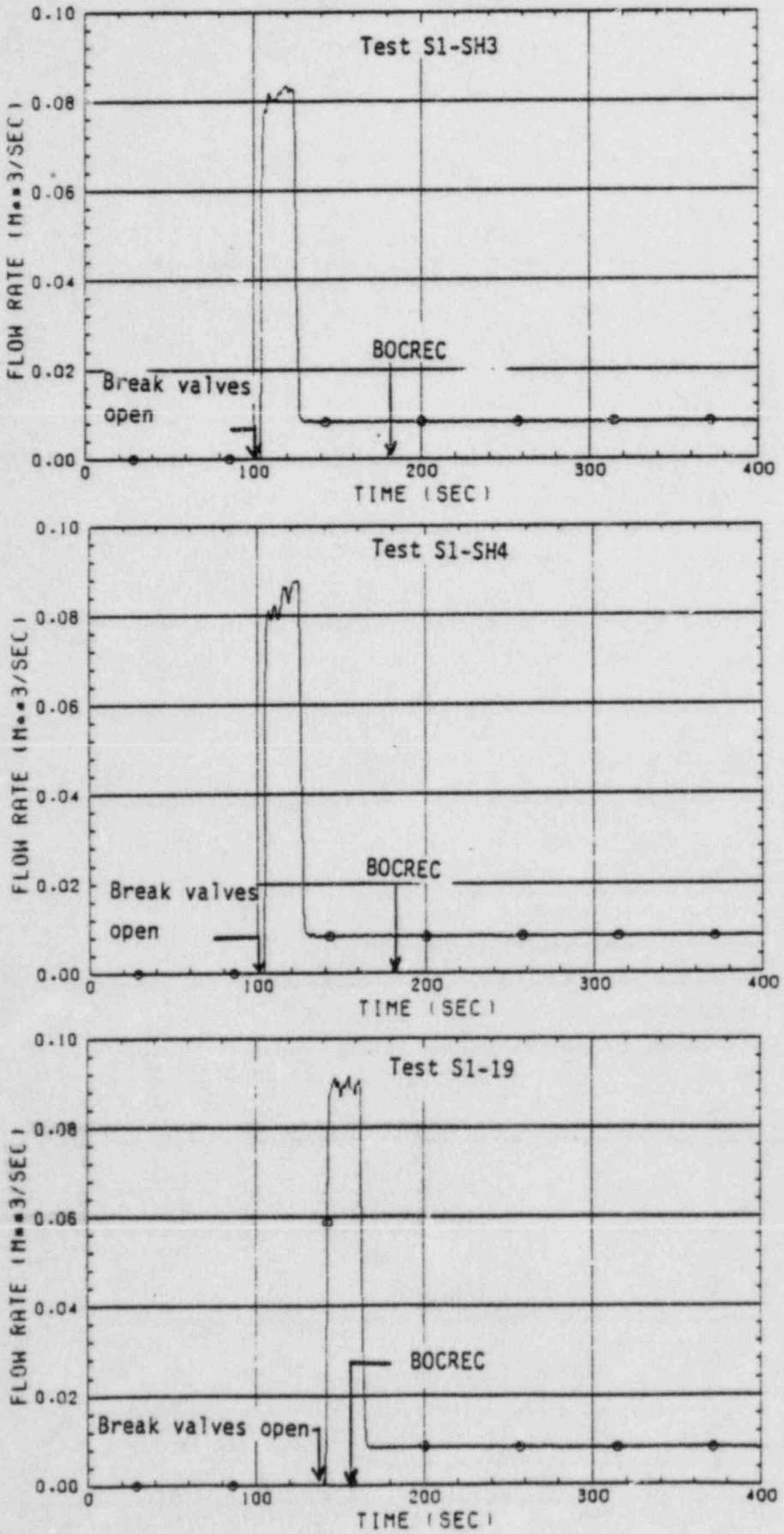

Fig. 3-1 ECC water injection rates into intact cold leg

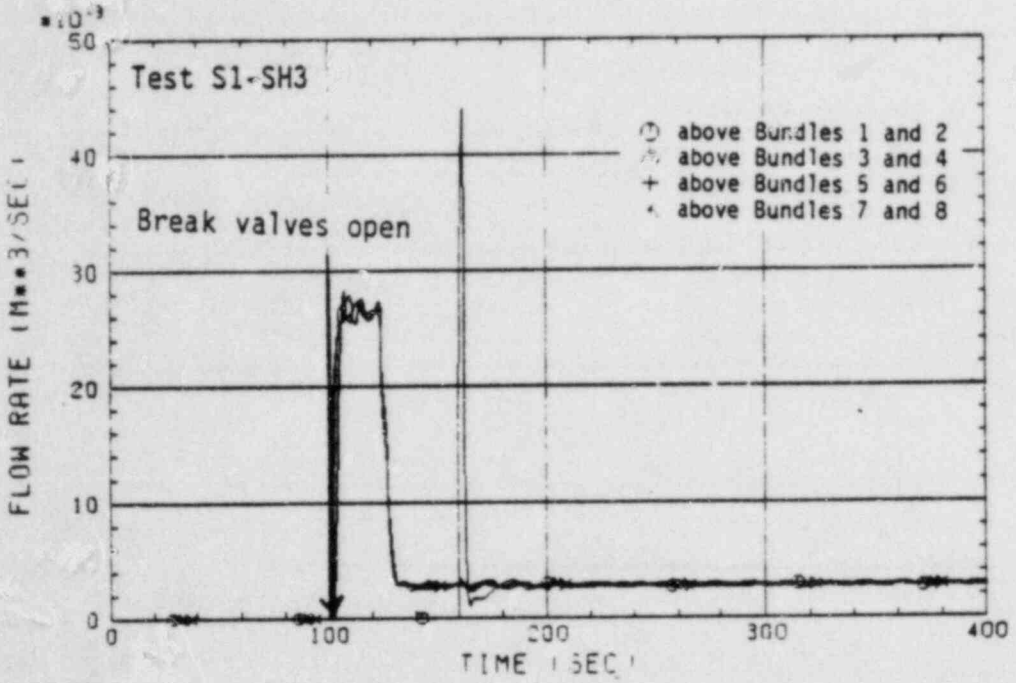

(1)

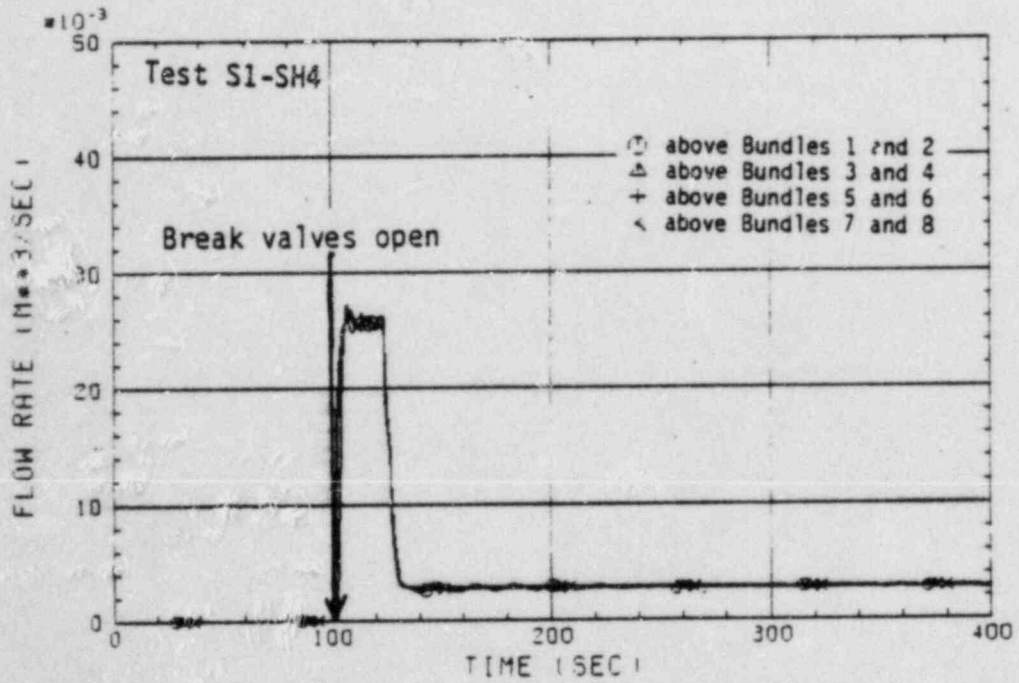

(2)

Fig. 3-2 ECC water injection rates into upper plenum

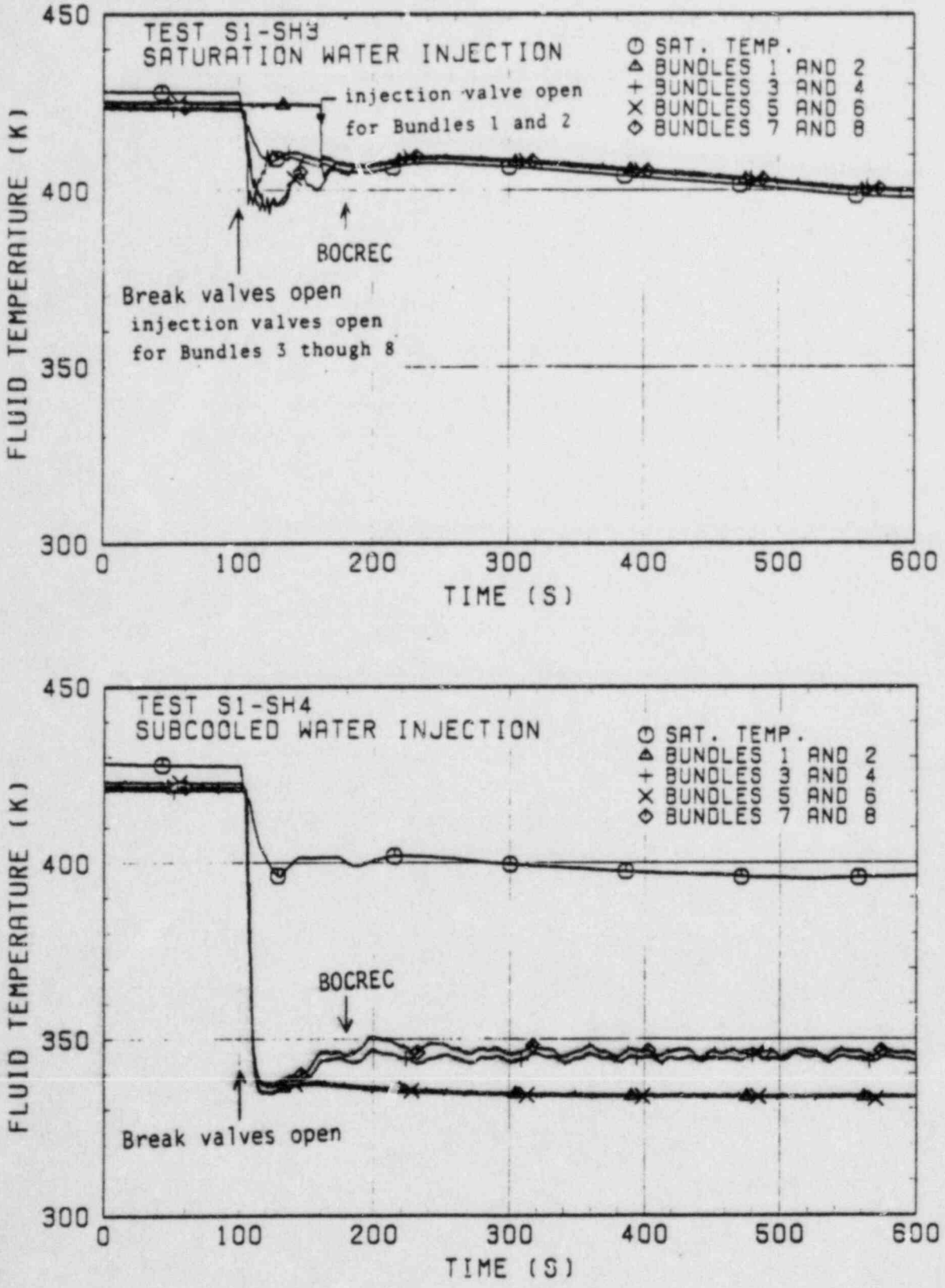

Fig. 3-3 Temperatures of ECC water injected into upper plenum

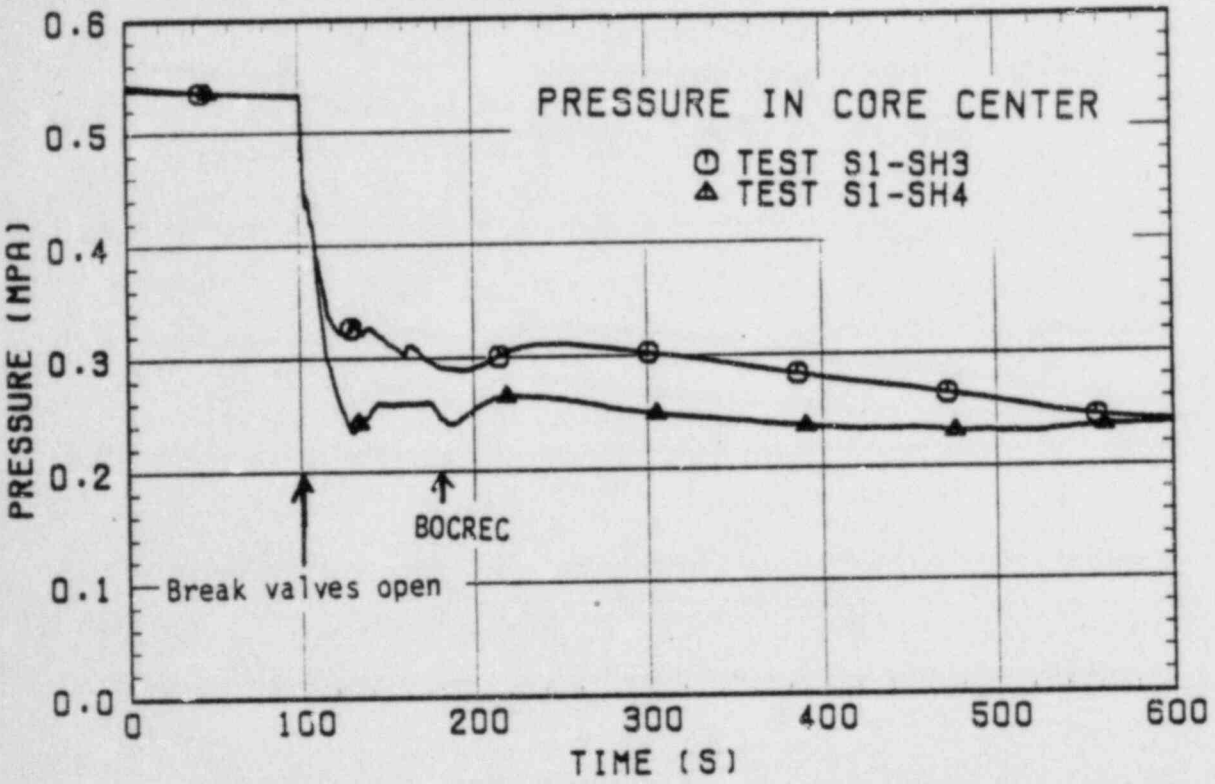

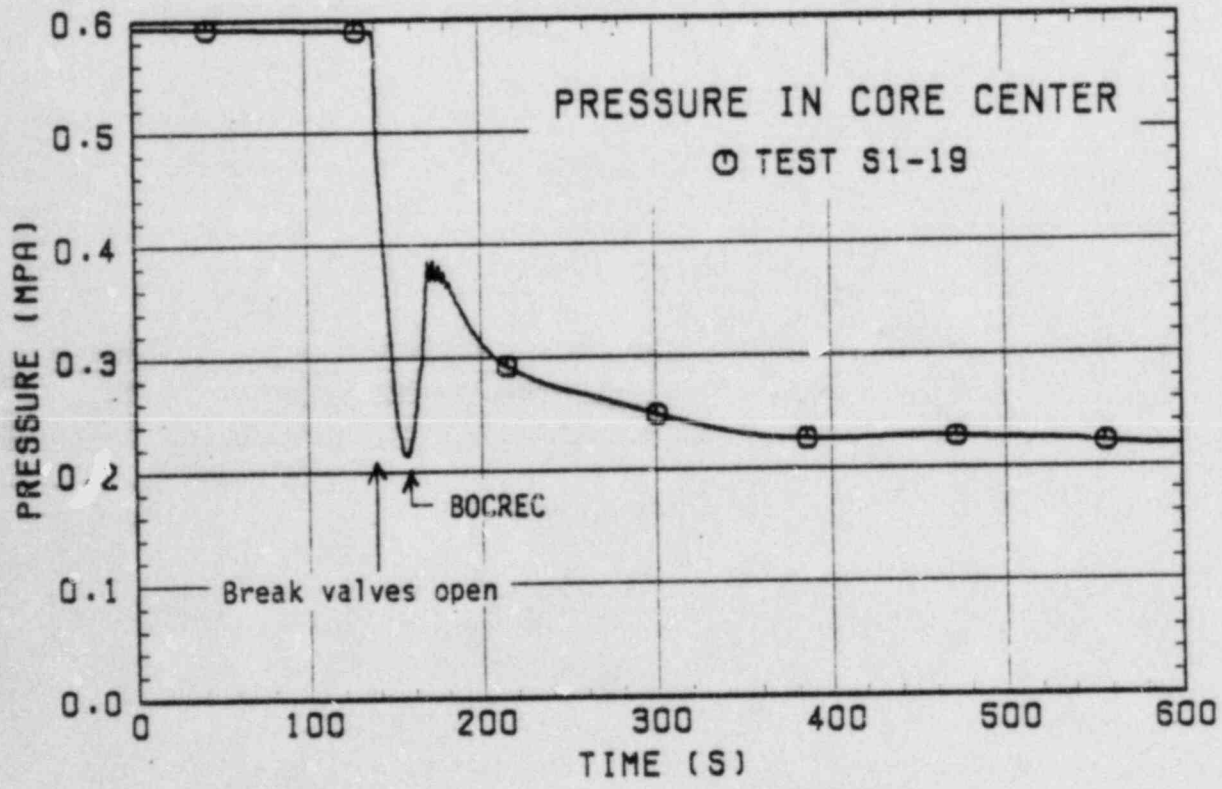

Fig. 3-4 Pressure transients in core center

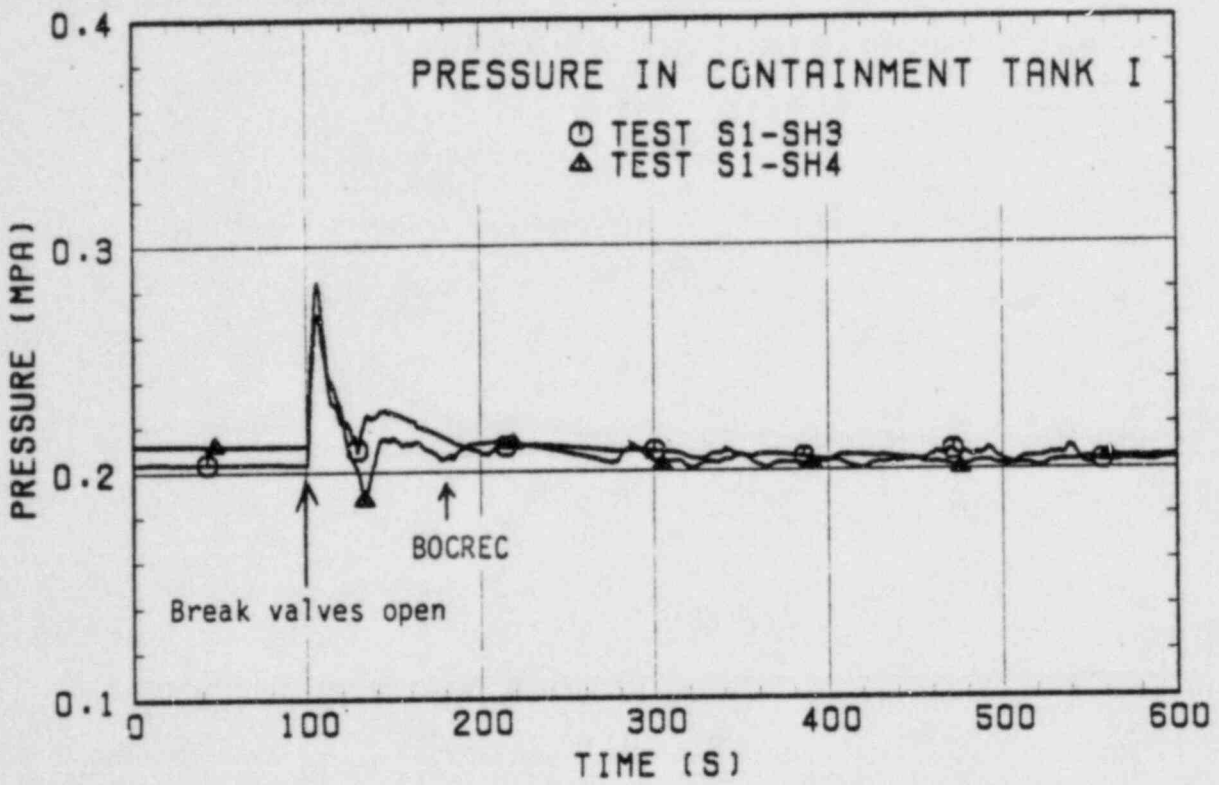

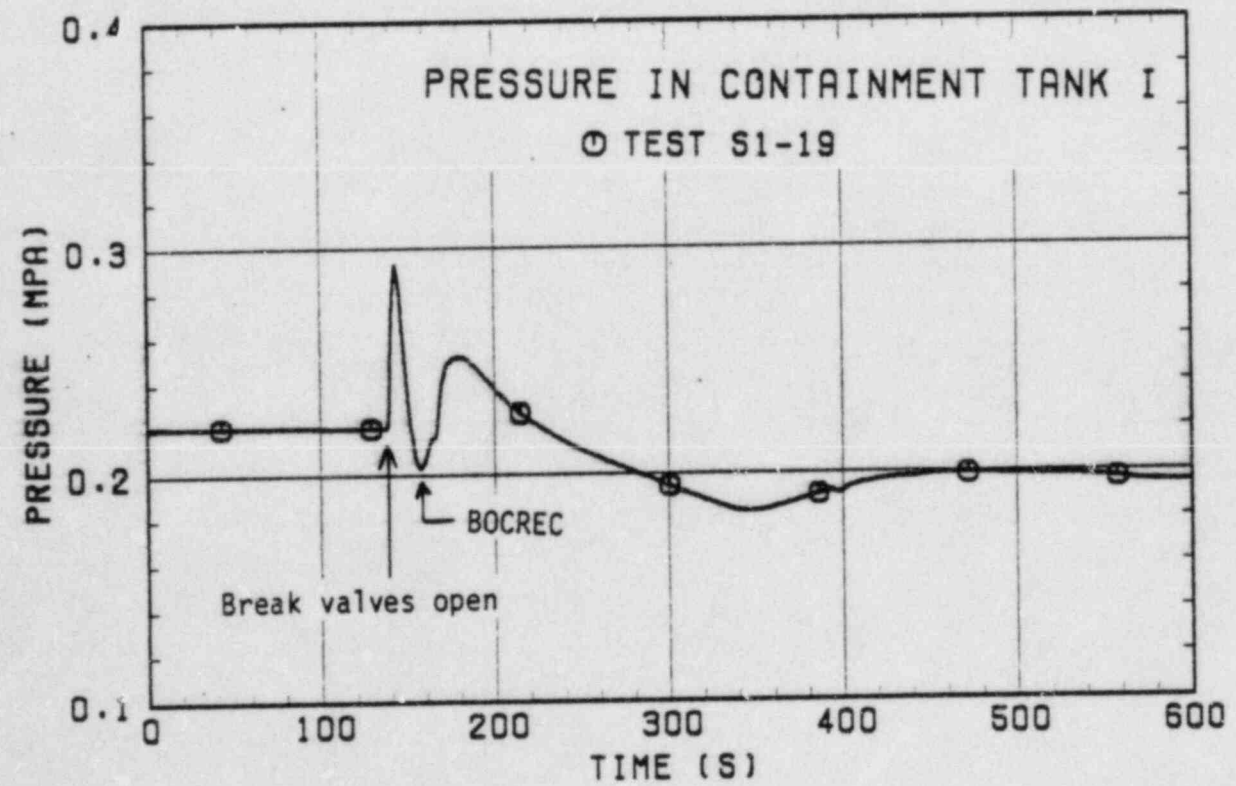

Fig. 3-5 Pressure transients at top of containment tank-I

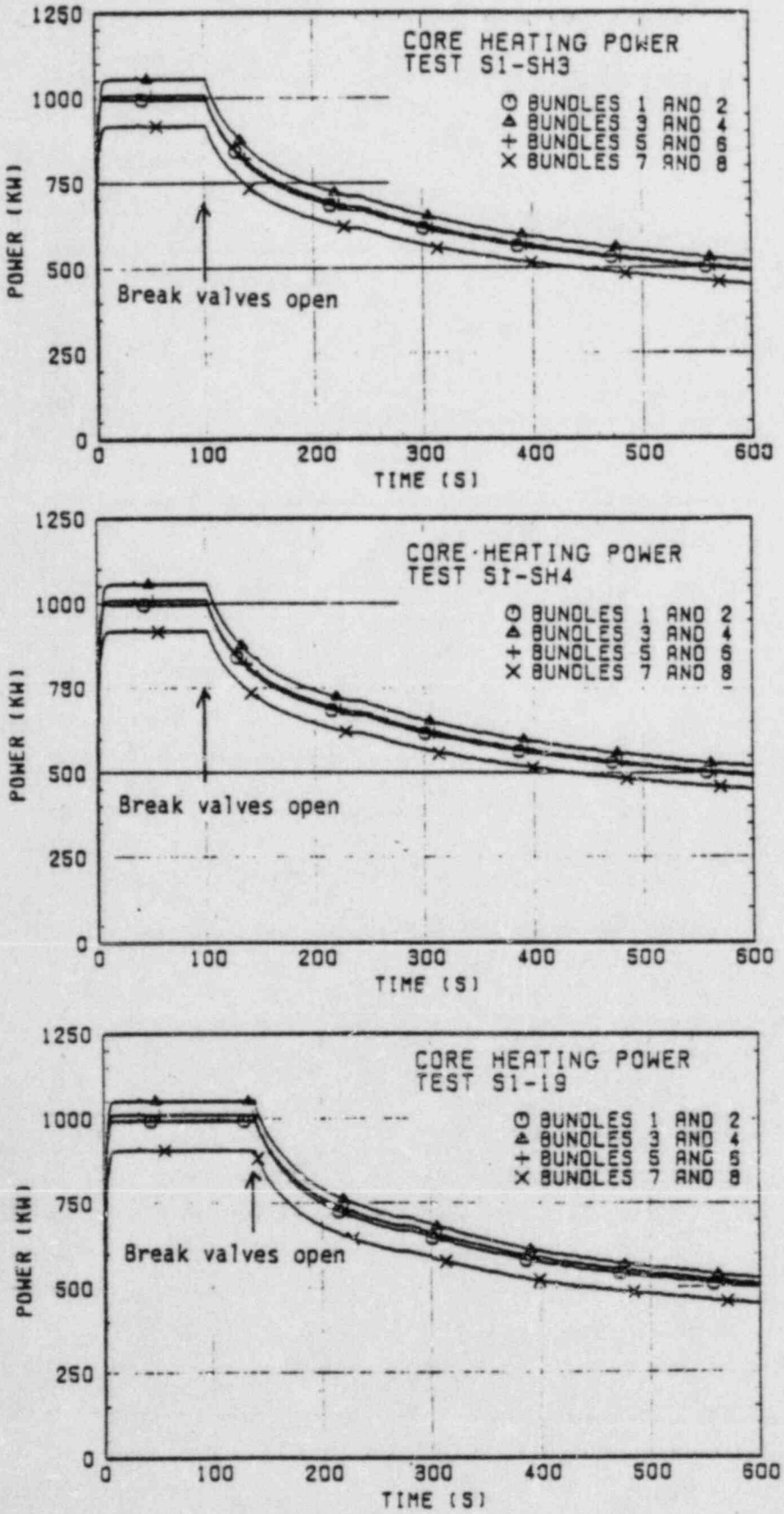

Fig. 3-6 Core heating powers

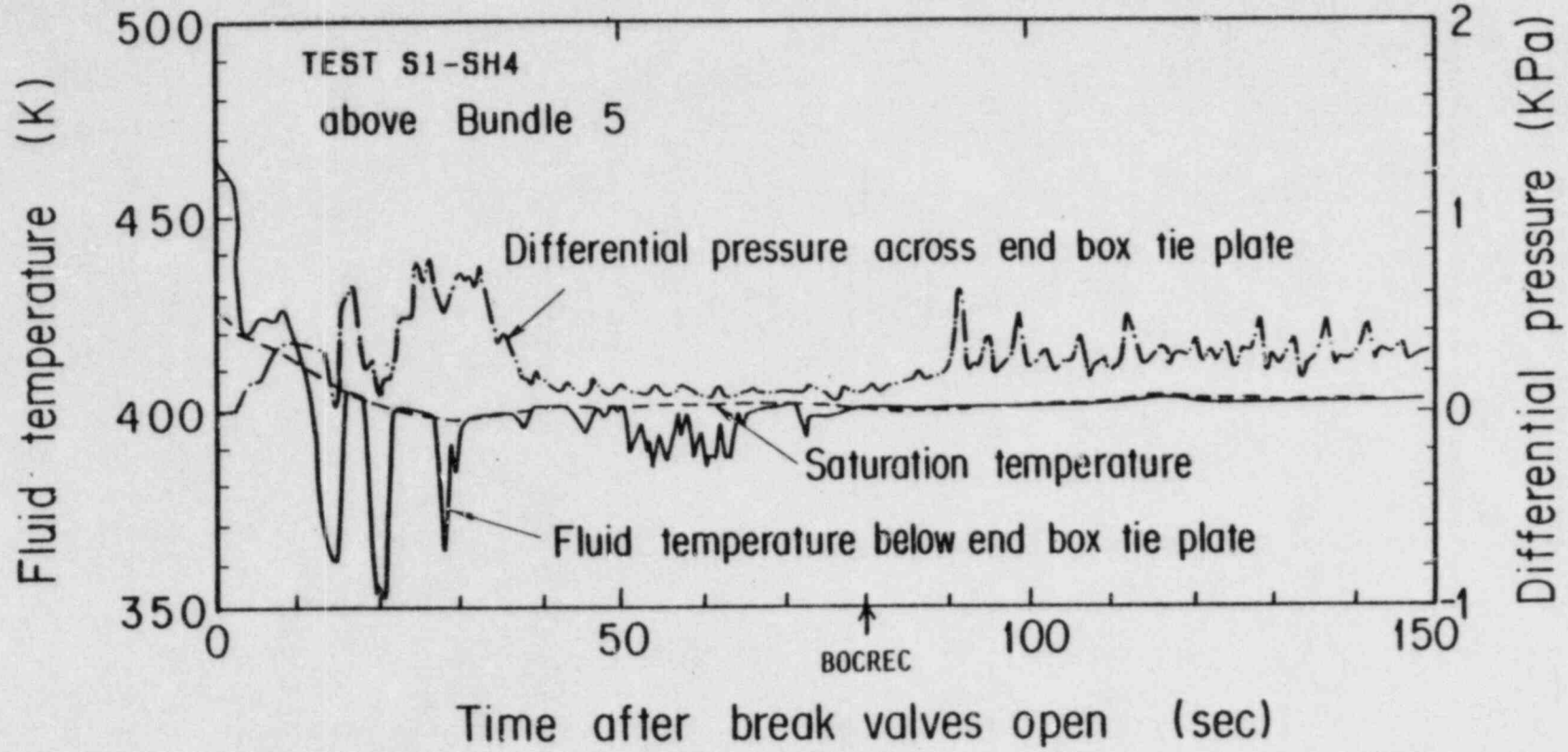

Fig. 3-7 Differential pressure across end box tie plate and fluid temperature just below end box tie plate above bundle 4 in Test S1-SH4

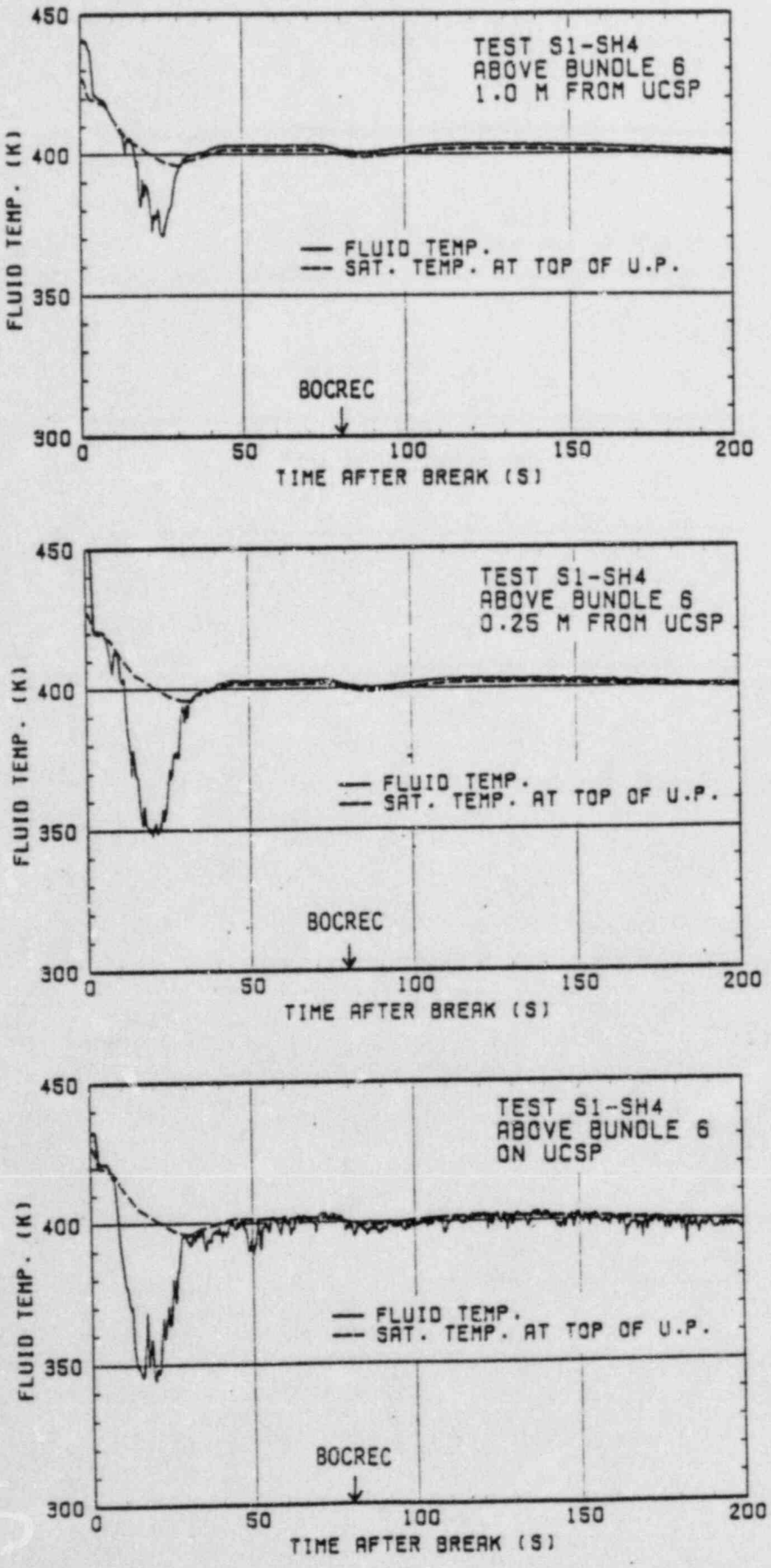

Fig. 3-8 Fluid temperatures in upper plenum

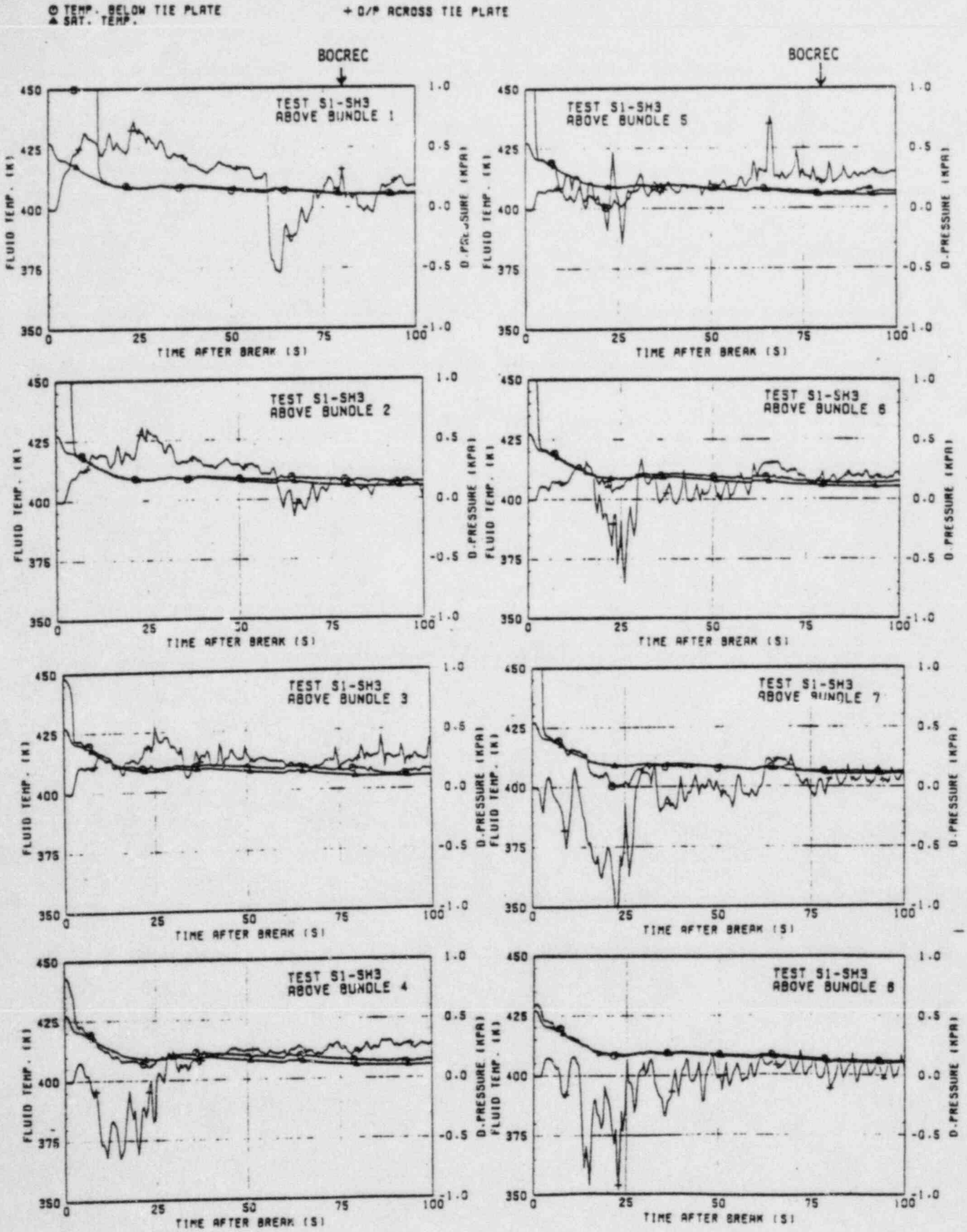

Fig. 3-9 Comparisons of fluid temperatures just below end box tie plate and differential pressures across end box tie plate over 8 bundles in Test S1-SH3

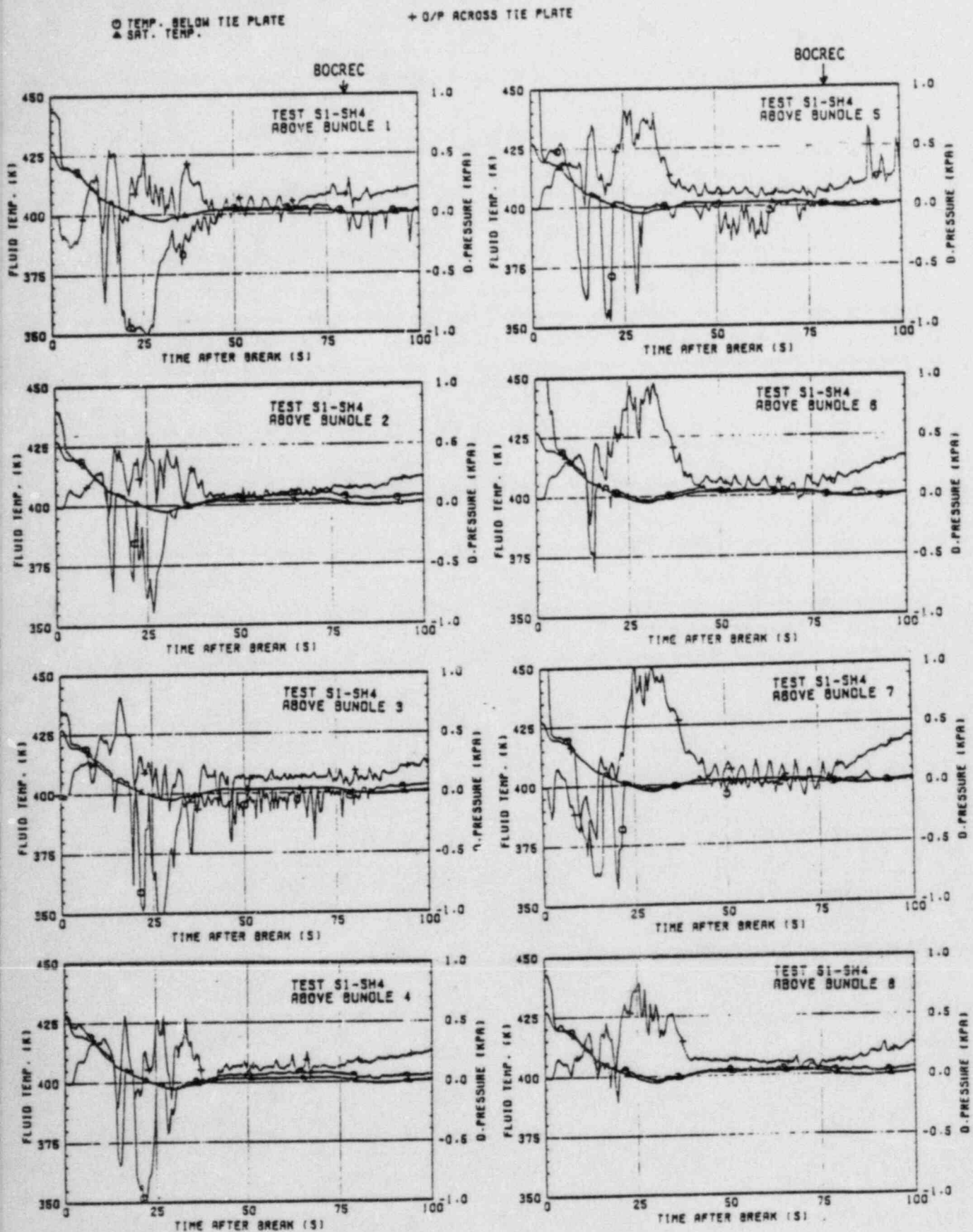

Fig. 3-10 Comparisons of fluid temperatures just below end box tie plate and differential pressures across end box tie plate over 8 bundles in Test S1-SH4

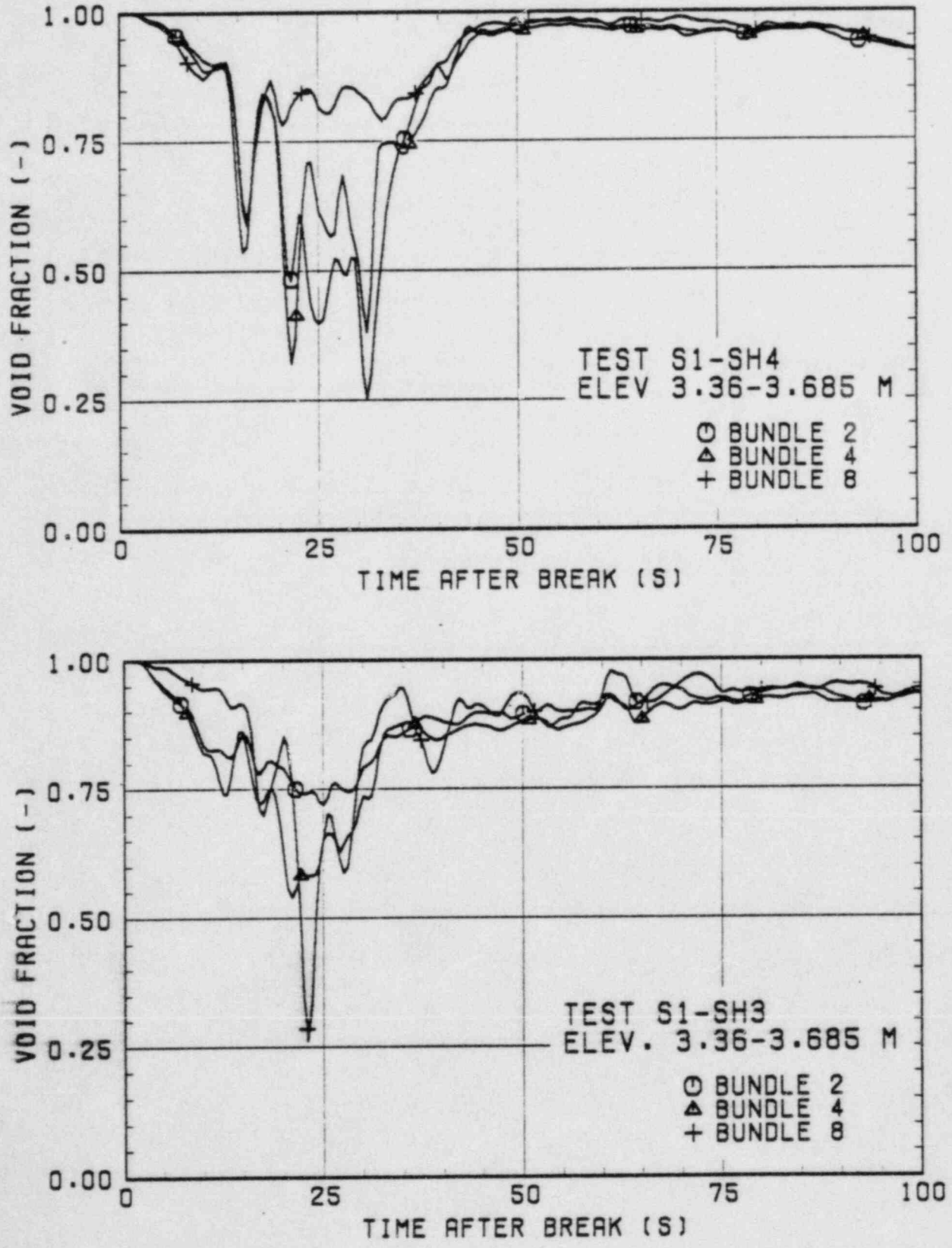

Fig. 3-11 Void fractions in Bundles 2, 4 and 8 at upper part of core

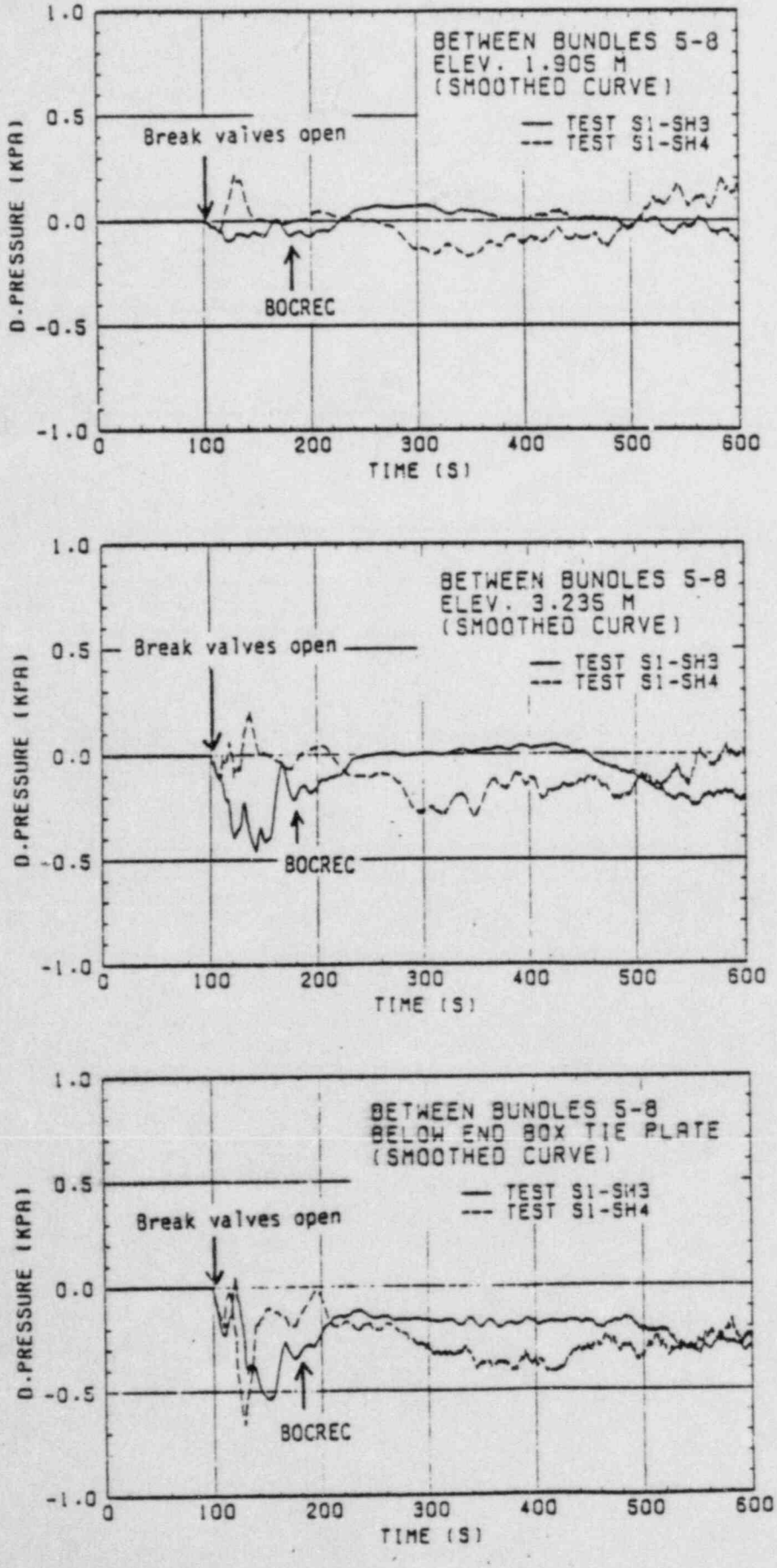

Fig. 3-12 Horizontal differential pressures between Bundles 5 and 8

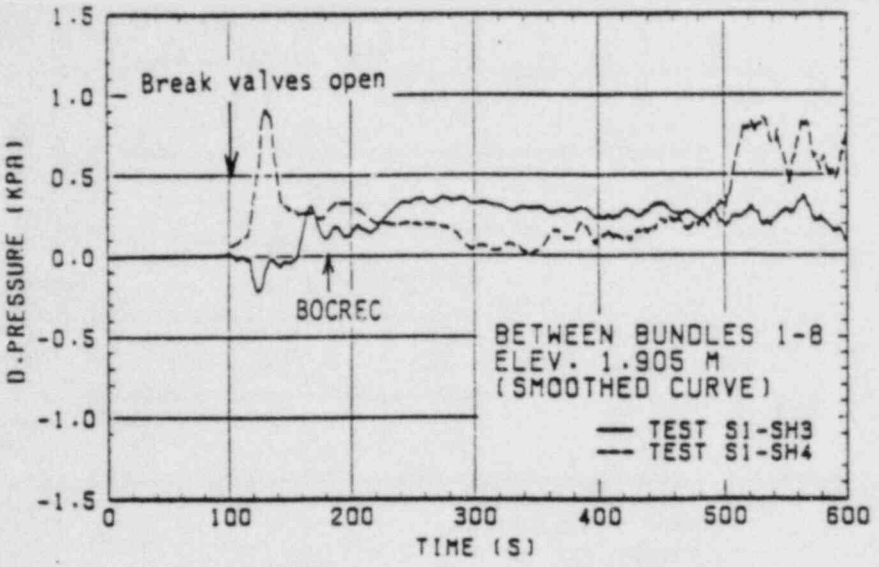

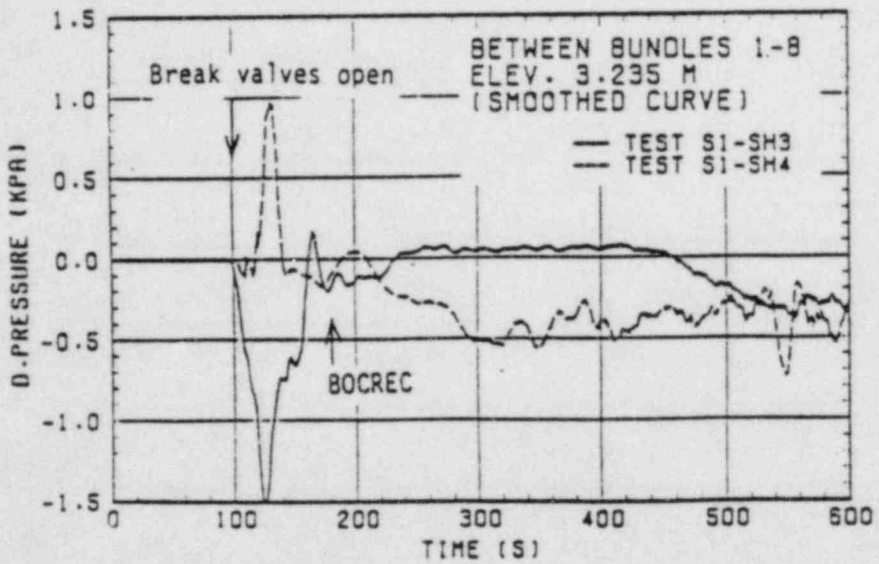

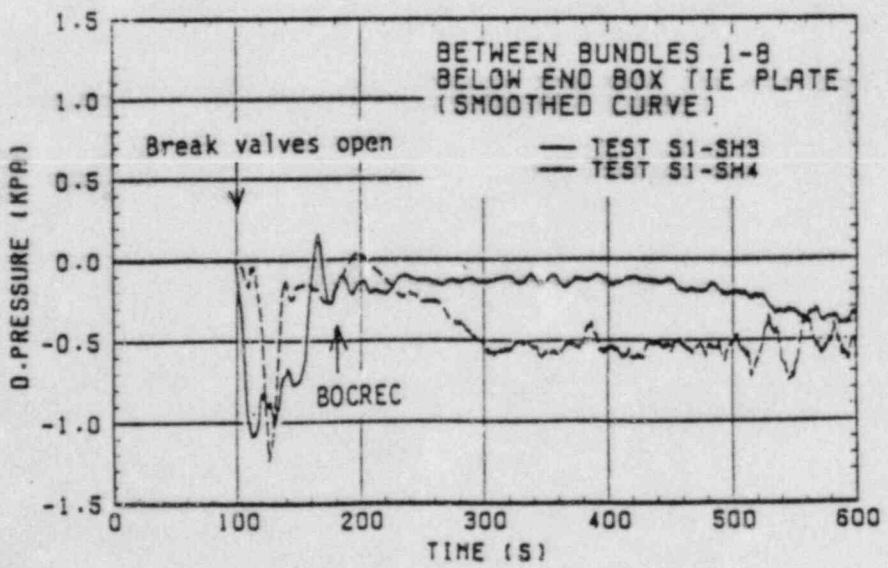

Fig. 3-13 Horizontal differential pressures between Bundles 1 and 8

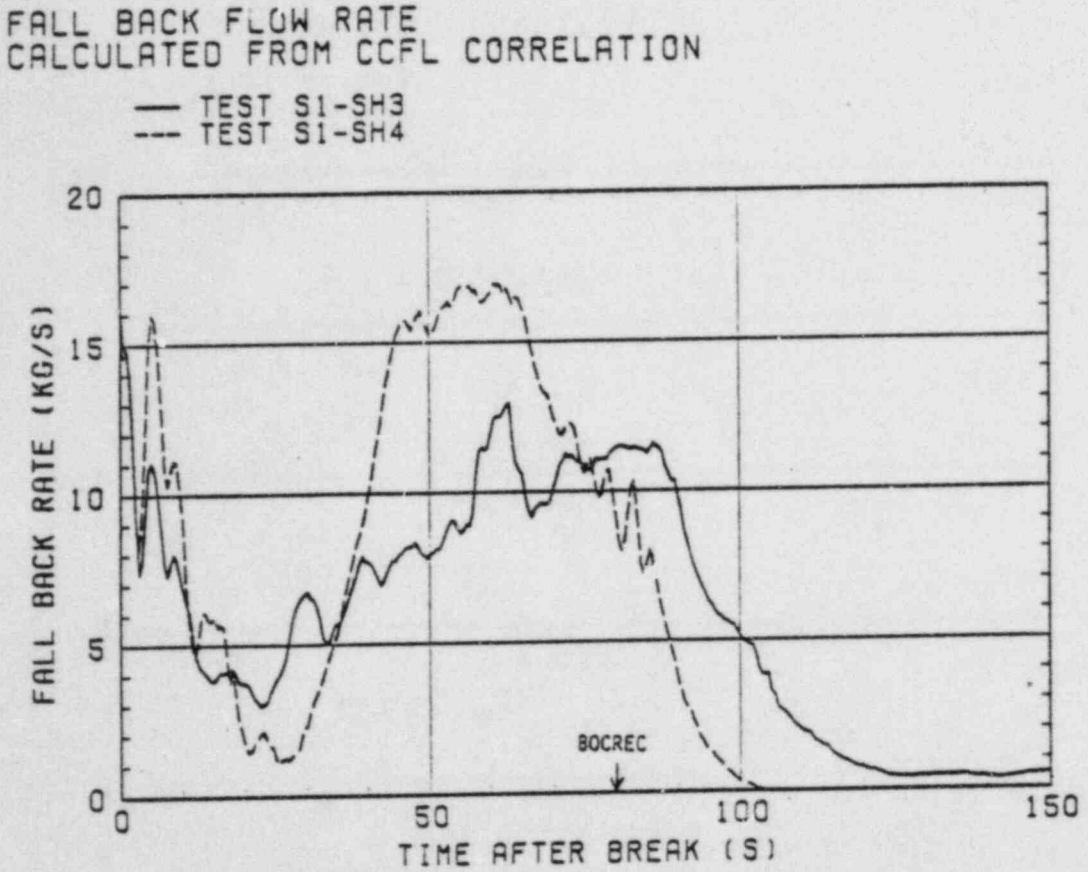

Fig. 3-14 Estimated fall back mass flow rates with CCFL correlation

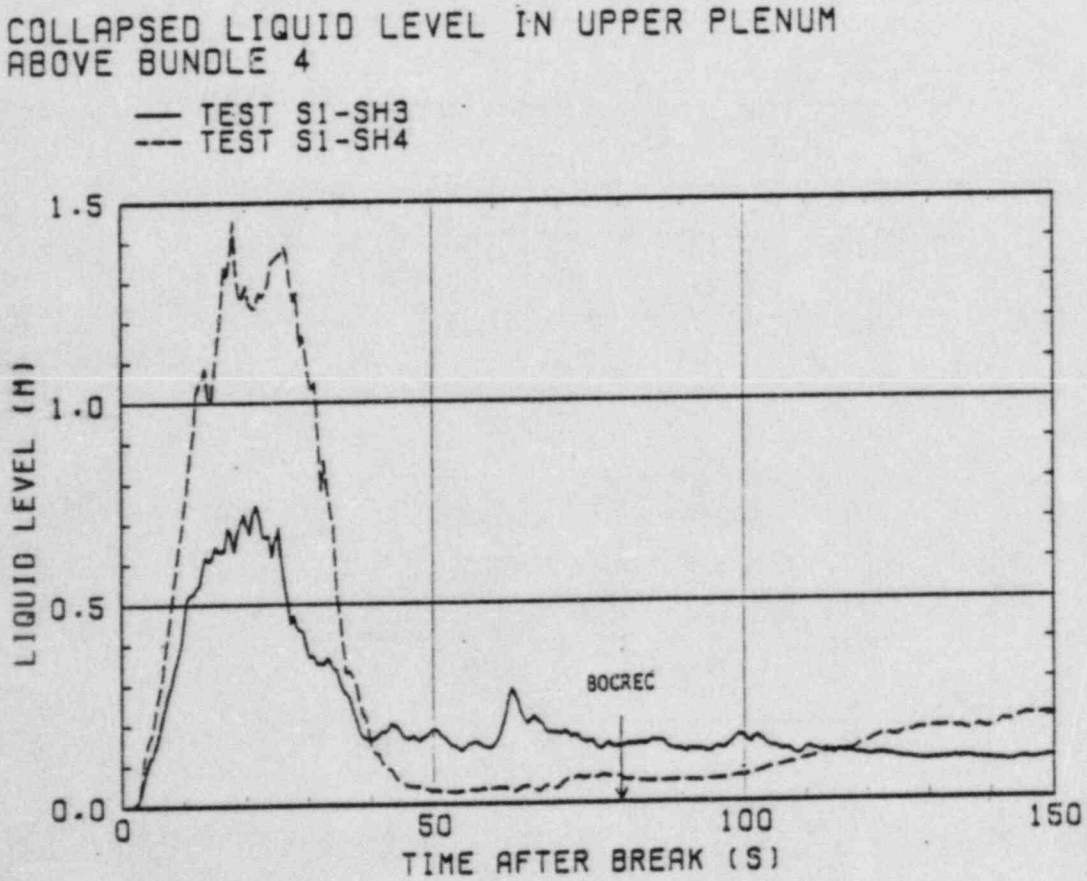

Fig. 3-15 Liquid levels in upper plenum

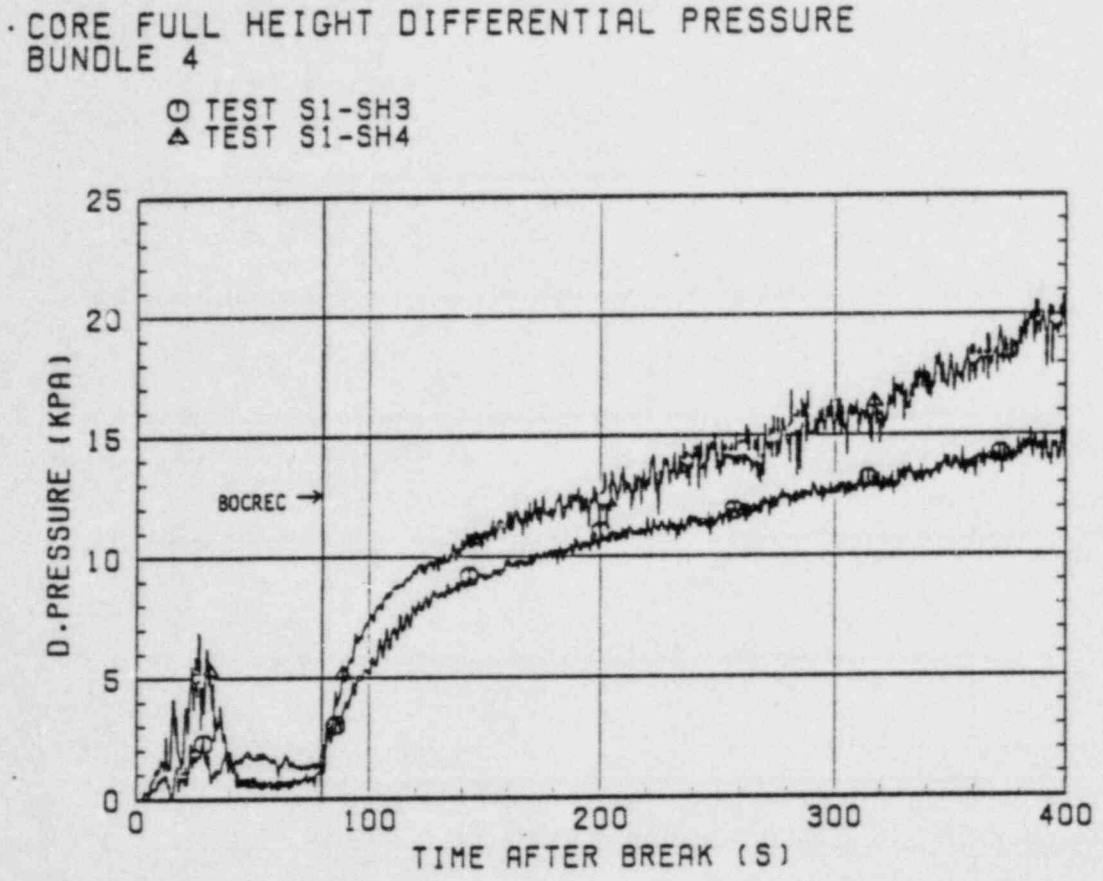

Fig. 3-16 Vertical differential pressures across core full height

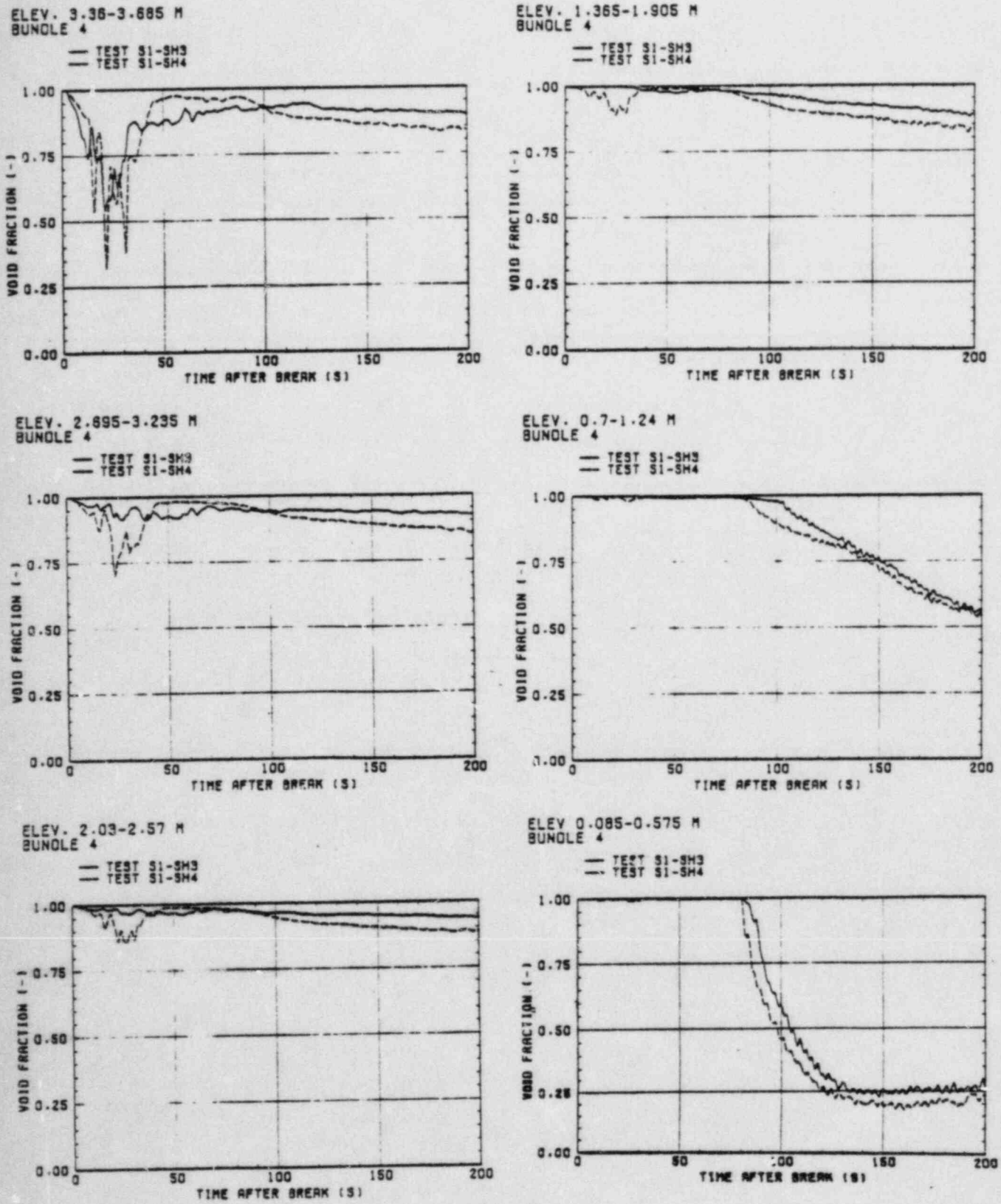

Fig. 3-17 Void fractions in core at six elevations

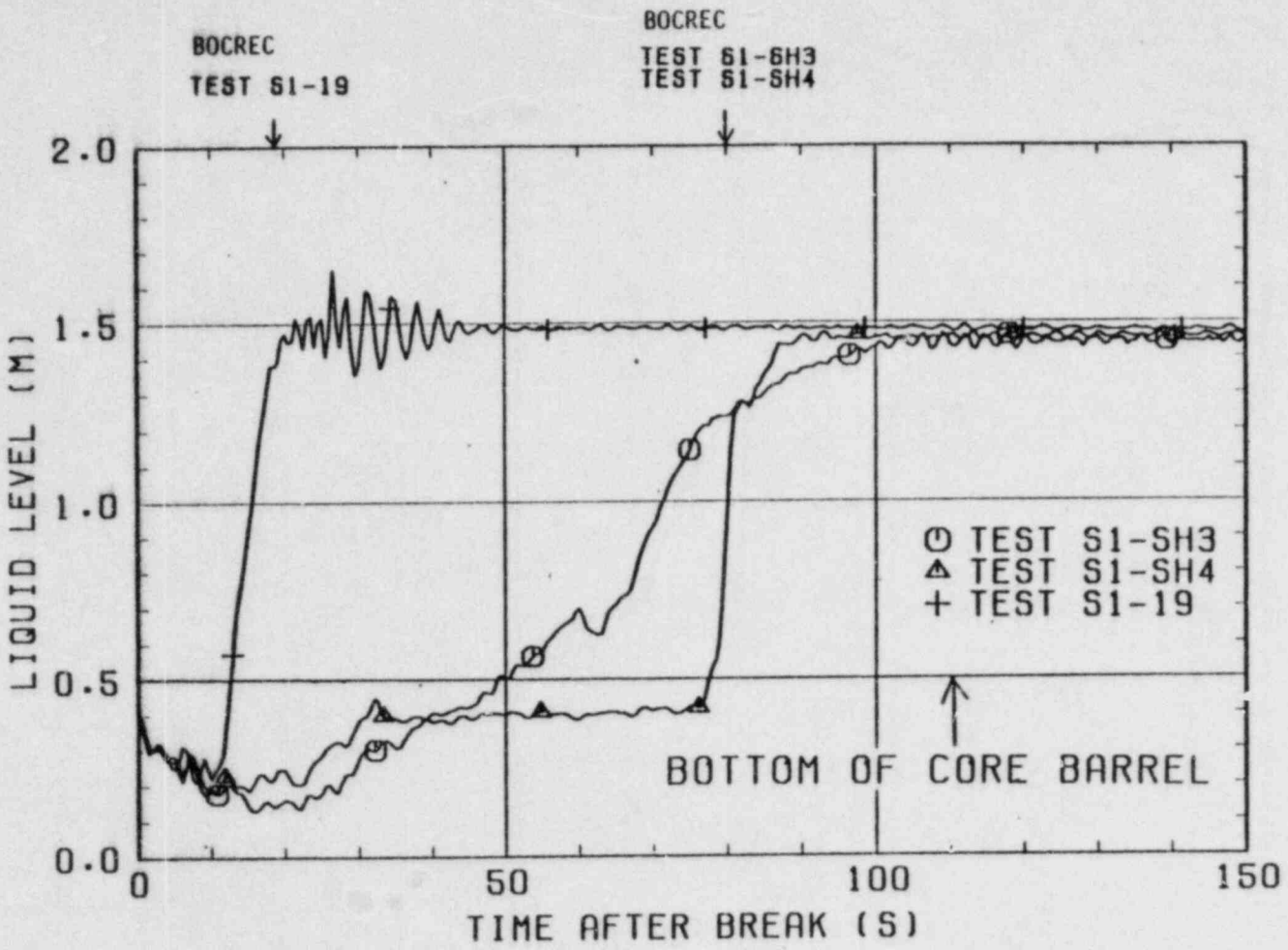

Fig. 3-18 Liquid levels in lower plenum

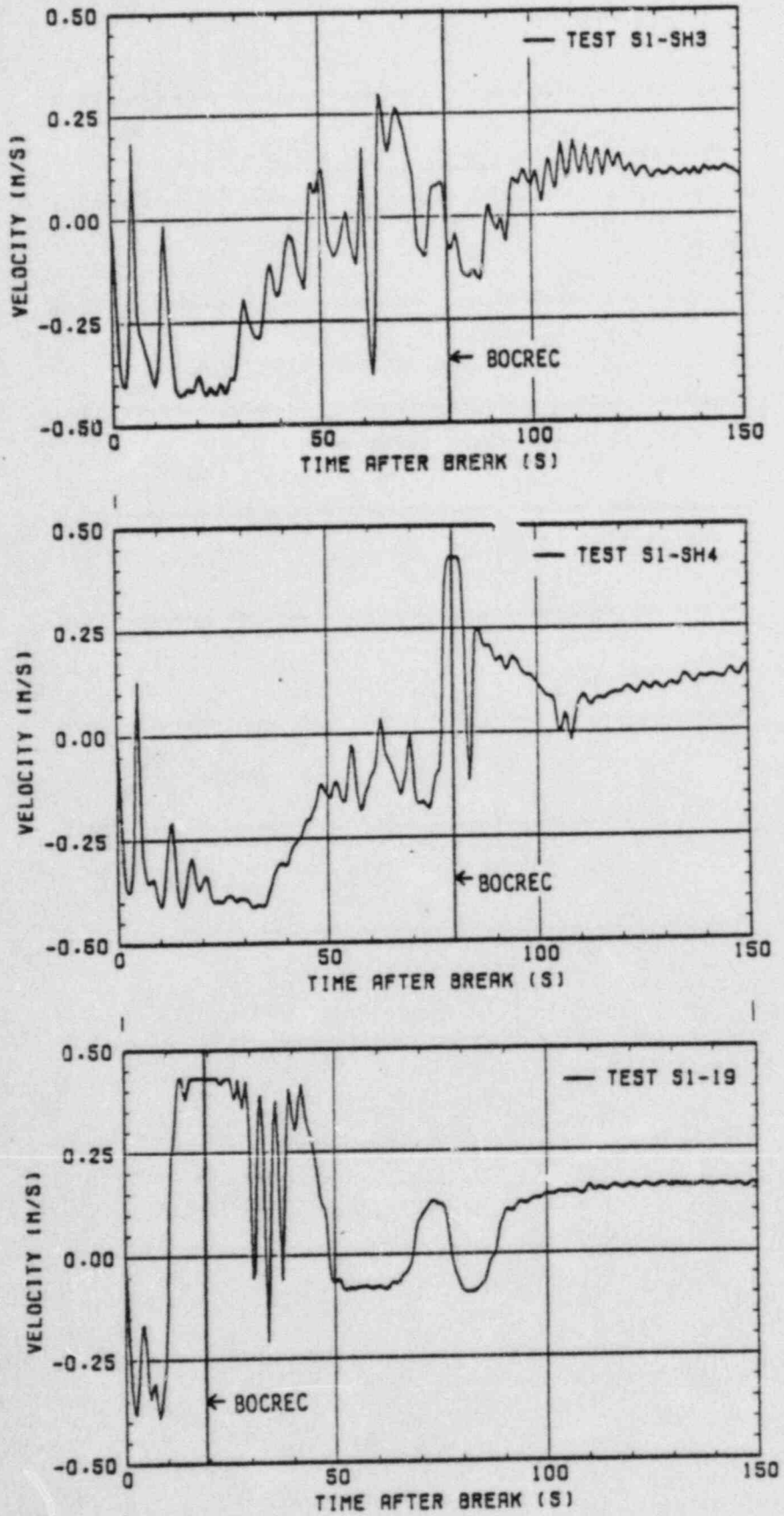

Fig. 3-19 Fluid velocities below core barrel

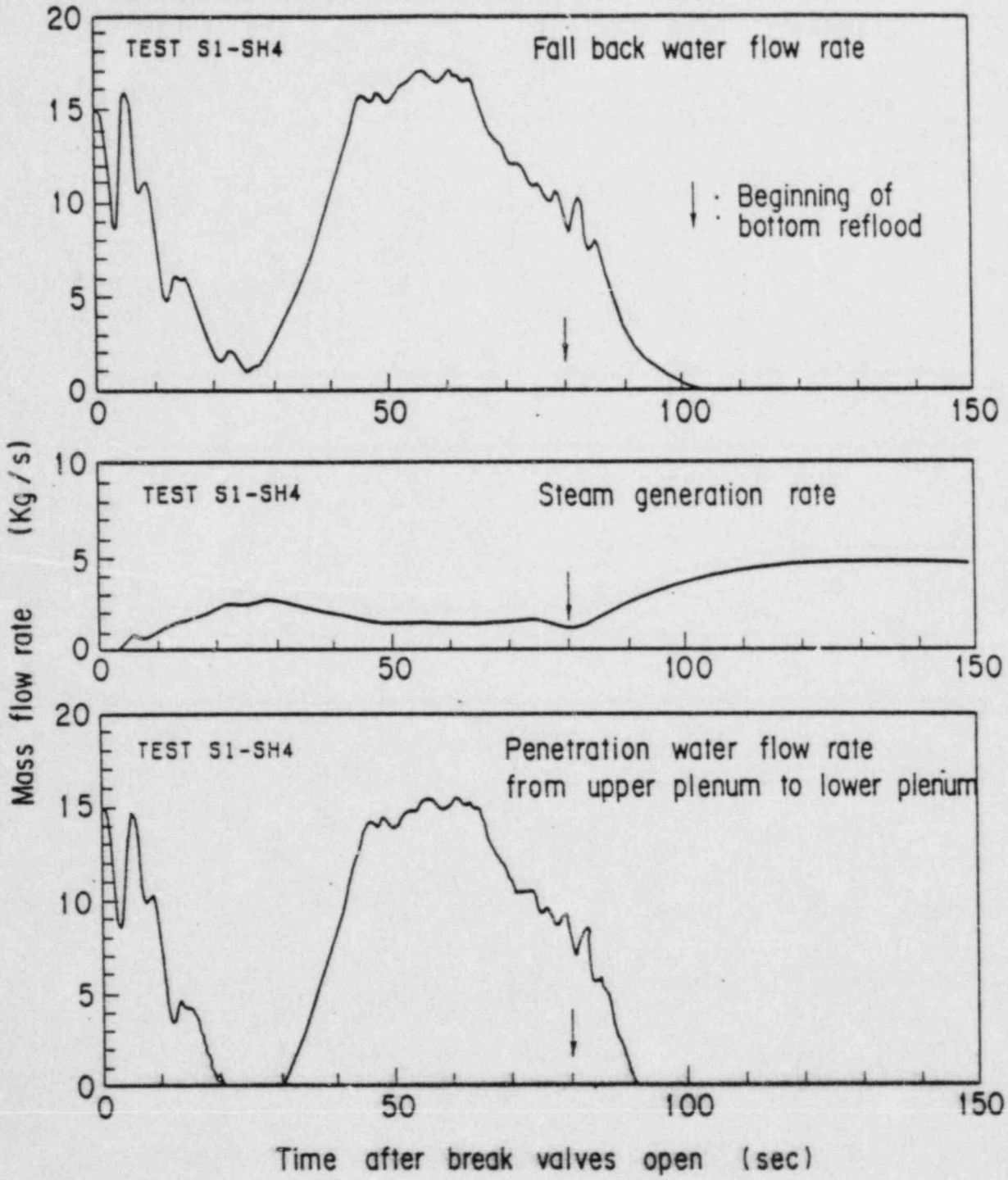

Fig. 3-20 Estimated penetration water flow rate from upper plenum to lower plenum in Test S1-SH4

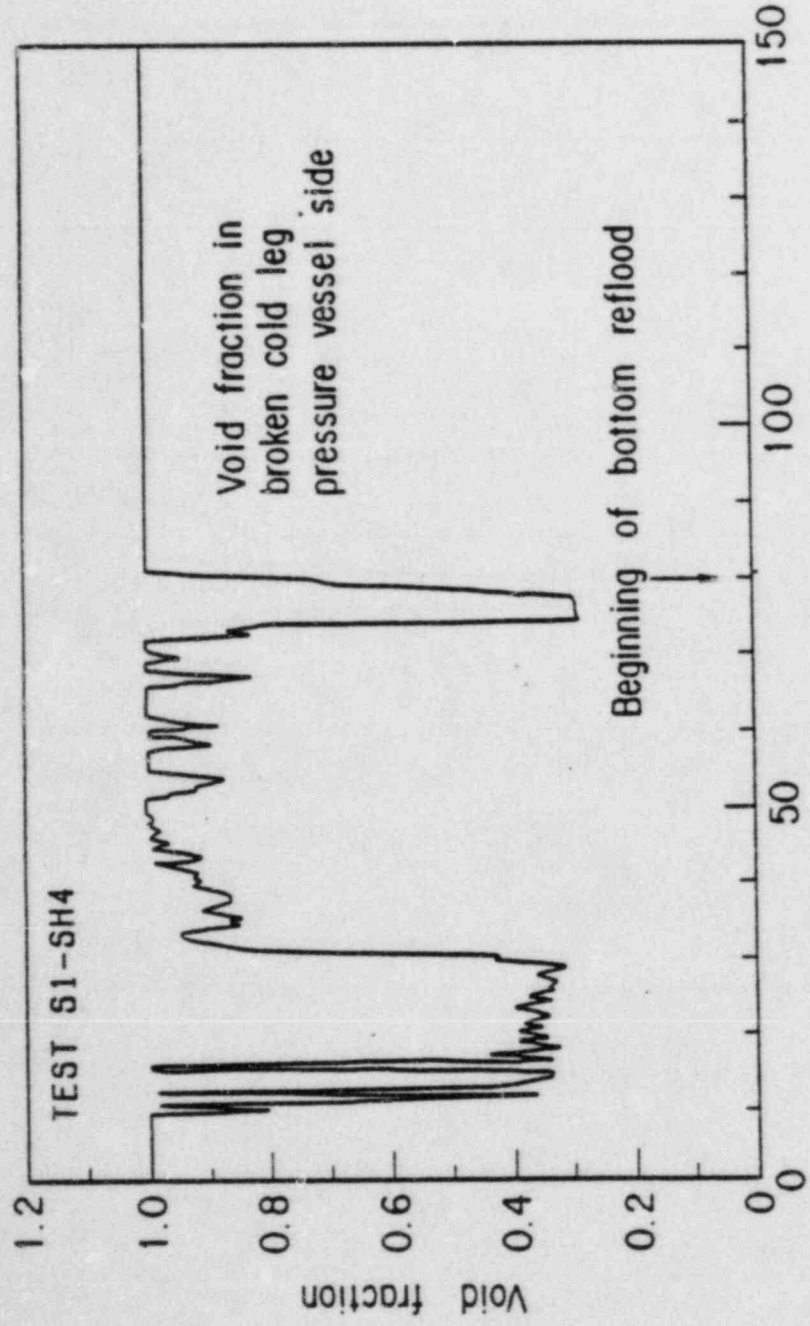

Fig. 3-21 Void fraction in broken cold leg pressure vessel side in Test S1-SH4

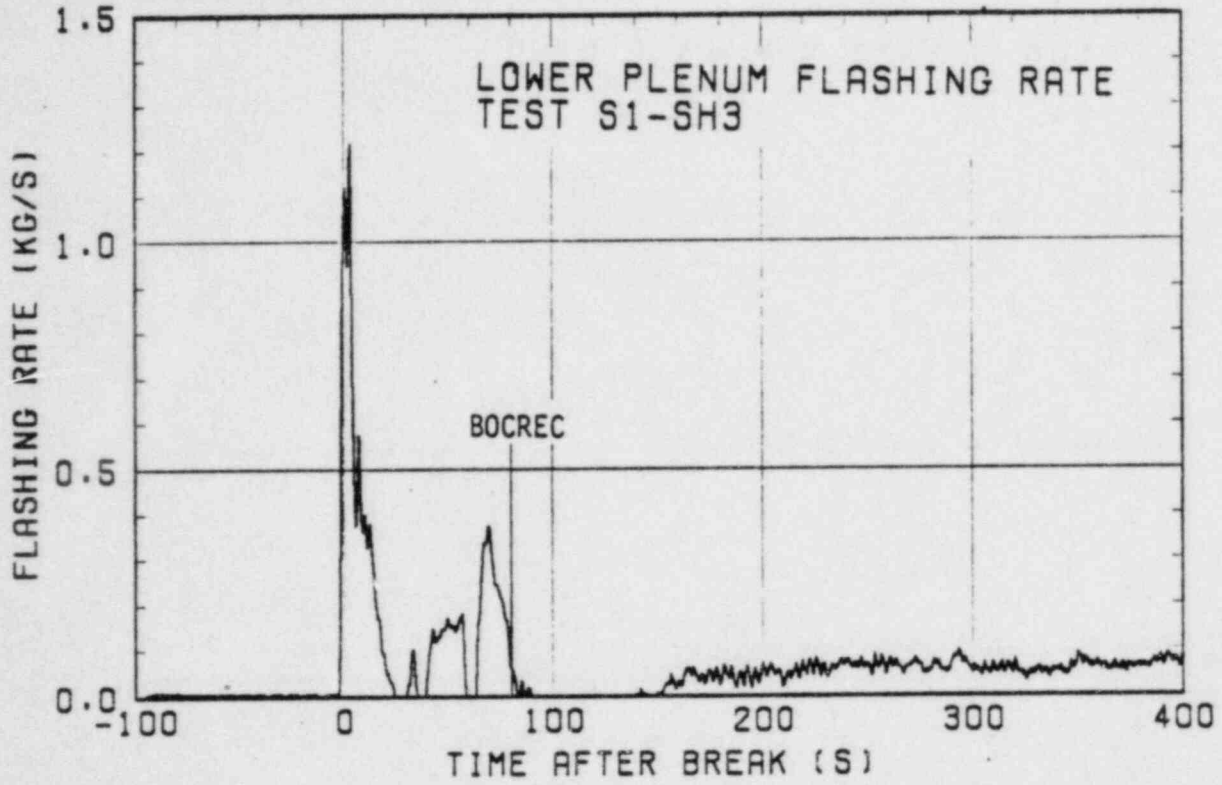

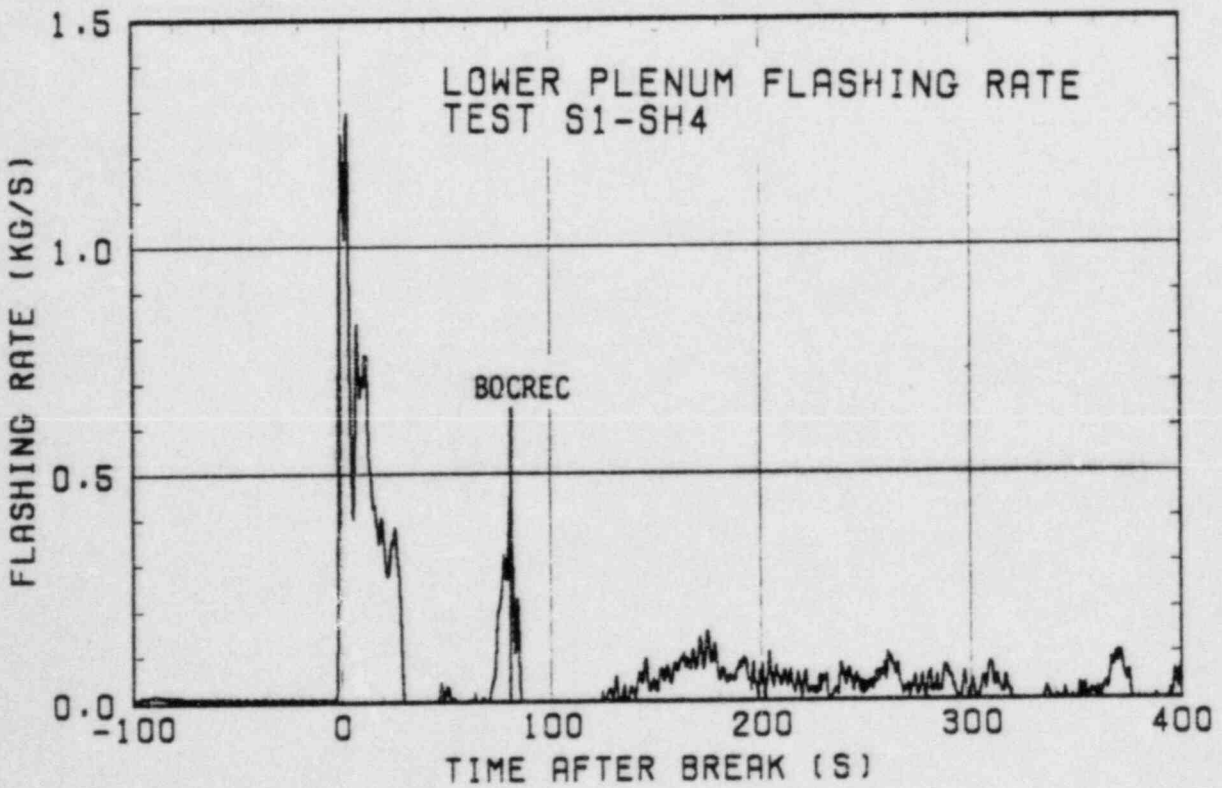

Fig. 3-22 Flashing rates in lower plenum

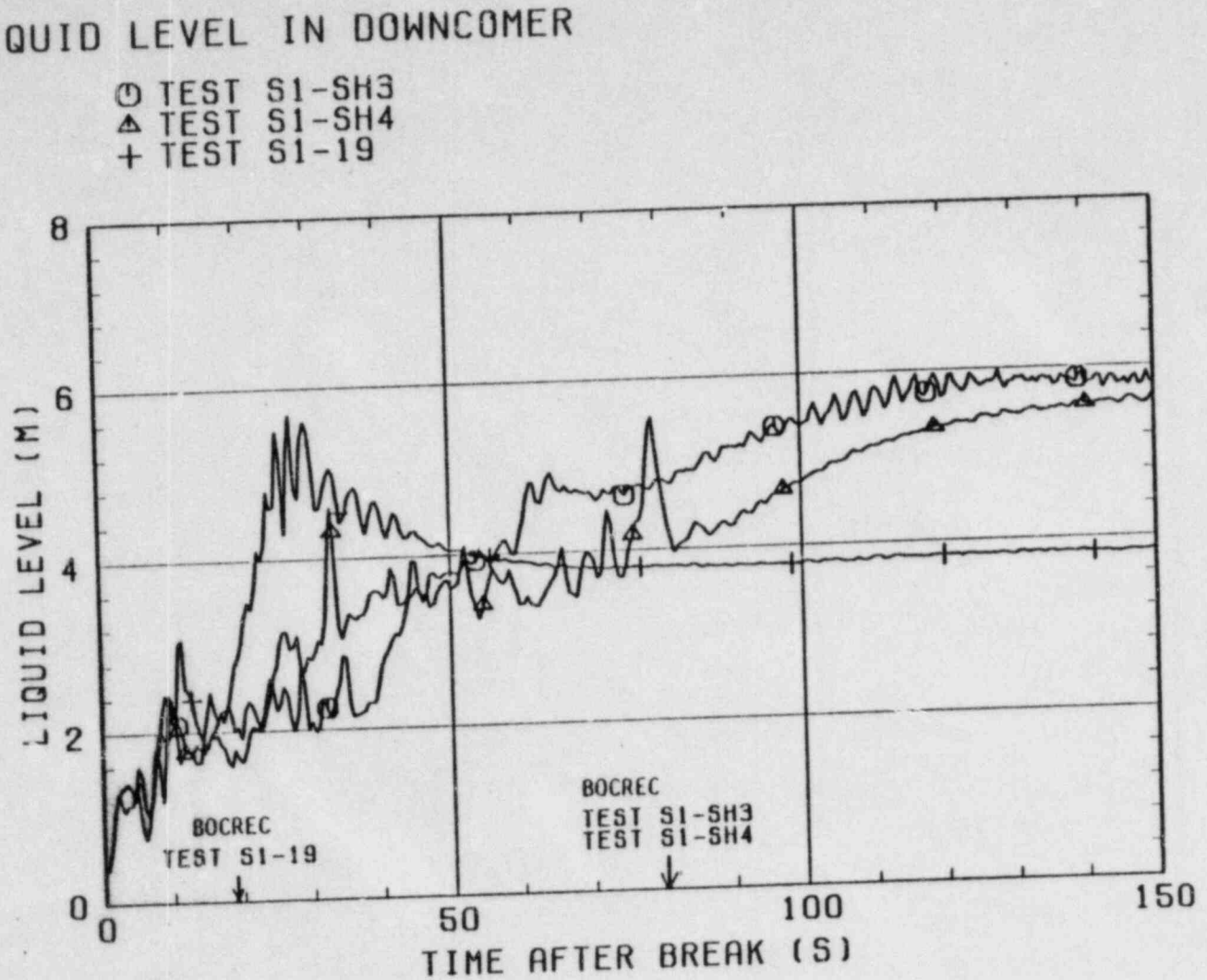

Fig. 3-23 Liquid levels in downcomer

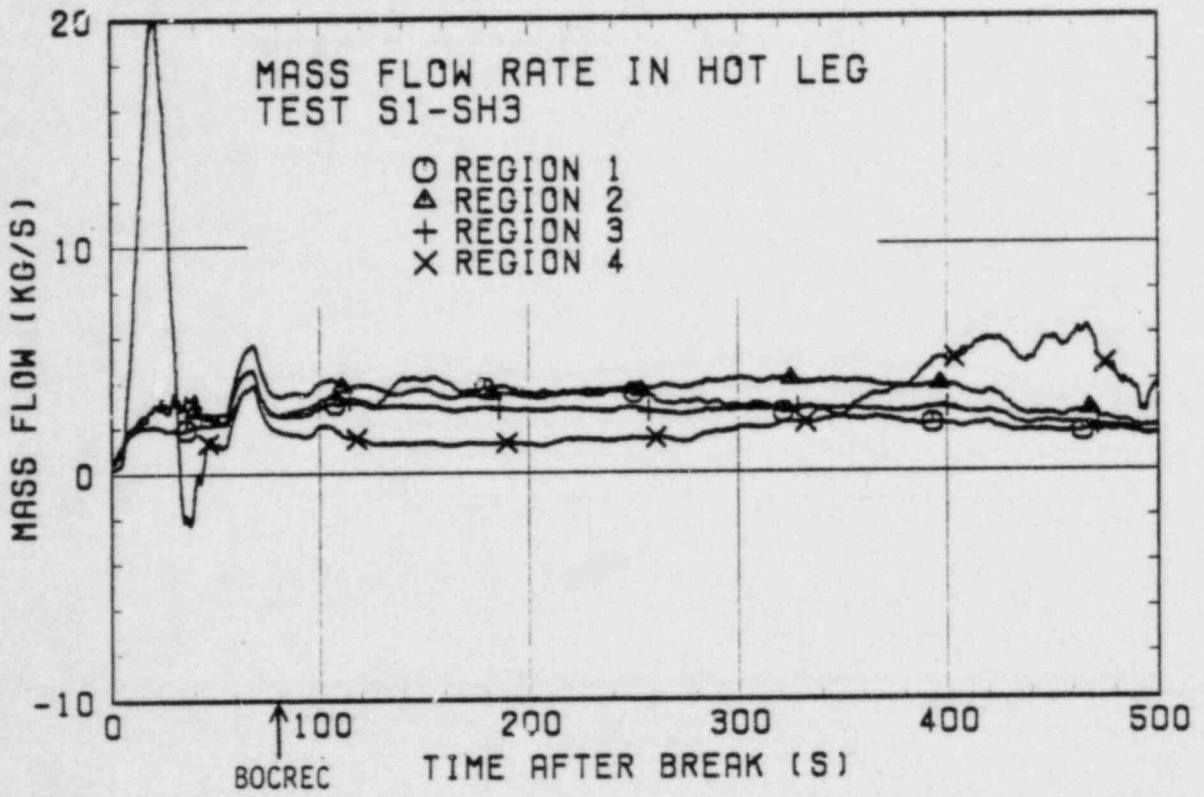

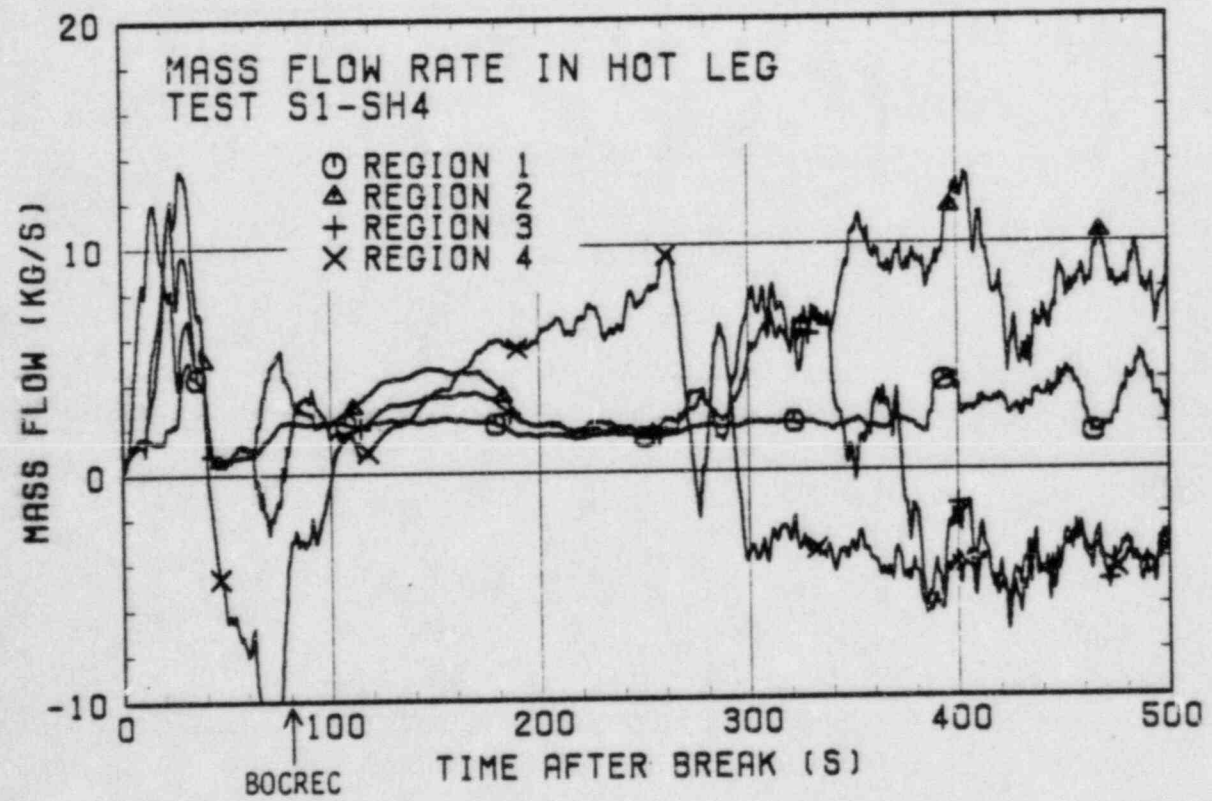

Fig. 3-24 Mass flow rates in four regions of hot leg

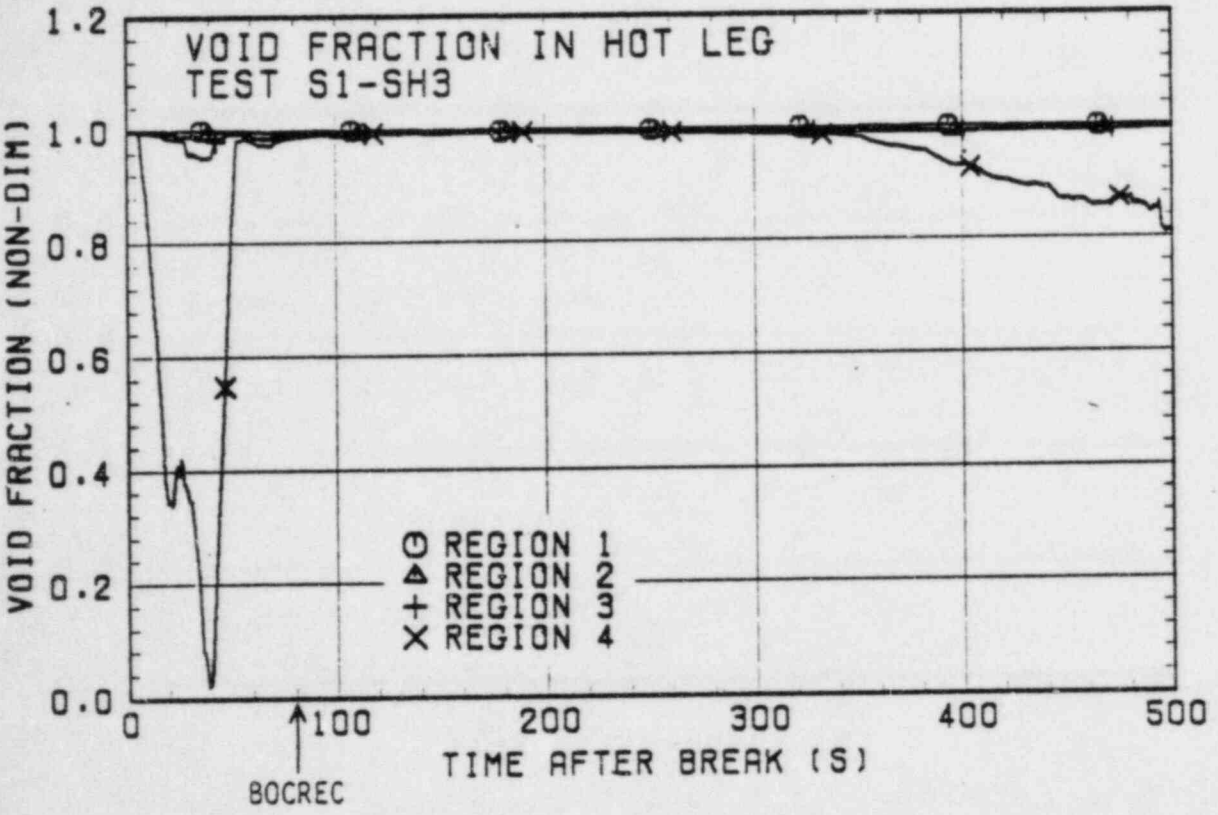

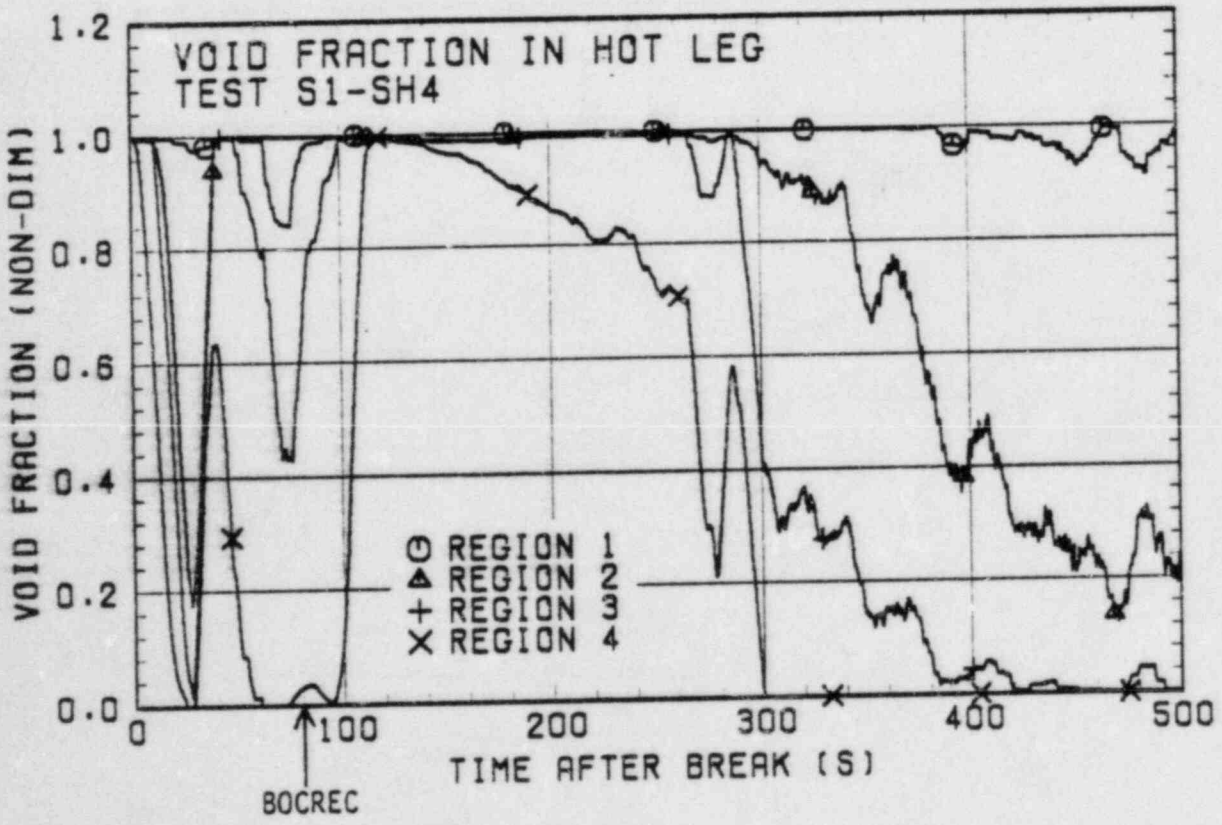

Fig. 3-25 Void fractions in four regions of hot leg

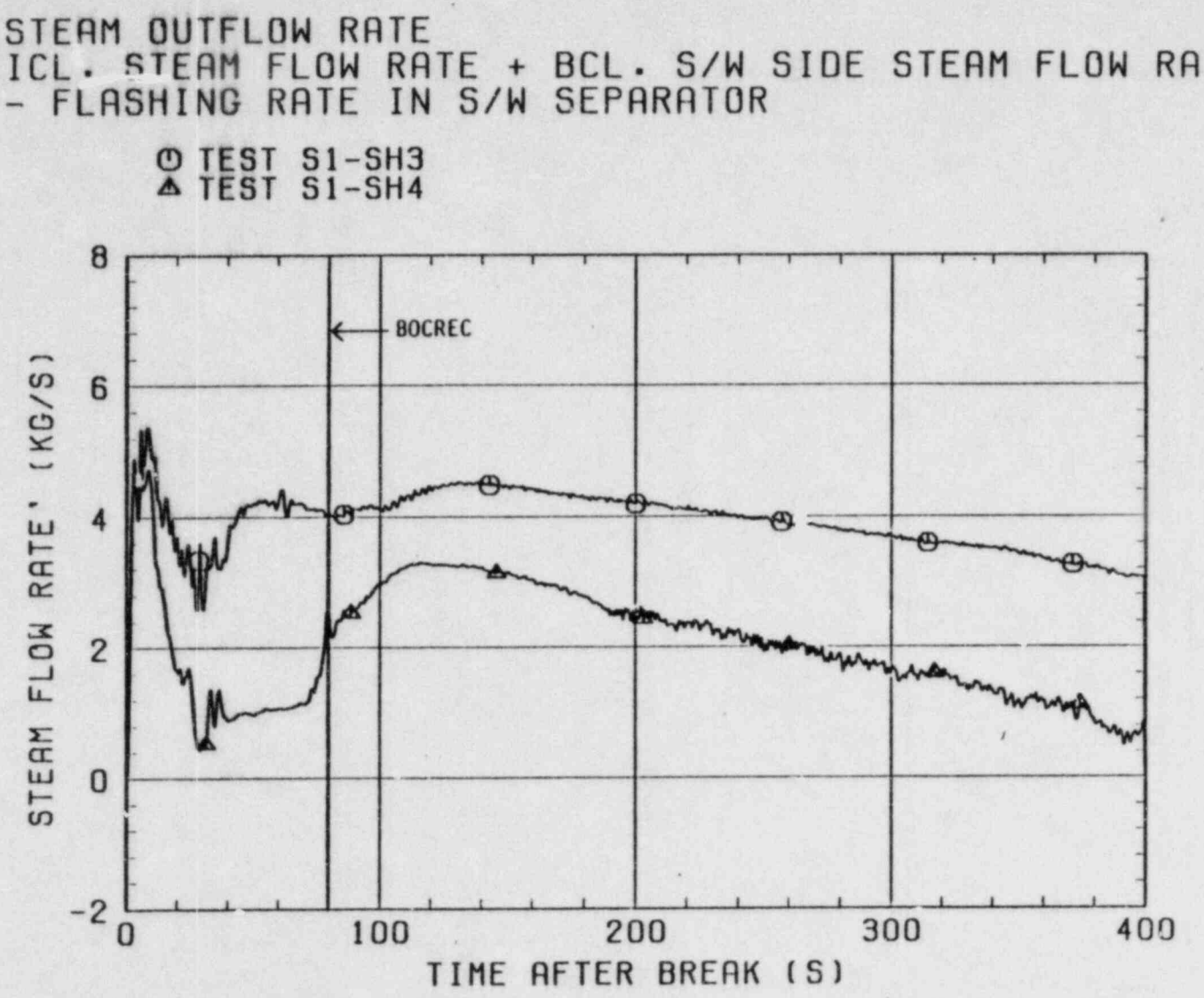

Fig. 3-26 Steam outflow rate through hot leg

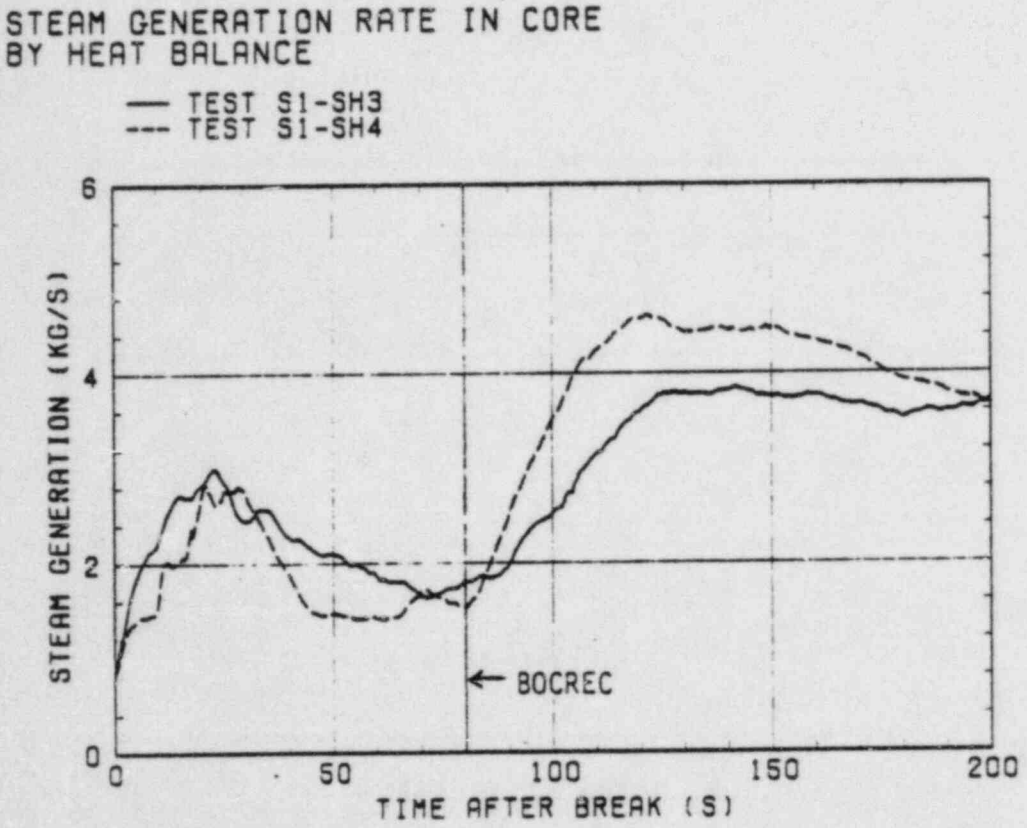

Fig. 3-27 Steam generation rates obtained from heat balance calculation

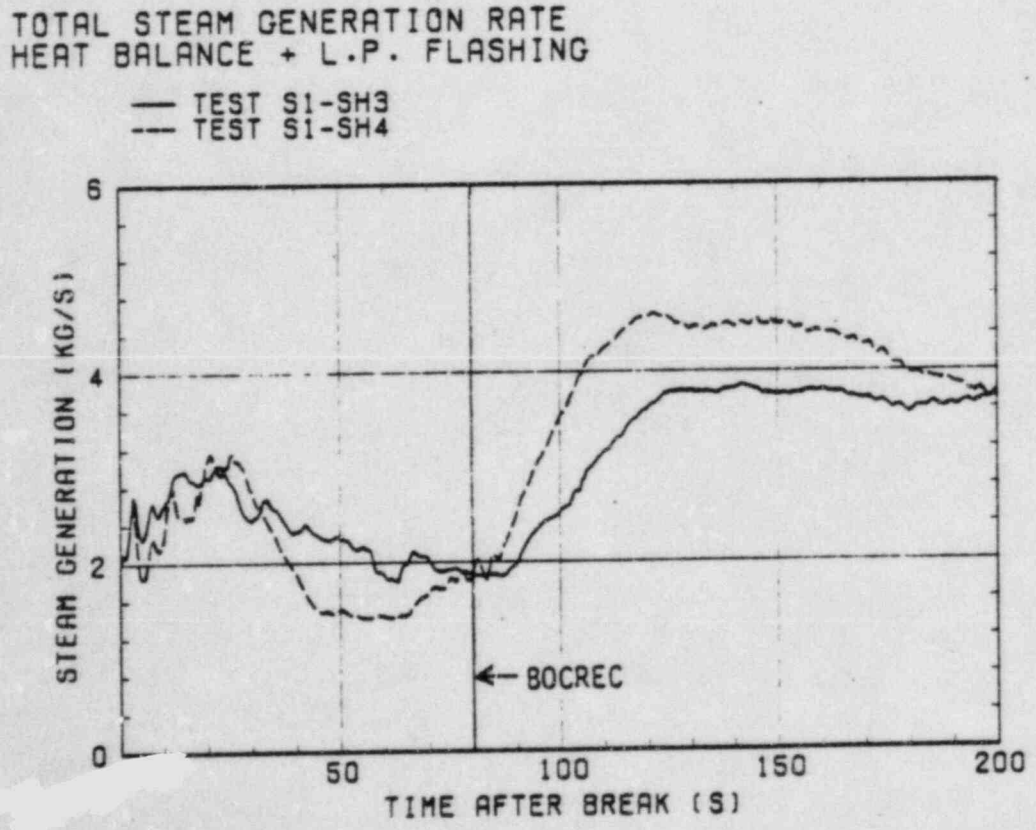

Fig. 3-28 Total steam generation rates obtained from heat balance and lower plenum flashing

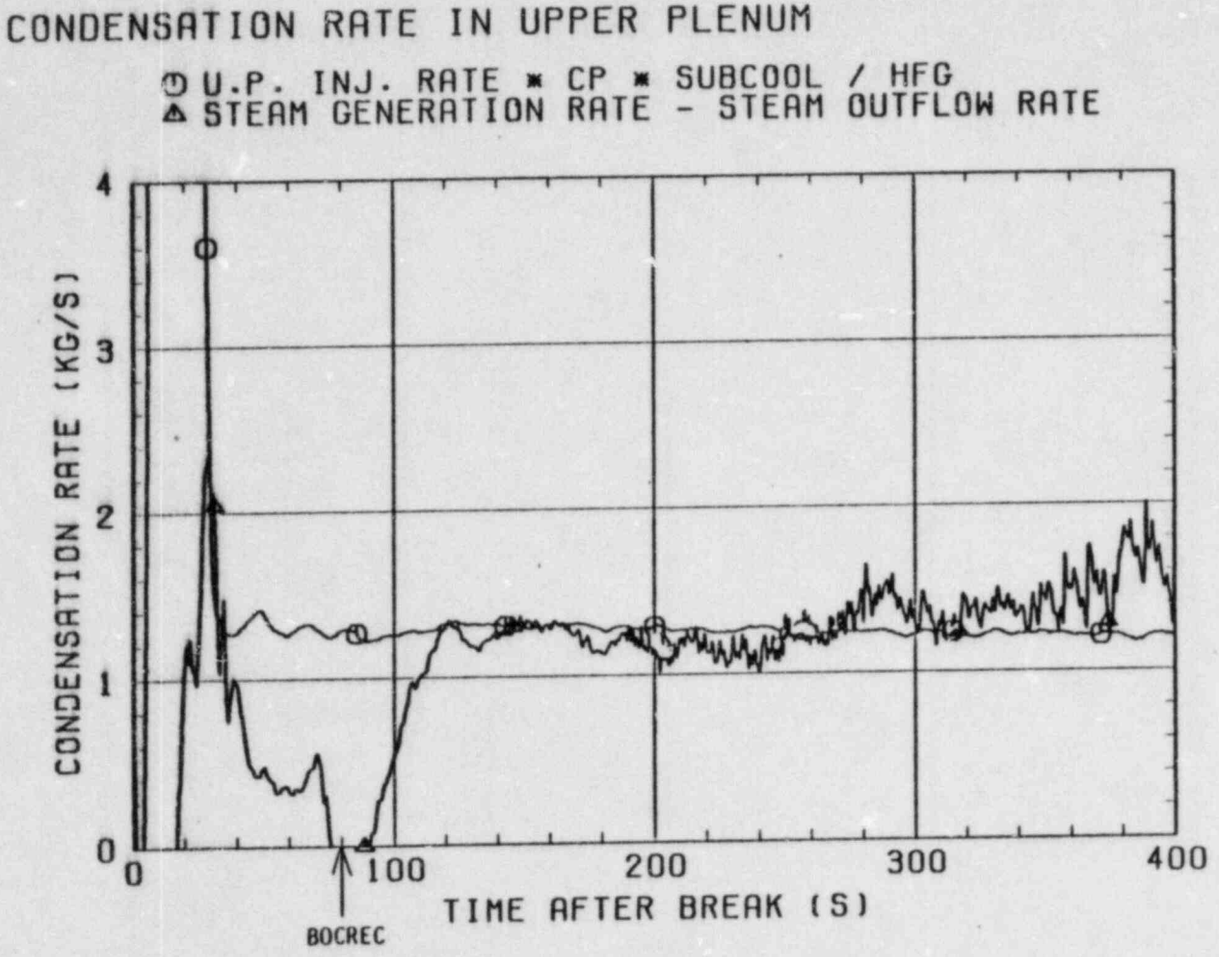

Fig. 3-29 Steam condensation rate in upper plenum in Test S1-SH4

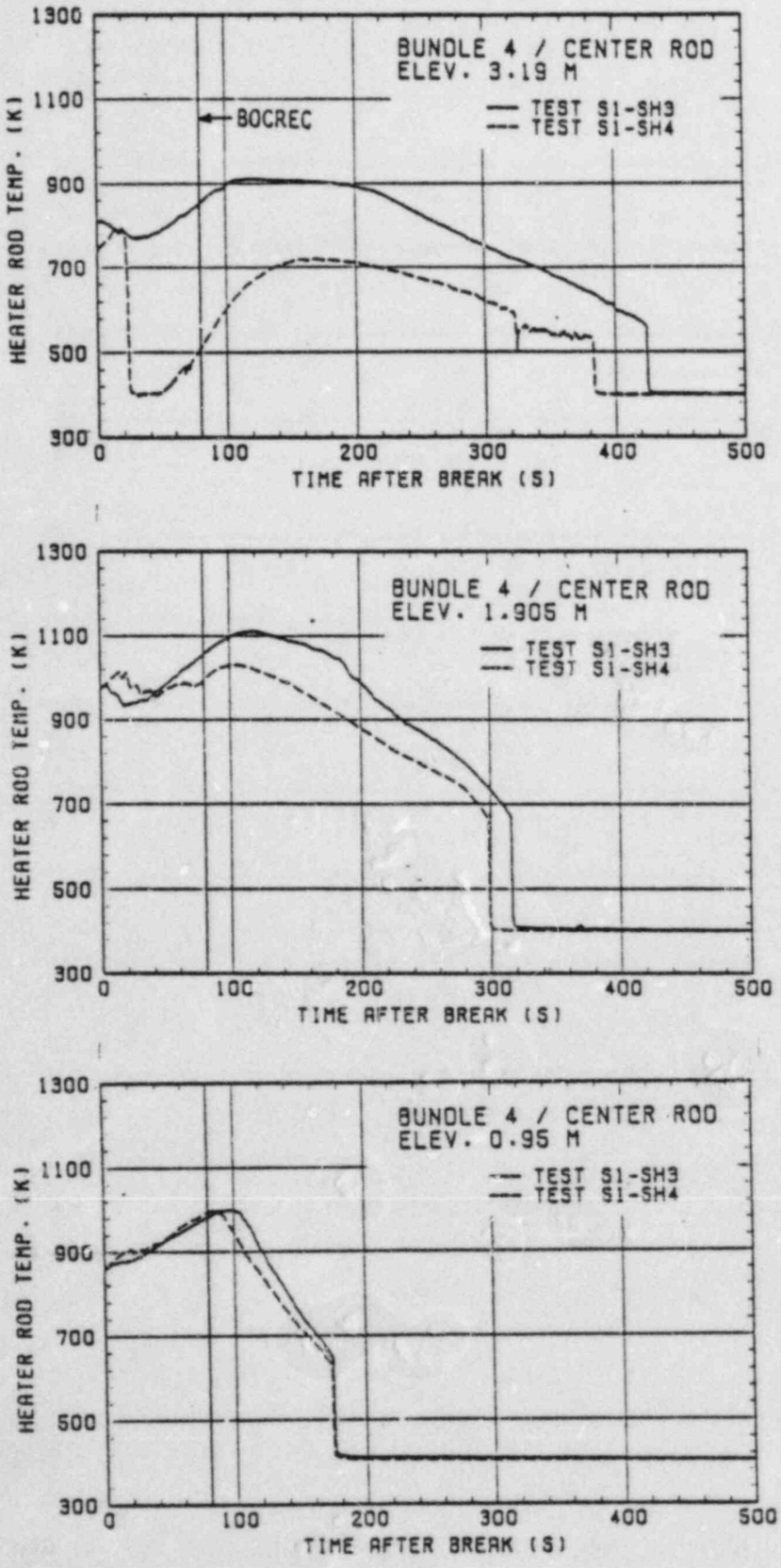

Fig. 3-30 Heater rod surface temperatures at elevations of 3.19, 1,905 and 0.95 m

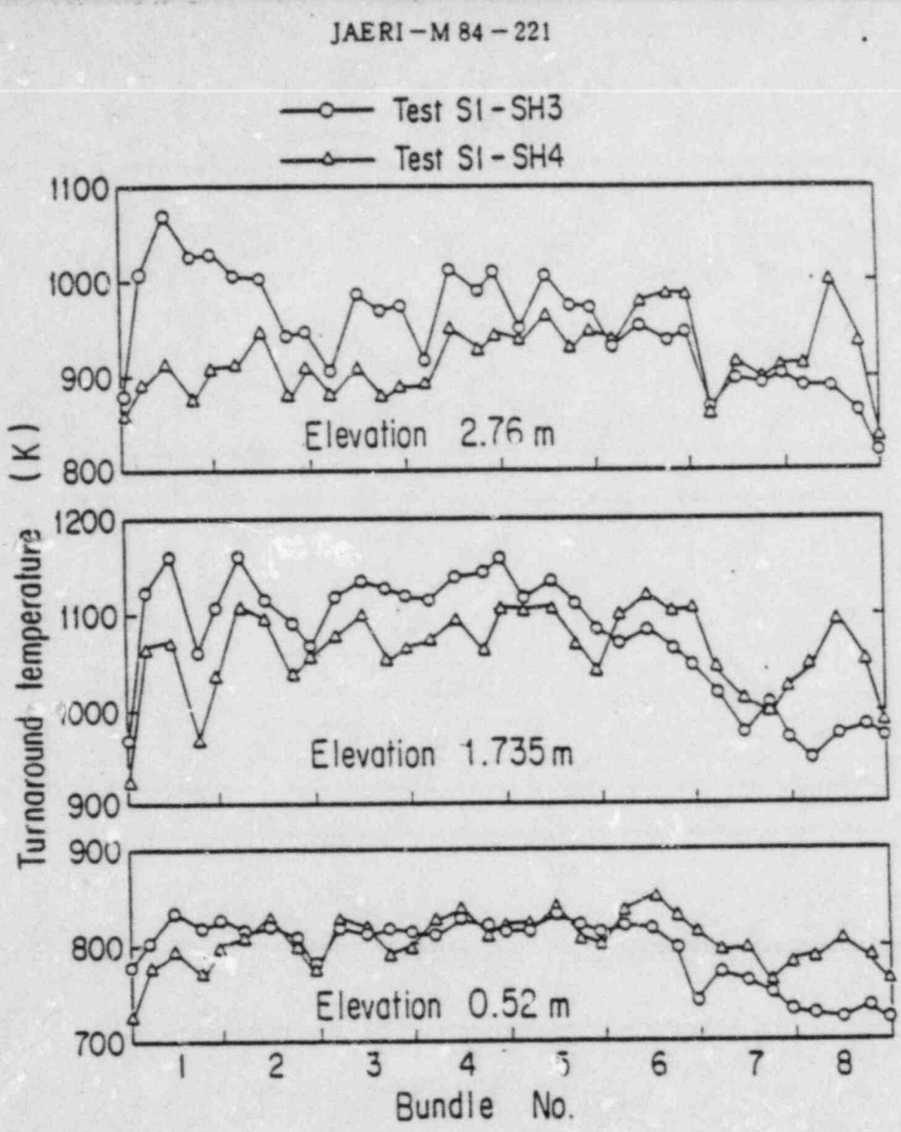

Fig. 3-31 Horizontal distributions of turnaround temperatures at elevations of 2.76, 1.735 and 0.52 m

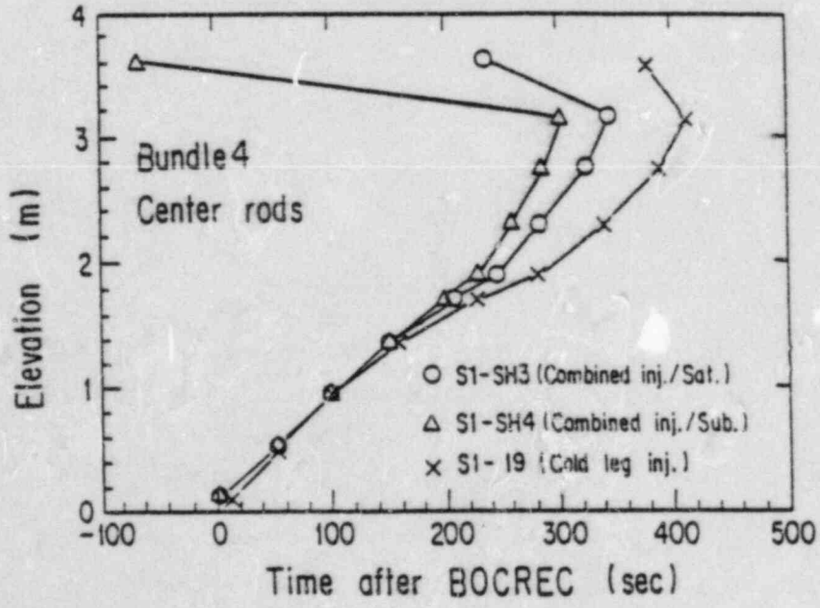

Fig. 3-32 Quench envelopes in Bundle 4

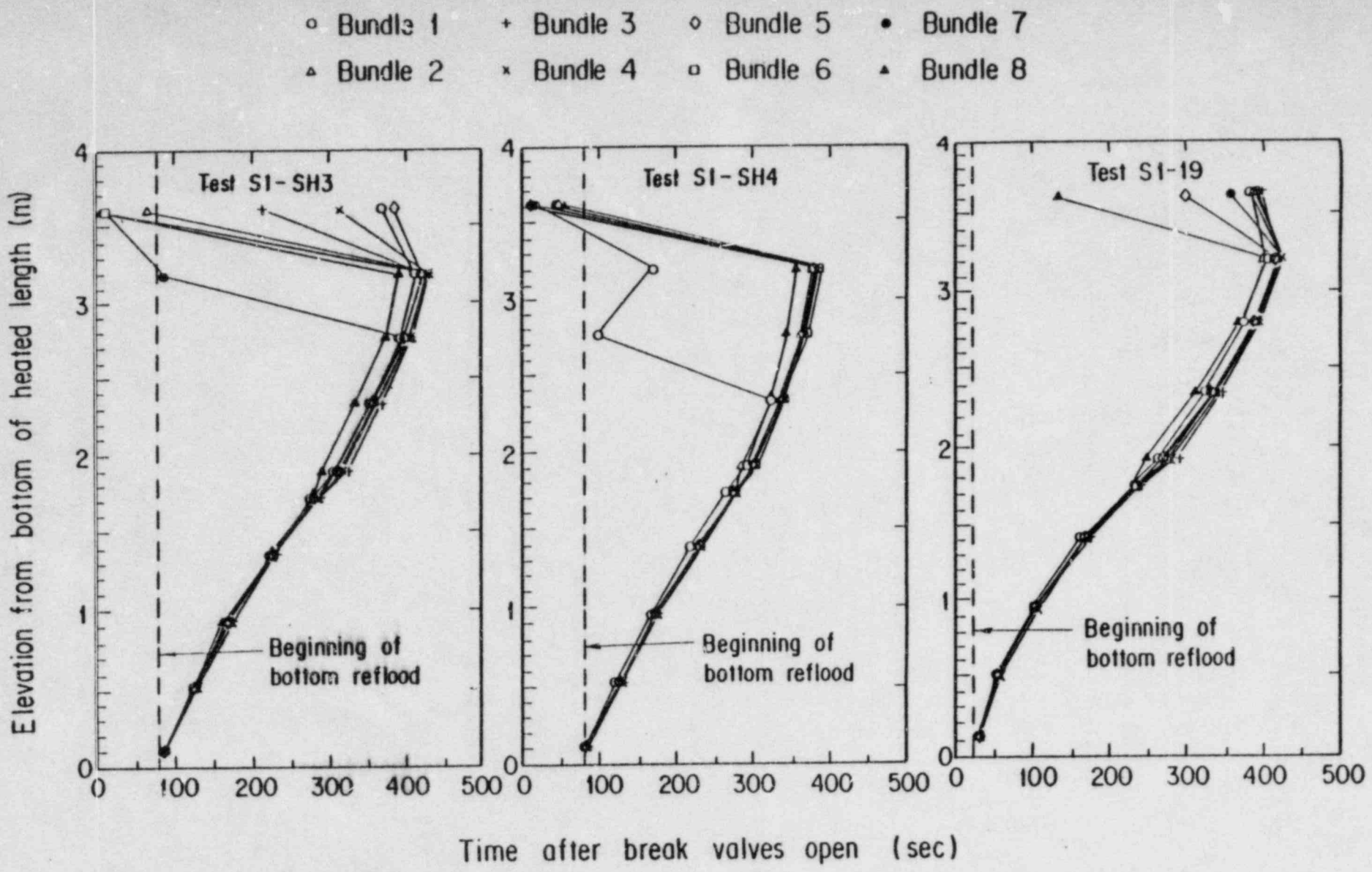

Fig. 3-33 Comparison of quench envelopes in all bundles

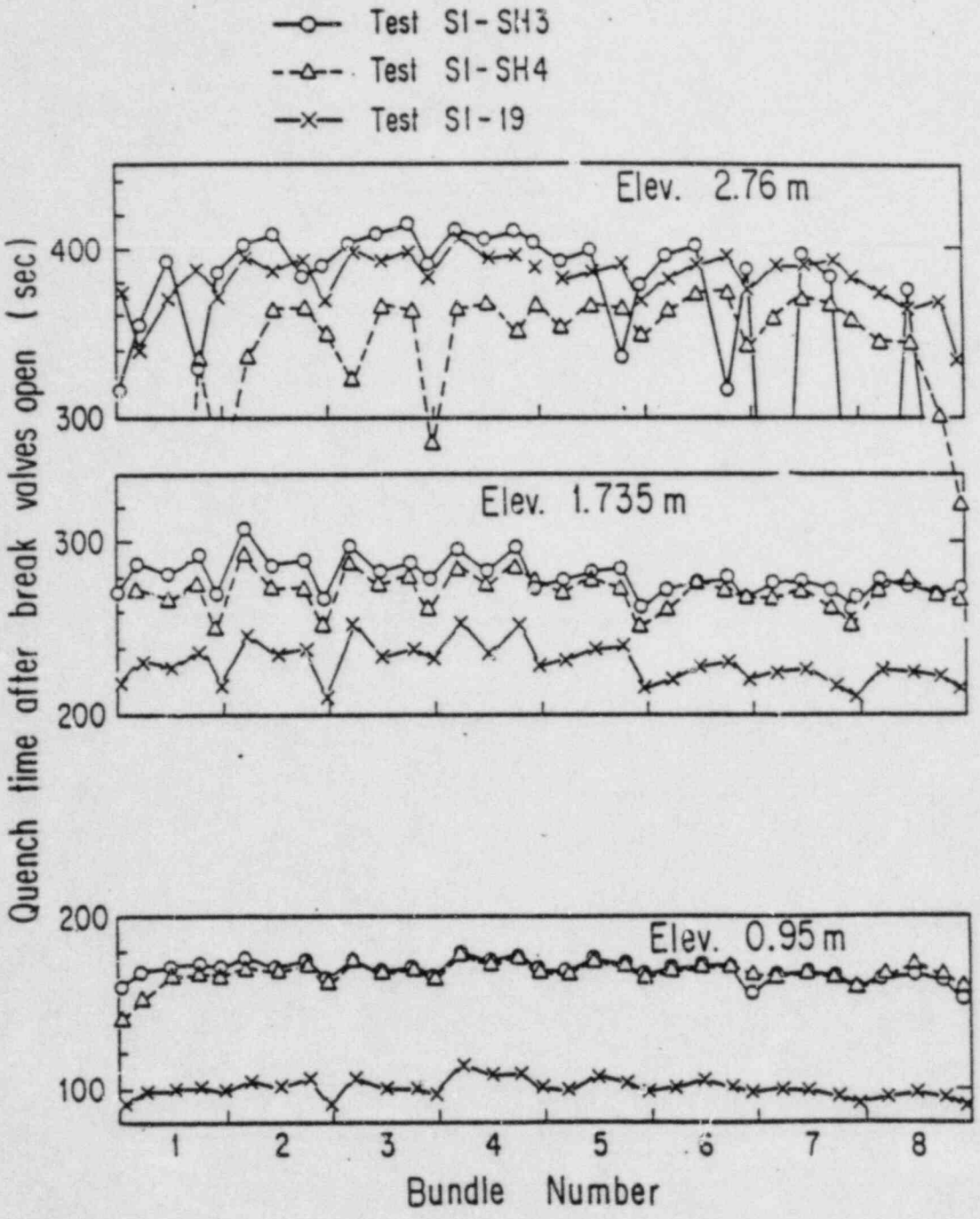

Fig. 3-34 Radial distributions of quench times at elevations of 2.76, 1.735 and 0.95 m

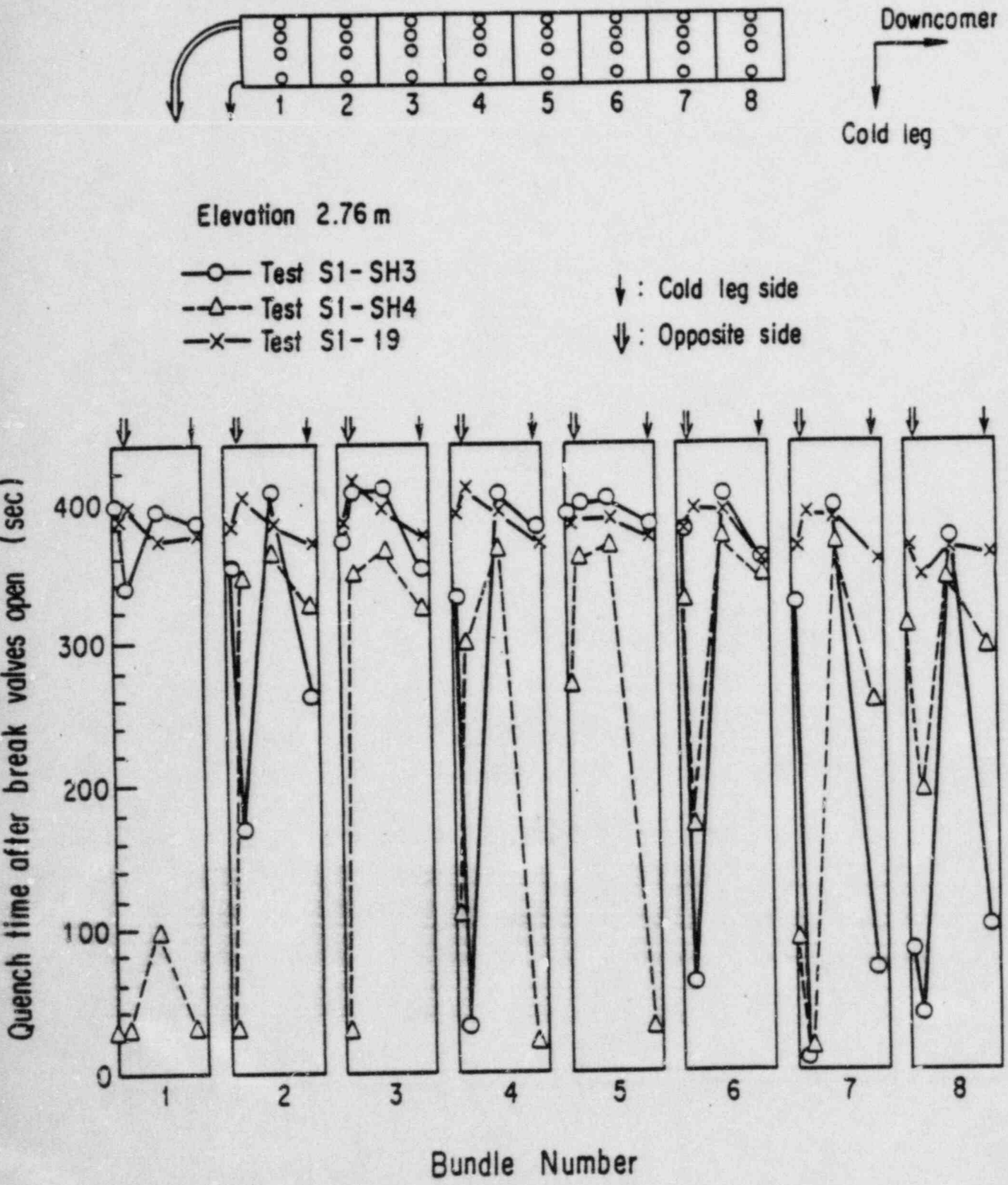

Fig. 3-35 Azimuthal distributions of quench times at elevation of 2.76 m

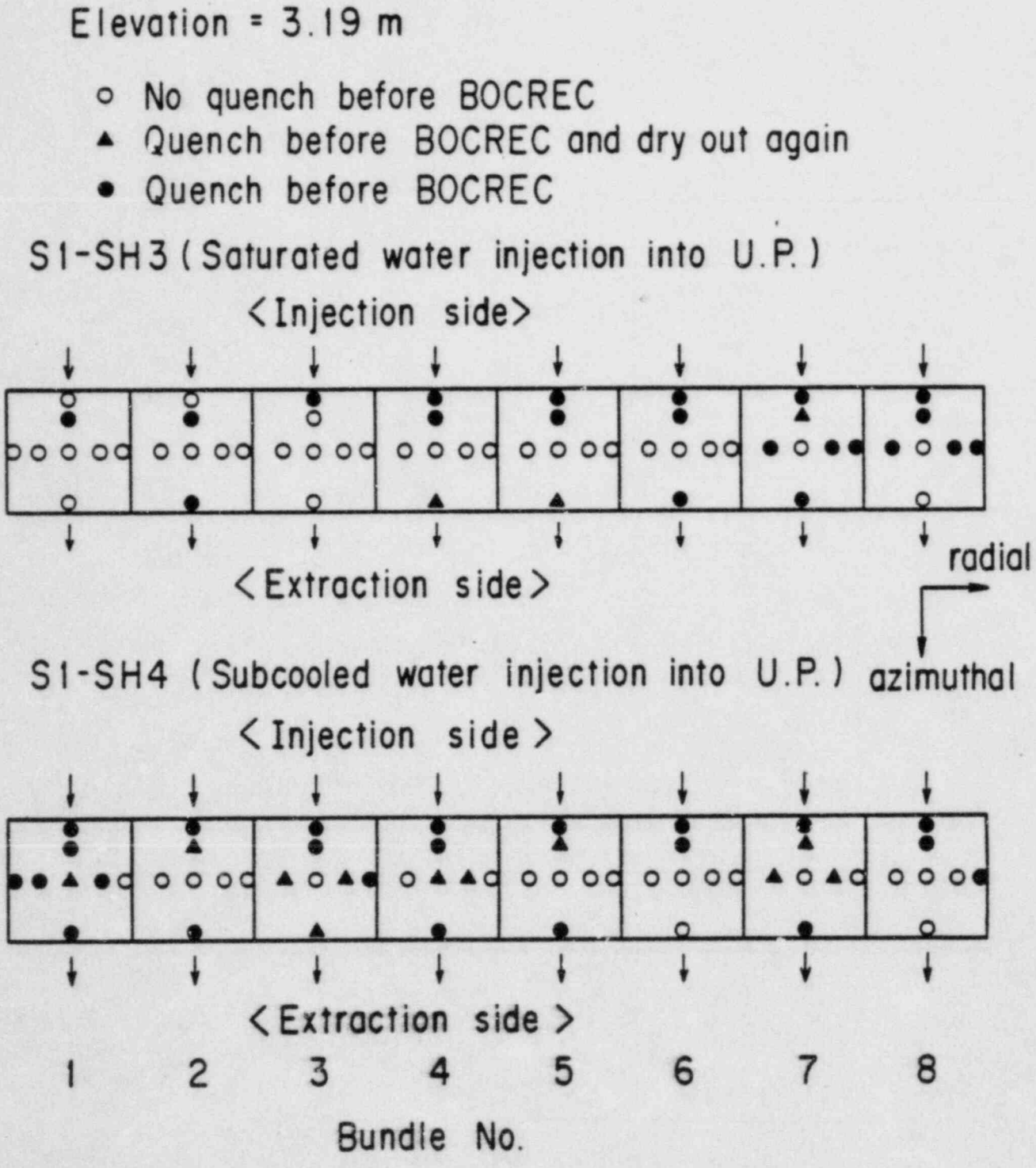

Fig. 3-36 Horizontal distributions of early quenched rods at elevation of 3.19 m in Tests Tests S1-SH3 and S1-SH4

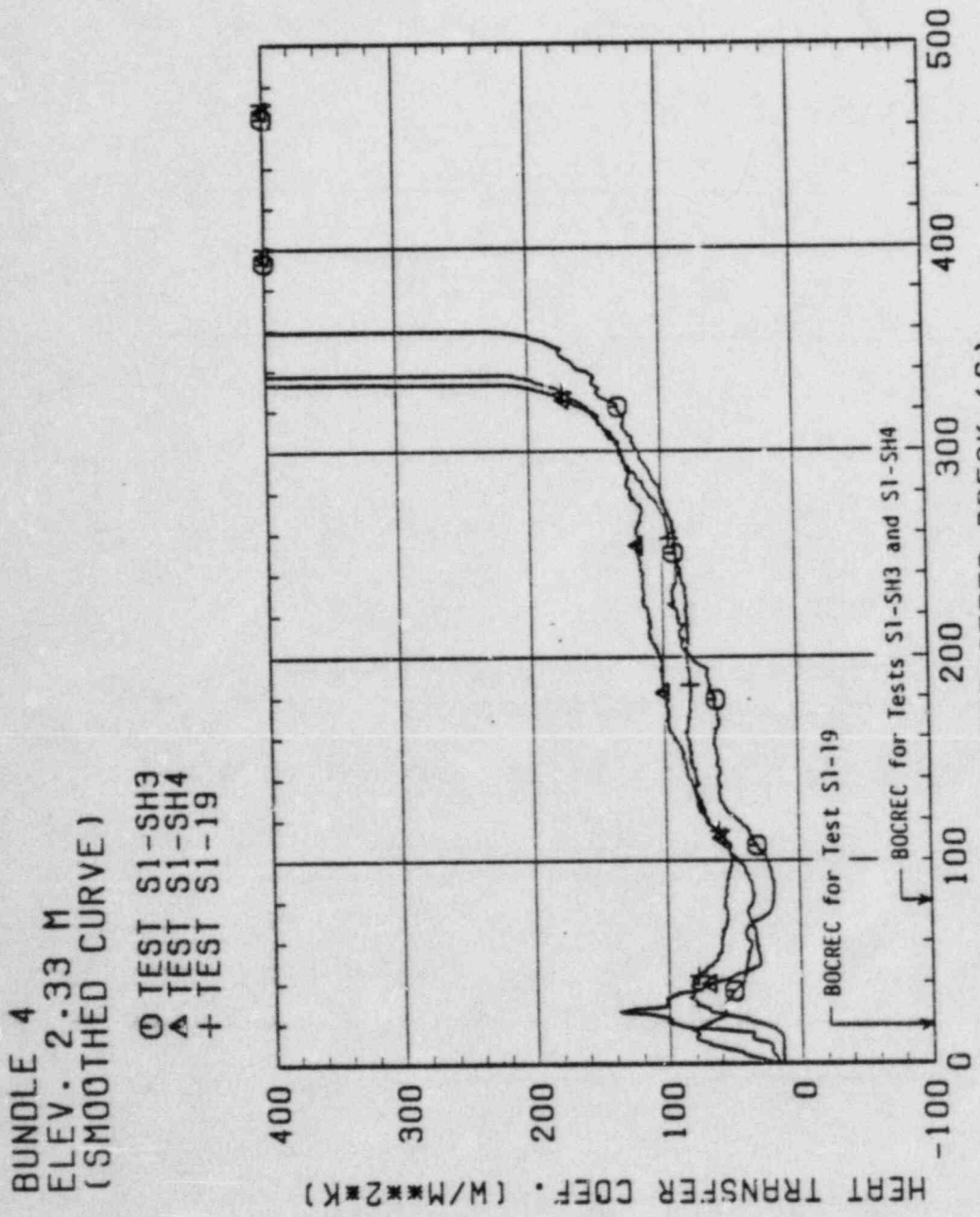

Fig. 3-37 Heat transfer coefficients at 2.33 m in Bundle 4.

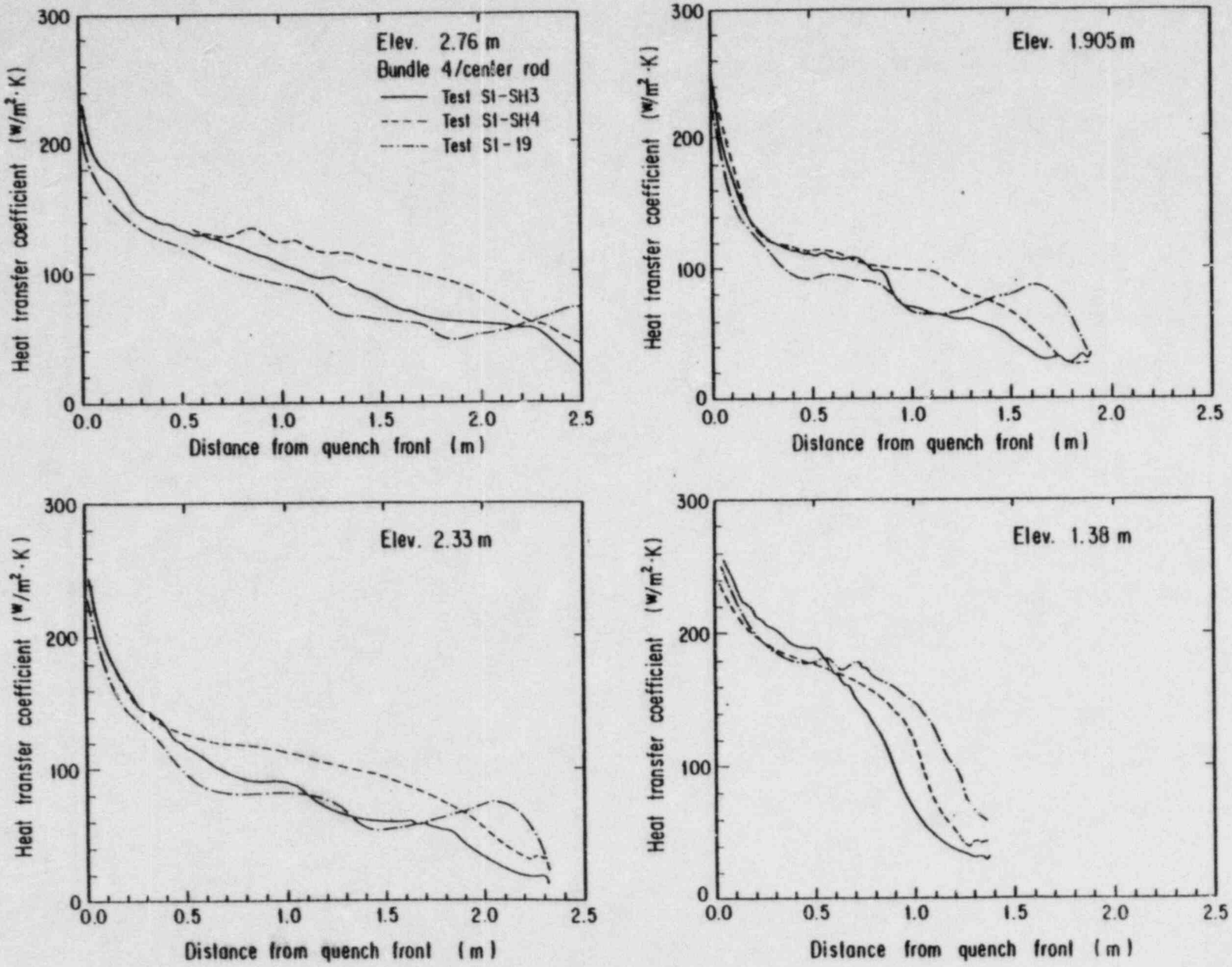

Fig. 3-38 Heat transfer coefficients vs. distance from quench front at elevations of 2.76, 2.33, 1.905 and 1.38 m in Bundle 4

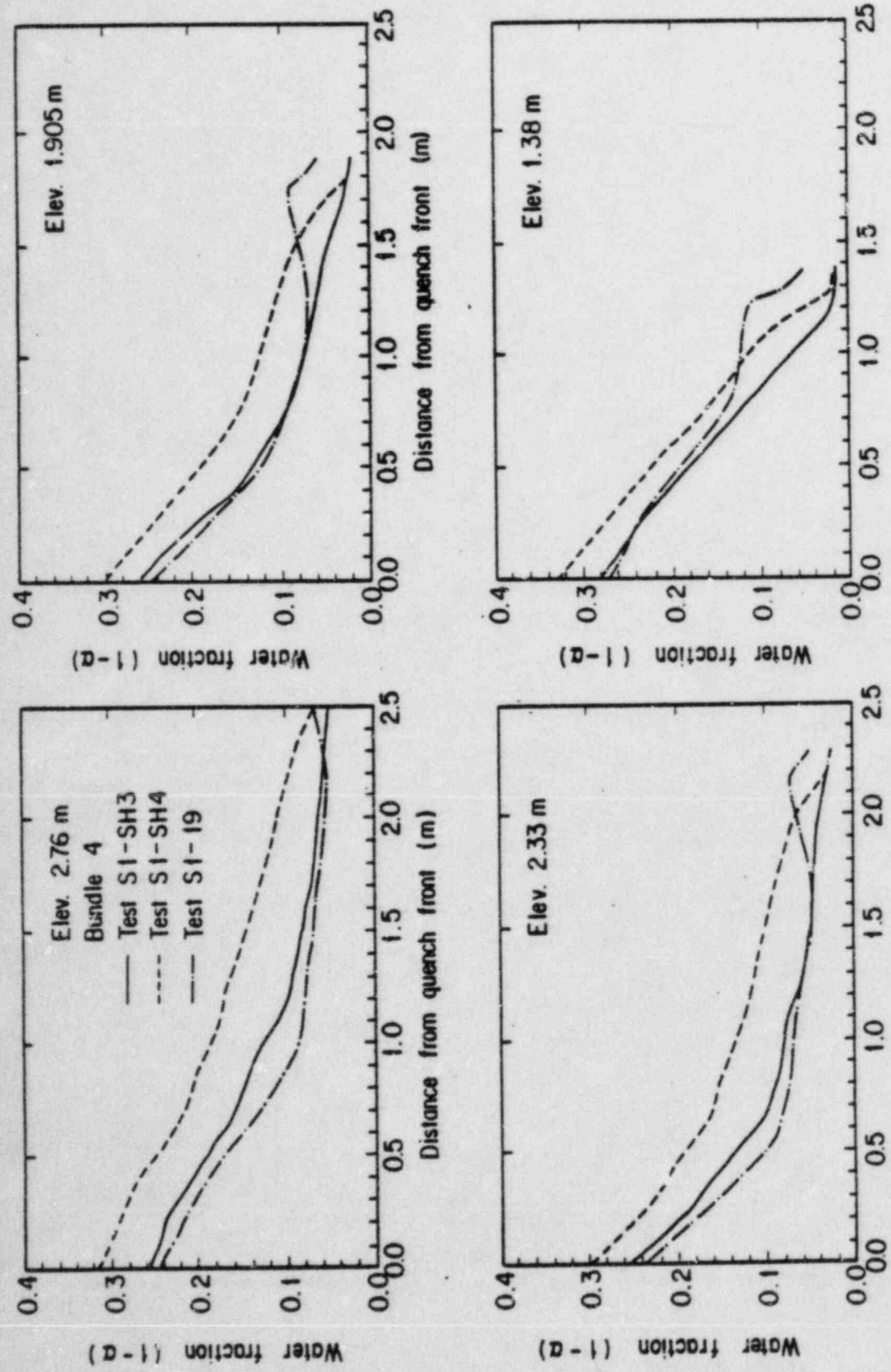

Fig. 3-39 Water fractions vs. distance from quench front at elevations of 2.76, 2.33, 1.905 and 1.38 m in Bundle 4

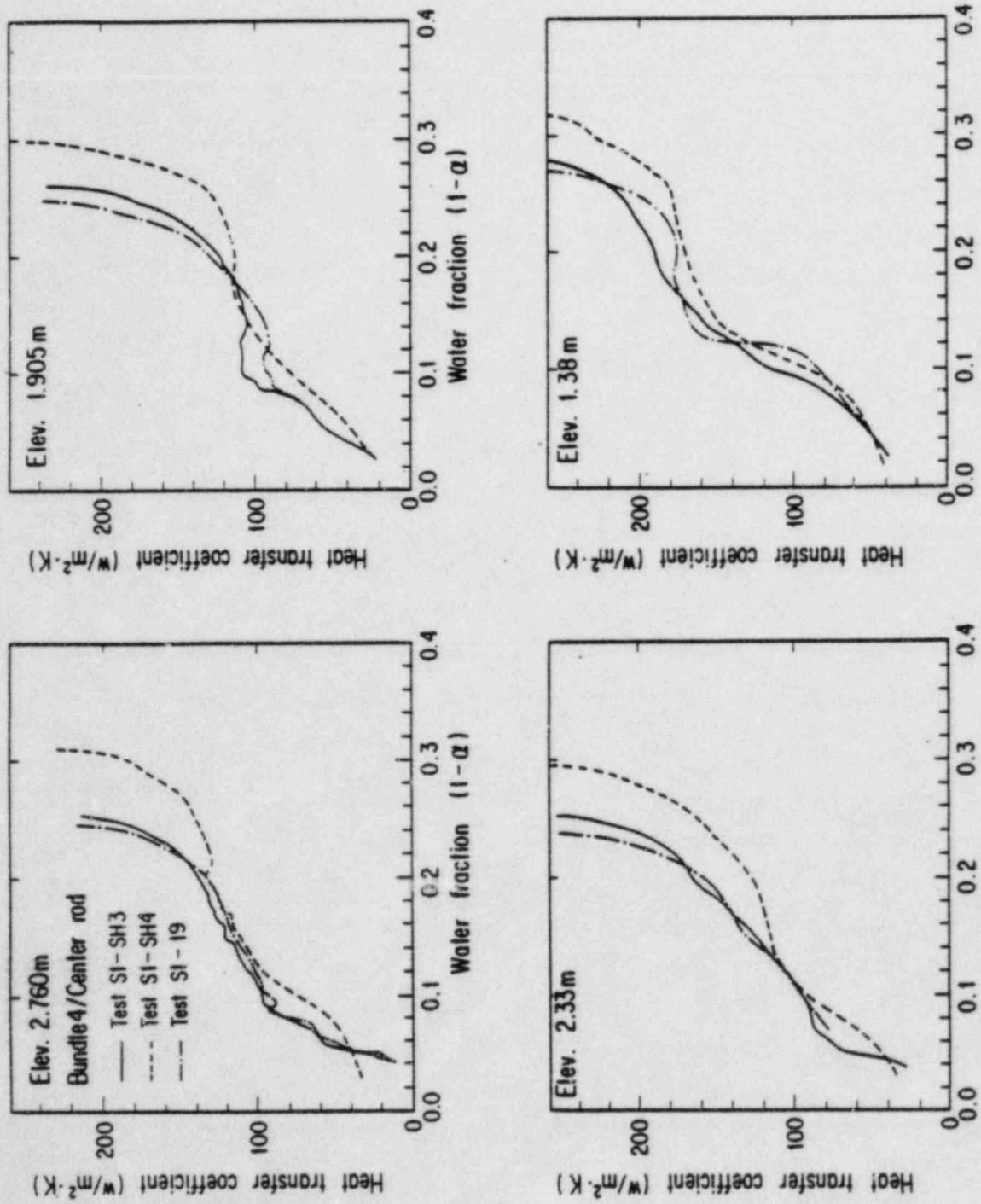

Fig. 3-40 Heat transfer coefficients vs. water fraction at elevations of 2.76, 2.33, 1.905 and 1.38 m in Bundle 4

Appendix A Slab Core Test Facility (SCTF) Core-I

A.1 Test Facility

The Slab Core Test Facility was designed under the following design phylosophy and design criteria:

a. Design Philosophy

(1) The facility should provide the capability to study the two-dimensional, thermohydraulic behavior and core flow within the reactor vessel especially due to the radial power distribution during the end of blowdown, refill and reflood phases of a simulated LOCA for a pressurized water reactor.

(2) To properly simulate the core heat transfer and hydrodynamics, a special emphasis is put on the proper simulation of the components in the pressure vessel. As the components in the pressure vessels are provided a simulated core, downcomer, core baffle region, lower plenum, upper plenum and upper head. On the other hand, simplified primary coolant loops are provided. As the primary coolant loops are provided a hot leg, an intact cold leg, broken cold legs and a steam water separator. The object of the steam/water separator is to measure the flow rate of carryover water coming out of the upper plenum.

b. Design Criteria

(1) The reference reactor for simulation to the SCTF is the Trojan reactor in the United States which is a four loop 3300 MWt PWR. The Ooi reactor in Japan is also referred which is of the similar type to the Trojan reactor.

(2) A full scale radial and axial section of a pressurized water reactor is provided as a simulated core of the SCTF with single bundle width.

(3) The simulated core consists of 8 bundles arranged in a row. Each bundle has electrically heated rods simulating fuel rods and non-heated rod with 16 × 16 array.

(4) The flow area and fluid volume of components are scaled down based on the core flow area scaling.

(5) To properly simulate the flow behavior of carryover water and entrainment, the elevations of hot leg and cold legs are designed to be the same as the PWRs as much as possible.

(6) The honeycomb structure is used as the side walls which accomodate the slab core, upper plenum and the upper part of lower plenum, so

as to minimize the effect of walls on the disturbance of the core heat transfer and hydrodynamics.

(7) To investigate the effect of flow resistance in the primary loops are provided the orifices of which dimension is changeable.

(8) The maximum allowable temperature of the simulated fuel rods is 1900°C and the maximum allowable pressure of the facility is 6 kg/cm^2 absolute.

(9) The facility is equipped with a hot leg equivalent to four actual hot legs connecting the upper plenum and the steam water separator, an intact cold leg equivalent to three actual intact cold legs connecting the steam water separator and the downcomer and two broken cold legs, one is for the steam water separator side and the other for the pressure vessel side.

(10) The ECCS consists of an Acc., a LPCI and a combined injection systems.

(11) ECC water injection ports are the cold leg, hot leg, upper plenum, downcomer, lower plenum and above the upper core support plate. These portions are to be chosen according to the object of the test.

(12) For better simulation of lower plenum flow resistance, simulated fuel rods do not penetrate through the bottom plate of the lower plenum but terminate below the bottom of the core.

(13) For measurements in the pressure vessel including core measurements, the feature of the slab geometry of the pressure vessel is utilized as much as possible. Design and arrangement of the instruments are done so as to be able to carry out installation calibration and removal of the instruments.

(14) View windows are provided where flow pattern recognition is important. The locations are, the interface between the core and the upper plenum, hot leg, pressure vessel side broken cold leg and the downcomer.

(15) The blocked bundle test is carried out in Core-I in order to investigate the effect of the ballooned fuel rods and the unblocked normal bundle test for the Core-II and -III.

(16) Simulated types of break are cold leg break and hot leg break.

(17) The components and systems such as the containment tanks and ECC water supply system in the CCTF are shared with the SCTF to the maximum extent.

The overall schematic diagram of the SCTF is shown in Fig.A-1. The principal dimensions of the facility is shown in Table A-1, and the

comparison of dimensions between the SCTF and the referred PWR is shown in Fig.A-2.

A.1.1 Pressure Vessel and Internals

The pressure vessel is of slab geometry as shown in Fig.A-3. The height of the components in the pressure vessel is almost the same as the reference reactor's, and the flow area and the fluid volume of each component are scaled down based on the nominal core flow area scaling.

The core consists of 8 bundles in a row and each bundles include simulated fuel rods and non-heated rods with 16 × 16 array. The core arrangement for the SCTF Core-I is shown in Fig.A-4, which includes 6 normal bundles and 2 blocked bundles. The core is enveloped by the honeycomb thermal insulator which is attached on the barrel.

The downcomer is located at one end of the pressure vessel which corresponds to the periphery of the actual reactor. The core baffle region is, on the other hand, located between the core and the downcomer. For better understanding, the cross section of the pressure vessel at the elevation of midplane of the core is shown in Fig.A-5.

The design of upper plenum internals is based on that of the new Westinghouse 17 × 17 array fuel assemblies. The internals consist of control rod guide tubes, support columns, orifice plates and open holes and those arrangements is shown in Fig.A-6. The radius of each internal is scaled down by factor 8/15 from that of an actual reactor. Flow resistance baffles are inserted into the guide tubes. The elevation and the configuration of baffles plates are shown in Fig.A-7 and A-8.

The height of the hot leg and cold legs are designed as close to the actual PWR as possible. However, in order to avoid the interference of the nozzles in the downcomer, the height of nozzles for the broken cold leg and the intact cold leg are shifted down compared to that of the hot leg as shown in Fig.A-3.

A.1.2 Heater Rod Assembly

The heater rod assembly for the SCTF Core-I consists of 8 bundles arranged in a row. These bundles are composed of 6 normal unblocked bundles which are located at the 1st, 2nd and 5th to 8th bundles and 2 blocked bundles which are 3rd and 4th bundles as shown in Fig.A-4. Each bundle has 234 electrically heated rods and 22 non-heated rods. The dimensions of the heater rods are based on a 15 × 15 fuel rod bundle,

and the heated length and the outer diameter of each heater rod are 3.66 m and 10.7 mm, respectively. A heater rod consists of a nichrome heater element, magnesium oxide (MgO) and Nichrofer-7216 sheath (equialent to Inconel 600). The sheath wall thickness is about 1.0 mm and is thicker than the actual fuel cladding because of the requirements for thermocouple installation. The heating element is a helical coil and has a 17 step chopped cosine axial power profile as shown in Fig.A-9. The peaking factor is 1.4.

Non-heated rods are either stainless steel pipes or solid rods of 13.8 mm O.D. The heater rods and non-heated rods are fixed at the top of the core allowing the rods to move downward when the thermal expansion occurs. In Fig.A-10 the axial position where blockage sleeves for simulating the balooned fuel rod are equipped is shown. The blockage sleeves consist of three types of sleeve, one is used for the rods at the corner adjacent to the next blocked bundle, another for the rods adjacent to the side walls and the third for the rods except for the periphery of the blocked bundle. These are named A, B and C respectively in the Fig.A-11 and these configurations for these are shown in Fig.A-12.

For better simulation for flow resistance in the lower plenum the simulated rods do not penetrate through the bottom plate of the lower plenum as shown in Fig.A-10.

A.1.3 Primary Loops and ECCS.

Primary loops consist of a hot leg equivalent to the four actual hot legs, a steam/water separator for measuring the flow rate of carry over water, an intact cold leg equivalent to the three actual intact loops, a broken cold leg on the pressure vessel side and a broken cold leg on the steam water separator side. These two broken cold legs are connected to two containment tanks through break valves, respectively. The arrangement of the primary loops is shown in Fig.A-13. The flow area of each loop is scaled down based on the core flow area scaling. It should be emphasized that the cross section of the hot leg is a elongated circle to realize the proper flow pattern in the hot leg. The steam/water separator has a steam generator inlet plenum simulator to realize the flow characteristics of carryover water. The cross section of the hot leg and the configuration of the steam generator inlet plenum simulator are shown in Fig.A-14.

A pump simulator and a loop seal part are provided for the intact cold leg. The arrangement of the intact cold leg is shown in Fig.A-15.

The pump simulator consists of the casing and duct simulators and an orifice plate as shown in Fig.A-16. The loop resistance is adjusted with the orifice plate.

In principle, ECCS consists of an accumulator and a low pressure injection system. The injection port is located as already described in the design criteria. Besides, the UCSP extraction system is provided and the UCSP water injection and extraction systems will be used for combined injection tests.

A.1.4 Containment Tanks and Auxiliary System

Two containment tanks are provided to the SCTF. The containment tank-I is connected with the downcomer through the pressure vessel side broken cold leg and the containment tank-II is connected with the steam/water separator through the steam/water separator side broken cold leg. Especially in the containment tank-I, carryover water from the downcomer is measured by phase separation. These containment tanks and auxiliary system such as a pressurizer for injecting water from the Acc. tank, etc. are shared with the CCTF.

A.2 Instrumentation

The instrumentation in the SCTF has been provided both by JAERI and USNRC. The JAERI-provided instrumentation includes the measurement of temperatures, pressures, differential pressures, liquid levels, flow velocities, and heating powers. USNRC has provided film probes, impedance probes, string probes, liquid level detectors (LLDs), fluid distribution grids (FDGs), turbine meters, drag disks, γ-densitometers, spool pieces and video optical probes. The measurement items of the JAERI- and USNRC-provided instruments are listed in Tables A-2 and A-3, respectively. Location of each instrument is shown in Figs. A-17 through A-34.

Table A-1 Principal Dimensions of Test Facility

1. Core Dimension	
(1) Quantity of Bundle	8 Bundles
(2) Bundle Array	1 × 8
(3) Bundle Pitch	230 mm
(4) Rod Array in a Bundle	16 × 16
(5) Rod Pitch in a Bundle	14.3 mm
(6) Quantity of Heater Rod in a Bundle	234 rods
(7) Quantity of Non-Heated Rod in a Bundle	22 rods
(8) Total Quantity of Heater Rods	234 × 8 = 1872 rods
(9) Total Quantity of Non-Heated Rods	22 × 8 = 176 rods
(10) Effective Heated Length of Heater Rod	3660 mm
(11) Diameter of Heater Rod	10.7 mm
(12) Diameter of Non-Heateed Rod	13.8 mm
2. Flow Area & Fluid Volume	
(1) Core Flow Area* (nominal)	0.227 m^2
(2) Core Fluid Volume	0.92 m^3
(3) Baffle Region Flow Area	0.10 m^2
(4) Baffle Region Fluid Volume	0.36 m^3
(5) Downcomer Flow Area	0.121 m^2
(6) Upper Annulus Flow Area	0.158 m^2
(7) Upper Plenum Horizontal Flow Area	0.525 m^2
(8) Upper Plenum Fluid Volume	1.16 m^2
(9) Upper Head Fluid Volume	0.86 m^3
(10) Lower Plenum Fluid Volume	1.38 m^3
(11) Steam Generator Inlet Plenum Simulator Flow Area	0.626 m^2
(12) Steam Generator Inlet Plenum Simulator Fluid Volume	0.931 m^3
(13) Steam Water Separator Fluid Volume	5.3 m^3
(14) Flow Area at the Top Plate of Steam Generator Inlet Plenum Simulator	0.195 m^2
(15) Hot Leg Flow Area	0.0826 m^2
(16) Intact Cold Leg Flow Area (Diameter = 297.9 mm)	0.0697 m^2
(17) Broken Cold Leg Flow Area (Diameter = 151.0 mm)	0.0179 m^2

* Flow area in the core is 0.35 m^2, including the excess flow area of gaps between the bundle and the surface of thermal insulator and between the core barrel and the pressure vessel wall.

Table A-1 Principal Dimensions of Test Facility

(18) Containment Tank I Fluid Volume	30 m^3
(19) Containment Tank II Fluid Volume	50 m^3
3. Elevation & Height	
(1) Top Surface of Upper Core Support Plate (UCSP)	0 mm
(2) Bottom Surface of UCSP	-76 mm
(3) Top of the Effective Heated Length of Heater Rod	-393 mm
(4) Bottom of the Skirt in the Lower Plenum	-5270 mm
(5) Bottom of Intact Cold Leg	+724 mm
(6) Bottom of Hot Leg	+1050 mm
(7) Top of Upper Plenum	+2200 mm
(8) Bottom of Steam Generator Inlet Plenum Simulator	+1933 mm
(9) Centerline of Loop Seal Bottom	-2281 mm
(10) Bottom Surface of End Box	- 185.1 mm
(11) Top of the Upper Annulus	+2234 mm
(12) Height of Steam Generator Inlet Plenum Simulator	1595 mm
(13) Height of Loop Seal	3140 mm
(14) Inner Height of Hot Leg Pipe	737 mm
(15) Bottom of Lower Plenum	-5770 mm
(16) Top of Upper Head	+2887 mm

Table A-2 Measurement Items of SCTF (JAERI-provided instruments)

LOCATION	ITEM	PROBE	QUANTITY
1. CORE			
center	pressure	DP cell	1
short range of core	diff. press.	DP cell	22
half length of core	diff. press.	DP cell	16
full length of core	diff. press.	DP cell	8
across spacers	diff. press.	DP cell	7
across end box	diff. press.	DP cell	8
across 4 assemblies	diff. press.	DP cell	3
across 8 assemblies	diff. press.	DP cell	3
below and above end box	steam velocity	Pitot-tube	3
sub channel	steam velocity	Pitot-tube	13
below end box hole	fluid temp.	T/C	16
above end box hole	fluid temp.	T/C	16
core baffle	fluid temp.	T/C	6
non-heating rods	fluid temp.	T/C	96
	steam temp.	SSP	16
	clad temp.	T/C	108
heater rods	clad temp.	T/C	640
side walls	wall temp.	T/C	36
core baffle	wall temp,	T/C	6
core baffle	liquid level	DP cell	1
short range of core baffle	liquid level	DP cell	6
heated rod	power		8
			sum(1039)
2. UPPER PLENUM			
centre	pressure	DP cell	1
across end box tie plate	diff. press.	DP cell	8
core outlet-hot leg inlet	diff. press.	DP cell	4
periphery of UCSP hole	fluid temp.	T/C	4
centre of UCSP hole	fluid temp.	T/C	4
250mm & 1000mm above UCSP	fluid temp.	T/C	4
surface of UCSP	fluid temp.	T/C	4
above UCSP hole	steam temp.	SSP	4

Table A-2 Measurement Items of SCTF (JAERI-provided instruments)
(Continued)

LOCATION	ITEM	PROBE	QUANTITY
surface of structure	wall temp.	T/C	15
side walls	wall temp.	T/C	8
above end box tie plate	liquid level	DP cell	8
above UCSP	liquid level	DP cell	4
above UCSP (v.)	steam velocity	Pitot-tube	2
inter-structures (h.)	steam velocity	Pitot-tube	2
			sum(97)
3. LOWER PLENUM			
below bottom spacer	pressure	DP cell	1
lower plenum - upper plenum	diff. press.	DP cell	1
core inlet	fluid temp.	T/C	8
inlet from downcomer	fluid temp.	T/C	2
side & bottom walls	wall temp.	T/C	4
below bottom spacer	liquid level	DP cell	1
			sum(17)
4. DOWNCOMER			
upper position	pressure	DP cell	1
horizontal direction	diff. press.	DP cell	1
four levels	fluid temp.	T/C	8
side wall	wall temp.	T/C	2
inner wall	wall temp.	T/C	2
below cold leg level	liquid level	DP cell	1
above cold leg level	liquid level	DP cell	1
below core inlet level	liquid level	DP cell	1
bottom	momentum flux	Drag disk	2
			sum(19)
5. HOT LEG			
full length	diff. press.	DP cell	1
multiple points	fluid temp.	T/C	3
	steam temp.	SSP	3
	wall temp.	T/C	1
	liquid level	DP cell	2
			sum(10)

Table A-2 Measurement Items of SCTF (JAERI-provided instruments)

(Continued)

LOCATION	ITEM	PROBE	QUANTITY
6. S/W SEPARATOR SIDE BROKEN COLD LEG			
across resistance simulator	diff. press.	DP cell	1
S/W separator to containment tank II	flow rate	venturi	1
multiple points	fluid temp.	T/C	1
	steam temp.	SSP	1
	wall temp.	T/C	1
			sum(5)
7. INTACT COLD LEG			
full length	diff. press.	DP cell	1
across resistance simulator	diff. press.	DP cell	1
across pump simulator	diff. press.	DP cell	1
	flow rate	venturi	1
near resistance simulator	fluid temp.	T/C	1
pump simulator	fluid temp.	T/C	3
	wall temp.	T/C	1
			sum(9)
8. PV SIDE BROKEN COLD-LEG	pressure	DP cell	1
full length	diff. press.	DP cell	1
across resistance simulator	diff. press.	DP cell	1
multiple points	fluid temp.	T/C	4
	wall temp.	T/C	2
	liquid level	DP cell	2
			sum(11)
9. VENT LINE			
across the length	diff. pres.	DP cell	1
			sum(1)

Table A-2 Measurement Items of SCTF (JAERI-provided instruments)
(Continued)

LOCATION	ITEM	PROBE	QUANTITY
10. S/W SEPARATOR			
	pressure	DP cell	1
between inlet and outlet	diff. press.	DP cell	1
SG plenum simulator	diff. press.	DP cell	1
SG plenum simulator	fluid temp.	T/C	2
top and bottom	fluid temp.	T/C	2
wall	wall temp.	T/C	2
full height	liquid level	DP cell	1
liquid extraction	flow rate	DP cell	1
			sum(11)
11. CONTAINMENT TANK-I			
	pressure	DP cell	1
downcomer-CT-I	diff. press.	DP cell	1
CT-I - CT-II	diff. press.	DP cell	1
	flow rate	DP cell	1
full height	liquid level	DP cell	1
		float	1
top, middle & bottom	fluid temp.	T/C	3
wall	wall temp.	T/C	1
			sum(10)
12. CONTAINMENT TANK-II			
	pressure	DP cell	1
upper plenum - CT-II	diff. press.	DP cell	1
separator - CT-II	diff. press.	DP cell	1
steam blow line	flow rate	DP cell	1
full height	liquid level	DP cell	1
top, middle & bottom	fluid temp.	T/C	3
			sum(8)
13. ECC INJECTION SYSTEM			
ACC tank	pressure	DP cell	1
total and LPCI	flow rate	E-M flow meter	2
			1
ACC tank	fluid temp.	T/C	1

Table A-2 Measurement Items of SCTF (JAERI-provided instruments)
(Continued)

LOCATION	ITEM	PROBE	QUANTITY
13. ECC INJECTION SYSTEM			
header	fluid temp.	T/C	2
ACC tank	liquid level	DP cell	1
			sum(8)
14. UCSP WATER EXTRACTION SYSTEM			
extraction line	flow rate	E-M flow meter	4
steam line	flow rate	DP cell	4
extraction line	fluid temp.	T/C	5
steam line	fluid temp.	T/C	1
extraction line	liquid level	DP cell	4
			sum(18)
15. SATURATED WATER TANK			
	fluid temp	T/C	1
	liquid level	DP cell	1
			sum(2)
16. NITROGEN GAS SYSTEM			
	flow rate	DP cell	1
injection port	fluid temp.	T/C	1
			sum(2)

Total 1267

Table A-3 Measurement Items of SCTF (USNRC-provided instruments)

LOCATION	ITEM	PROBE	QUANTITY
1. CORE			
non-heated rods	liquid level	LLD	20×4 = 80
non-heated rods	film thickness and velocity	film probe	6
non-heated rods	void fraction and droplet velocity	flag probe	8
side walls	film thickness and velocity	film probe	8
sub-channel	fluid density	γ-densitometer	10
end box	fluid density	γ-densitometer	5
end box	flow pattern	video optical probe	1
2. UPPER PLENUM			
full height	liquid level	FDG	8×8 = 64
structure surface	film thickness and velocity	film probe	6
side walls	film thickness and velocity	film probe	6
inter structure	void fraction	prong probe	8
above UCSP hole	velocity	turbine	8
inter structure	velocity	turbine	4
inter structure	fluid density	γ-densitometer	4
hot leg inlet	flow pattern	video optical probe	1
3. LOWER PLENUM			
core inlet	velocity	turbine	4
bottom	reference conductivity	reference probe	1
4. DOWNCOMER			
full height	liquid level	FDG	2×3×7 = 42
two levels	velocity	drag disk	3
two levels	void fraction	string probe	3

Table A-3 Measurement Items of SCTF (USNRC-provided instruments)

(Continued)

LOCATION	ITEM	PROBE	QUANTITY
5. HOT LEG	mass flow rate fluid density void fraction	spool piece	1
6. PV SIDE BROKEN COLD-LEG	mass flow rate fluid density void fraction	spool piece	1
7. VENT LINE	mass flow rate void fraction	spool piece	1

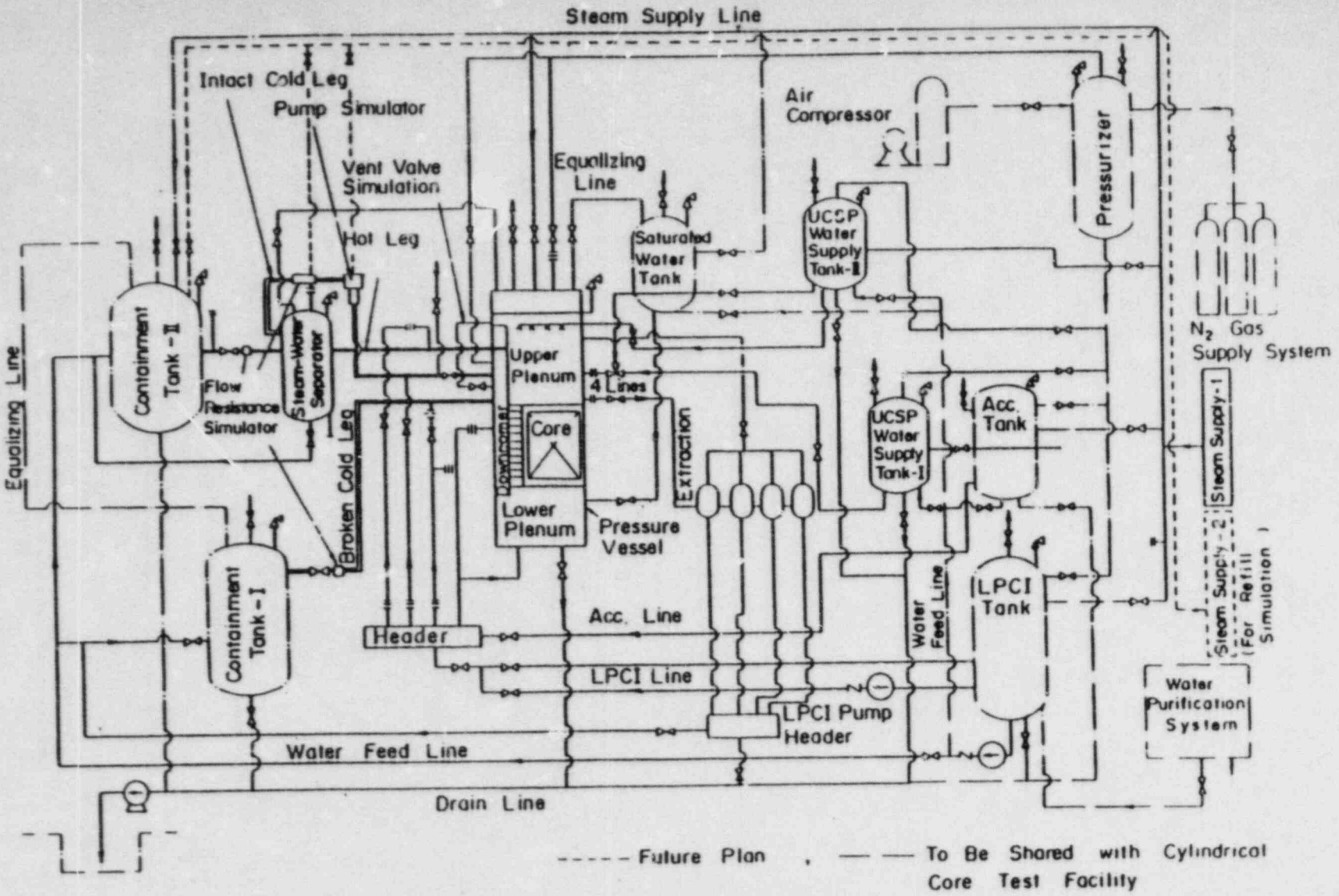

Fig. A-1 Schematic Diagram of Slab Core Test Facility

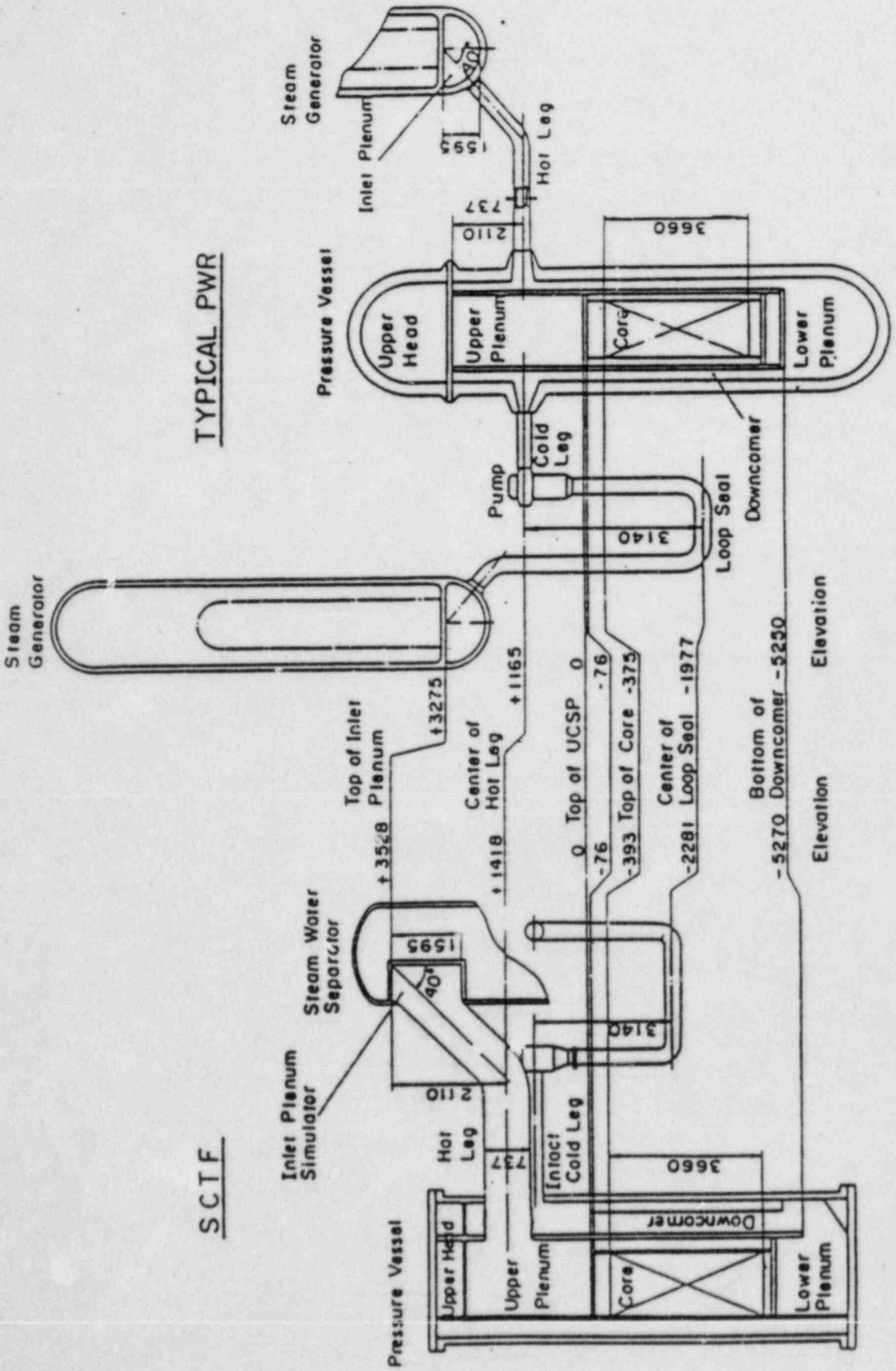

Fig. A-2 Comparison of Dimensions between SCTF and a Reference PWR

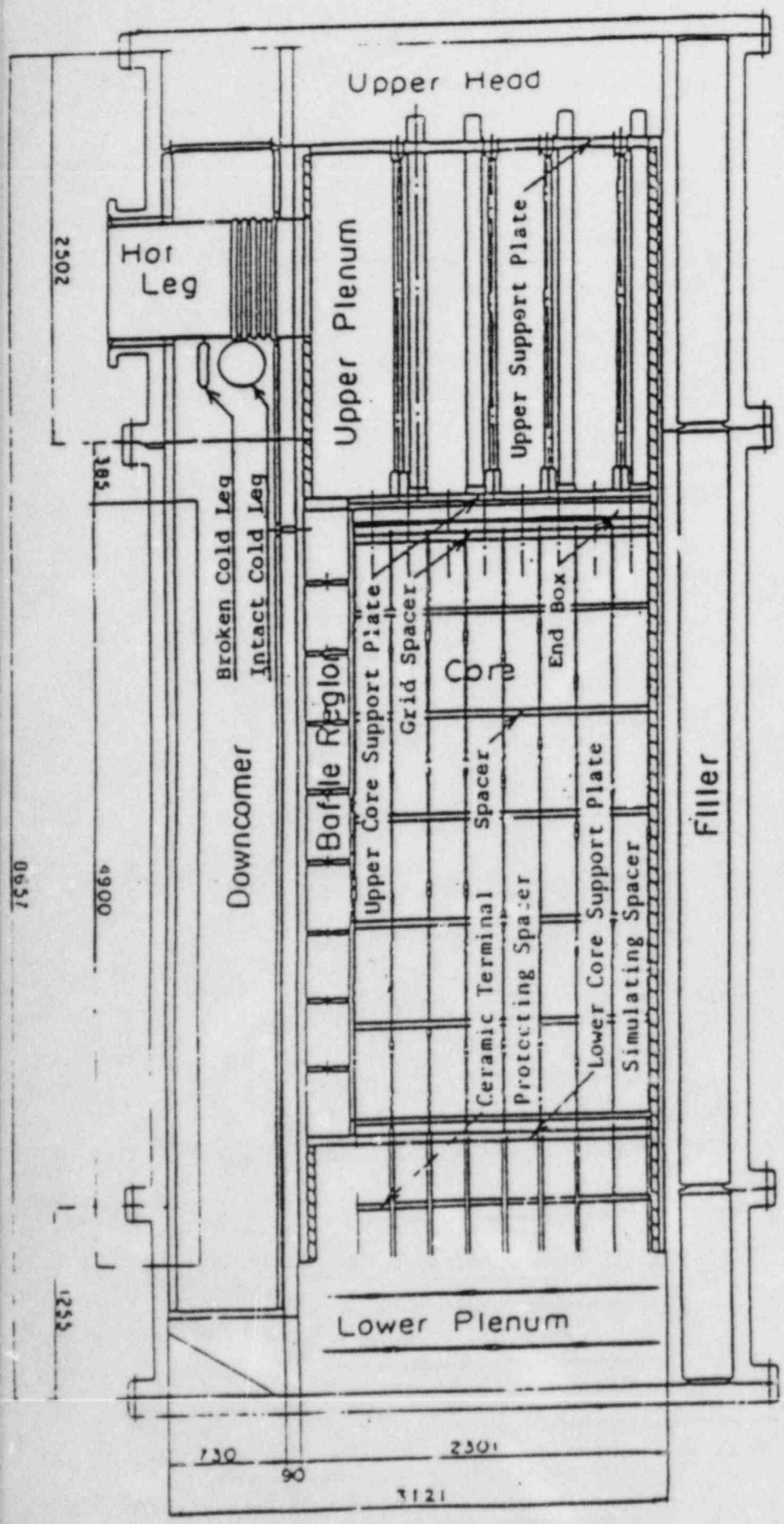

Fig. A-3 Vertical Cross Section of the Pressure Vessel

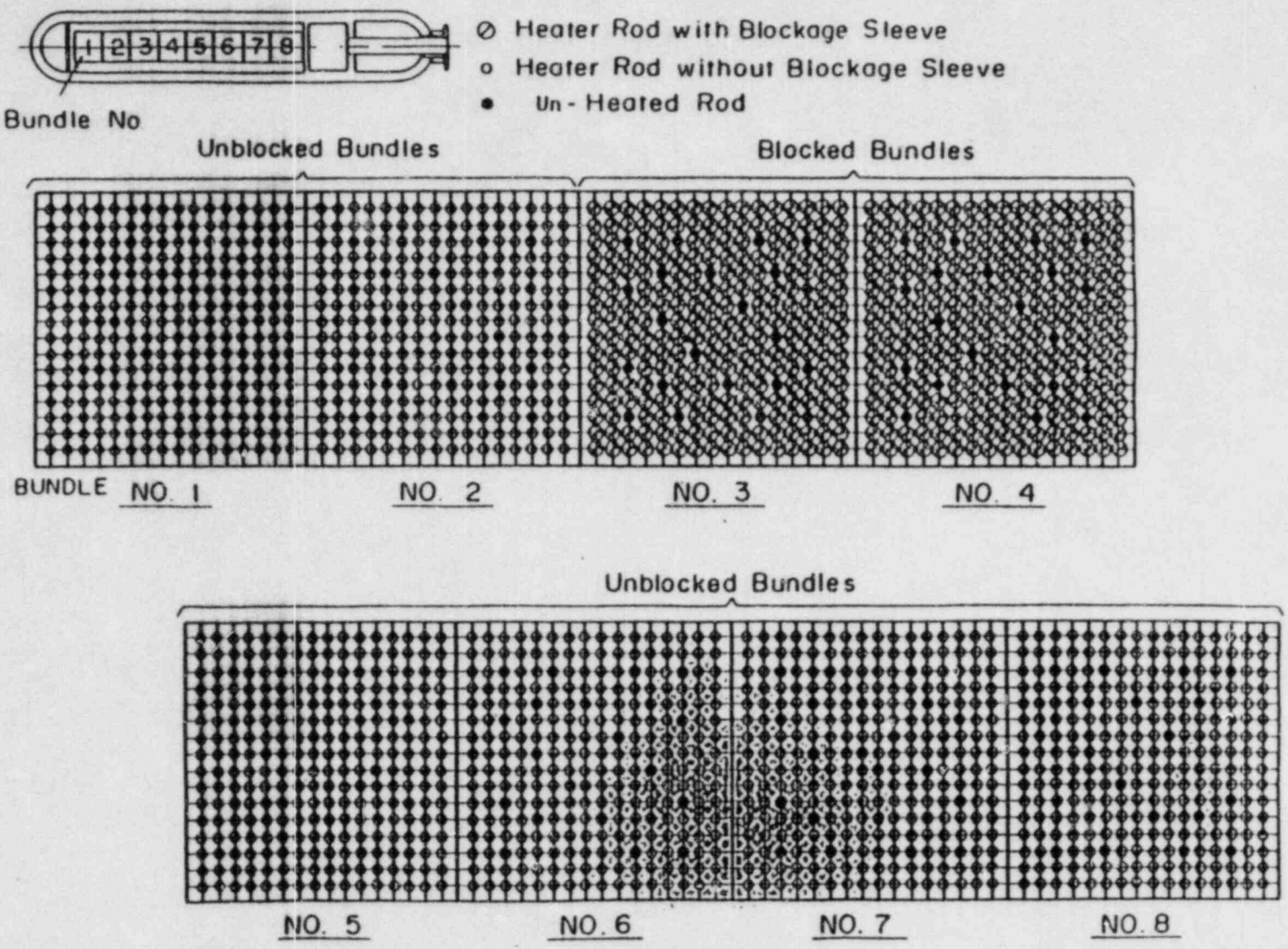

Fig. A-4 Arrangement of Heater Bundles

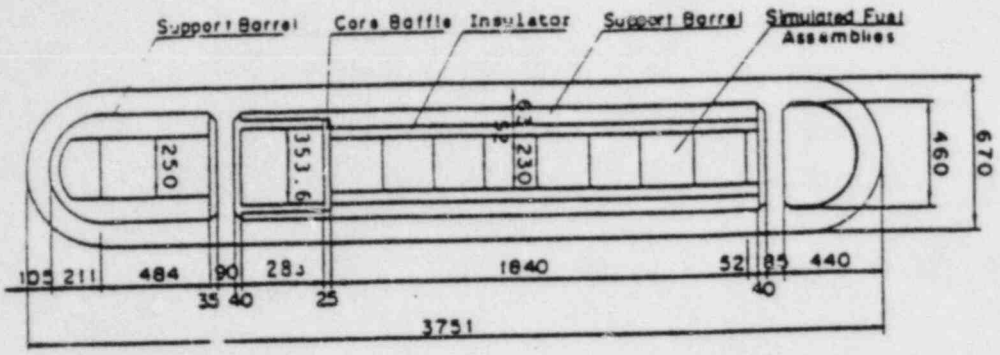

Fig. A-5 Horizontal Cross Section of the Pressure Vessel (1)

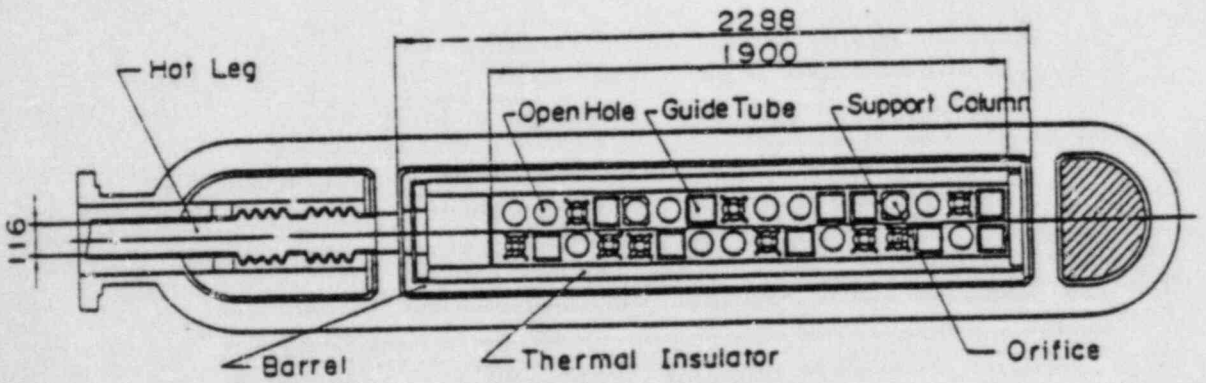

Upper Plenum Cross Section

Fig. A-6 Horizontal Cross Section of the Pressure Vessel (2)

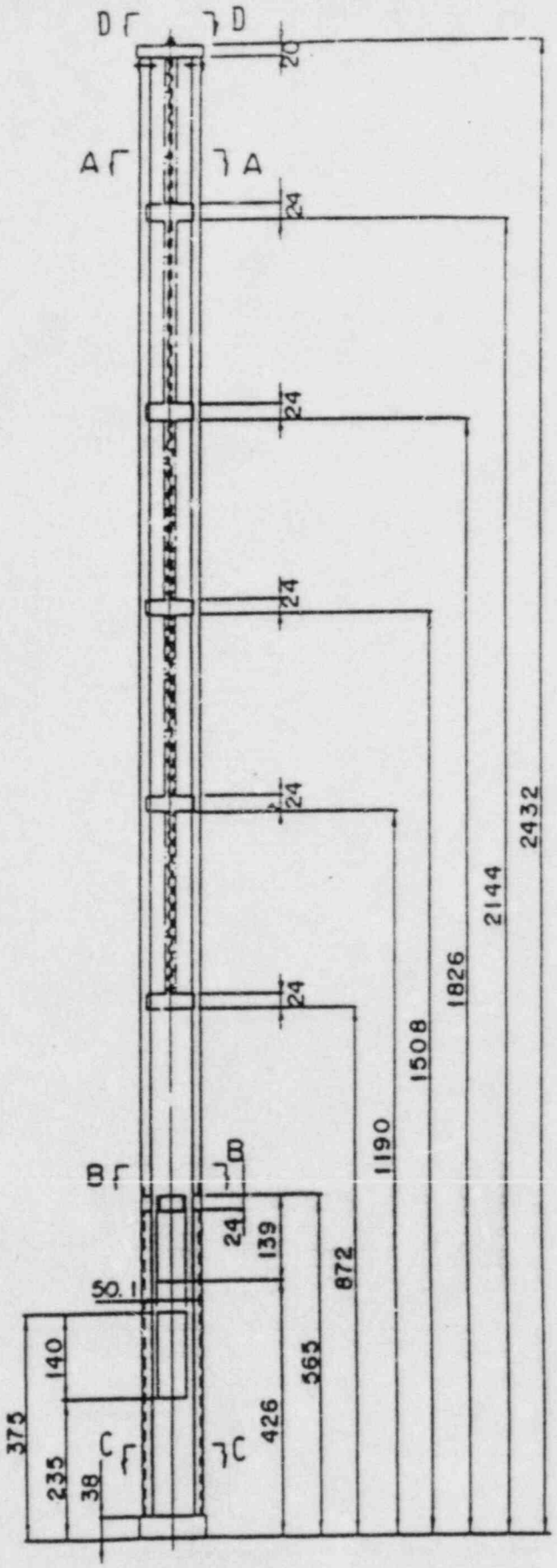

Fig. A-7 Dimension of Guide Tube (1)

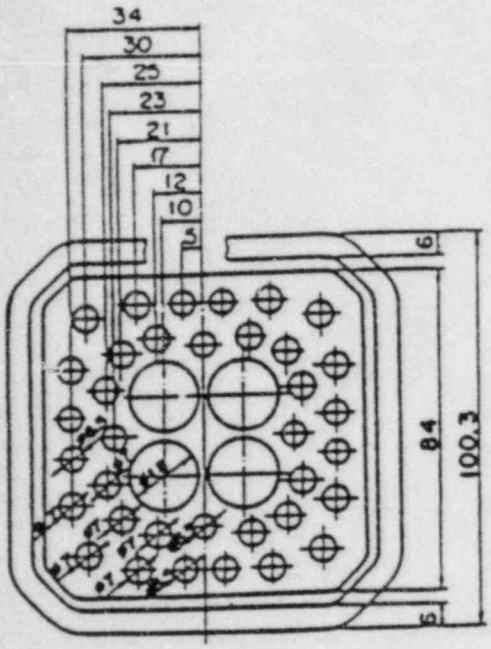

SECTION A-A

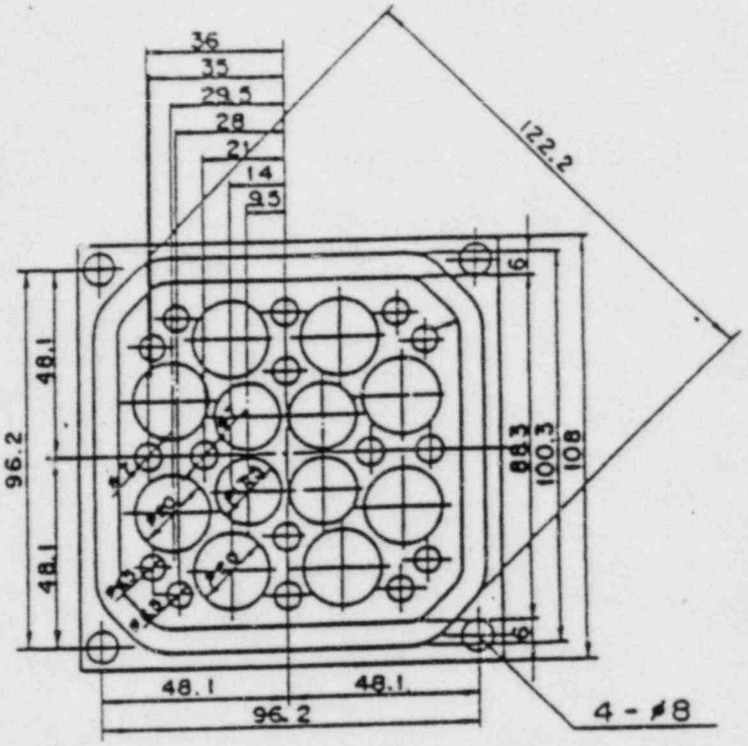

SECTION C-C

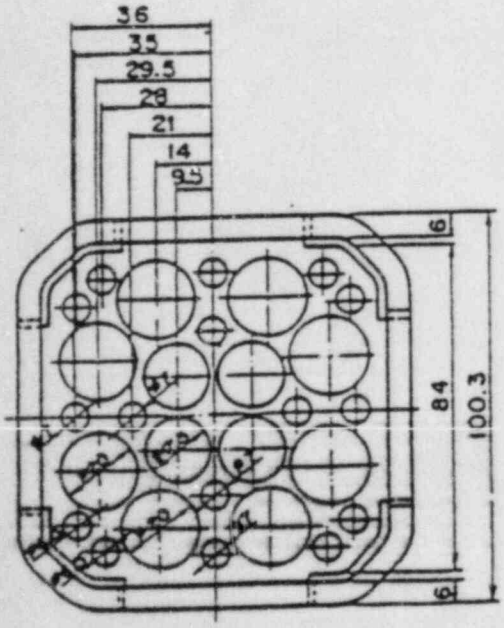

SECTION B-B

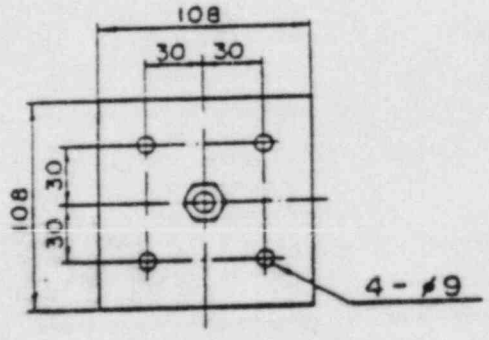

SECTION D-D

Fig. A-8 Dimension of Guide Tube (2)

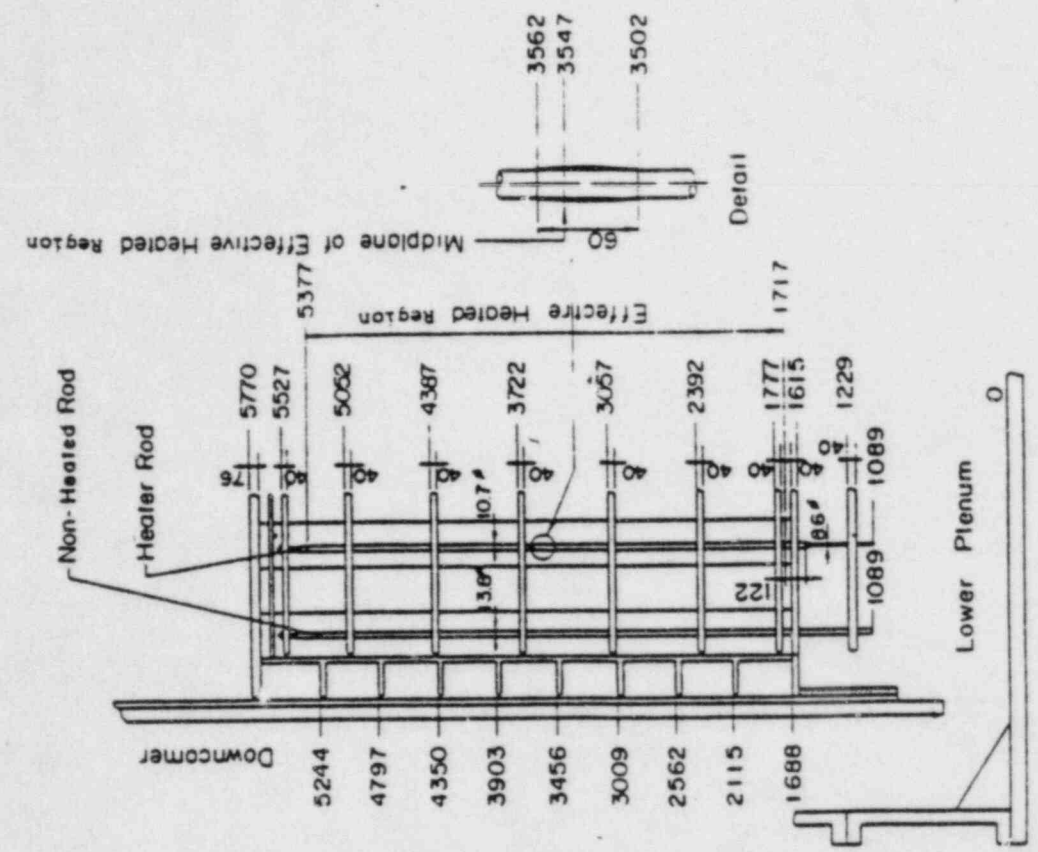

Fig. A-10 Relative Elevation and Dimension of the Core in SCTF

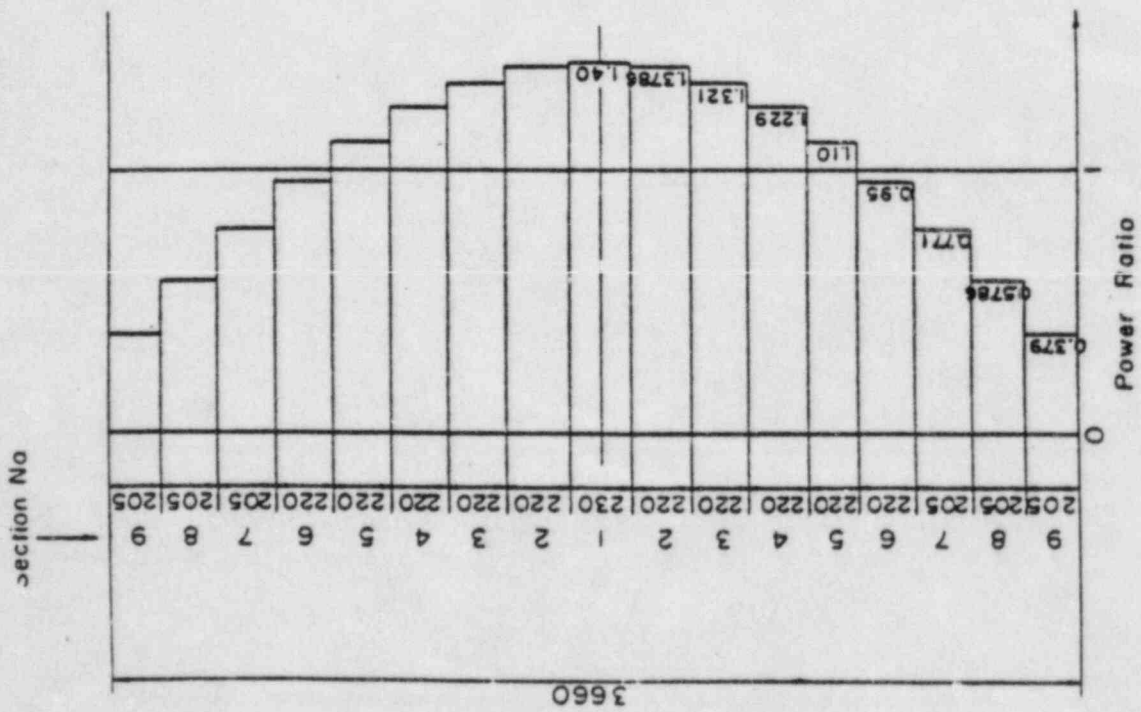

Fig. A-9 Axial Power Distribution of Heater Rod

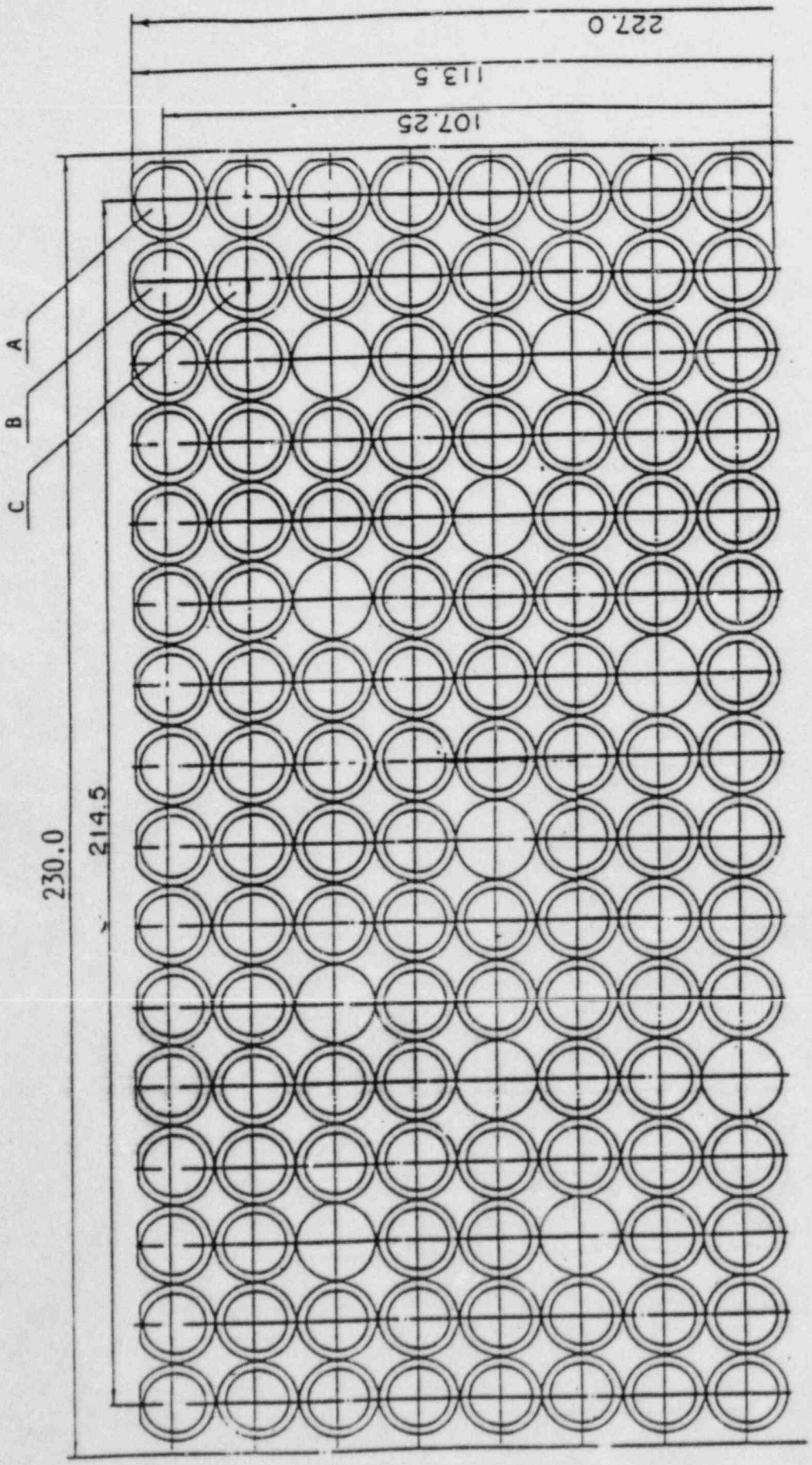

Fig. A-11 Arrangement of the Heater Rods with Three Kinds of Blockage Sleeve

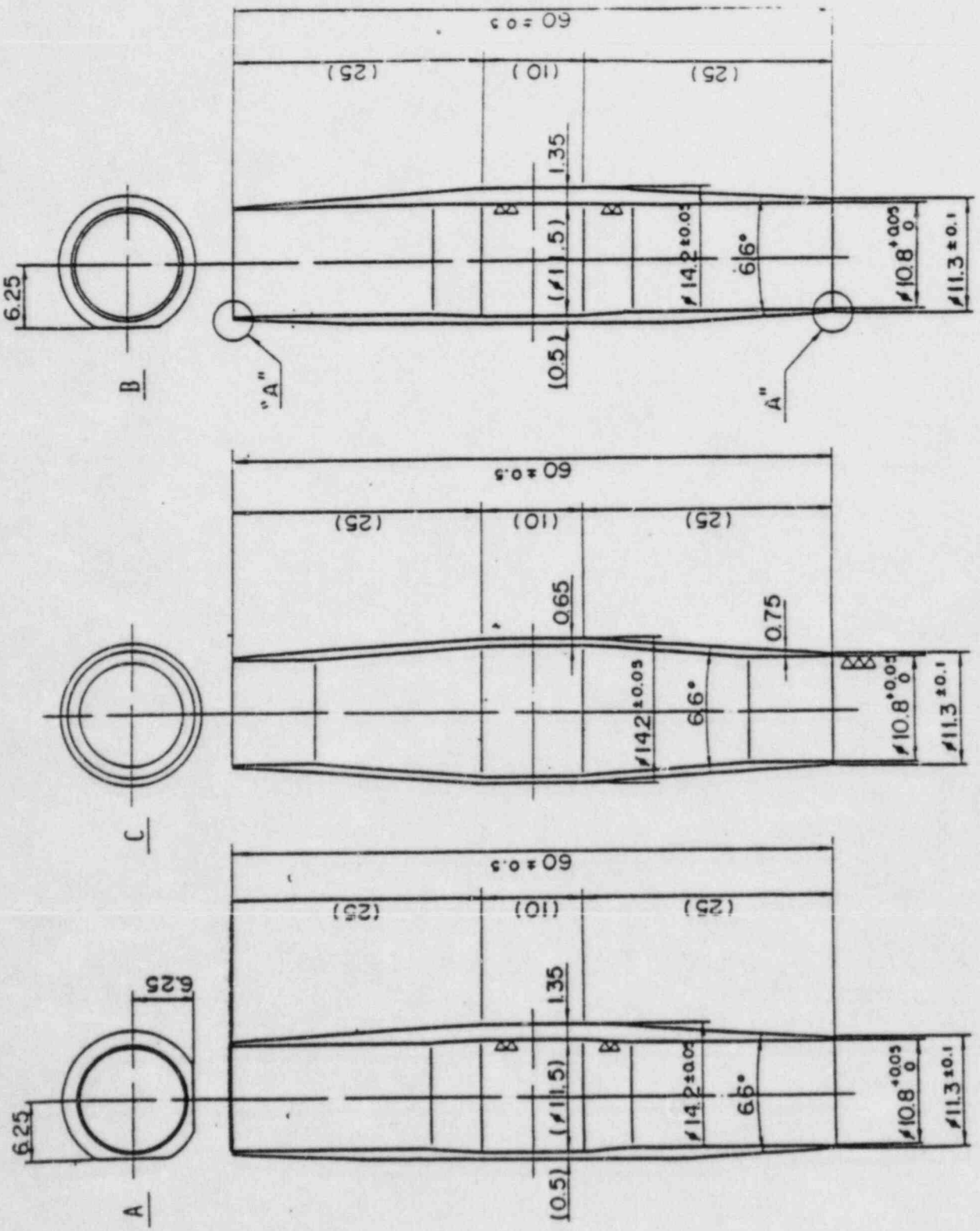

Fig. A-12 Configuration and Dimension of the Thre Blockage Sleeves

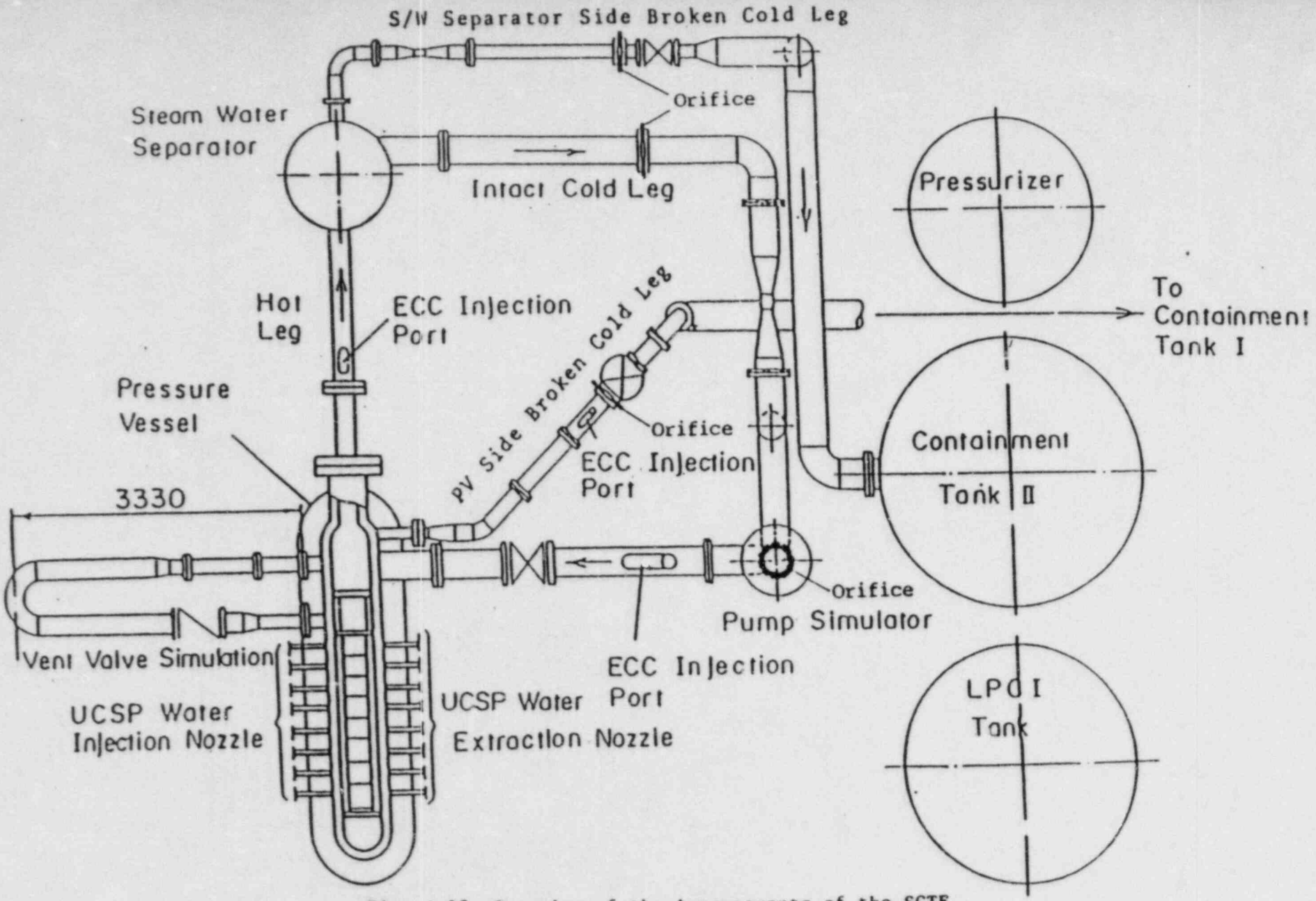

Fig. A-13 Overview of the Arrangements of the SCTF

JAERI-M 84-221

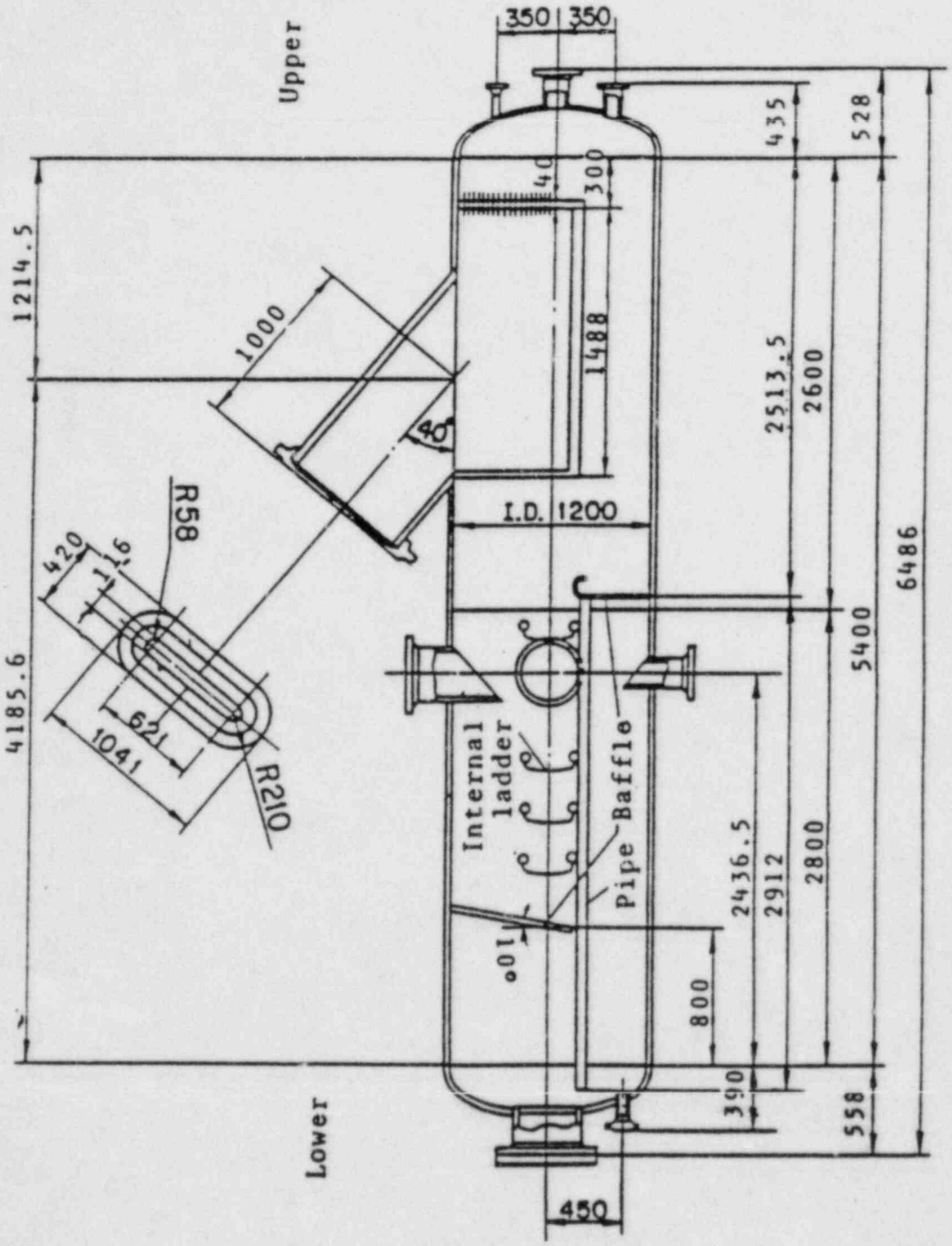

Fig. A-14 Steam-Water Separator

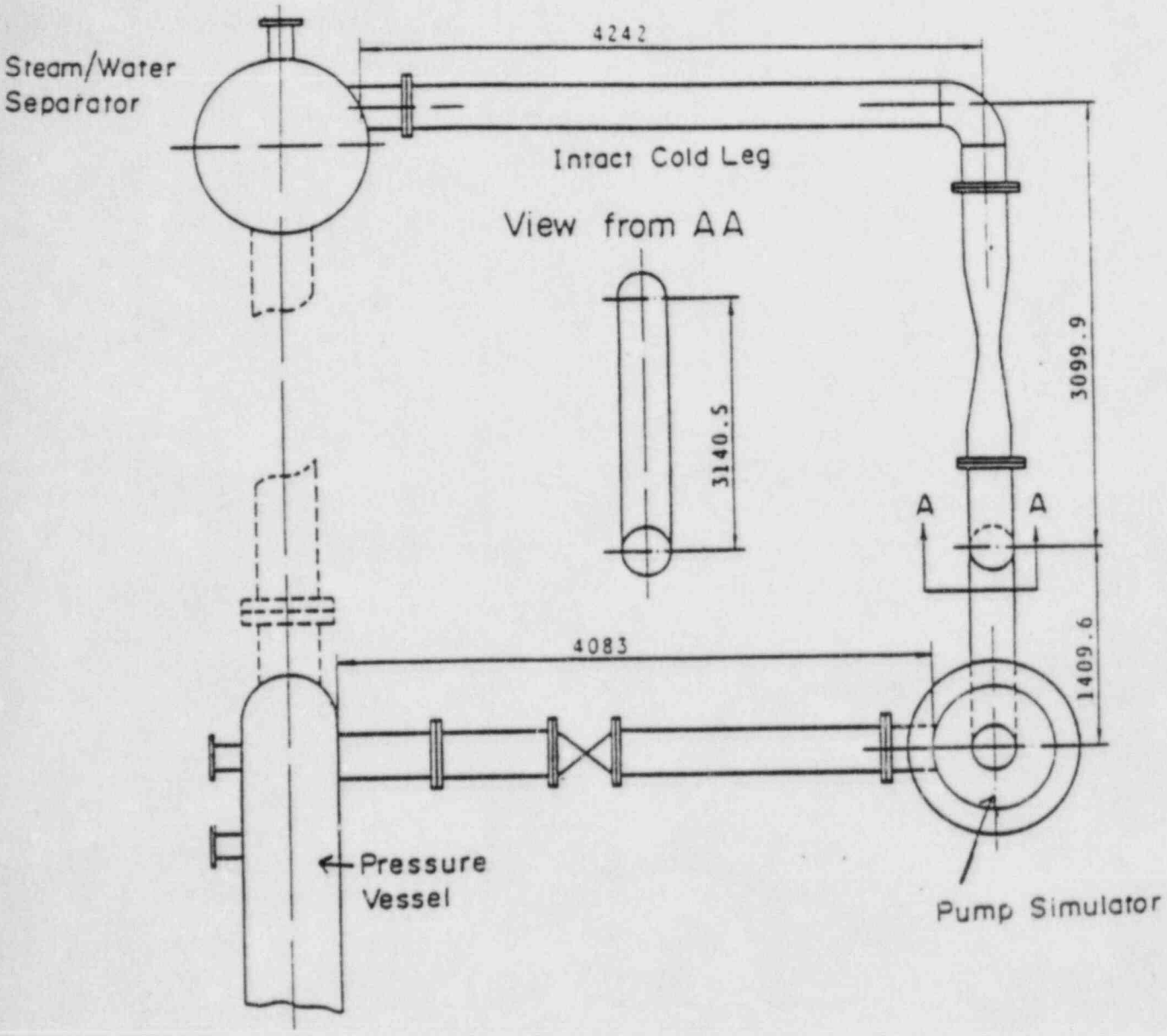

Fig. A-15 Arrangement of Intact Cold Leg

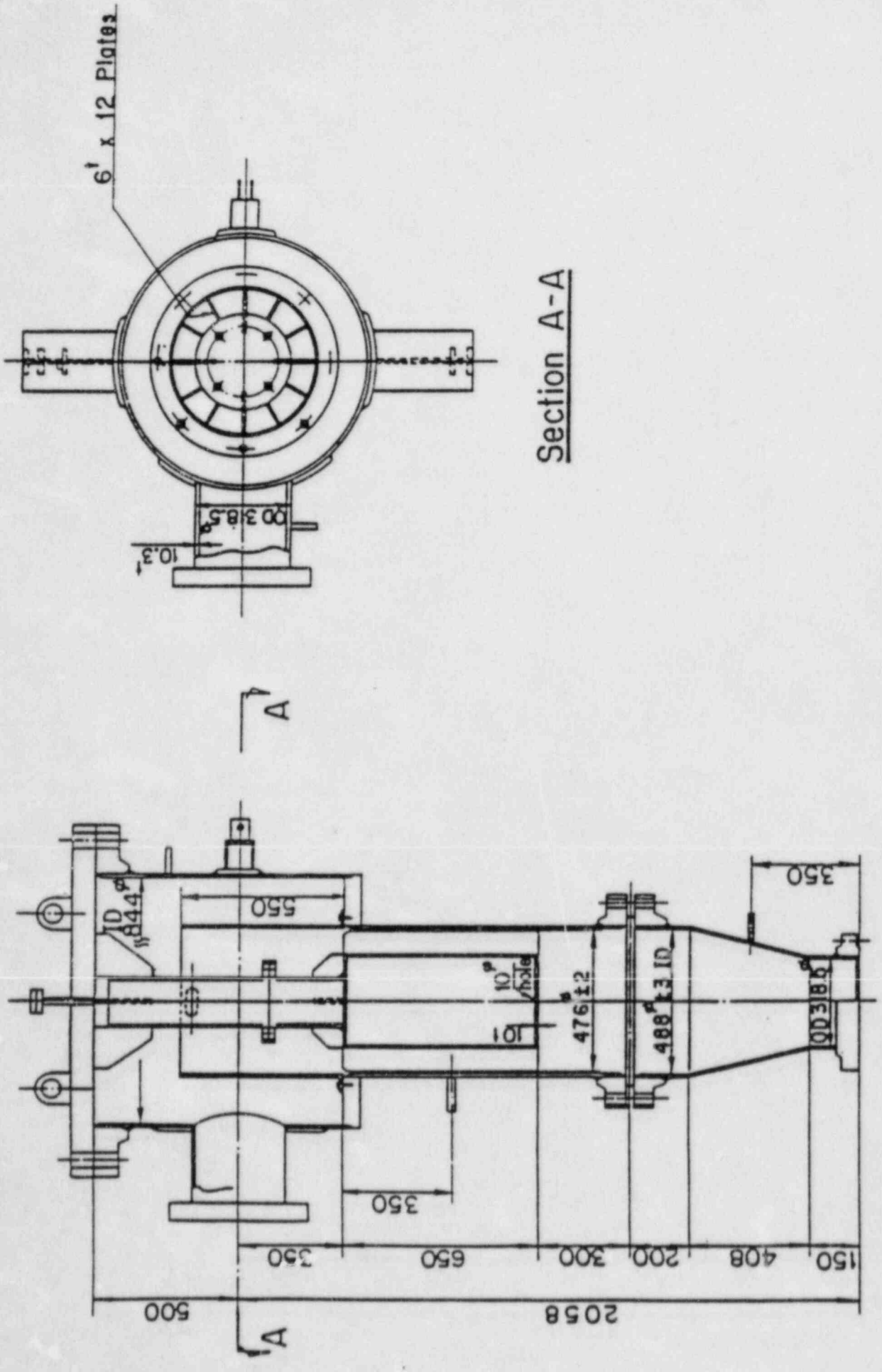

Fig. A-16 Configuration and Dimension of Pump Simulator

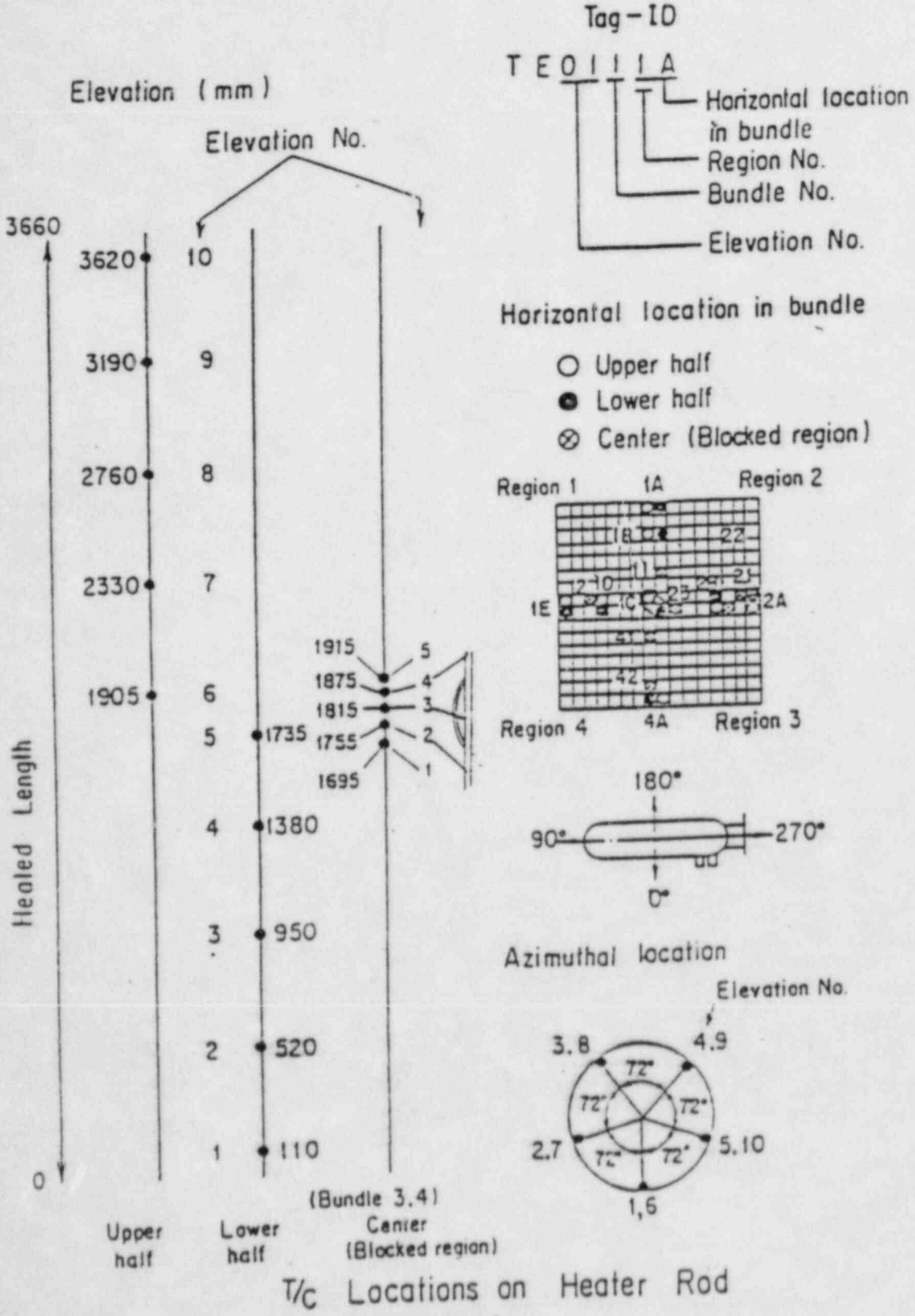

Fig. A-17 Thermocouple Locations of Heater Rod Surface Temperature Measurements

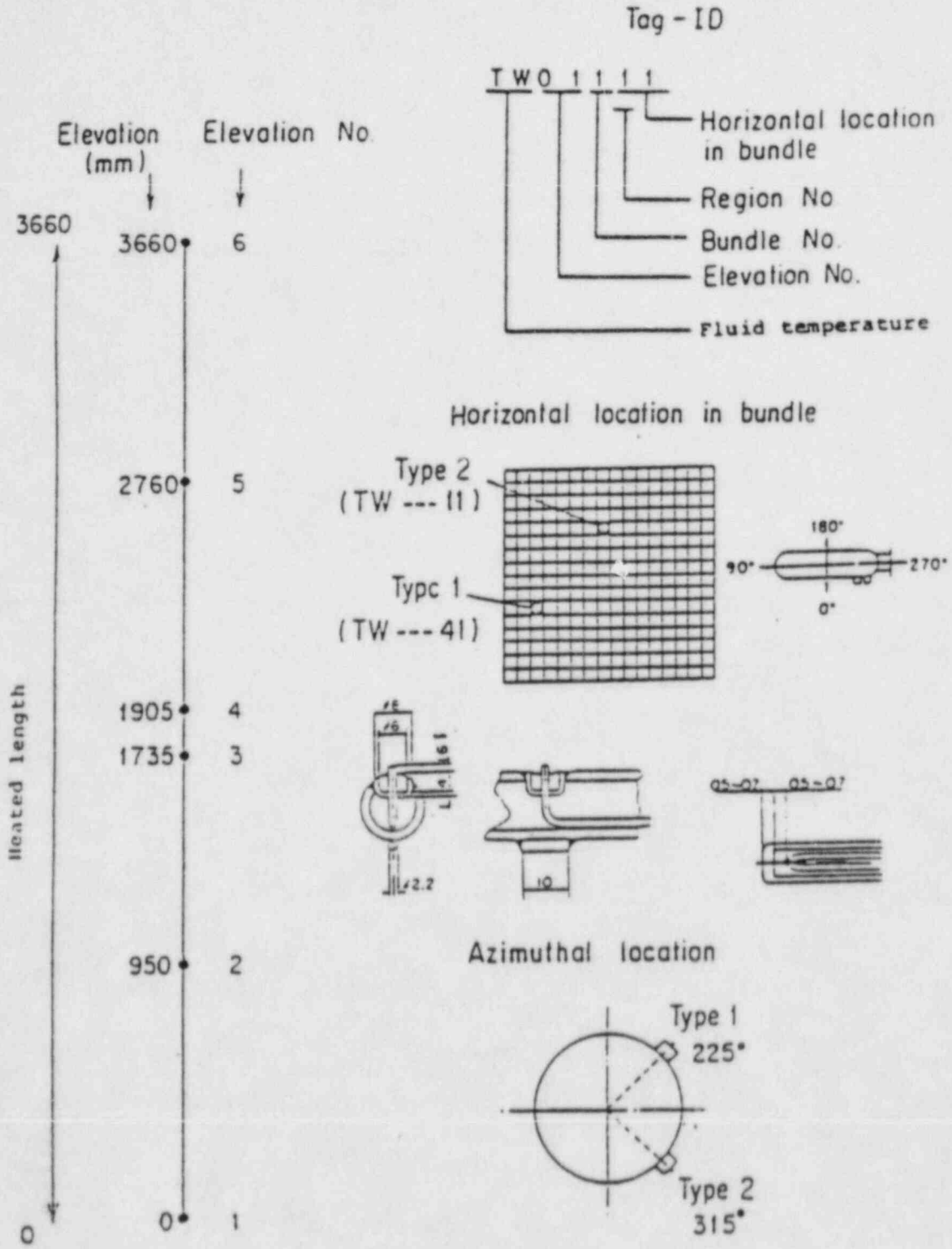

Fig. A-18 Thermocouple Locations of Fluid Temperature Measurements in Core

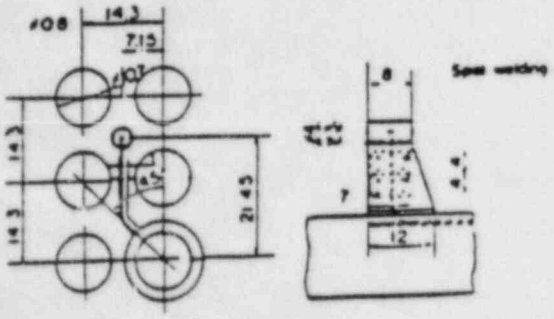

Steam temperature T/C

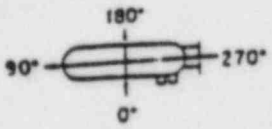

Tag－ID

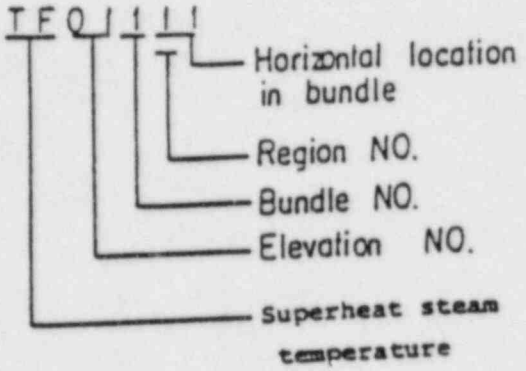

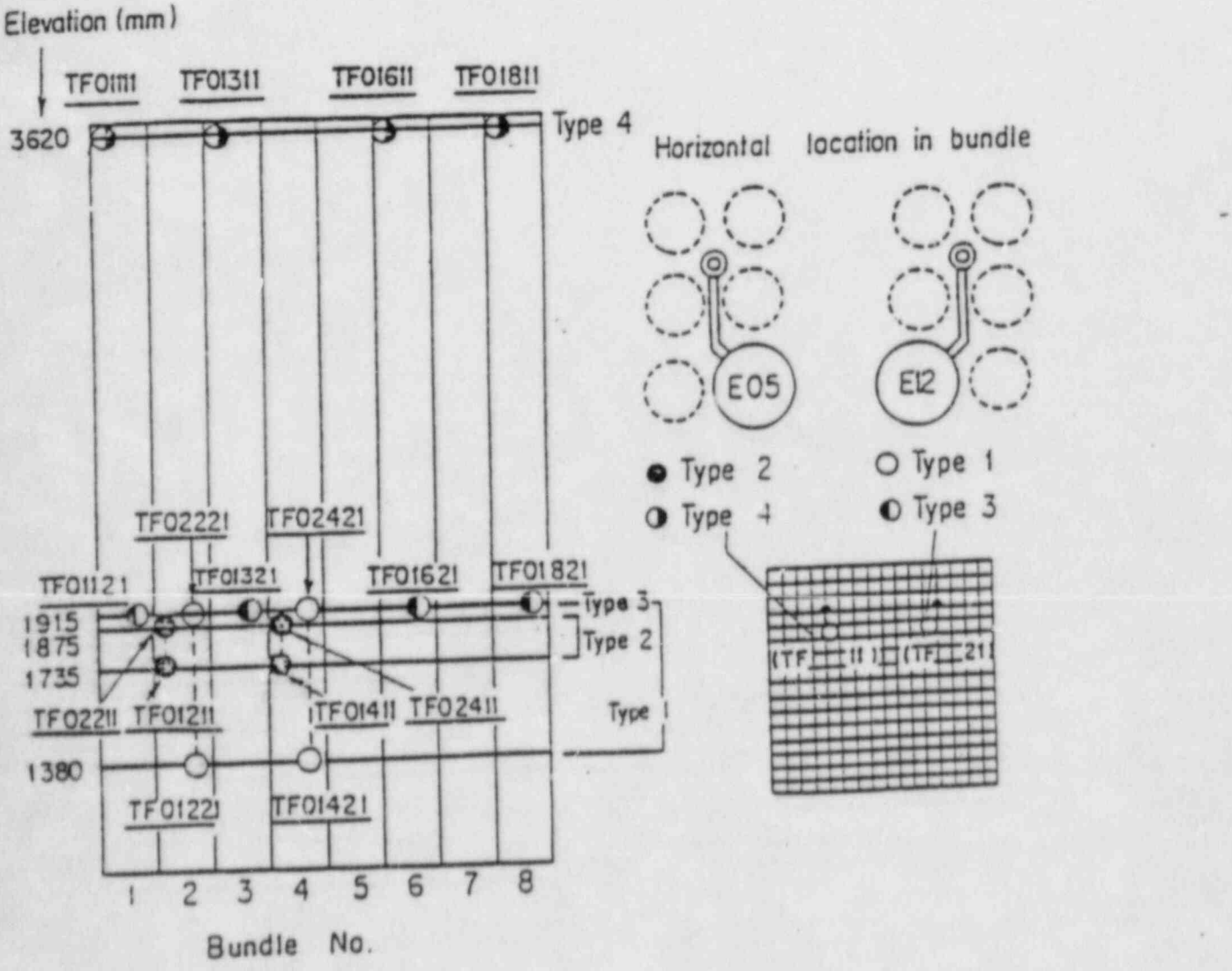

Fig. A-19 Thermocouple Locations of Steam Temperature Measurements in Core

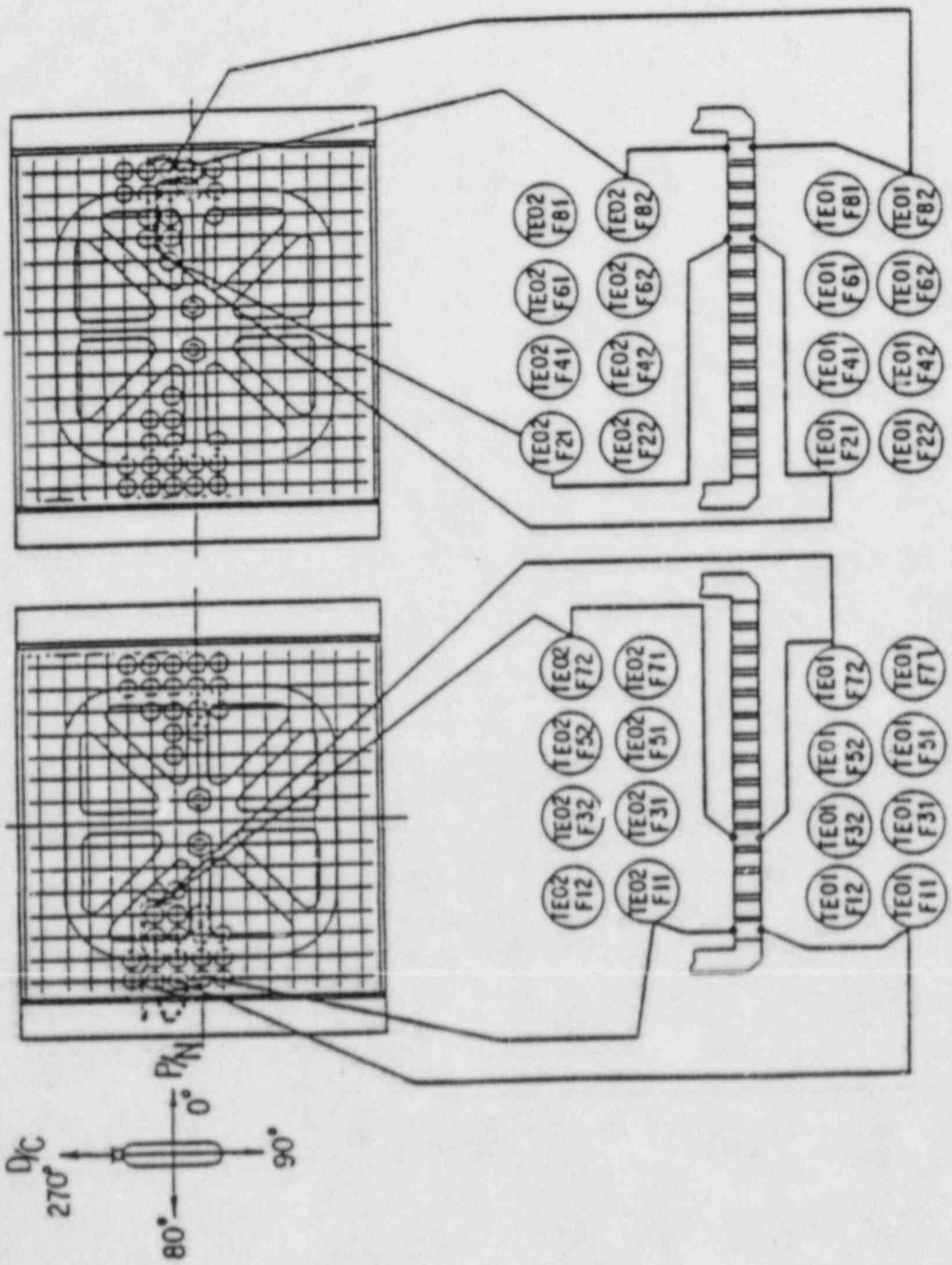

Fig. A-20 Thermocouple Locations of Fluid Temperature Measurements Just above and below End Box Tie Plate

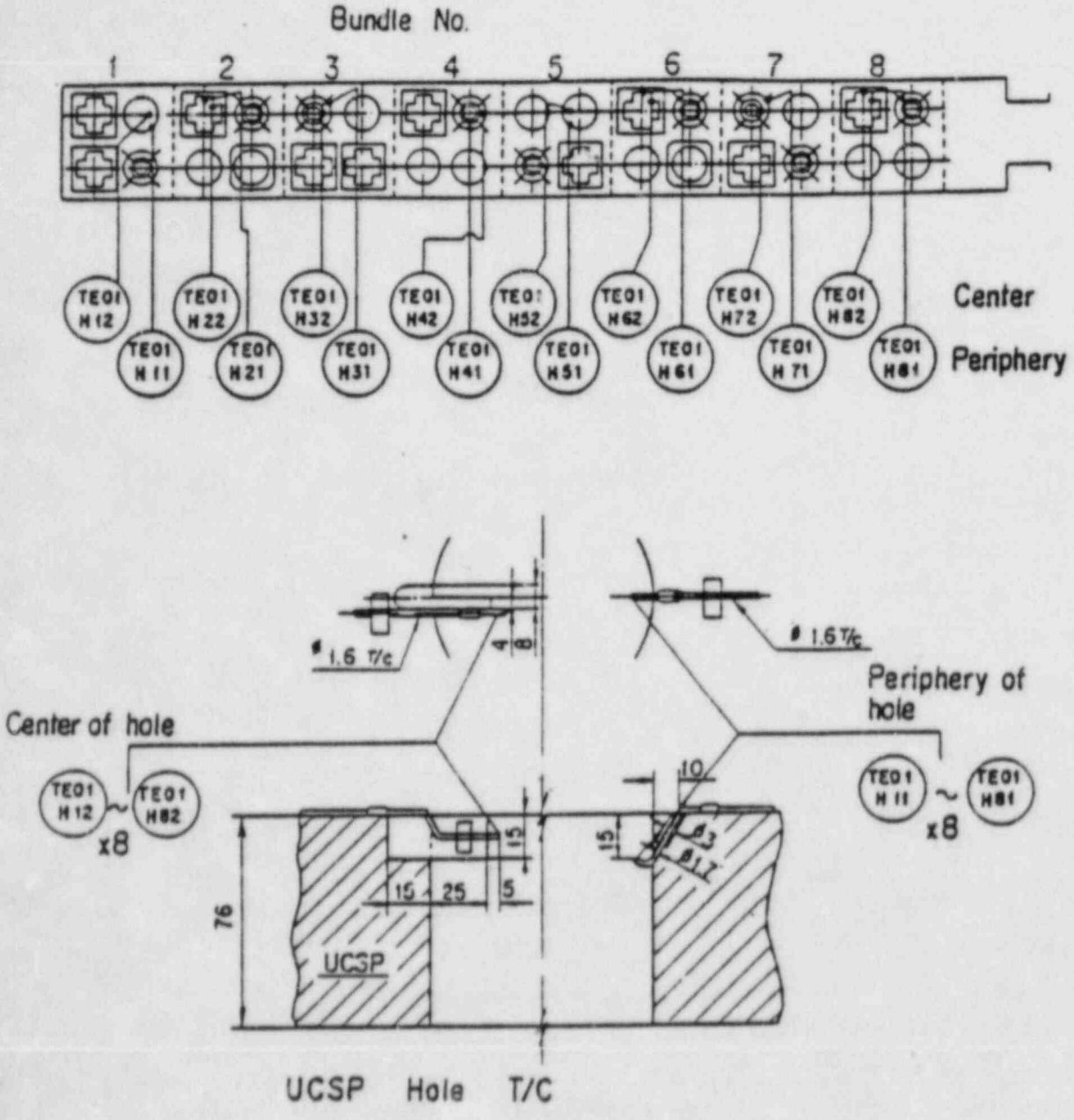

Fig. A-21 Thermocouple Locations of Fluid Temperature Measurements at Center and Periphery of UCSP Holes

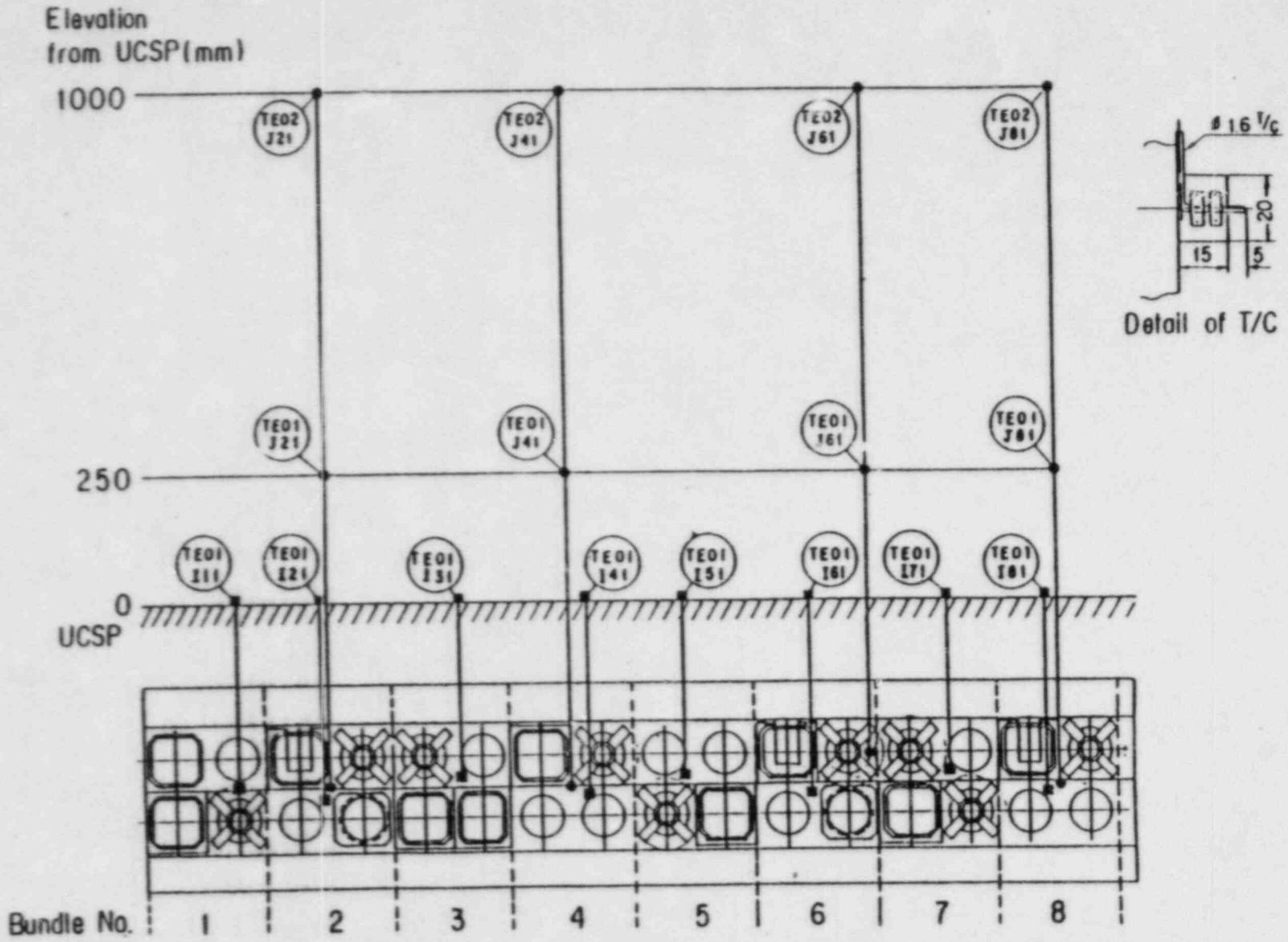

Fig. A-22 Thermocouple Locations of Fluid Temperature Measurements on and above UCSP

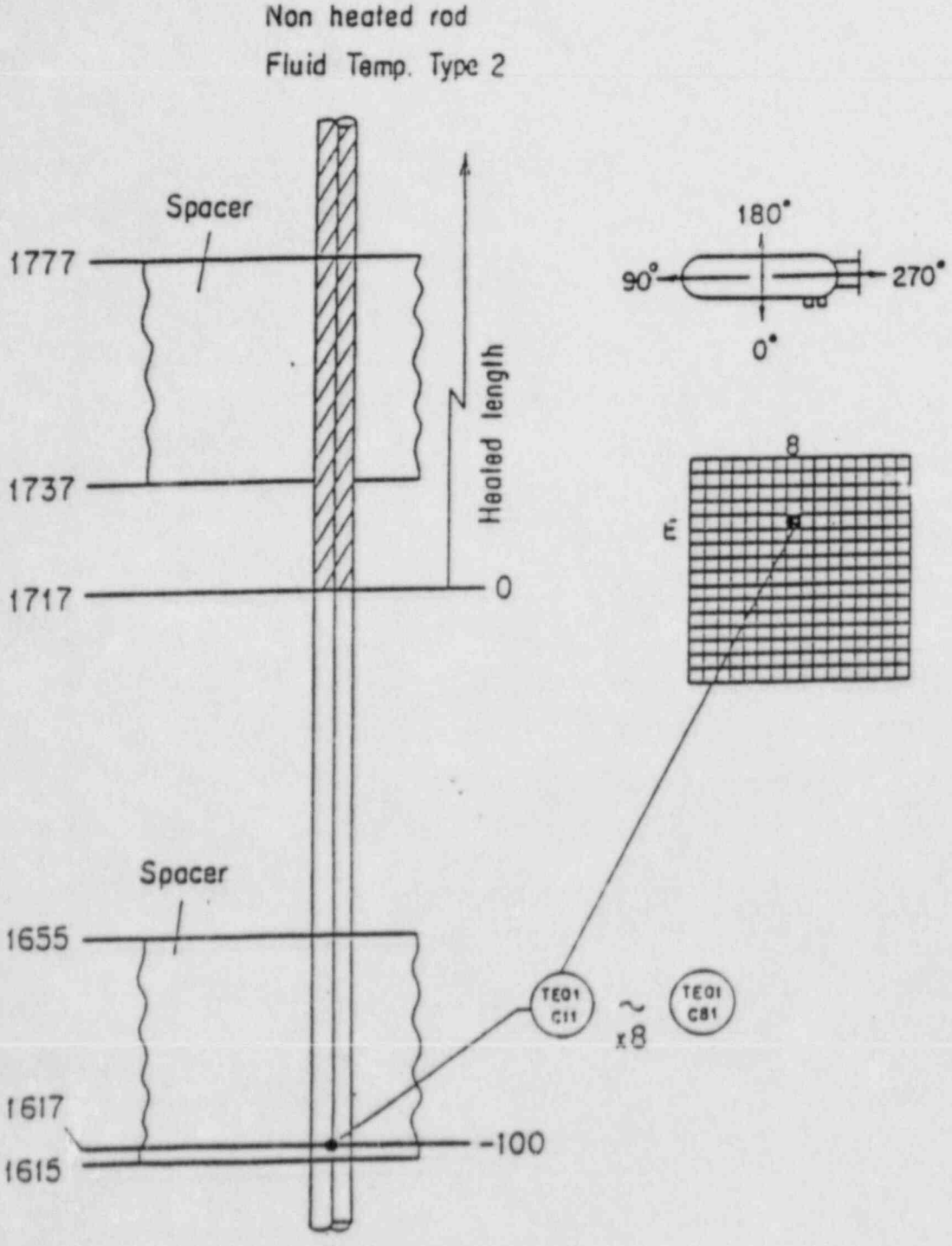

Fig. A-23 Thermocouple Locations of Fluid Temperature Measurements at Core Inlet

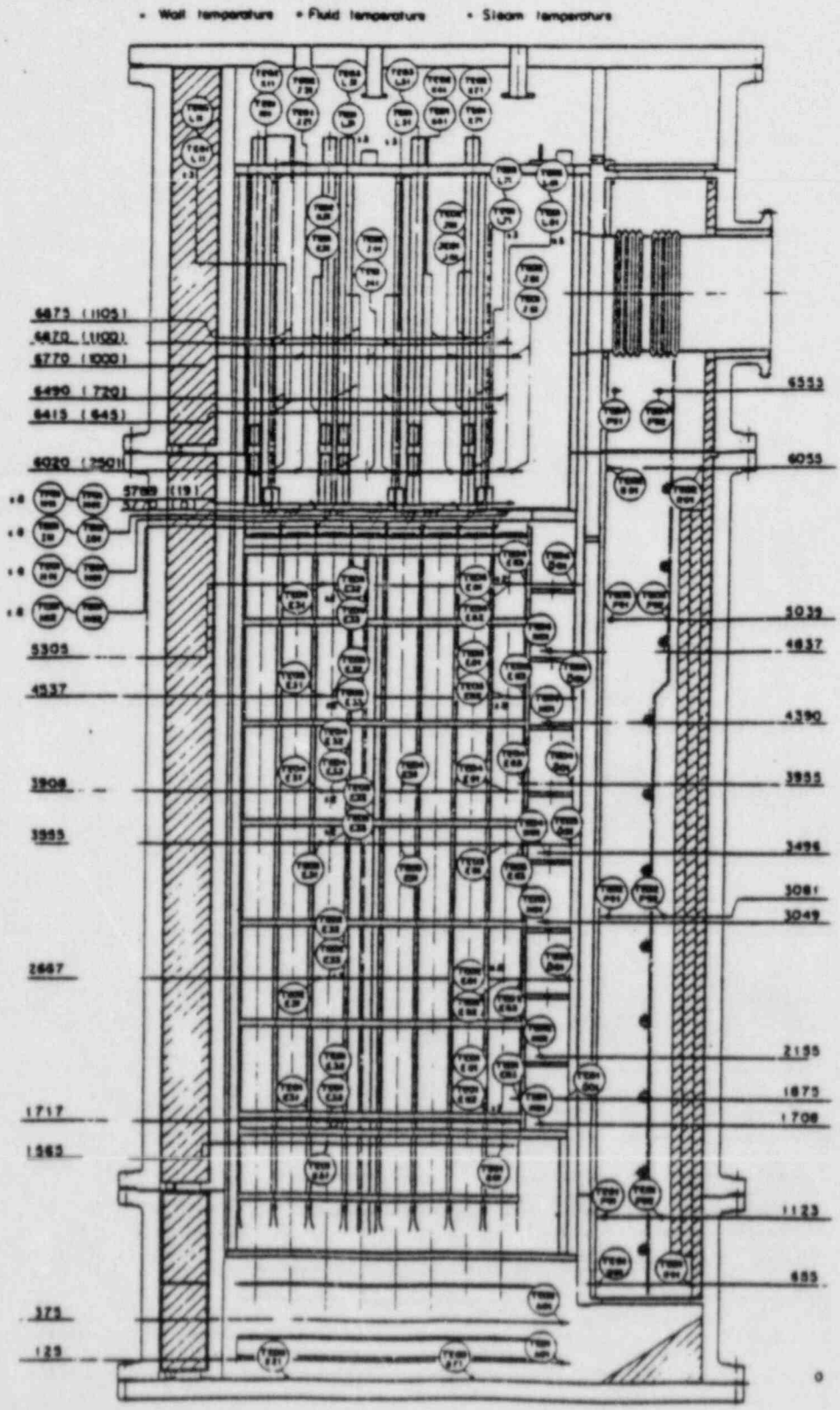

Fig. A-24 Thermocouple Locations of Temperature Measurements in Pressure Vessel except Core Region (Vertical View)

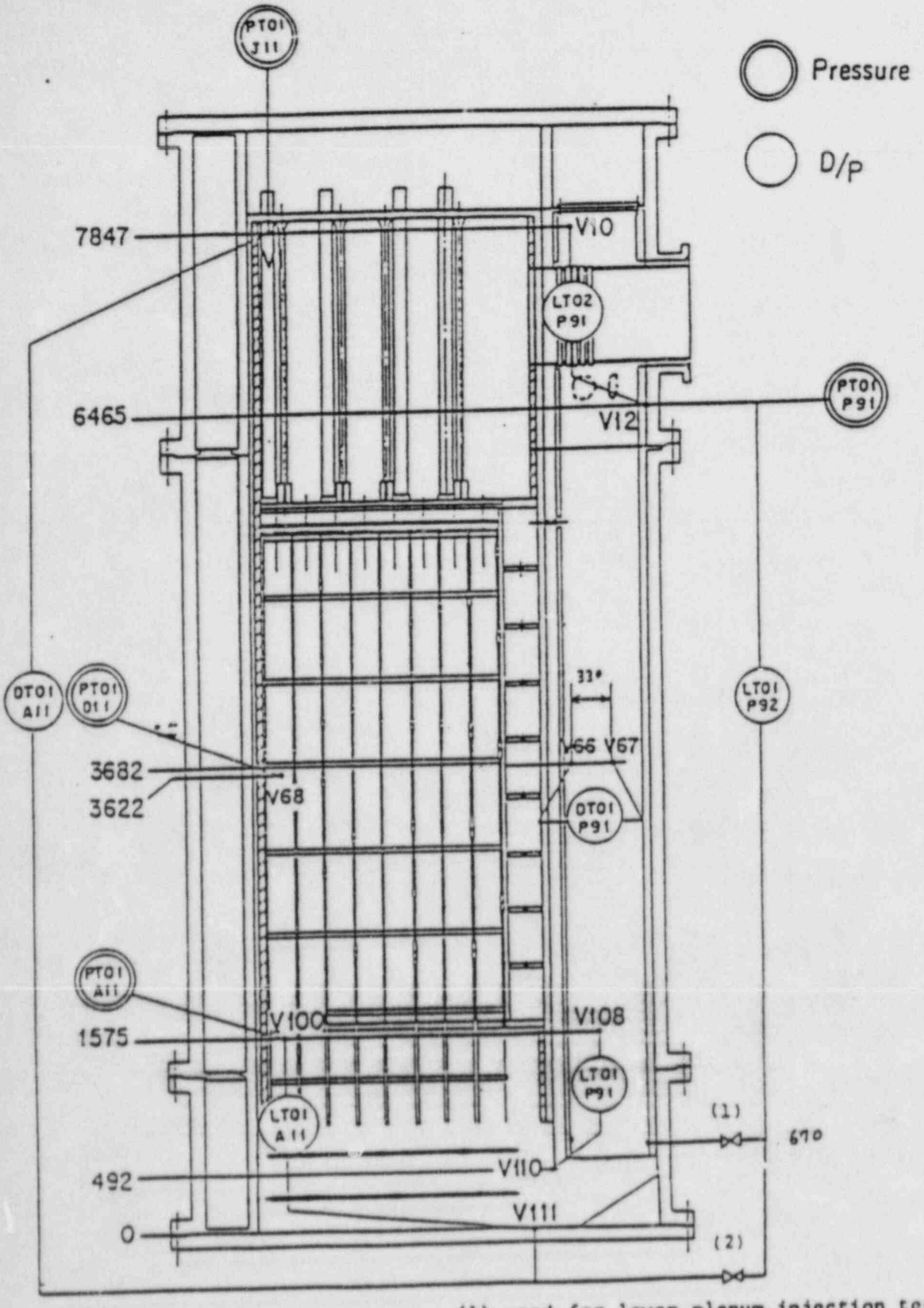

(1) used for lower plenum injection test
(the bottom of downcomer is blocked)
(2) used for the other tests

Fig. A-25 Location of Pressure Measurements in Pressure Vessel, Differential Pressure Measurements between Upper and Lower Plenums and Liquid Level Measurements in Downcomer and Lower Plenum

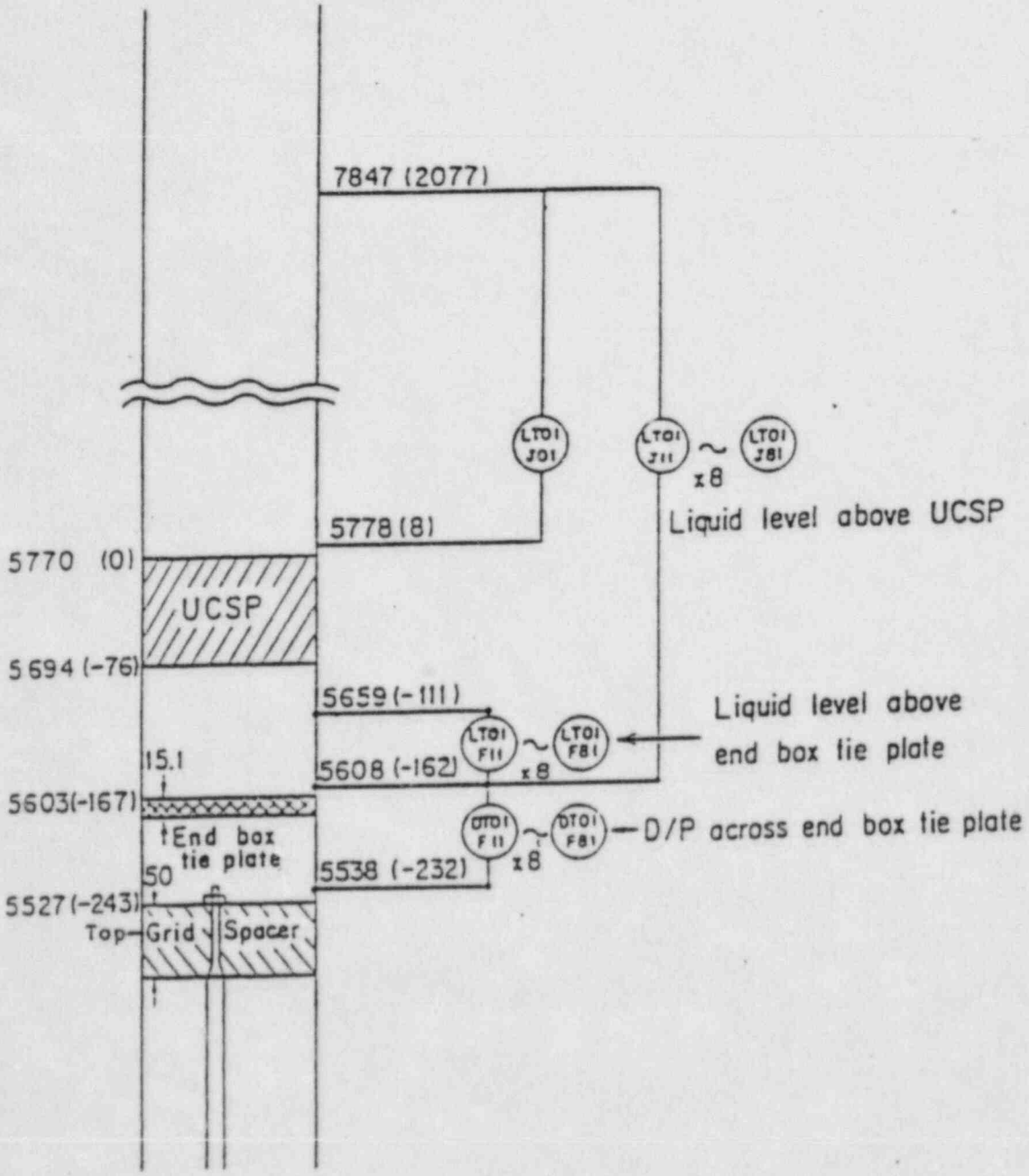

Fig. A-26 Locations of Differential Pressure Measurements across End Box Tie Plate and Liquid Level Measurements above UCSP and End Box Tie Plate

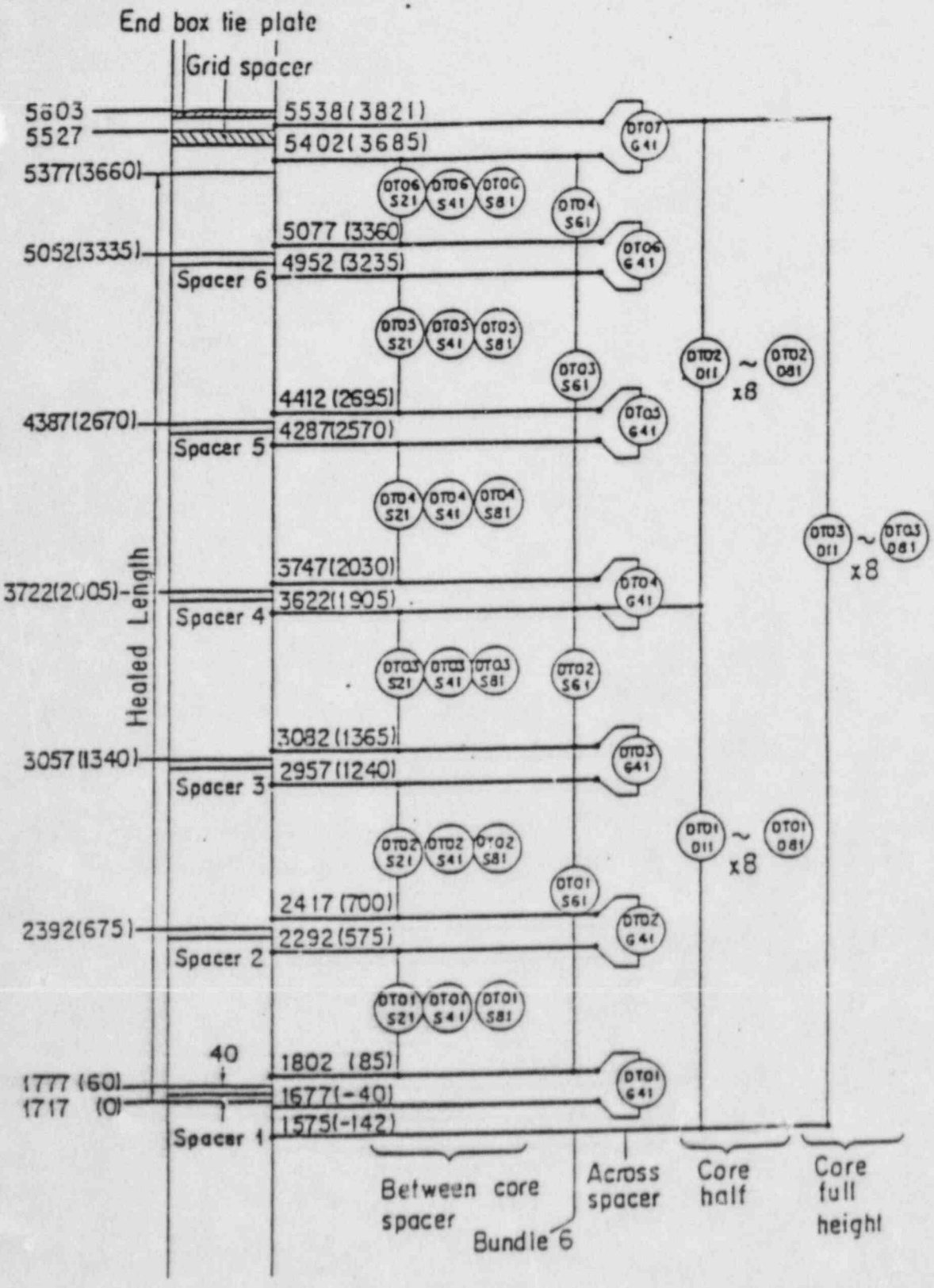

Fig. A-27 Locations of Vertical Differential Pressure Measurements in Core

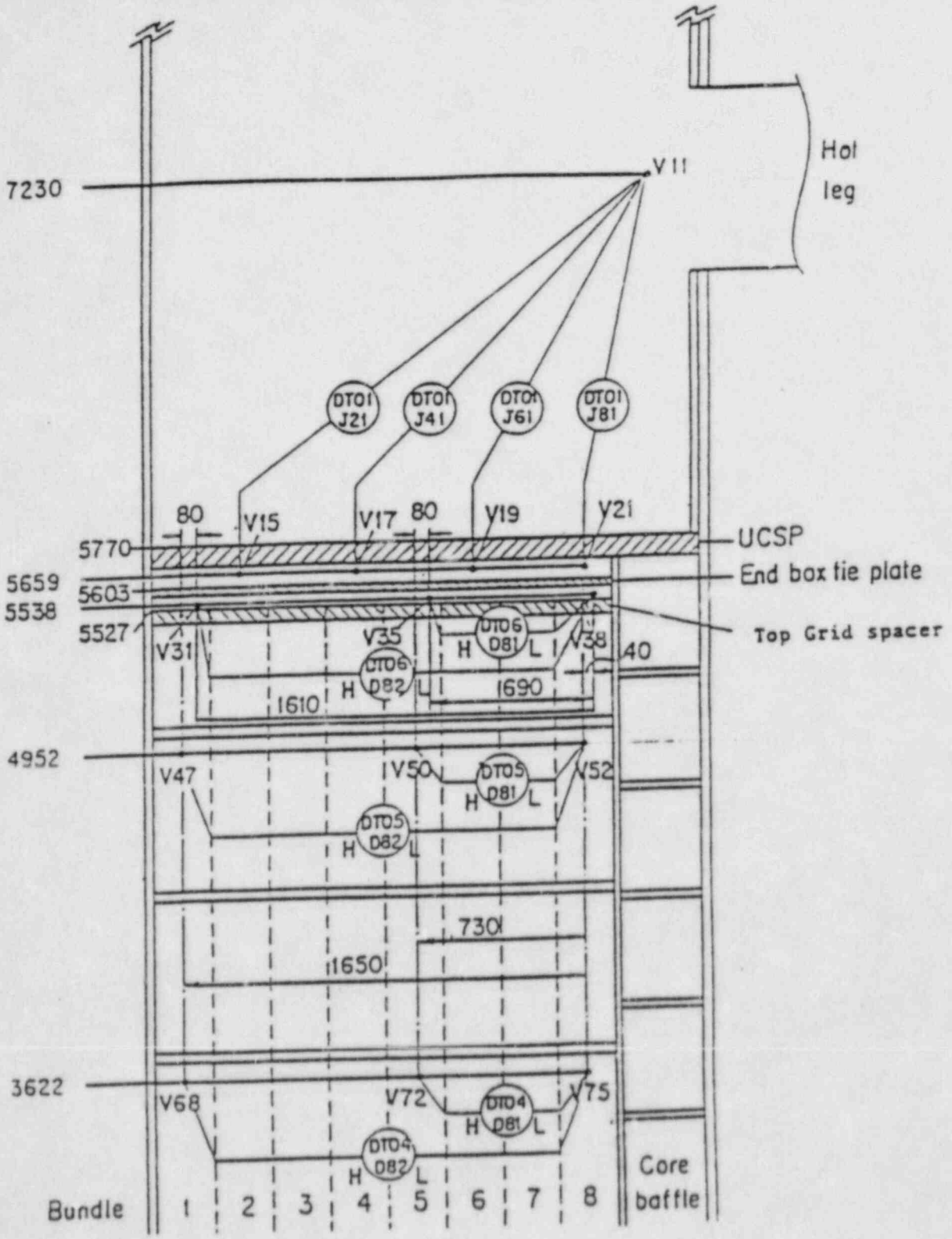

Fig. A-28 Locations of Horizontal Differential Pressure Measurements in Core and Differential Pressure Measurements between End Box and Inlet of Hot Leg

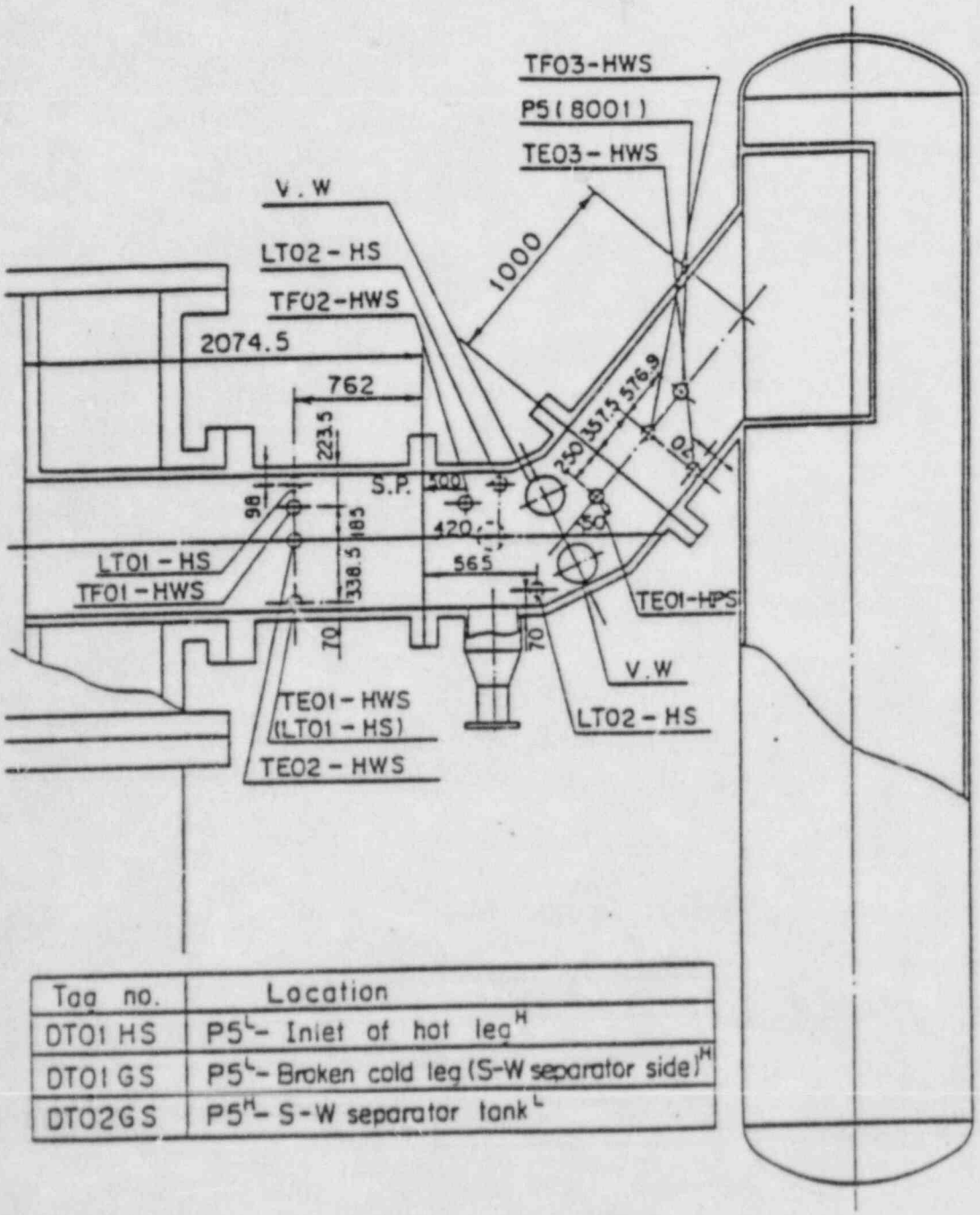

Tag no.	Location
DT01 HS	P5[L]- Inlet of hot leg[H]
DT01 GS	P5[L]- Broken cold leg (S-W separator side)[H]
DT02GS	P5[H]- S-W separator tank[L]

Fig. A-29 Locations of Hot Leg Instrumentation

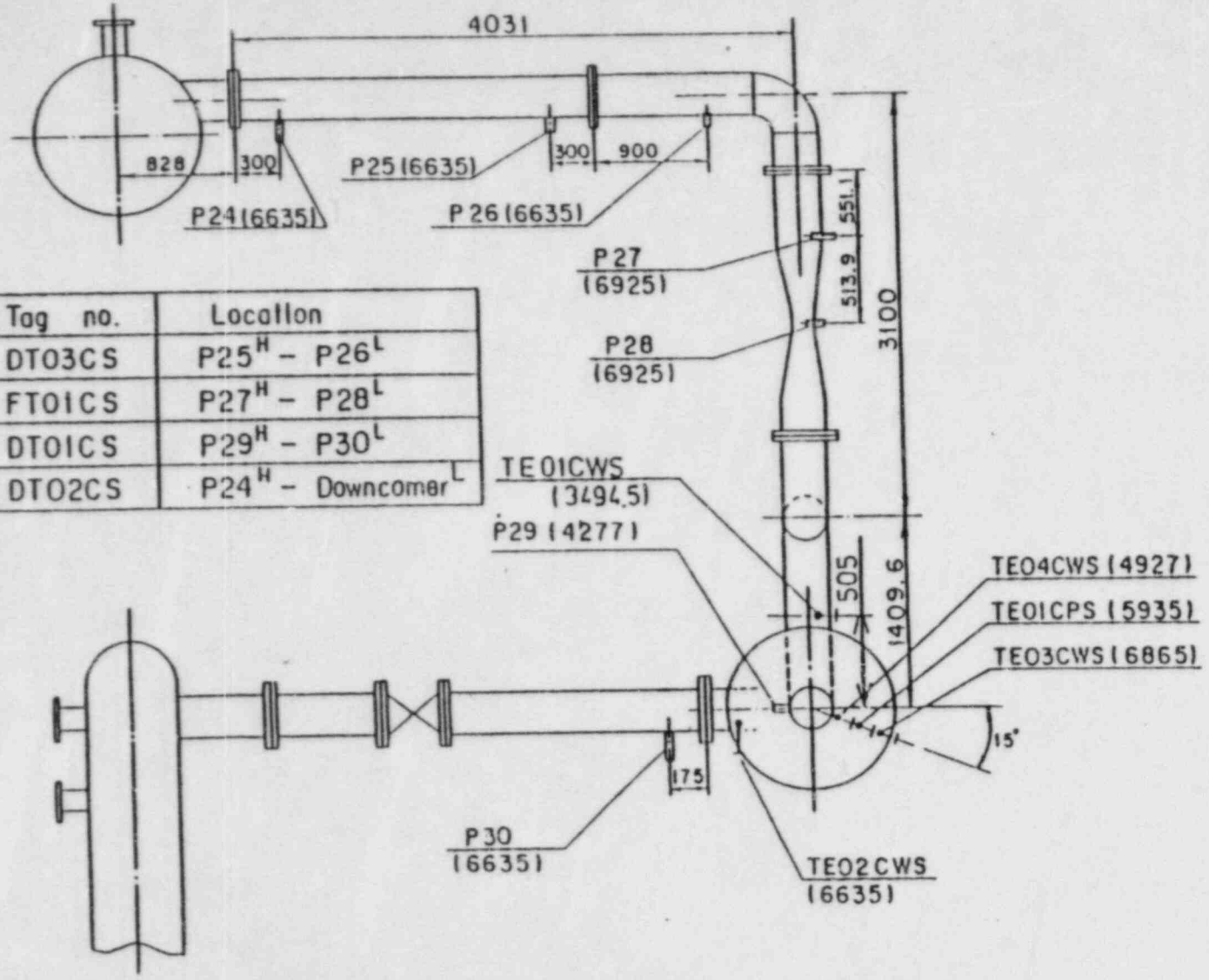

Tag no.	Location
DT03CS	$P25^{H} - P26^{L}$
FT01CS	$P27^{H} - P28^{L}$
DT01CS	$P29^{H} - P30^{L}$
DT02CS	$P24^{H} - \text{Downcomer}^{L}$

Fig. A-30 Locations of Intact Cold Leg Instrumentation

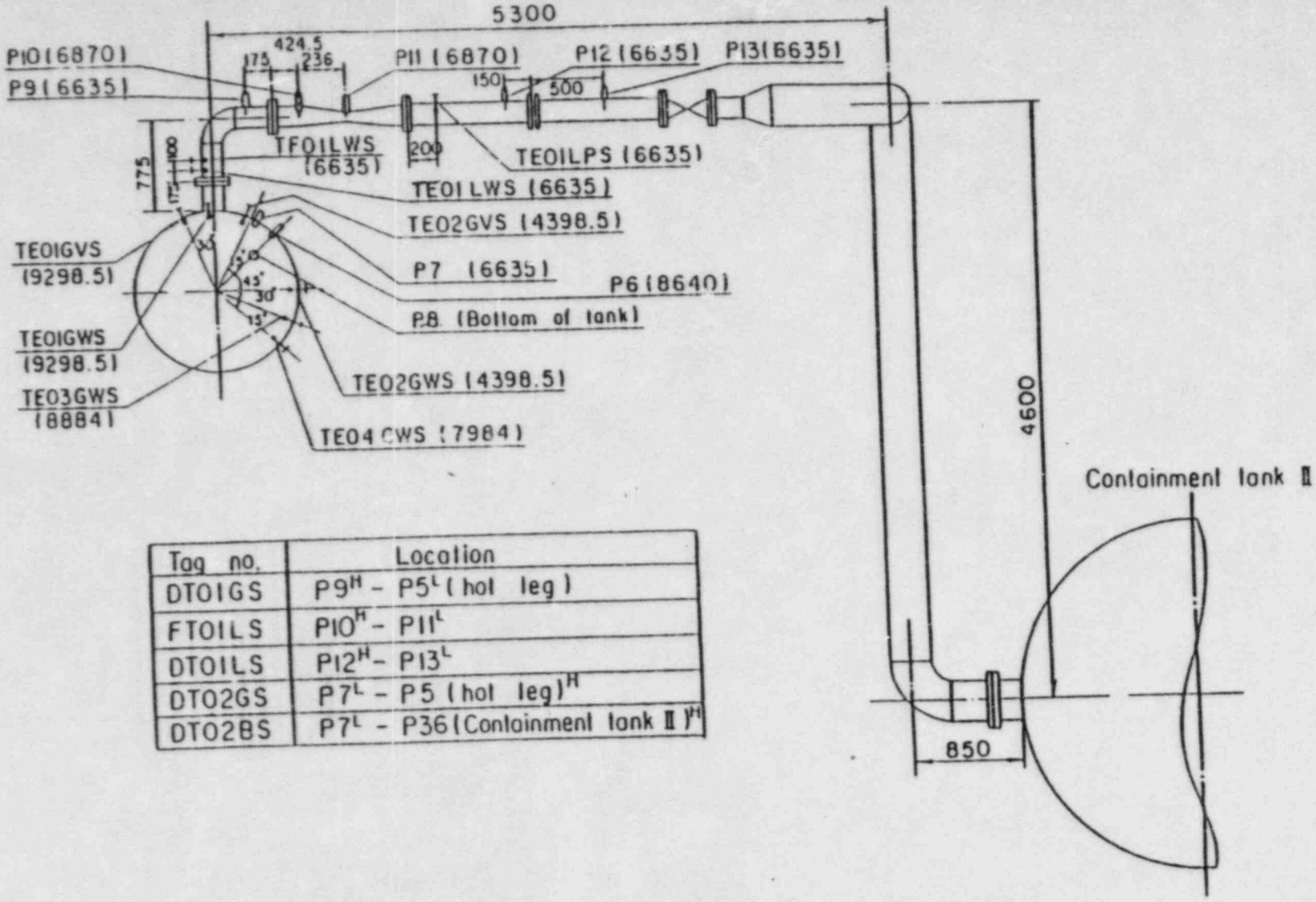

Tag no.	Location
DT01GS	$P9^{H}$ - $P5^{L}$ (hot leg)
FT01LS	$P10^{H}$ - $P11^{L}$
DT01LS	$P12^{H}$ - $P13^{L}$
DT02GS	$P7^{L}$ - P5 (hot leg)^{H}
DT02BS	$P7^{L}$ - P36 (Containment tank II)^{H}

Fig. A-31 Measurement Location of Steam/Water Separator Side Broken Cold Leg

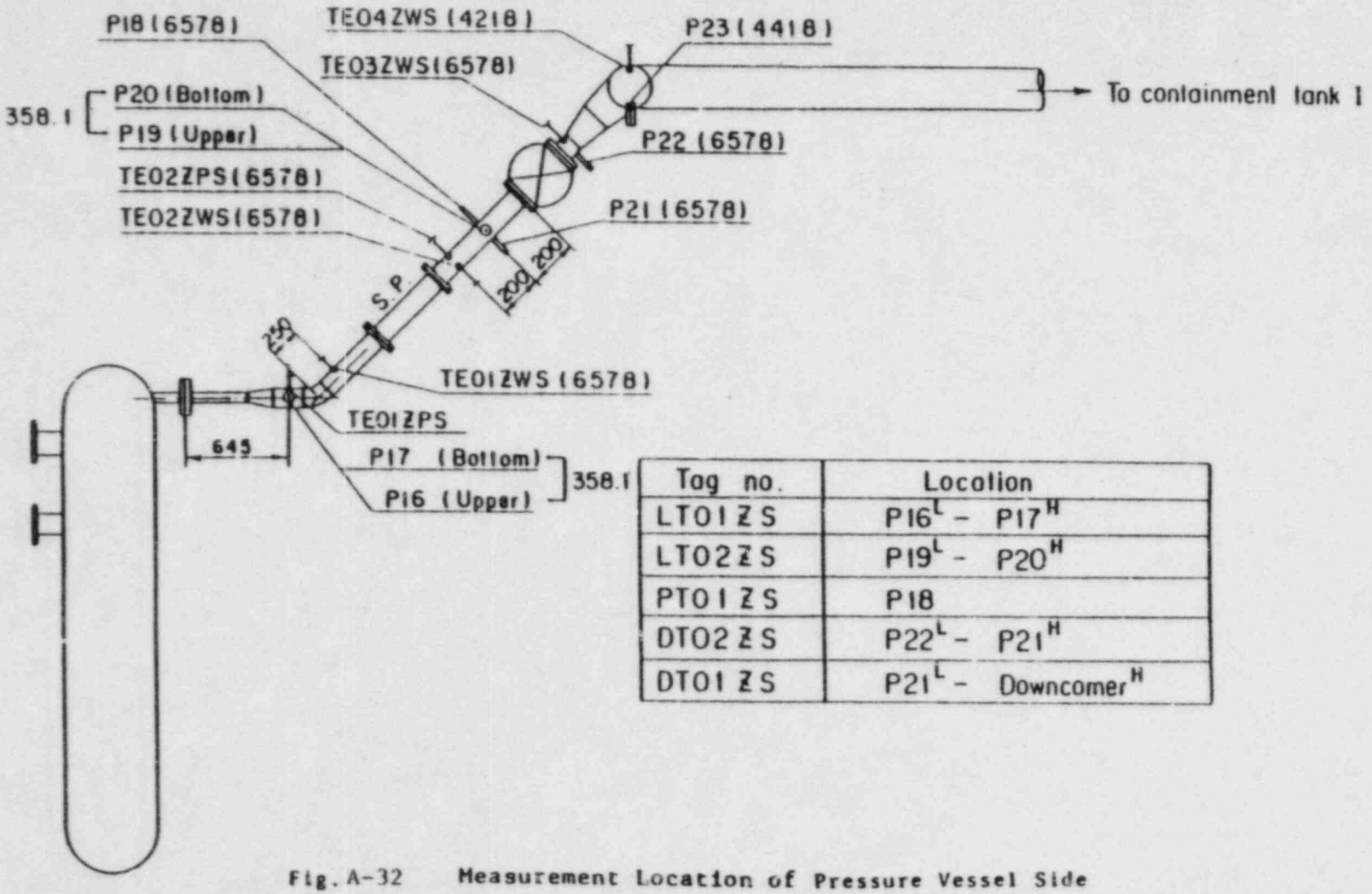

Tag no.	Location
LT01ZS	$P16^{L}$ - $P17^{H}$
LT02ZS	$P19^{L}$ - $P20^{H}$
PT01ZS	P18
DT02ZS	$P22^{L}$ - $P21^{H}$
DT01ZS	$P21^{L}$ - Downcomer^{H}

Fig. A-32 Measurement Location of Pressure Vessel Side Broken Cold Leg

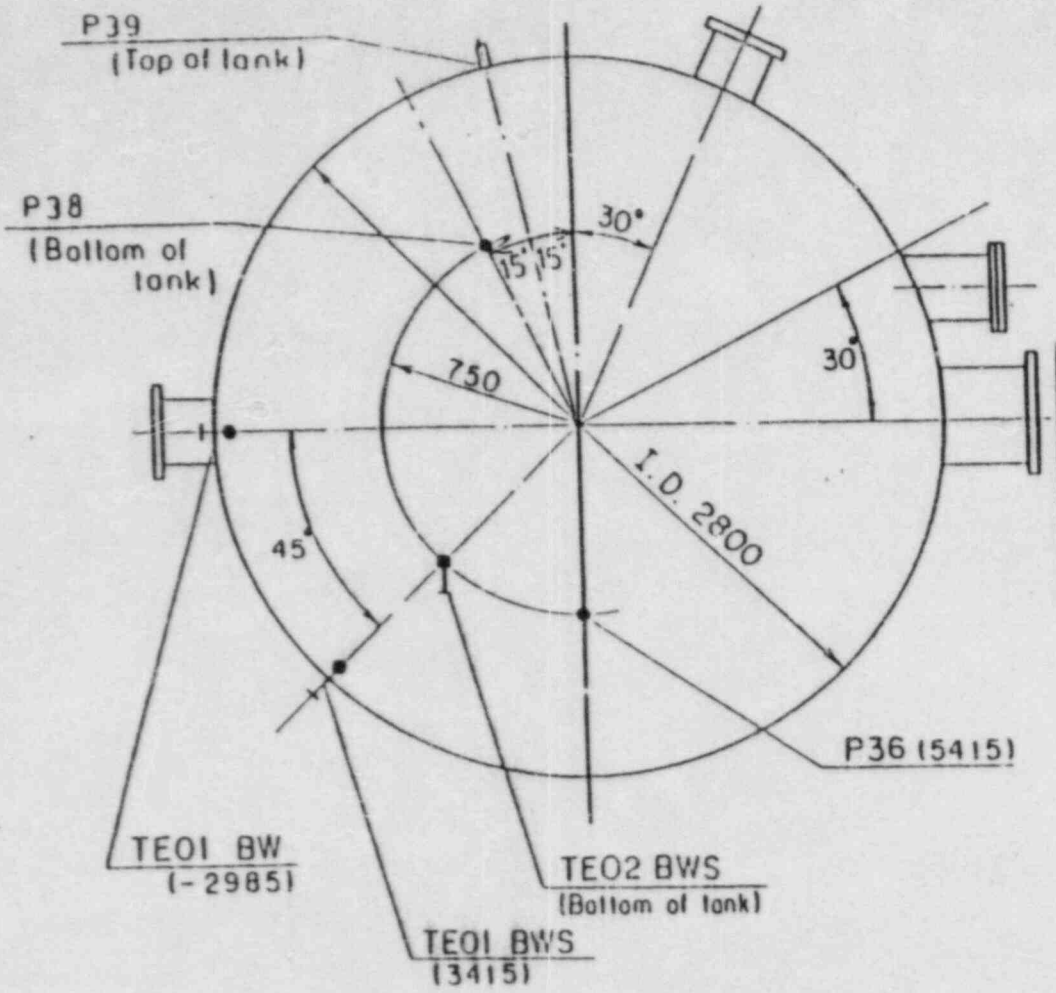

Tag no.	Location
DT01 BS	$P36^{H}$ – Upper plenum^{L}
DT02 BS	$P36^{H}$ – S-W Separator^{L}
DT01 E	$P36^{L}$ – P35 (C.T.I)^{H}
PT01 B	P36
LT01 1B	$P38^{H}$ – $P39^{L}$

Fig. A-33 Locations of Containment Tank-II Instrumentation

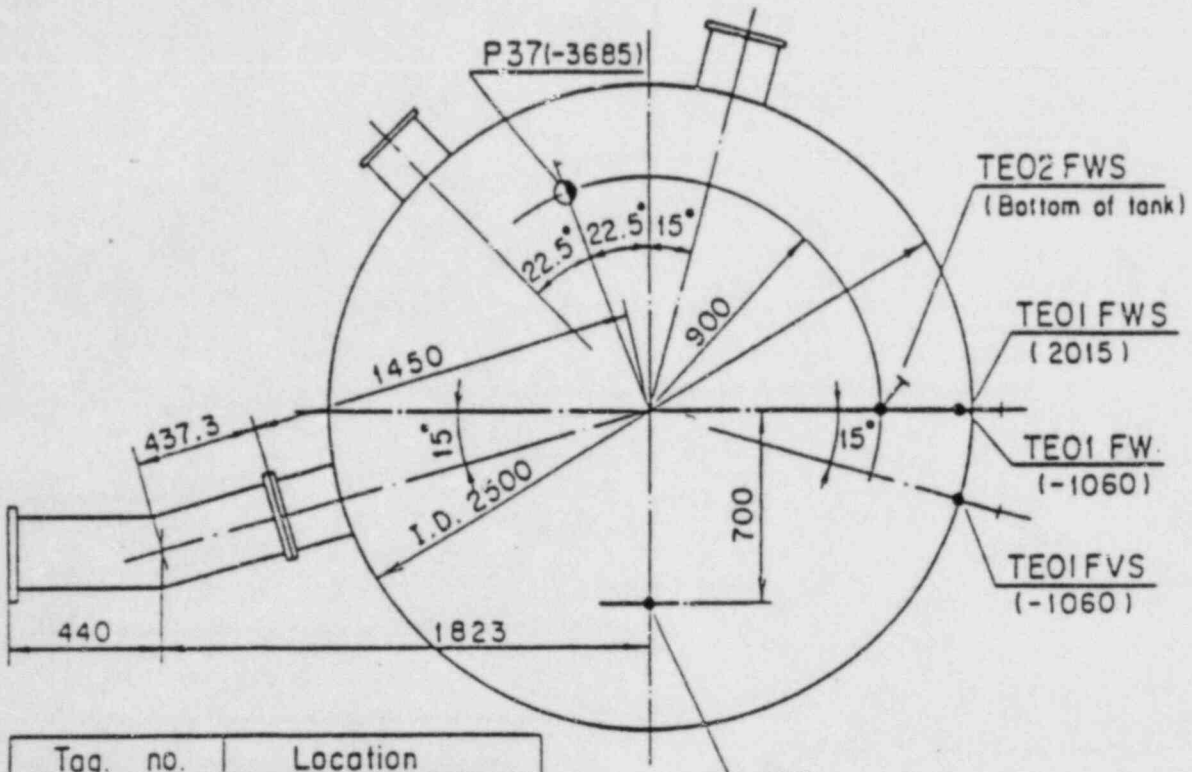

Tag. no.	Location
LT01 FS	$P35^{L}$ – $P37^{H}$
DT01 FS	$P35^{H}$ – $Downcomer^{L}$
DT01E	$P35^{H}$ – P36(C.T. II)^{H}
PT01F	P35

Fig. A-34 Locations of Containment Tank-I Instrumentation

Appendix B Selected Data of Test S1-SH3 (Run 528)

Fig. No.	Measurement item
B-1 ∿ B-16	Heater rod temperature
B-17 ∿ B-20	Fluid temperature in core
B-21 ∿ B-22	Steam temperature in core
B-23 ∿ B-24	Fluid temperature just above end box tie plate
B-25 ∿ B-28	Fluid temperature in UCSP holes
B-29 ∿ B-30	Fluid temperature on UCSP surface
B-31 ∿ B-32	Fluid temperature above UCSP
B-33 ∿ B-34	Fluid temperature at core inlet
B-35	Fluid temperature in downcomer
B-36	Fluid temperature in hot leg
B-37	Fluid temperature in intact cold leg
B-38	Fluid temperature in broken cold leg (steam/water separator side)
B-39	Fluid temperature in broken cold leg (PV side)
B-40	Liquid level in downcomer
B-41 ∿ B-42	Liquid level above end box tie plate
B-43 ∿ B-44	Liquid level above UCSP
B-45	Liquid level in hot leg
B-46	Liquid level in broken cold leg (PV side)
B-47 ∿ B-48	Differential pressure of core full height
B-49 ∿ B-50	Differential pressure across end box the plate
B-51 ∿ B-52	Horizontal differential pressure in core
B-53	Differential pressure of hot leg
B-54	Differential pressure across steam/water separator
B-55	Differential pressure of intact cold leg
B-56	Differential pressure between steam/water separator and containment tank-II
B-57	Differential pressure between top of upper plenum and containment tank-II
B-58	Differential pressure between containment tanks I and II
B-59	Differential pressure of broken cold leg (PV side)
B-60	Pressures in pressure vessel
B-61, B-62	Bundle powers
B-63	ECC injection rate into intact cold leg
B-64	ECC injection rate into upper plenum
B-65 ∿ B-70	Void fractions in core

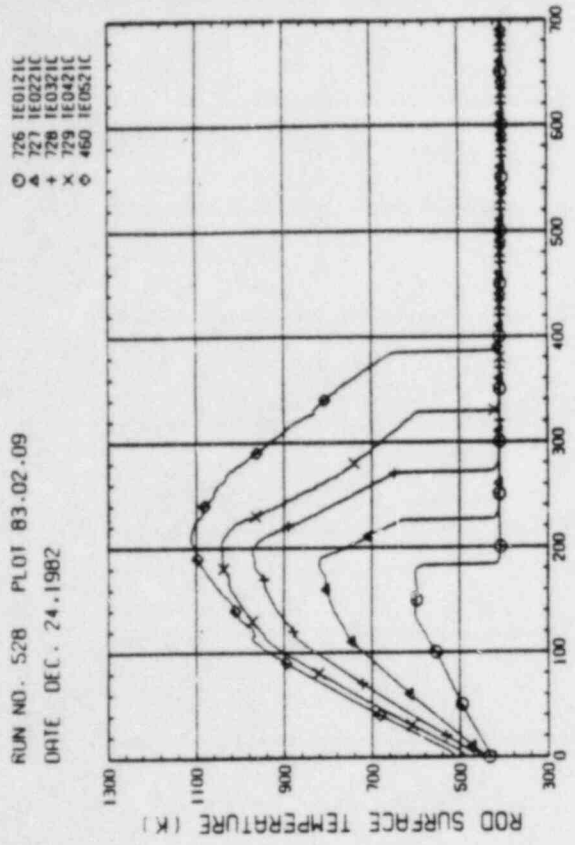

Fig. B-1 HEATER ROD TEMPERATURE (BUNDLE 1-1C, LOWER HALF)

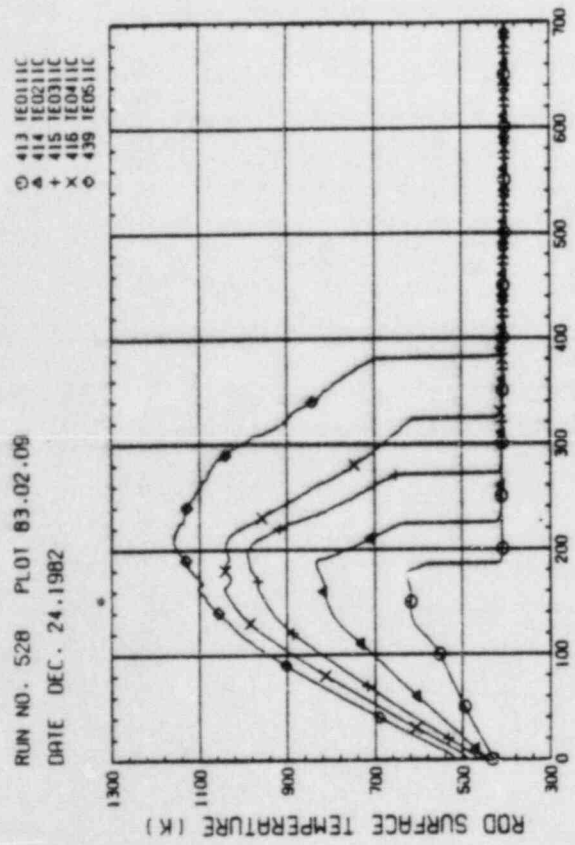

Fig. B-2 HEATER ROD TEMPERATURE (BUNDLE 1-1C, UPPER HALF)

Fig. B-3 HEATER ROD TEMPERATURE (BUNDLE 2-1C, LOWER HALF)

Fig. B-4 HEATER ROD TEMPERATURE (BUNDLE 2-1C, UPPER HALF)

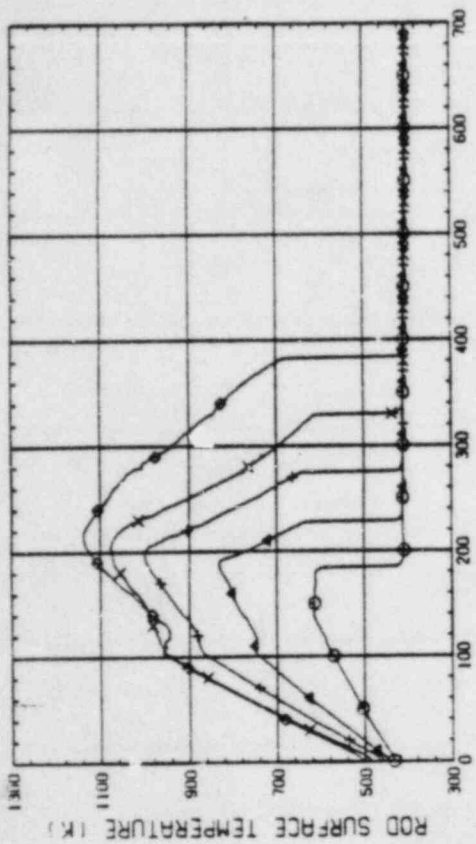

Fig. B-5 HEATER ROD TEMPERATURE (BUNDLE 3-1C, LOWER HALF)

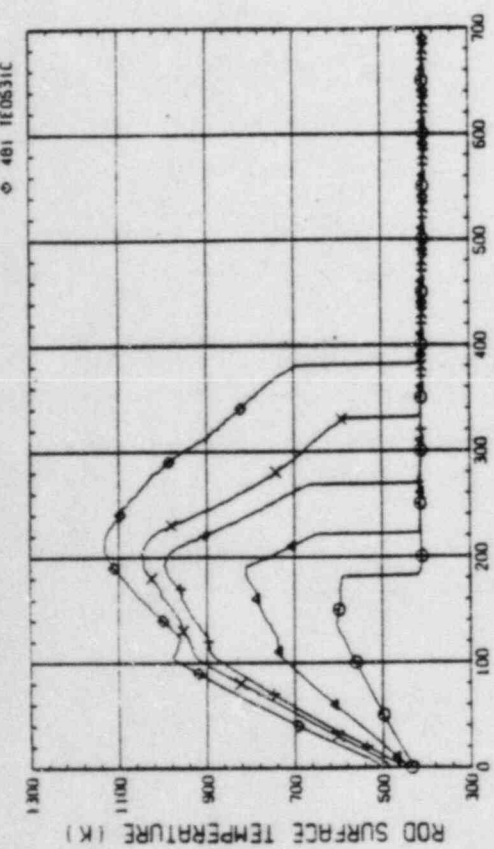

Fig. B-6 HEATER ROD TEMPERATURE (BUNDLE 3-1C, UPPER HALF)

Fig. B-7 HEATER ROD TEMPERATURE (BUNDLE 4-1C, LOWER HALF)

Fig. B-8 HEATER ROD TEMPERATURE (BUNDLE 4-1C, UPPER HALF)

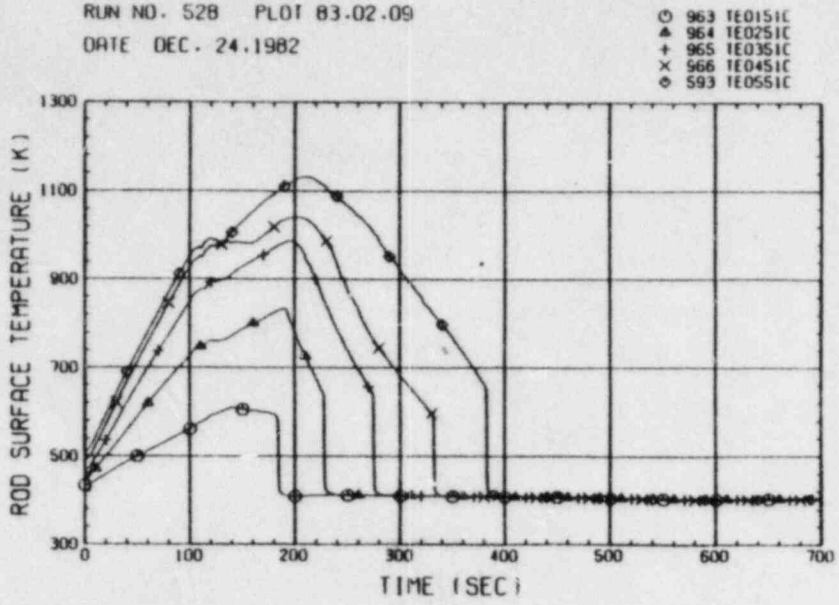

Fig. B-9 HEATER ROD TEMPERATURE (BUNDLE 5-1C, LOWER HALF)

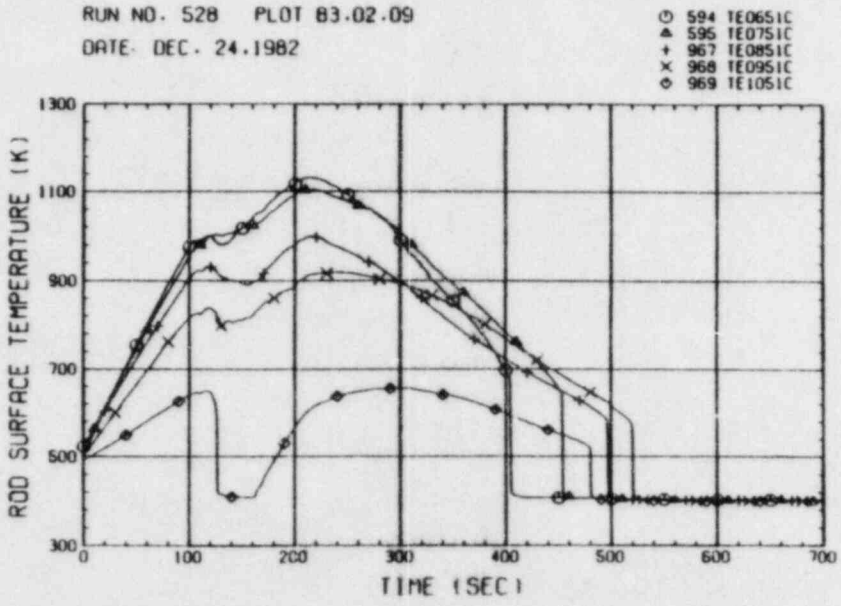

Fig. B-10 HEATER ROD TEMPERATURE (BUNDLE 5-1C, UPPER HALF)

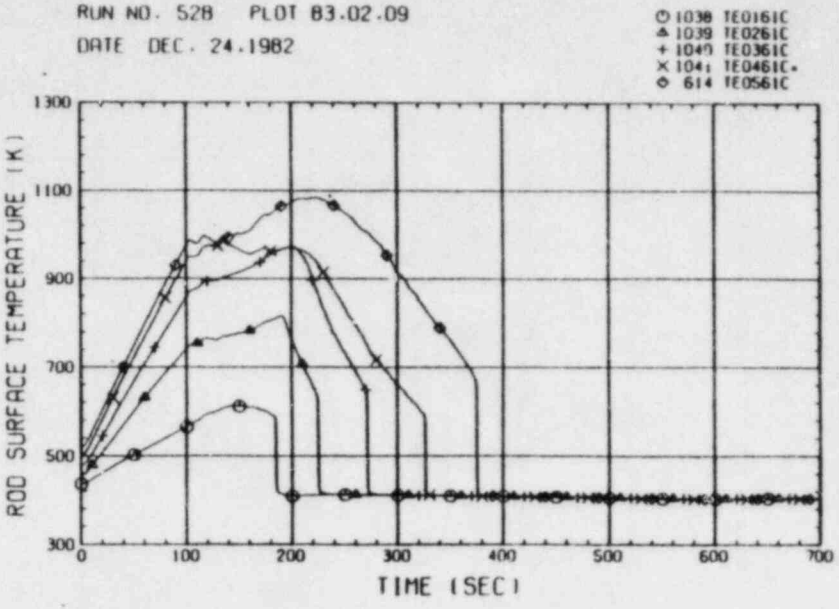

Fig. B-11 HEATER ROD TEMPERATURE (BUNDLE 6-1C, LOWER HALF)

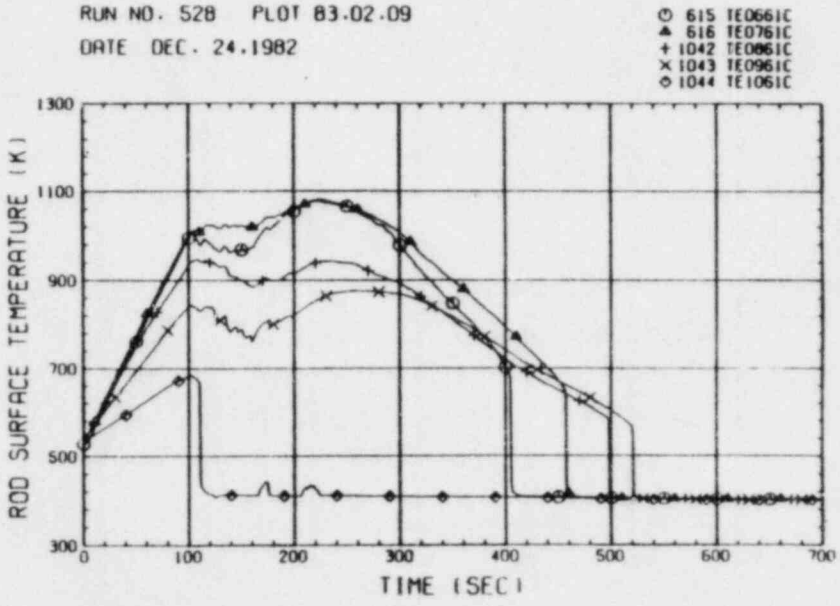

Fig. B-12 HEATER ROD TEMPERATURE (BUNDLE 6-1C, UPPER HALF)

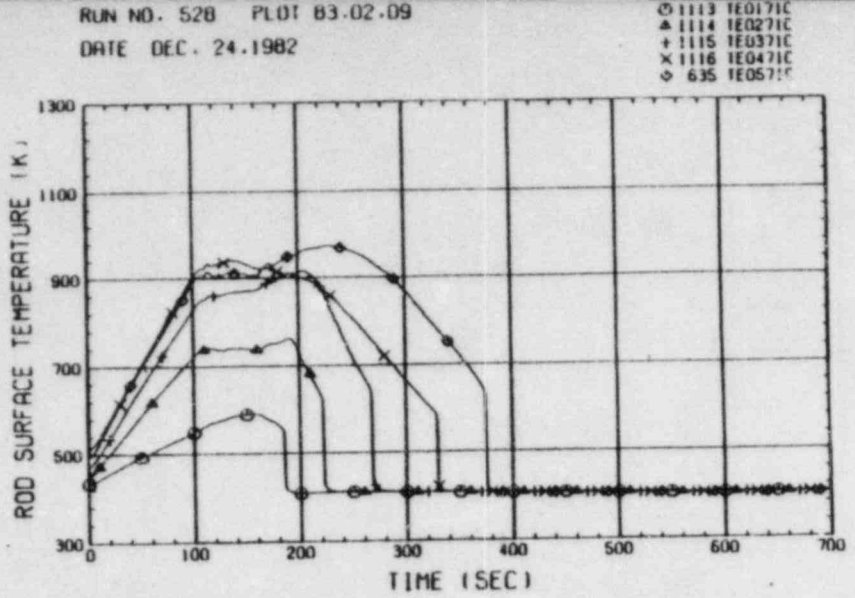

Fig. B-13 HEATER ROD TEMPERATURE (BUNDLE 7-1C, LOWER HALF)

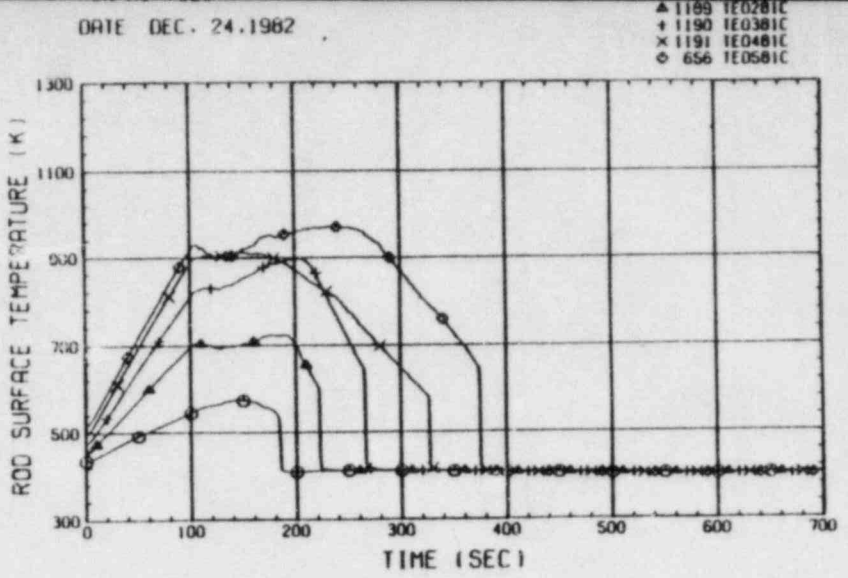

Fig. B-15 HEATER ROD TEMPERATURE (BUNDLE 8-1C, LOWER HALF)

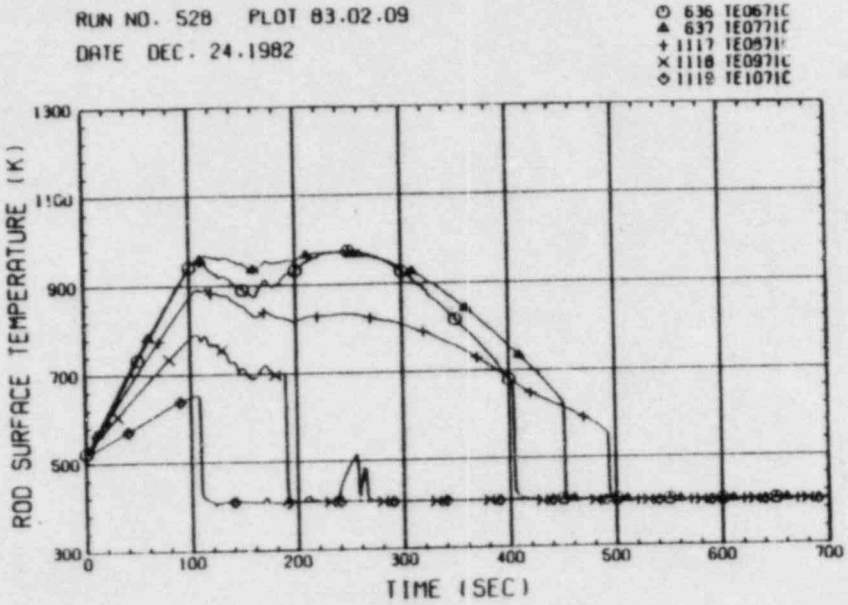

Fig. B-14 HEATER ROD TEMPERATURE (BUNDLE 7-1C, UPPER HALF)

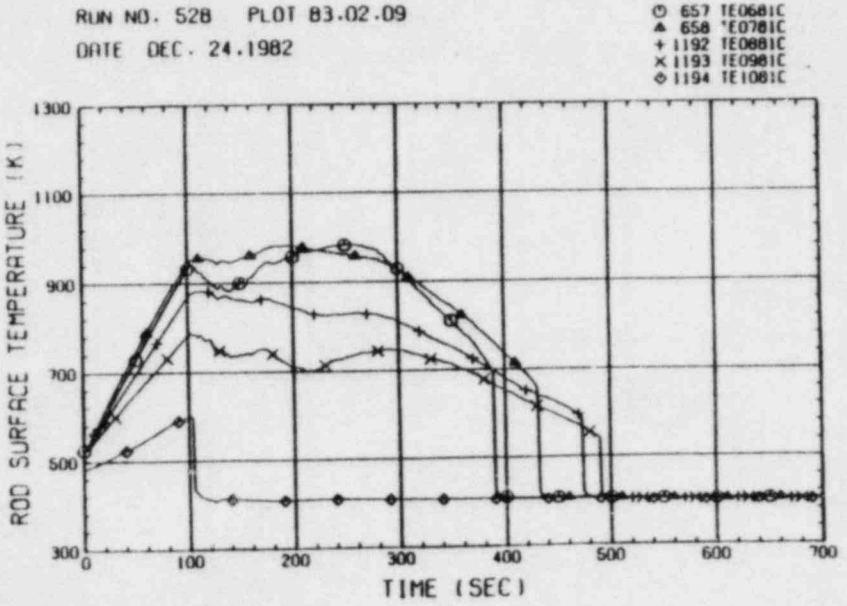

Fig. B-16 HEATER ROD TEMPERATURE (BUNDLE 8-1C, UPPER HALF)

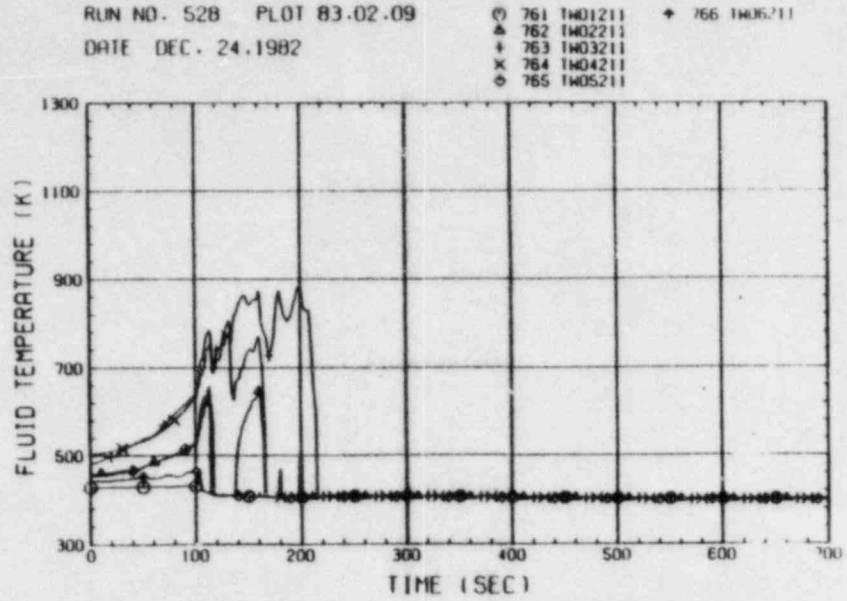

Fig. B-17 FLUID TEMPERATURE IN CORE (BUNDLE 2-1)

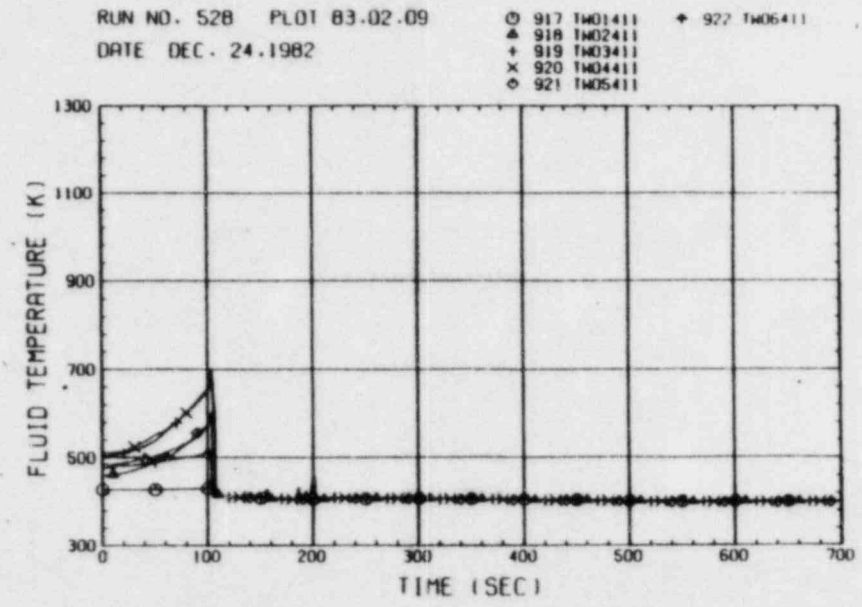

Fig. B-18 FLUID TEMPERATURE IN CORE (BUNDLE 4-1)

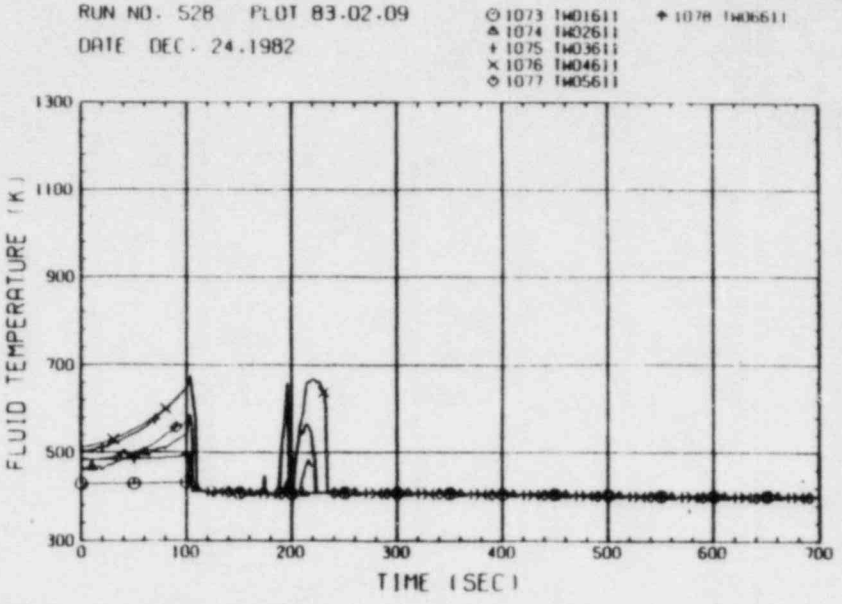

Fig. B-19 FLUID TEMPERATURE IN CORE (BUNDLE 6-1)

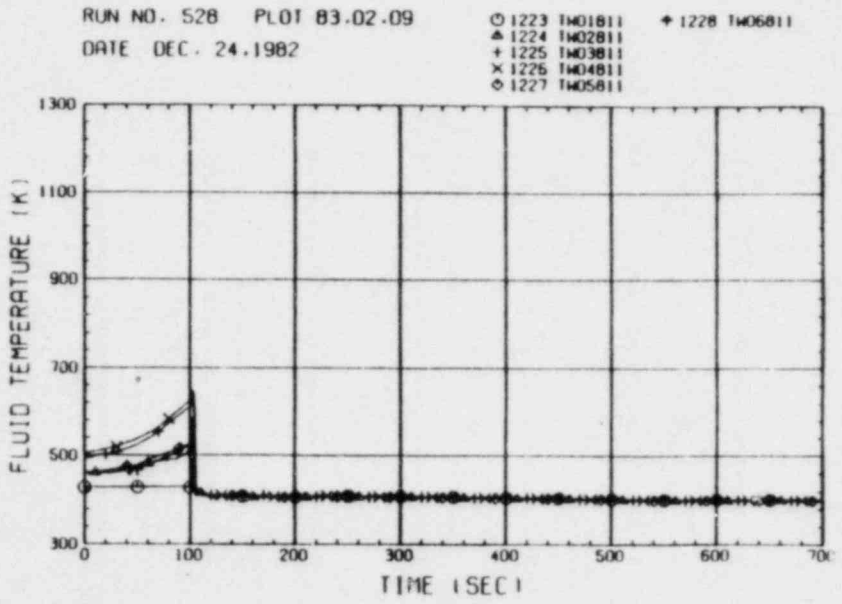

Fig. B-20 FLUID TEMPERATURE IN CORE (BUNDLE 8-1)

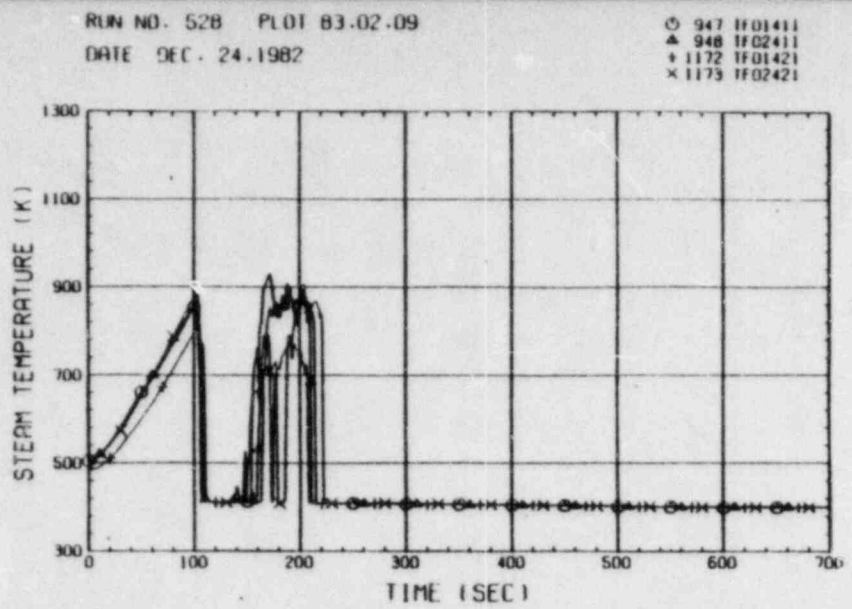

Fig. B-21 STEAM TEMPERATURE IN CORE, BUNDLE 4
(01411-1.735M, 02411-1.875M, 01421-1.38M, 02421-1.91[illegible])

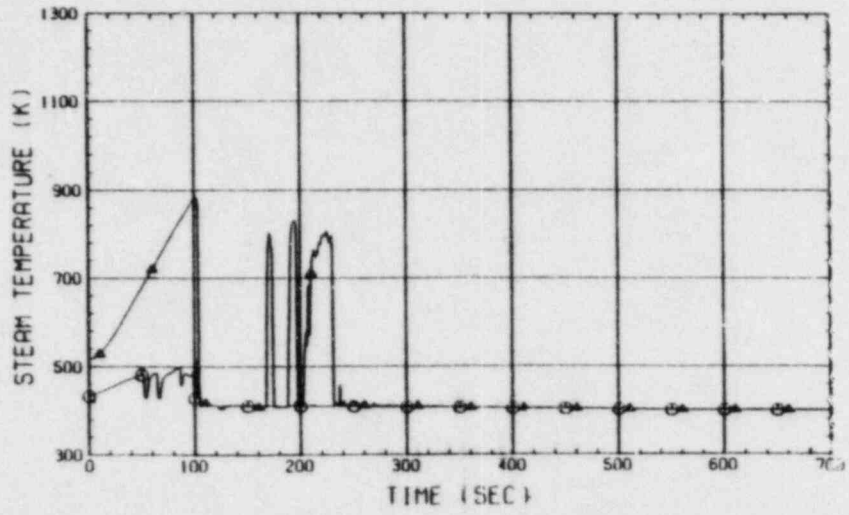

Fig. B-22 STEAM TEMPERATURE IN CORE, BUNDLE 6
(01611-3.62M, 01621-1.915M)

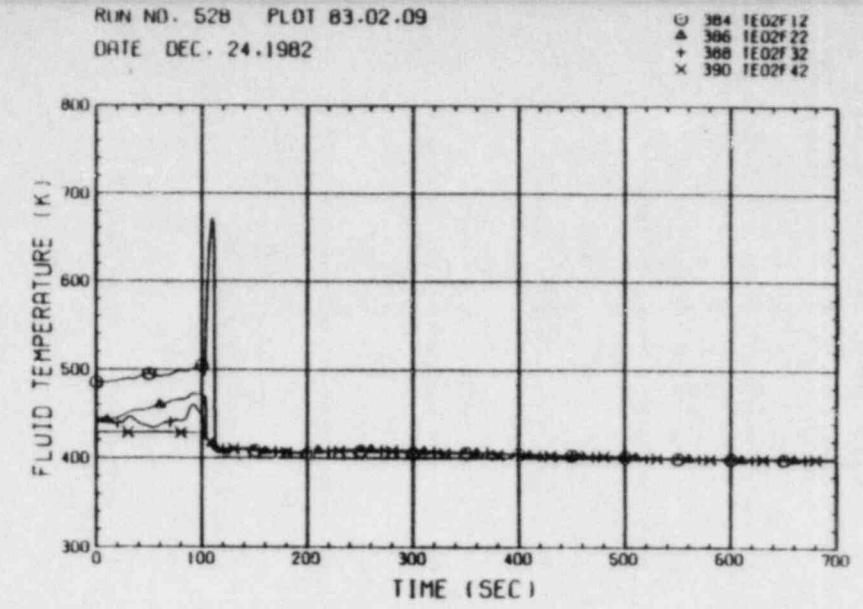

Fig. B-23 FLUID TEMPERATURE JUST ABOVE END BOX
(BUNDLE 1.2.3.4. COLD LEG SIDE)

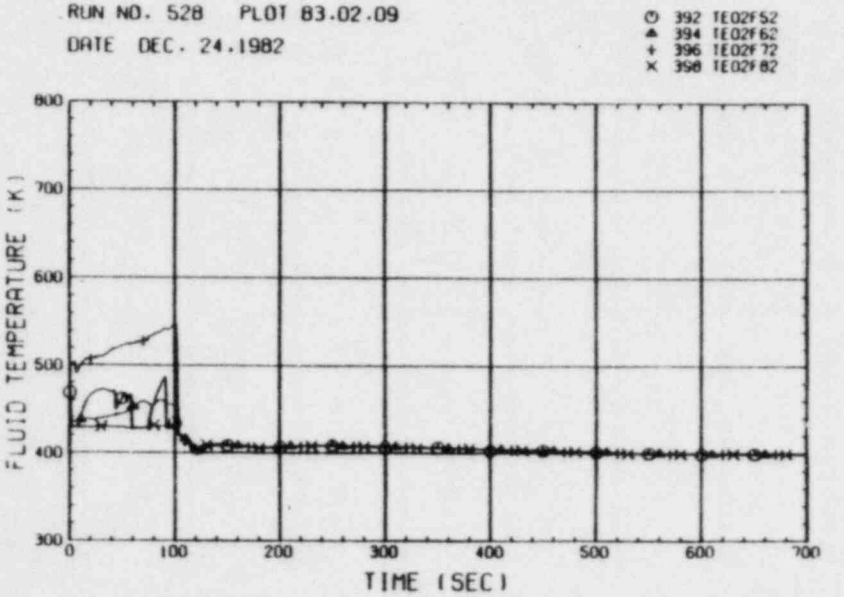

Fig. B-24 FLUID TEMPERATURE JUST ABOVE END BOX
(BUNDLE 5.6.7.8. COLD LEG SIDE)

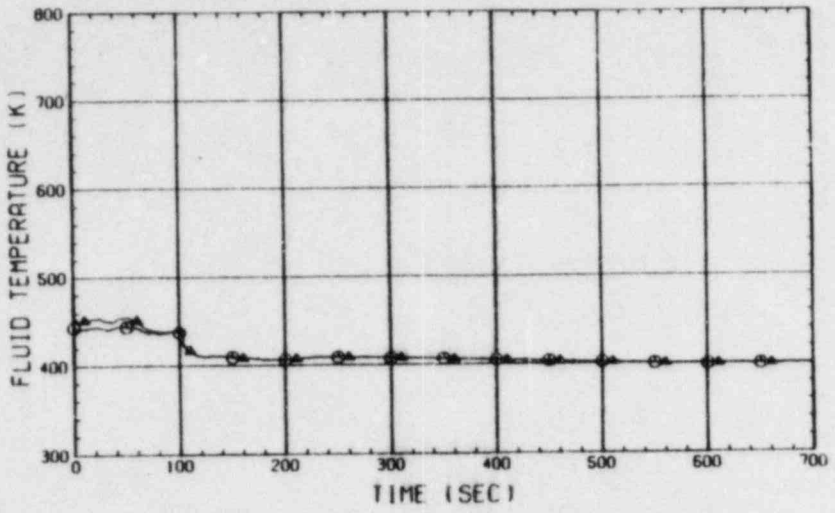

Fig. B-25 FLUID TEMPERATURE IN UCSP HOLE (BUNDLE 2. H21 - PERIPHERY. H22 - CENTER)

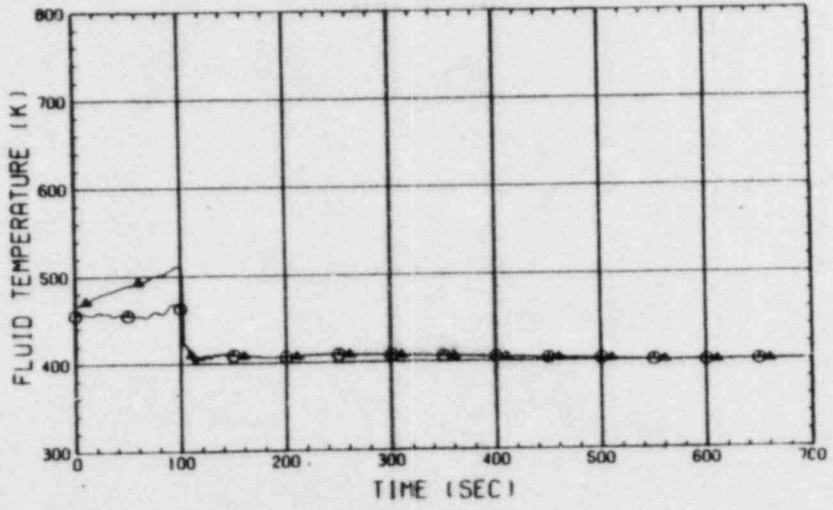

Fig. B-26 FLUID TEMPERATURE IN UCSP HOLE (BUNDLE 4. H41 - PERIPHERY. H42 - CENTER)

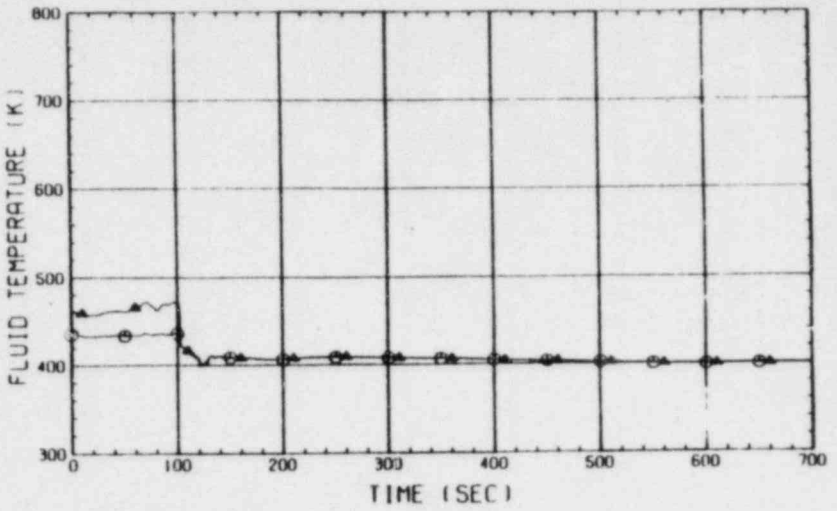

Fig. B-27 FLUID TEMPERATURE IN UCSP HOLE (BUNDLE 6. H61 - PERIPHERY. H62 - CENTER)

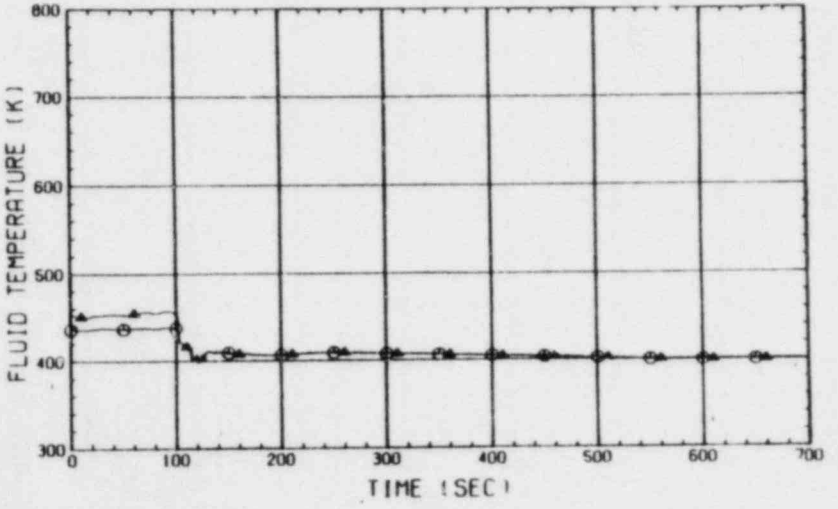

Fig. B-28 FLUID TEMPERATURE IN UCSP HOLE (BUNDLE 8. H81 - PERIPHERY. H82 - CENTER)

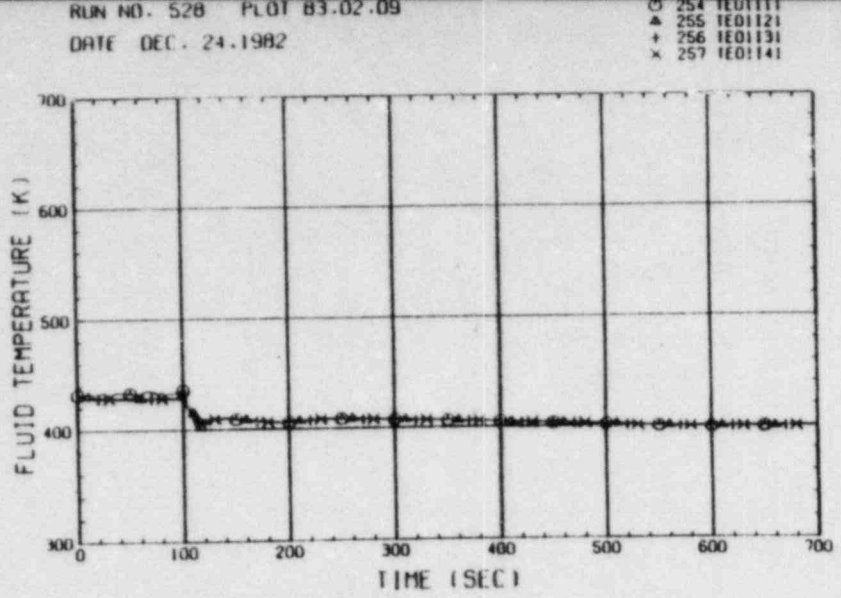

Fig. B-29 FLUID TEMPERATURE ON UCSP SURFACE (BUNDLE 1.2.3.4)

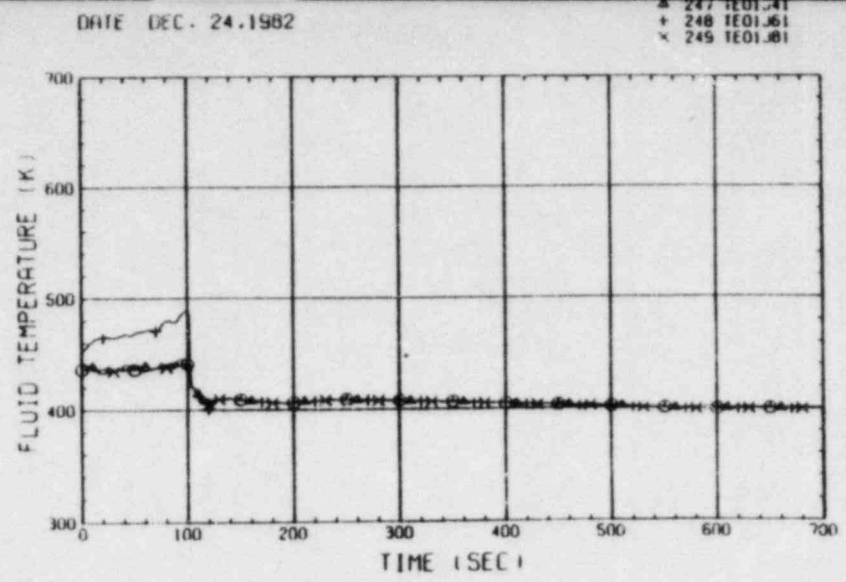

Fig. B-31 FLUID TEMPERATURE ABOVE UCSP (BUNDLE 2.4.6.8. 250MM ABOVE UCSP)

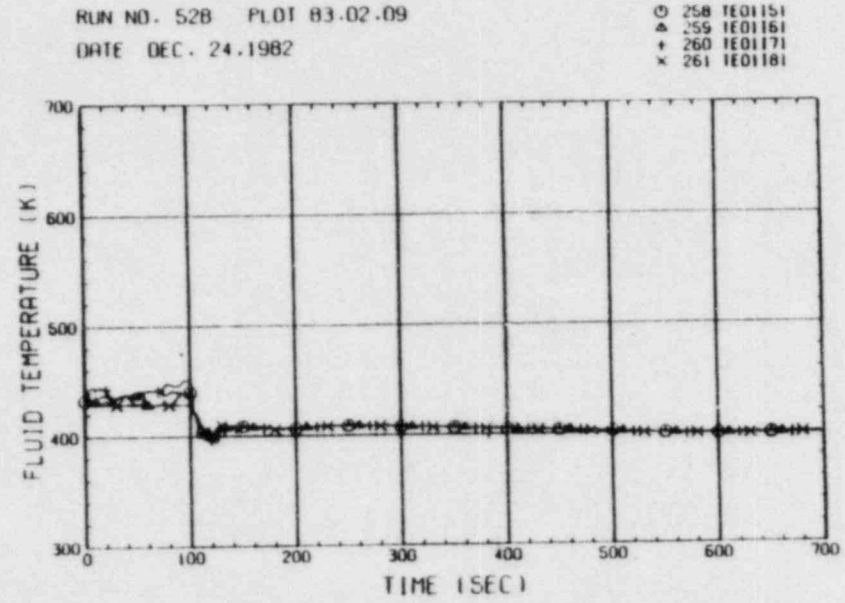

Fig. B-30 FLUID TEMPERATURE ON UCSP SURFACE (BUNDLE 5.6.7.8)

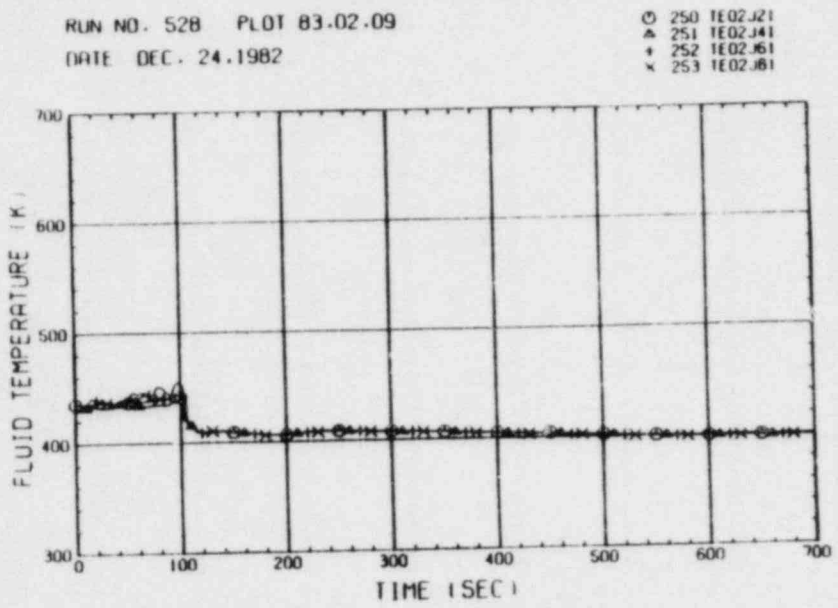

Fig. B-32 FLUID TEMPERATURE ABOVE UCSP (BUNDLE 2.4.6.8. 1000MM ABOVE UCSP)

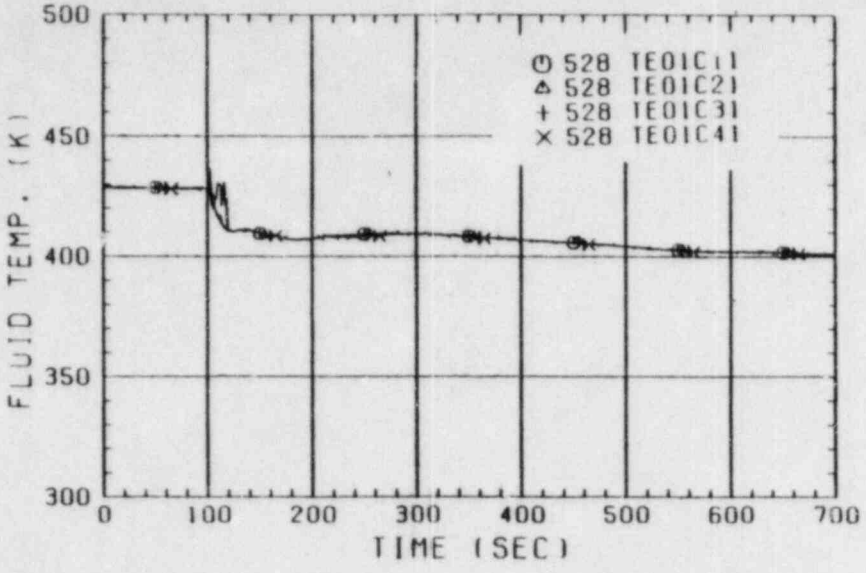

Fig. B-33 FLUID TEMPERATURE AT CORE INLET

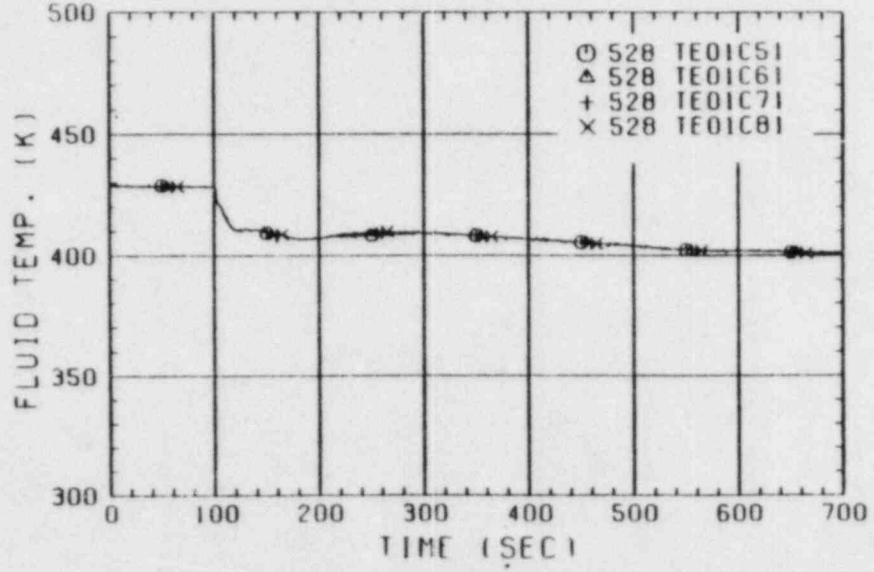

Fig. B-34 FLUID TEMPERATURE AT CORE INLET

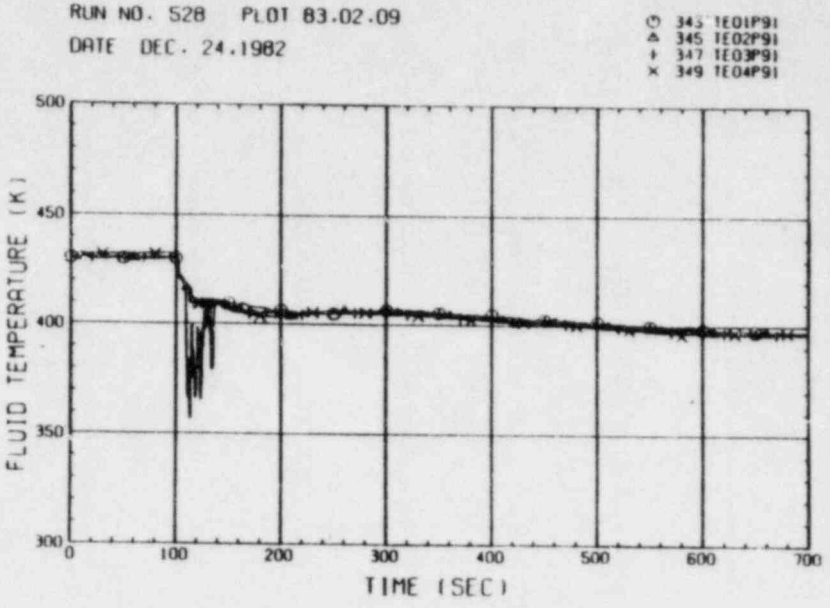

Fig. B-35 FLUID TEMPERATURE IN DOWNCOMER (BELOW INTACT COLD LEG)

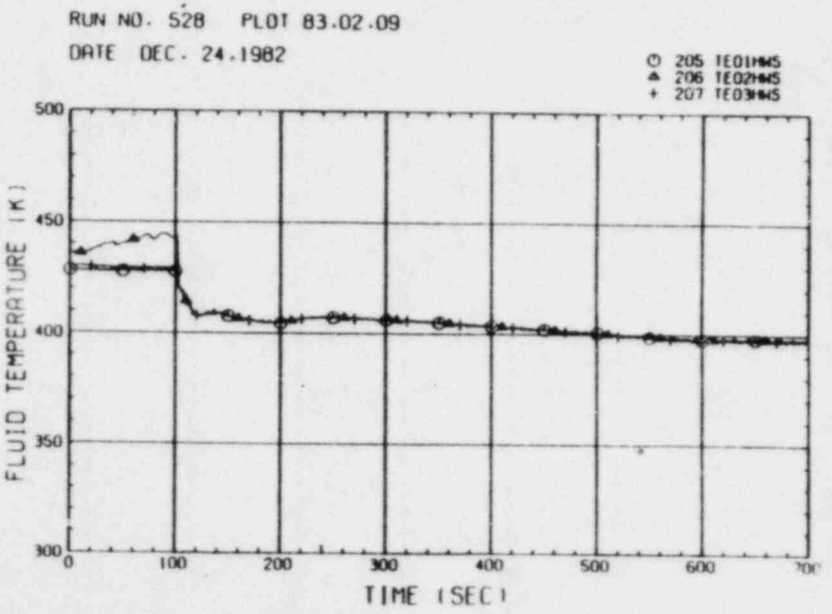

Fig. B-36 FLUID TEMPERATURE IN HOT LEG (01.02.03 - FROM PV TO STEAM/WATER SEPARATOR)

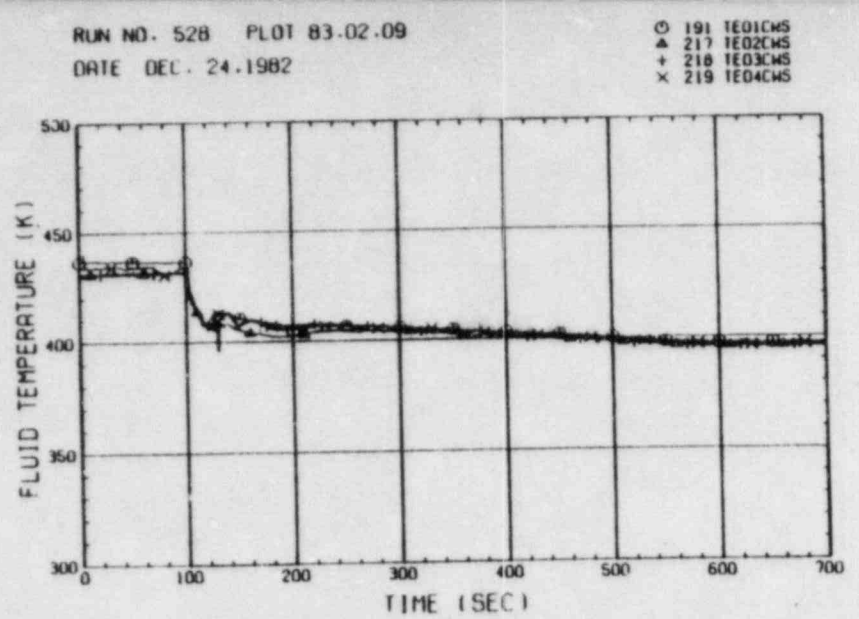

Fig. B-37 FLUID TEMPERATURE IN INTACT COLD LEG (01-BETWEEN PUMP SIMULATOR AND S/W SEPARATOR. 02.03.04-INSIDE PUMP)

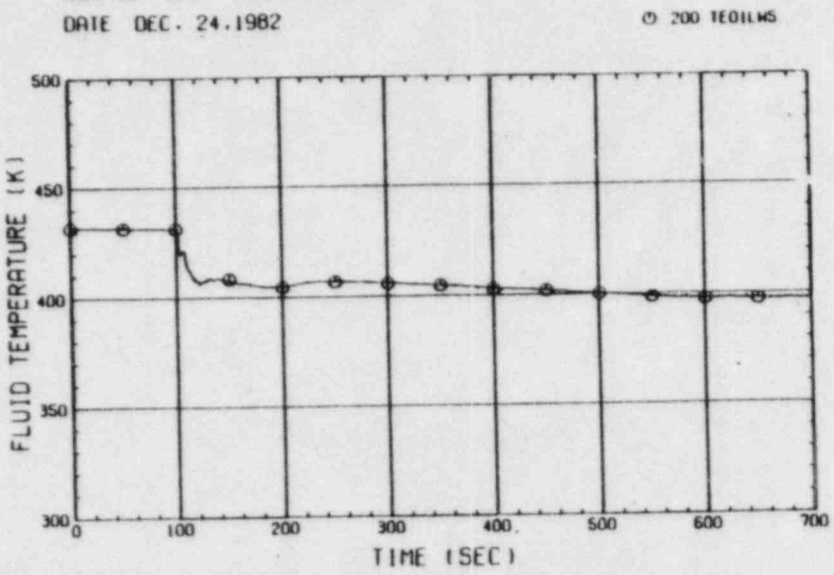

Fig. B-38 FLUID TEMPERATURE IN BROKEN COLD LEG - STEAM/WATER SEPARATOR SIDE

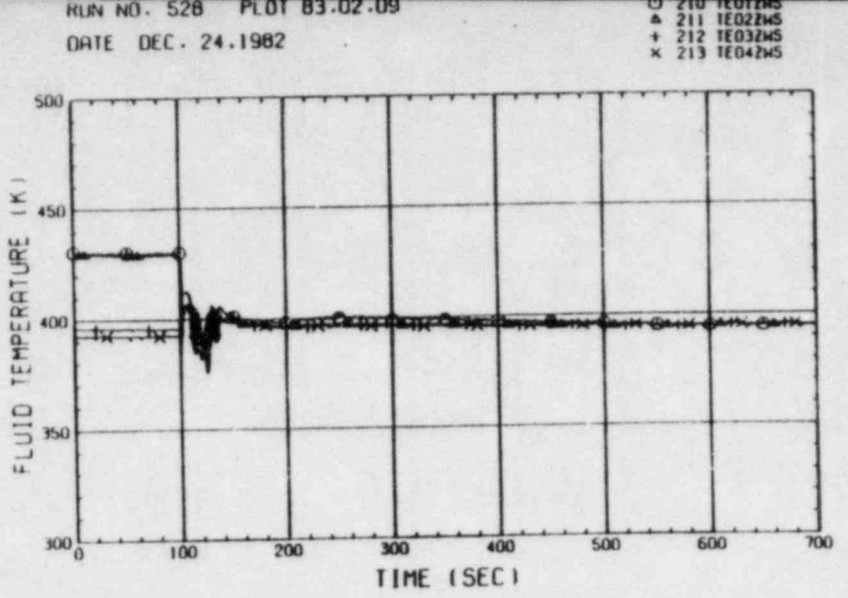

Fig. B-39 FLUID TEMPERATURE IN BROKEN COLD LEG - PV SIDE (01.02.03.04 - FROM PV TO CONTAINMENT TANK-1)

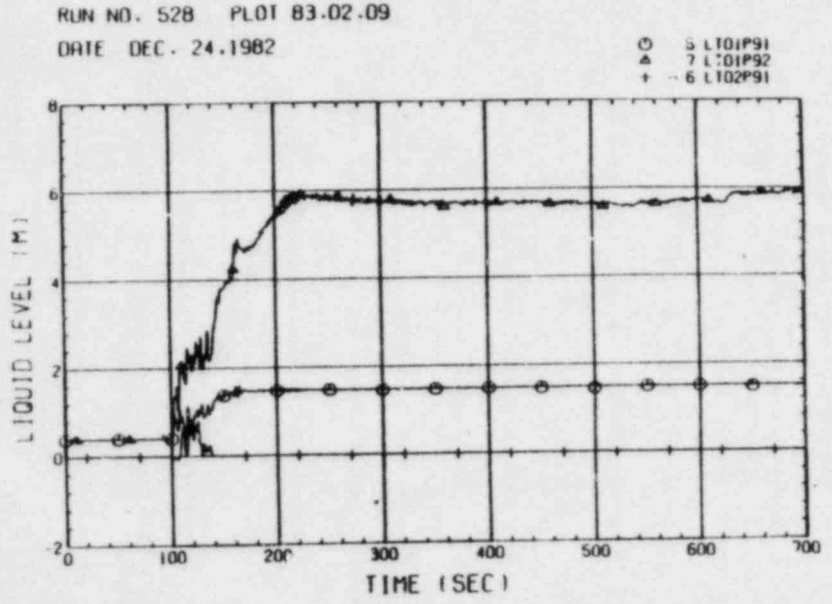

Fig. B-40 LIQUID LEVEL IN DOWNCOMER (01P91-BELOW CORE INLET. 01P92-BOTTOM TO COLD LEG. 02P91-COLD LEG TO TOP OF PV)

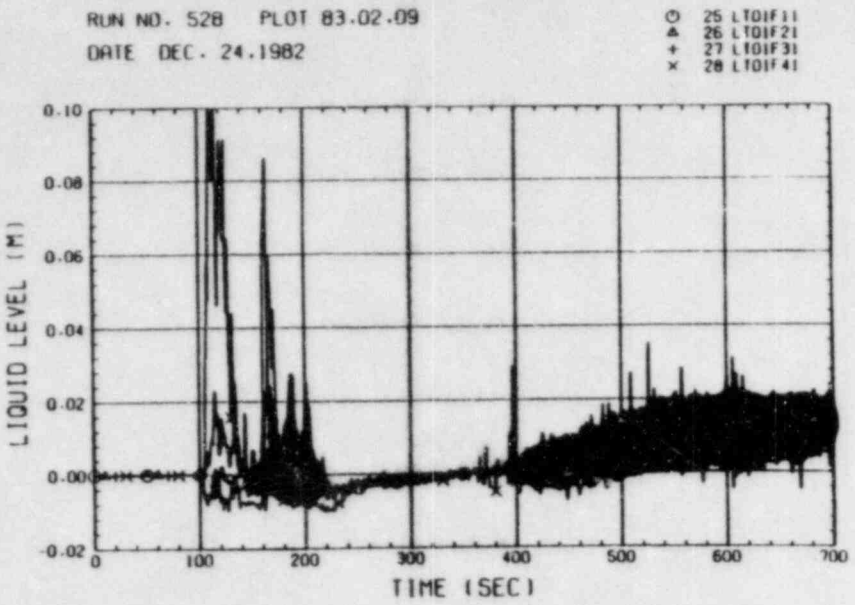

Fig. B-41 LIQUID LEVEL ABOVE END BOX TIE PLATE (BUNDLE 1.2.3.4)

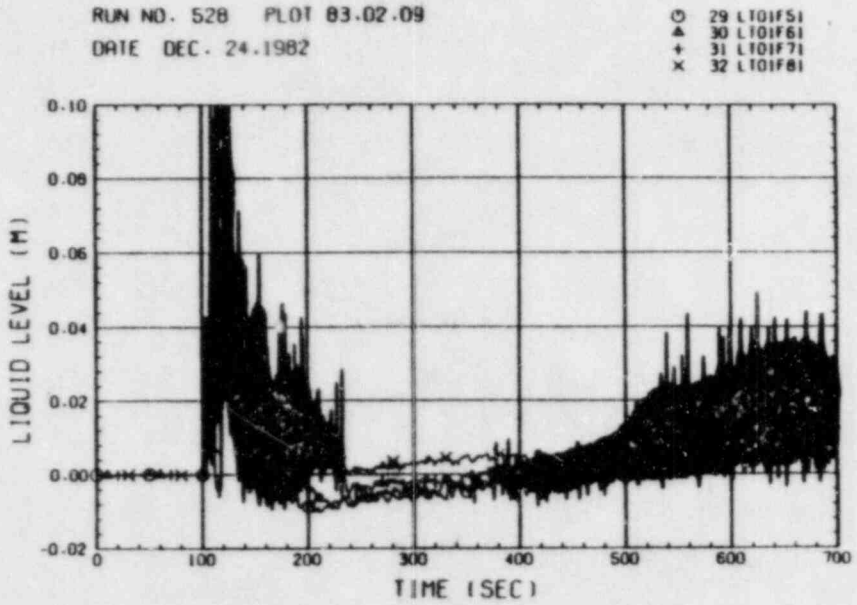

Fig. B-42 LIQUID LEVEL ABOVE END BOX TIE PLATE (BUNDLE 5.6.7.8)

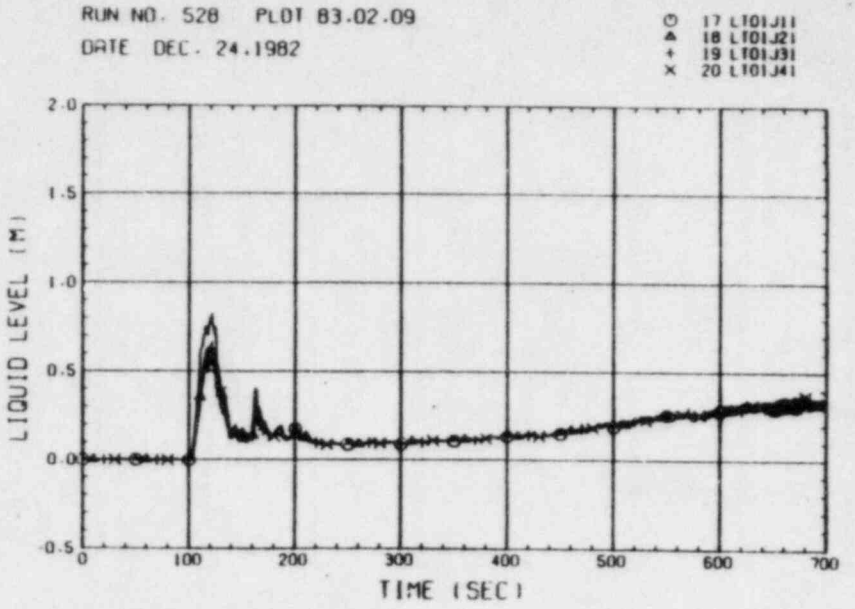

Fig. B-43 LIQUID LEVEL ABOVE UCSP (BUNDLE 1.2.3.4)

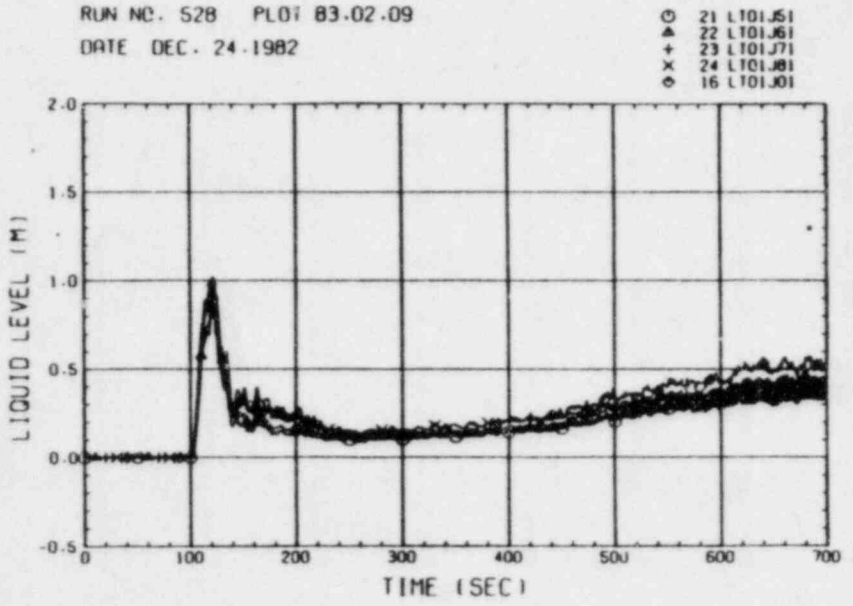

Fig. B-44 LIQUID LEVEL ABOVE UCSP (BUNDLE 5.6.7.8 AND CORE BAFFLE)

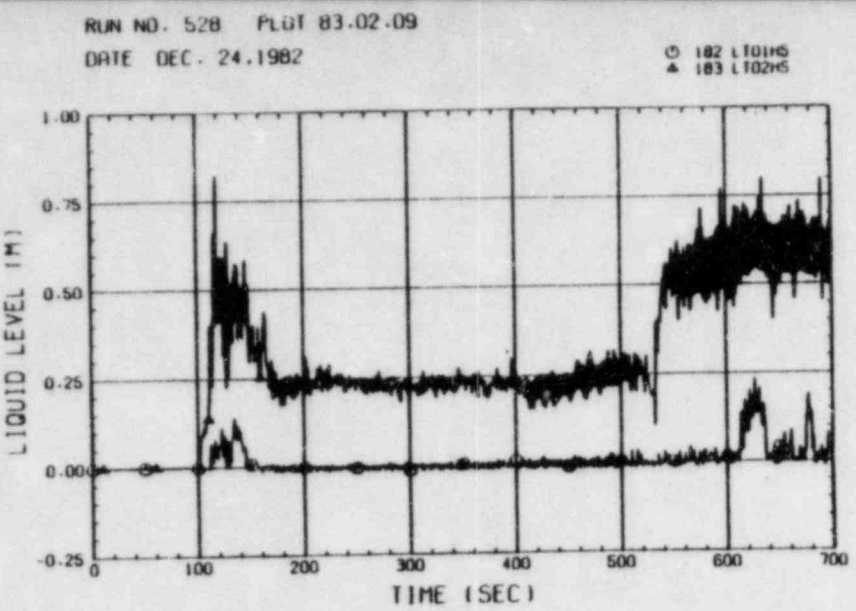

Fig. B-45 LIQUID LEVEL IN HOT LEG
(01HS - PV SIDE, 02HS - STEAM/WATER SEPARATOR SIDE)

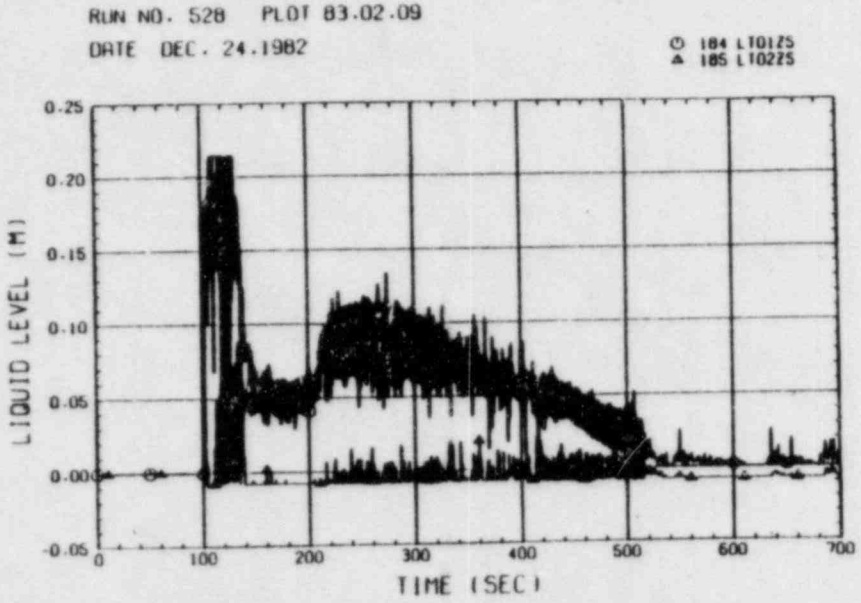

Fig. B-46 LIQUID LEVEL IN BROKEN COLD LEG - PV SIDE
(01 - DOWNCOMER SIDE, 02 - CONTAINMENT TANK-1 SIDE)

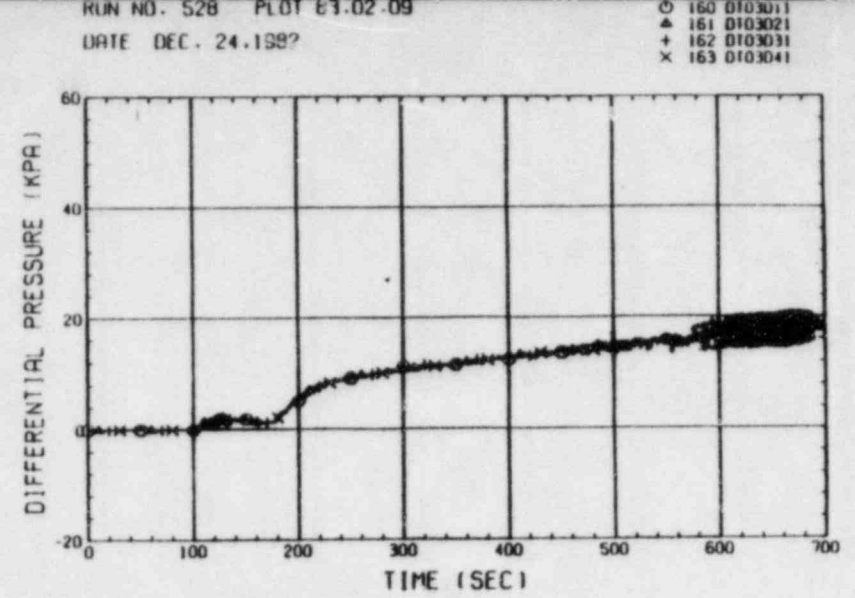

Fig. B-47 DIFFERENTIAL PRESSURE OF CORE FULL HEIGHT
(BUNDLE 1.2.3.4)

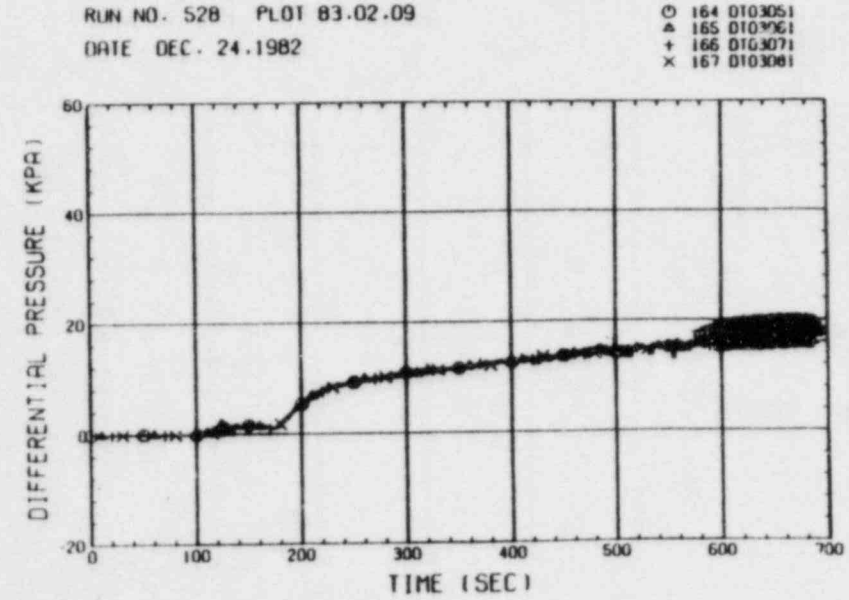

Fig. B-48 DIFFERENTIAL PRESSURE OF CORE FULL HEIGHT
(BUNDLE 5.6.7.8)

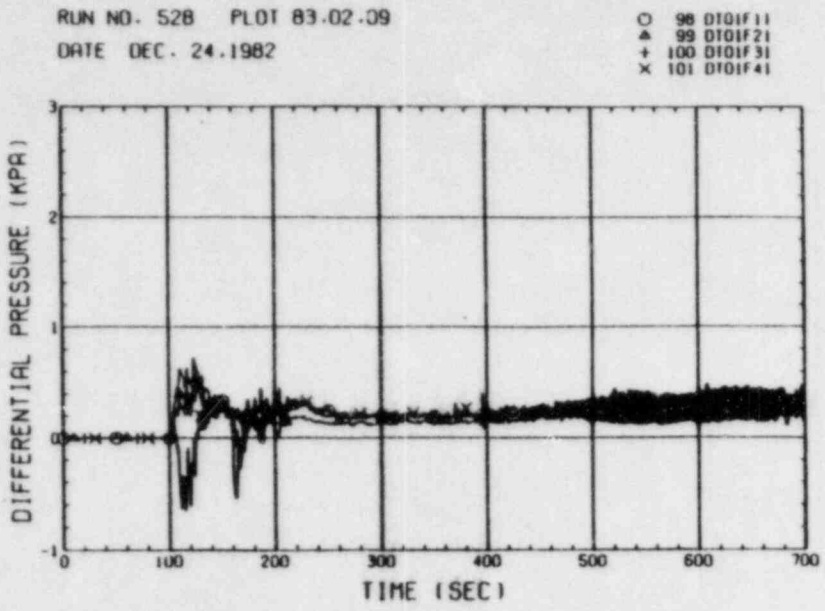

Fig. B-49 DIFFERENTIAL PRESSURE ACROSS END BOX TIE PLATE (BUNDLE 1.2.3.4)

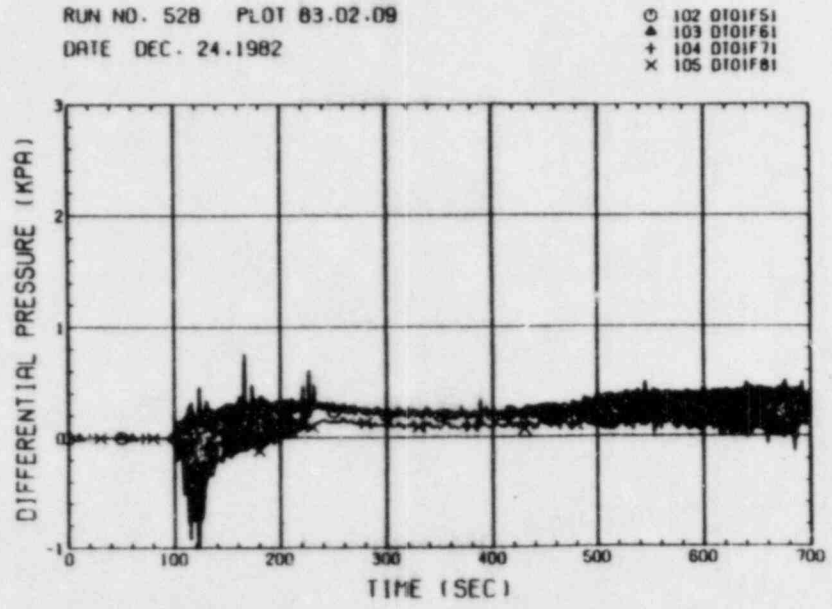

Fig. B-50 DIFFERENTIAL PRESSURE ACROSS END BOX TIE PLATE (BUNDLE 5.6.7.8)

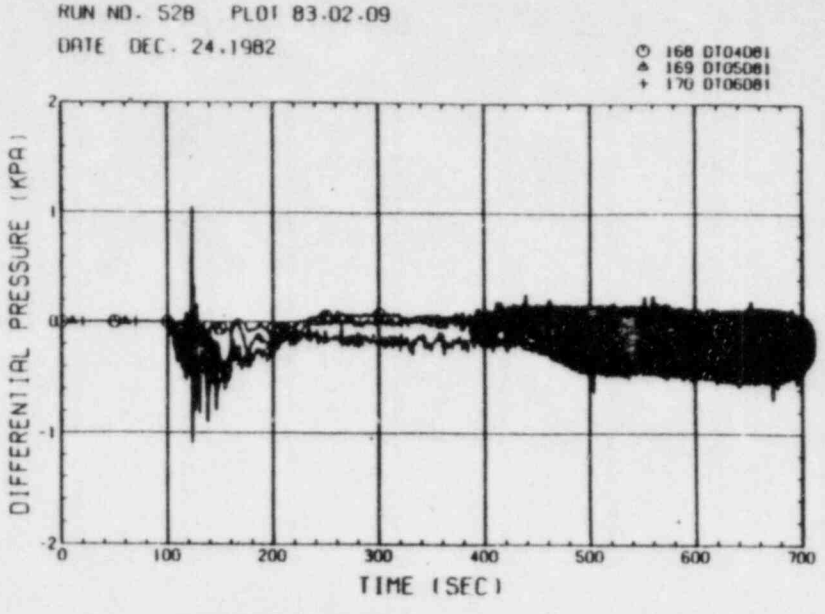

Fig. B-51 DIFFERENTIAL PRESSURE, HORIZONTAL, BUNDLE 5-8 (04-BELOW SPACER 4, 05-BELOW SPACER 6, 06-BELOW END BOX)

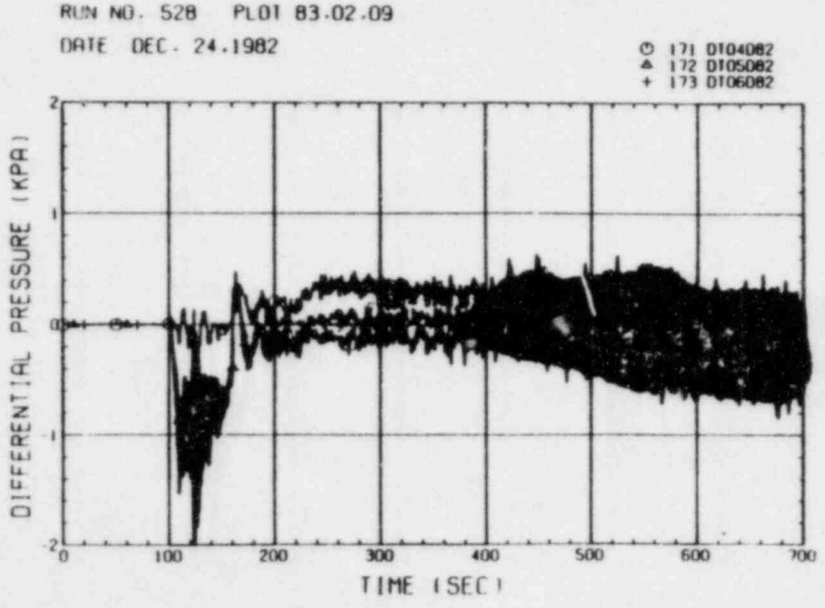

Fig. B-52 DIFFERENTIAL PRESSURE, HORIZONTAL, BUNDLE 1-8 (04-BELOW SPACER 4, 05-BELOW SPACER 6, 06-BELOW END BOX)

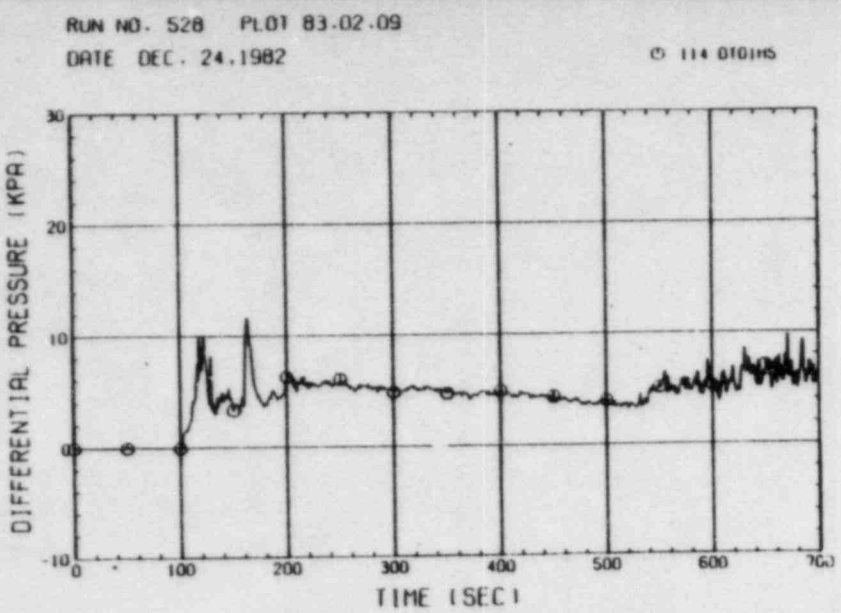

Fig. B-53 DIFFERENTIAL PRESSURE OF HOT LEG.
HOT LEG INLET - STEAM/WATER SEPARATOR INLET

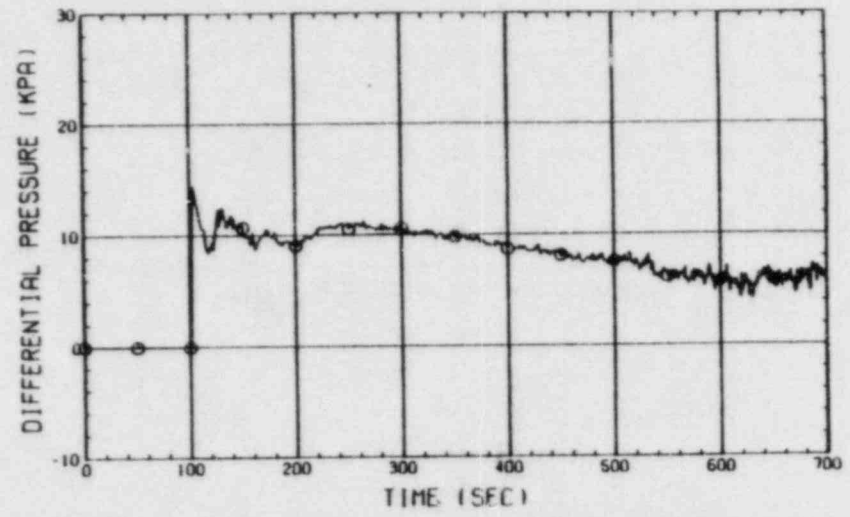

Fig. B-54 DIFFERENTIAL PRESSURE. STEAM/WATER SEPARATOR INLET -
BROKEN COLD LEG - S/W SEPARATOR SIDE NOZZLE

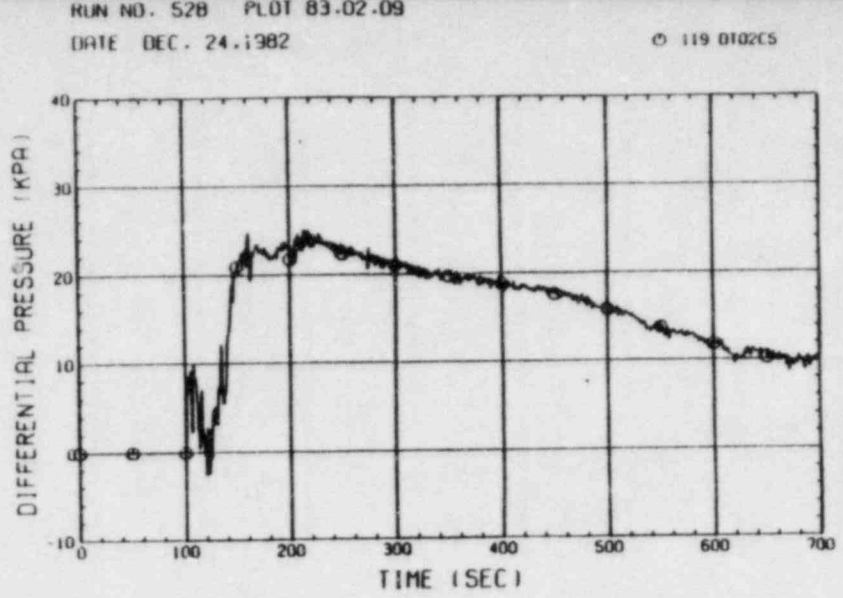

Fig. B-55 DIFFERENTIAL PRESSURE OF INTACT COLD LEG

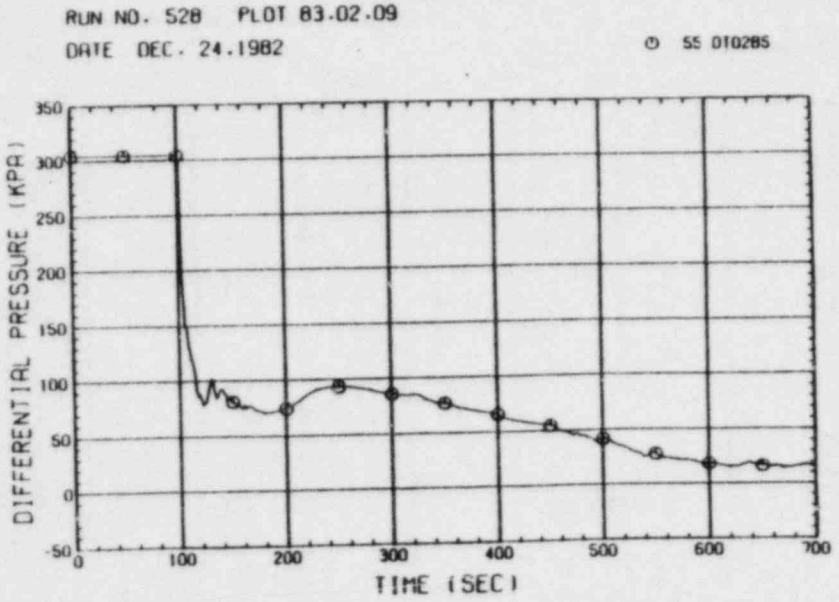

Fig. B-56 DIFFERENTIAL PRESSURE. STEAM/WATER SEPARATOR -
CONTAINMENT TANK-II

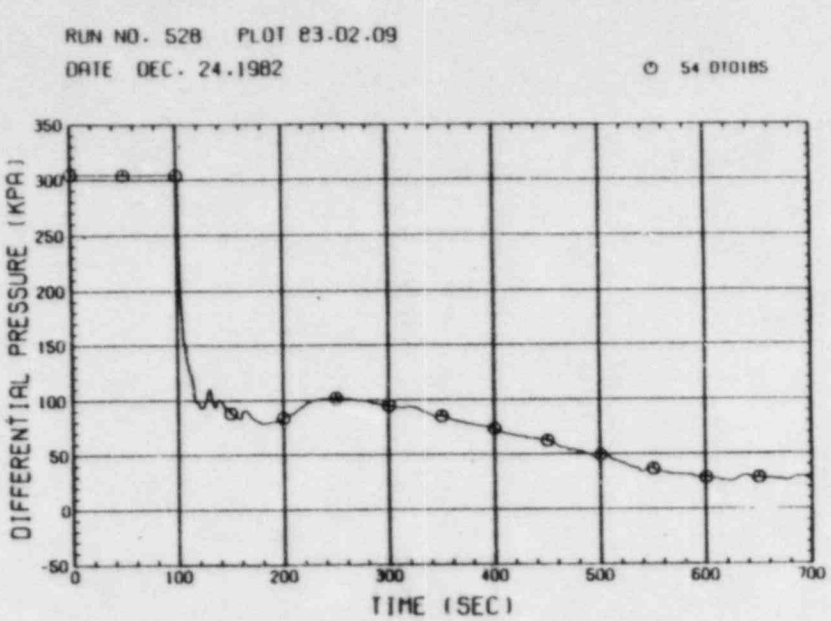

Fig. B-57 DIFFERENTIAL PRESSURE. TOP OF UPPER PLENUM - CONTAINMENT TANK-II

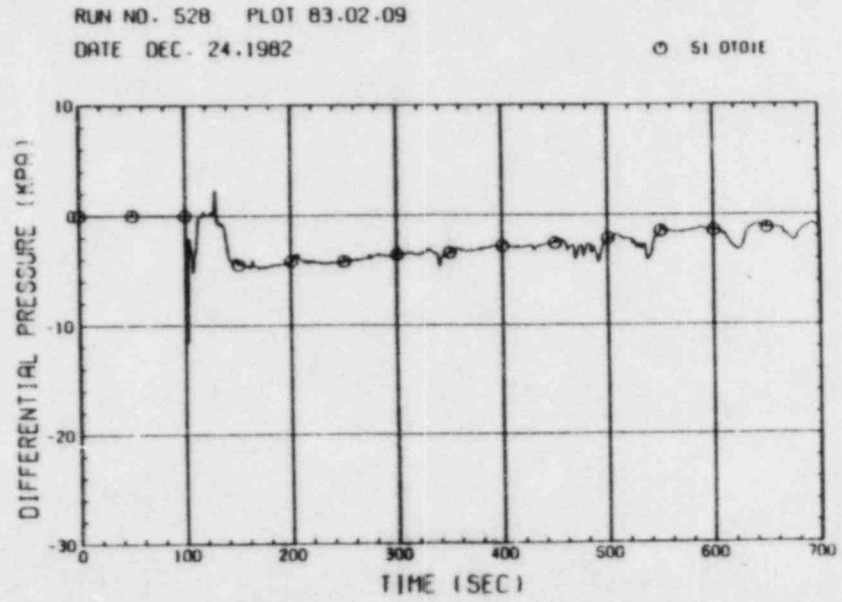

Fig. B-58 DIFFERENTIAL PRESSURE. CONTAINMENT TANK-II - CONTAINMENT TANK-I

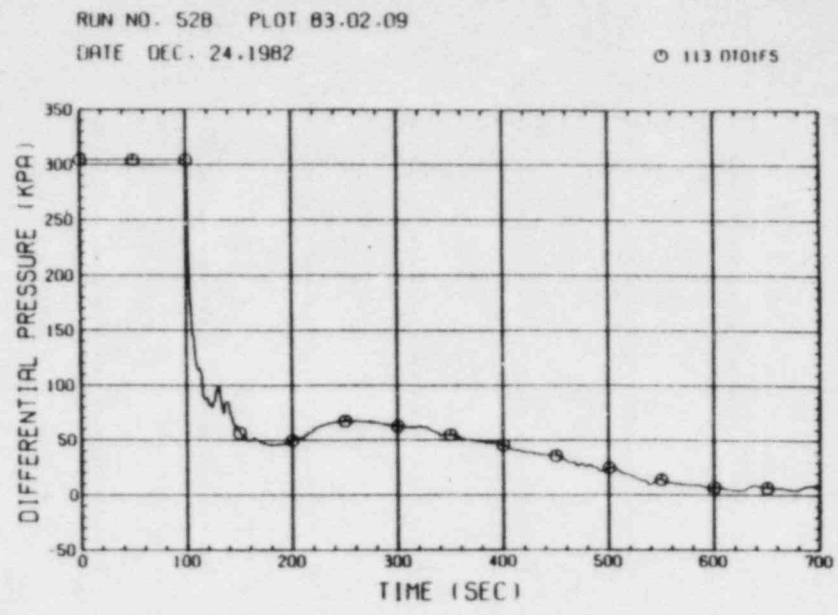

Fig. B-59 DIFFERENTIAL PRESSURE OF BROKEN COLD LEG - PV SIDE. DOWNCOMER - CONTAINMENT TANK-I

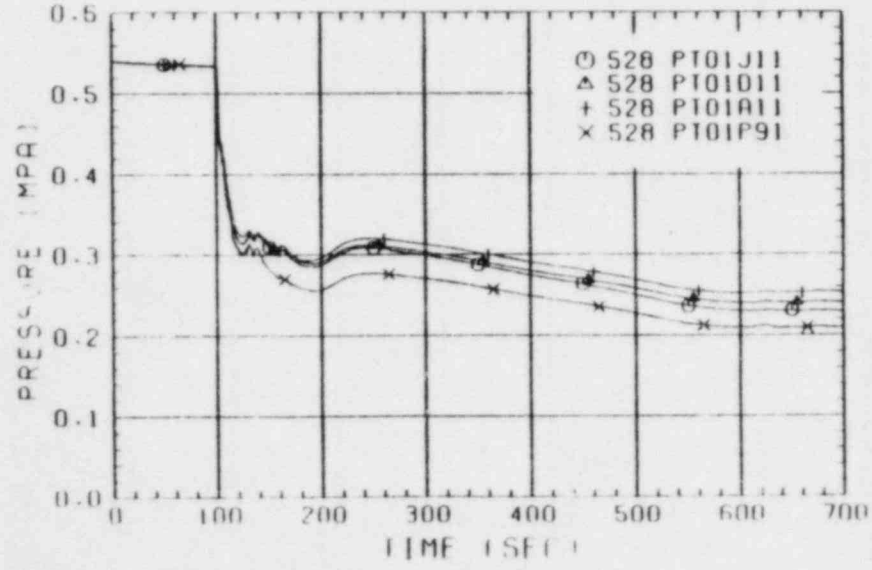

Fig. B-60 PRESSURE IN PV

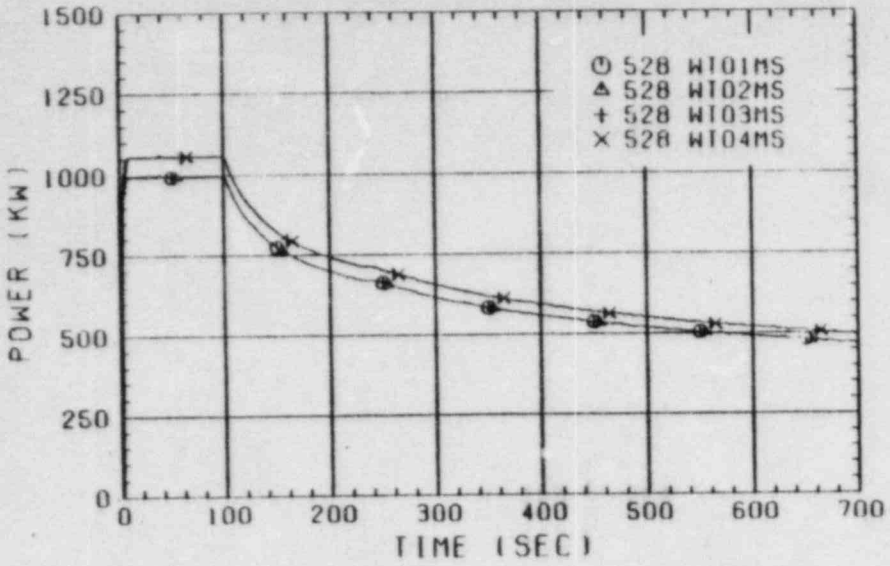

Fig. B-61 BUNDLE POWER . BUNDLE 1.2.3.4

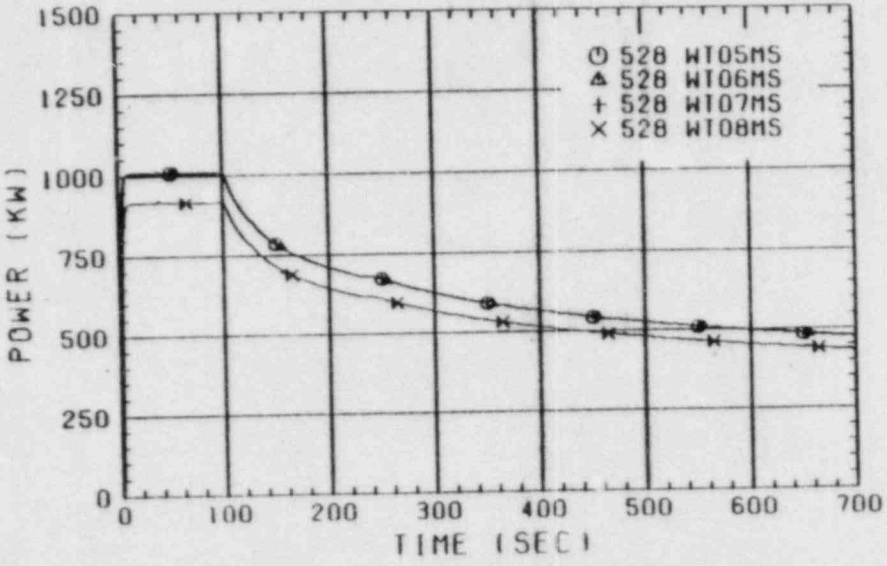

Fig. B-62 BUNDLE POWER . BUNDLE 5.6.7.8

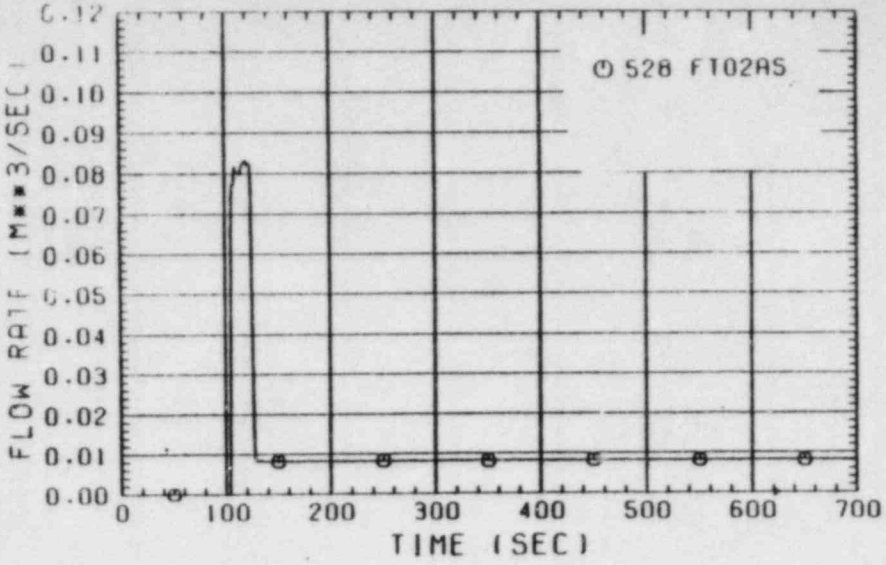

Fig. B-63 ECC INJECTION RATE INTO INTACT COLD LEG

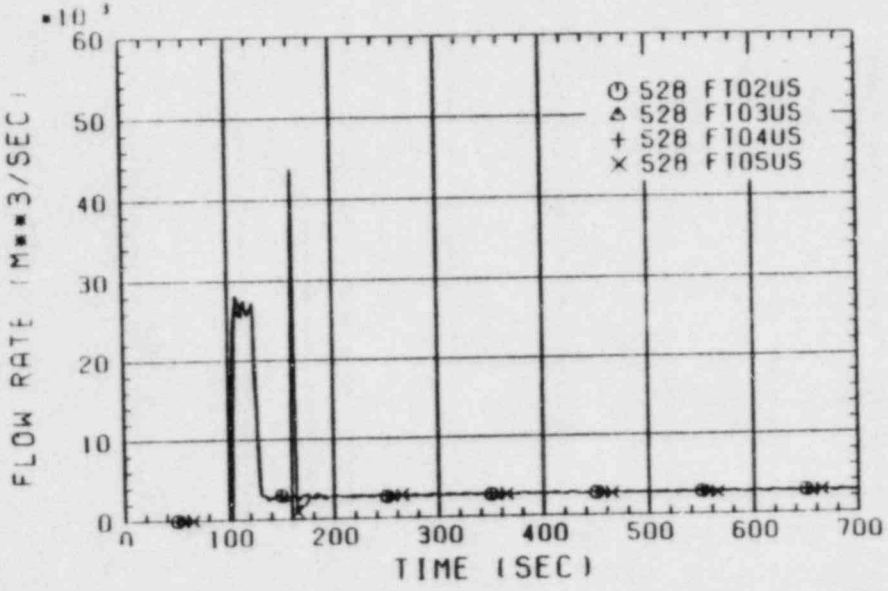

Fig. B-64 ECC INJECTION RATE INTO UPPER PLENUM

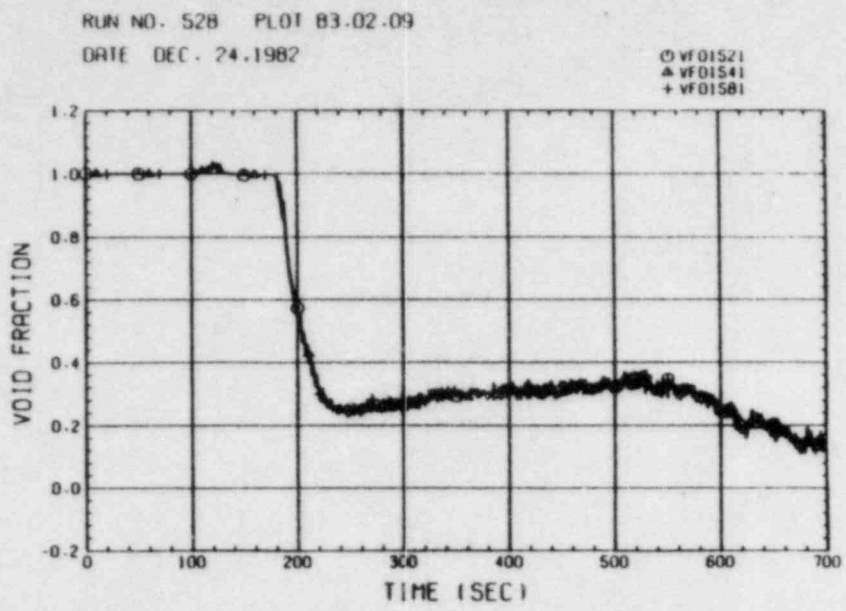

Fig. B-65 VOID FRACTION IN CORE, BUNDLE 2.4.8 (BETWEEN CORE SPACER 1 AND 2)

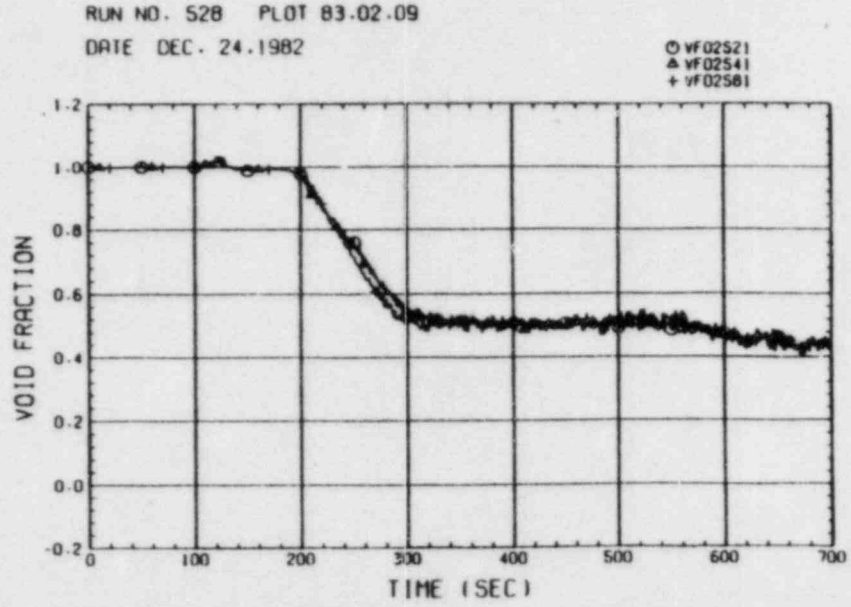

Fig. B-66 VOID FRACTION IN CORE, BUNDLE 2.4.8 (BETWEEN CORE SPACER 2 AND 3)

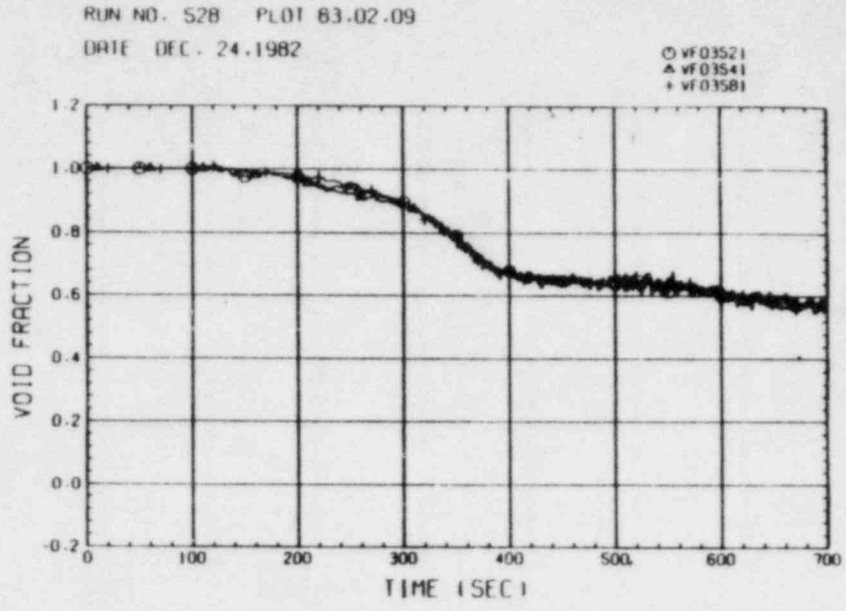

Fig. B-67 VOID FRACTION IN CORE, BUNDLE 2.4.8 (BETWEEN CORE SPACER 3 AND 4)

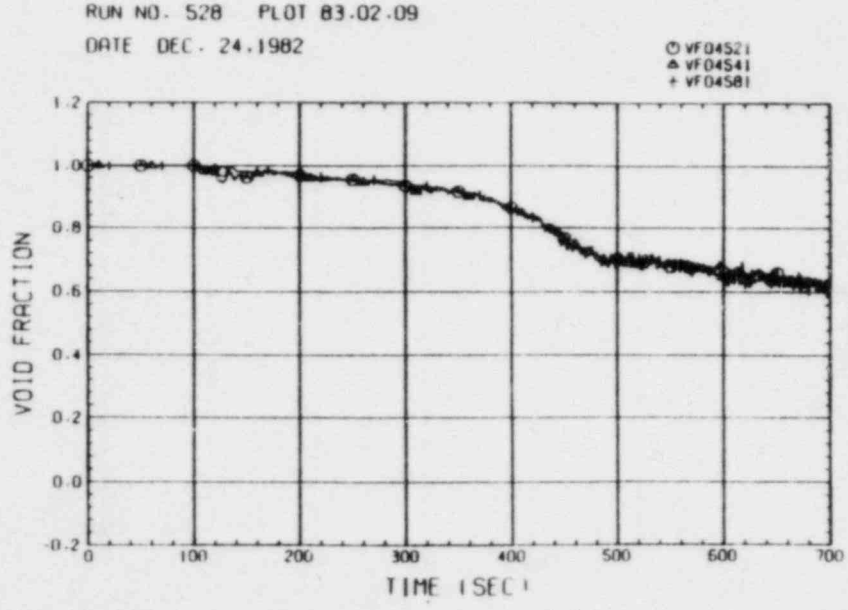

Fig. B-68 VOID FRACTION IN CORE, BUNDLE 2.4.8 (BETWEEN CORE SPACER 4 AND 5)

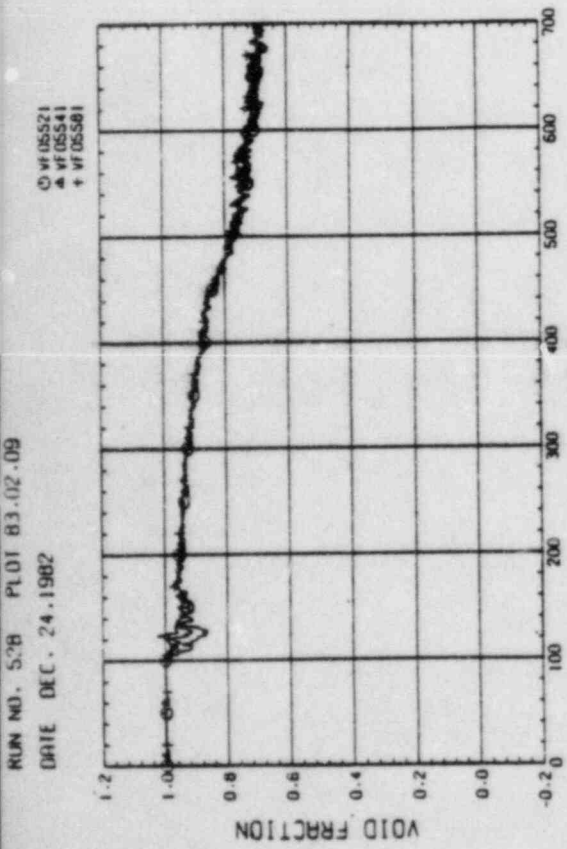

Fig. B-69 VOID FRACTION IN CORE, BUNDLE 2.4.8 (BETWEEN CORE SPACER 5 AND 6)

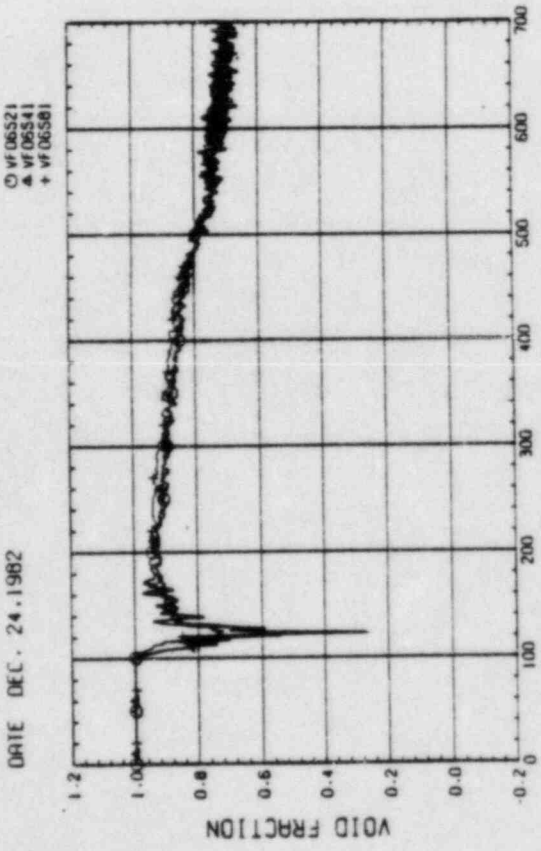

Fig. B-70 VOID FRACTION IN CORE, BUNDLE 2.4.8 (BETWEEN CORE SPACER 6 AND 7)

Appendix C Selected Data of Test S1-SH4 (Run 529)

Fig. No.	Measurement item
C- 1 ∿ C-16	Heater rod temperature
C-17 ∿ C-20	Fluid temperature in core
C-21 ∿ C-22	Steam temperature in core
C-23 ∿ C-24	Fluid temperature just above end box tie plate
C-25 ∿ C-28	Fluid temperature in UCSP holes
C-29 ∿ C-30	Fluid temperature on UCSP surface
C-31 ∿ C-32	Fluid temperature above UCSP
C-33 ∿ C-34	Fluid temperature at core inlet
C-35	Fluid temperature in downcomer
C-36	Fluid temperature in hot leg
C-37	Fluid temperature in intact cold leg
C-38	Fluid temperature in broken cold leg (steam/water separator side)
C-39	Fluid temperature in broken cold leg (PV side)
C-40	Liquid level in downcomer
C-41 ∿ C-42	Liquid level above end box tie plate
C-43 ∿ C-44	Liquid level above UCSP
C-45	Liquid level in hot leg
C-46	Liquid level in broken cold leg (PV side)
C-47 ∿ C-48	Differential pressure of core full height
C-49 ∿ C-50	Differential pressure across end box the plate
C-51 ∿ C-52	Horizontal differential pressure in core
C-53	Differential pressure of hot leg
C-54	Differential pressure across steam/water separator
C-55	Differential pressure of intact cold leg
C-56	Differential pressure between steam/water separator and containment tank-II
C-57	Differential pressure between top of upper plenum and containment tank-II
C-58	Differential pressure between containment tanks I and II
C-59	Differential pressure of broken cold leg (PV side)
C-60	Pressures in pressure vessel
C-61, C-62	Bundle powers
C-63	ECC injection rate into intact cold leg
C-64	ECC injection rate into upper plenum
C-65 ∿ C-70	Void fractions in core

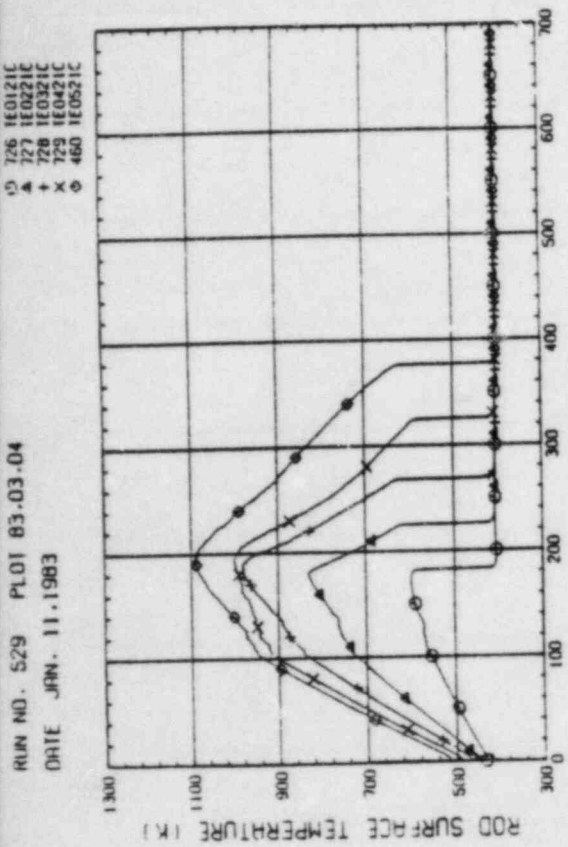

Fig. C-3 HEATER ROD TEMPERATURE (BUNDLE 2-1C, LOWER HALF)

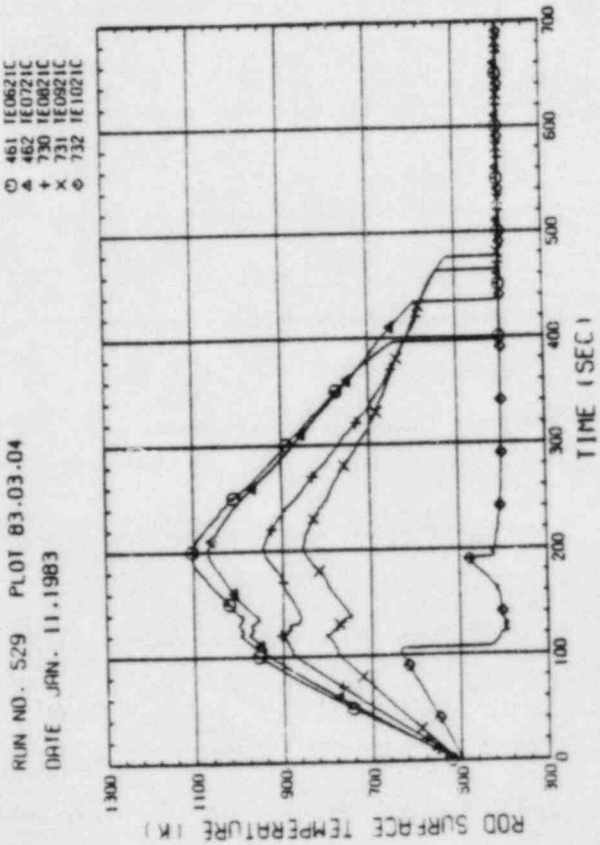

Fig. C-4 HEATER ROD TEMPERATURE (BUNDLE 2-1C, UPPER HALF)

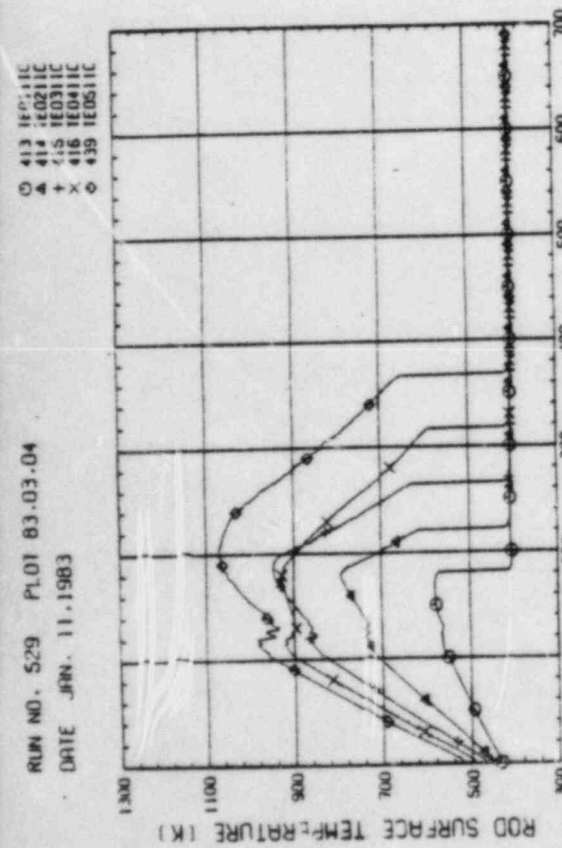

Fig. C-1 HEATER ROD TEMPERATURE (BUNDLE 1-1C, LOWER HALF)

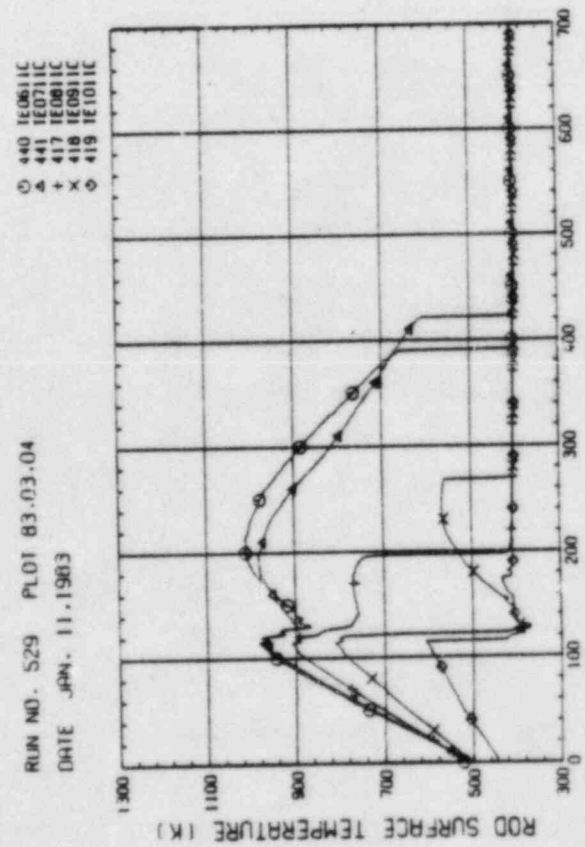

Fig. C-2 HEATER ROD TEMPERATURE (BUNDLE 1-1C, UPPER HALF)

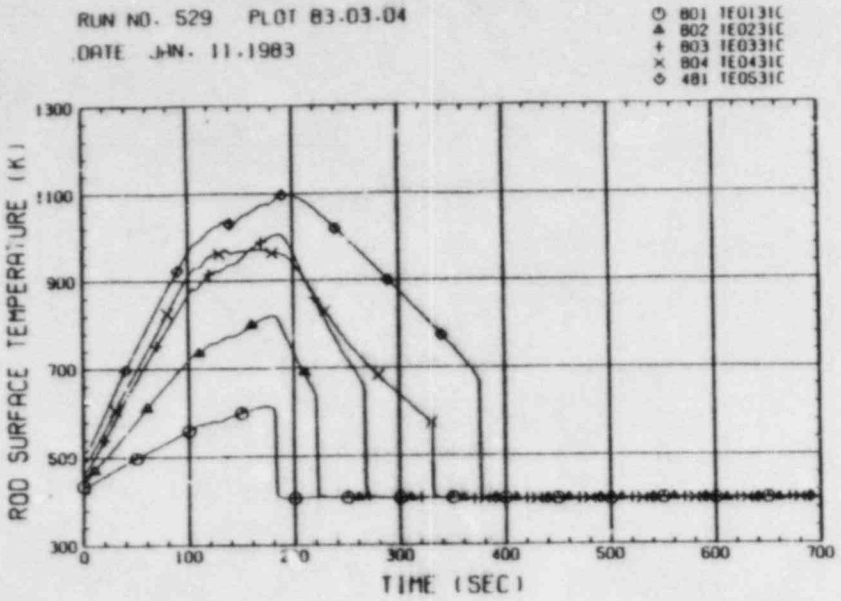

Fig. C-5 HEATER ROD TEMPERATURE (BUNDLE 3-1C, LOWER HALF)

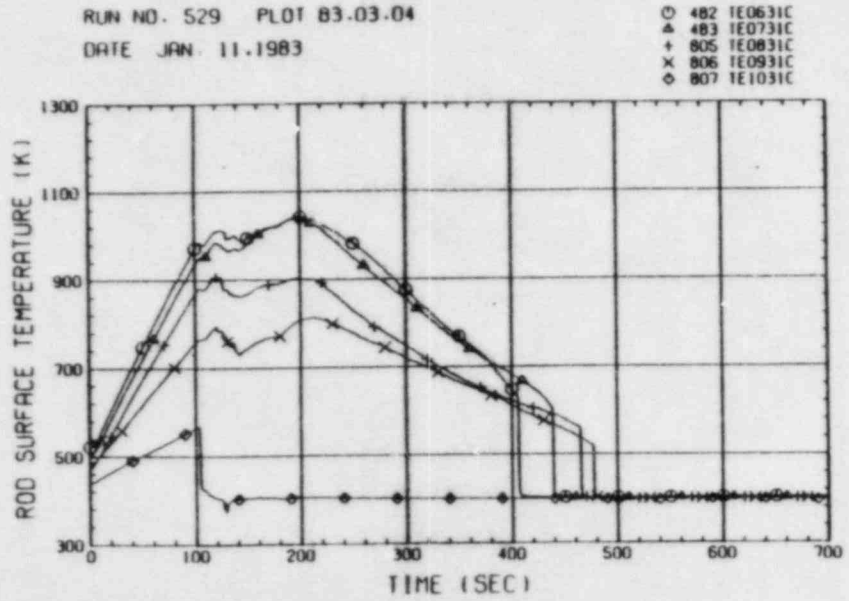

Fig. C-6 HEATER ROD TEMPERATURE (BUNDLE 3-1C, UPPER HALF)

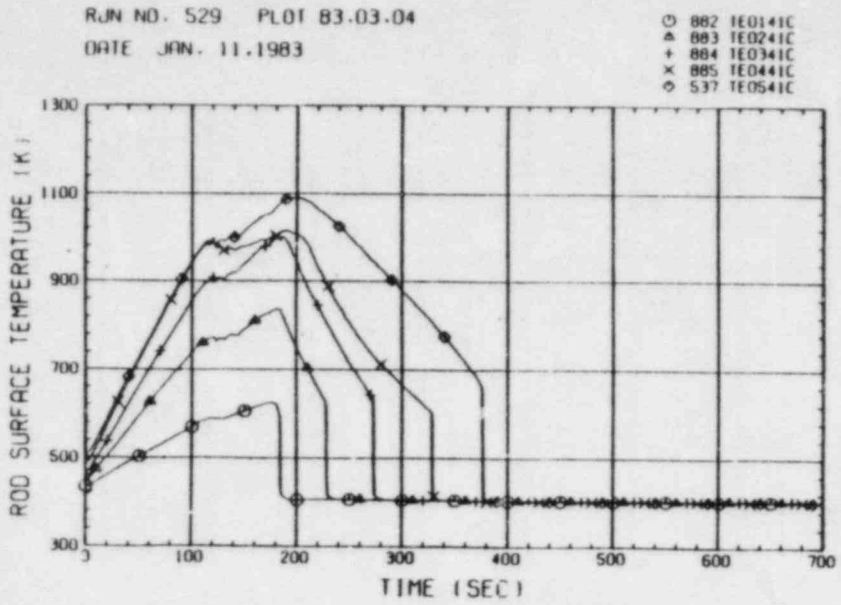

Fig. C-7 HEATER ROD TEMPERATURE (BUNDLE 4-1C, LOWER HALF)

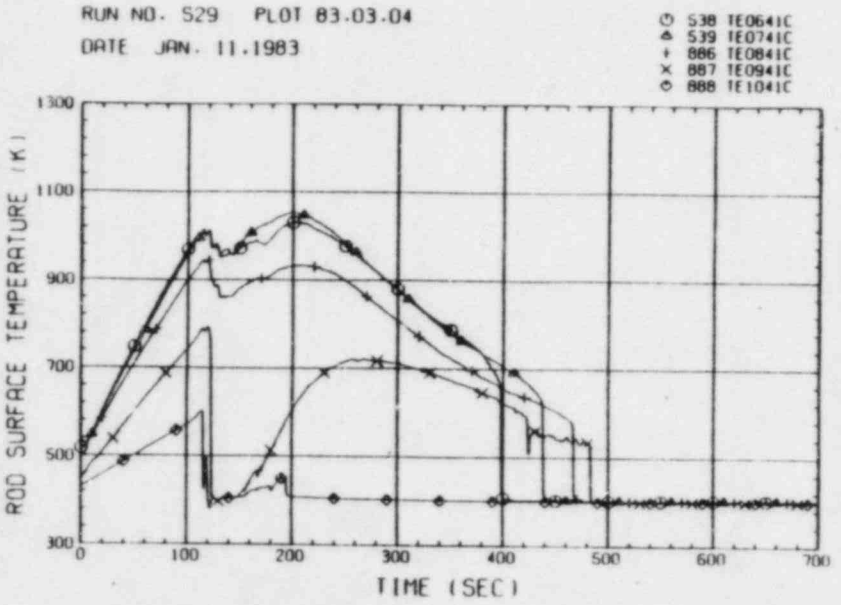

Fig. C-8 HEATER ROD TEMPERATURE (BUNDLE 4-1C, UPPER HALF)

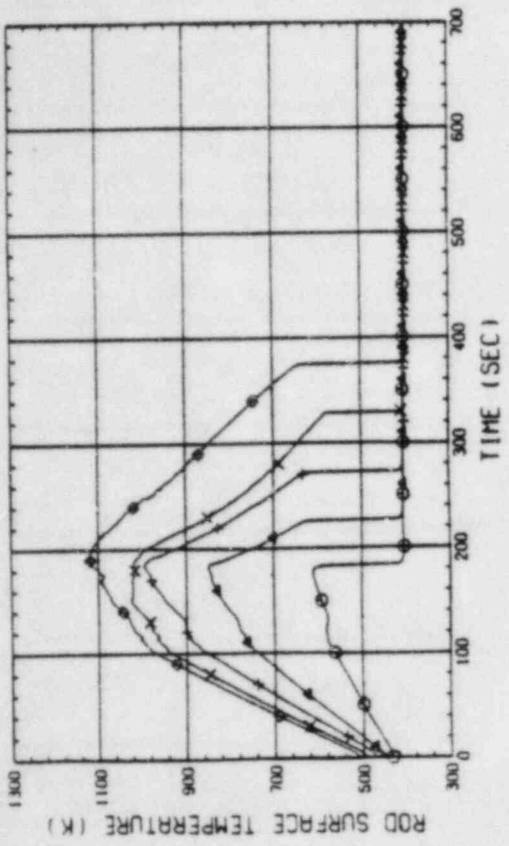

Fig. C-9 HEATER ROD TEMPERATURE (BUNDLE 5-1C, LOWER HALF)

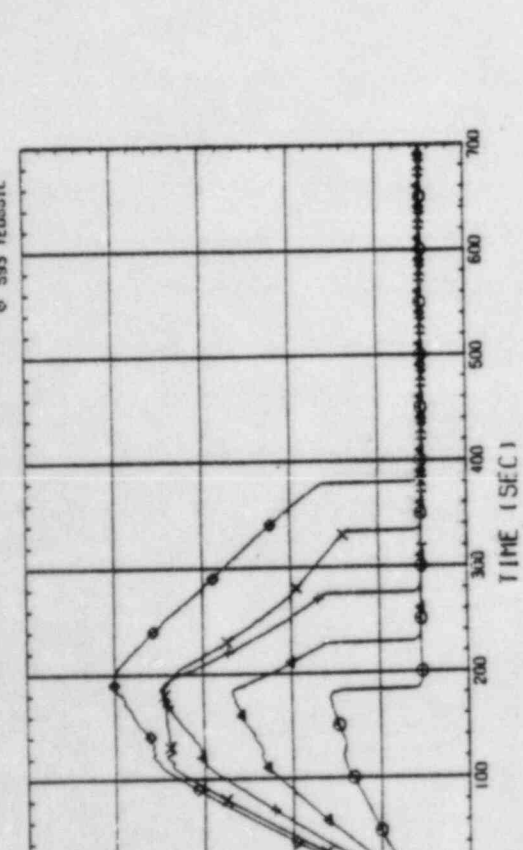

Fig. C-10 HEATER ROD TEMPERATURE (BUNDLE 5-1C, UPPER HALF)

Fig. C-11 HEATER ROD TEMPERATURE (BUNDLE 6-1C, LOWER HALF)

Fig. C-12 HEATER ROD TEMPERATURE (BUNDLE 6-1C, UPPER HALF)

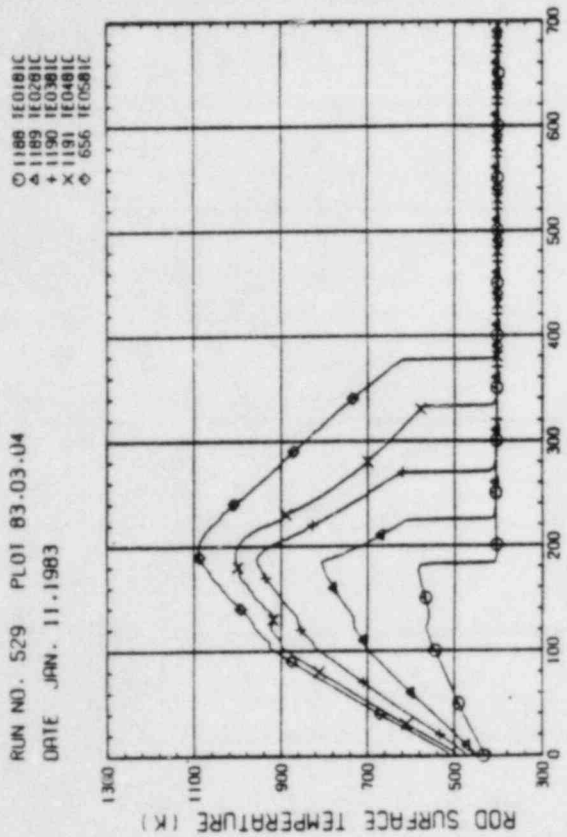

Fig. C-15 HEATER ROD TEMPERATURE (BUNDLE 8-IC, LOWER HALF)

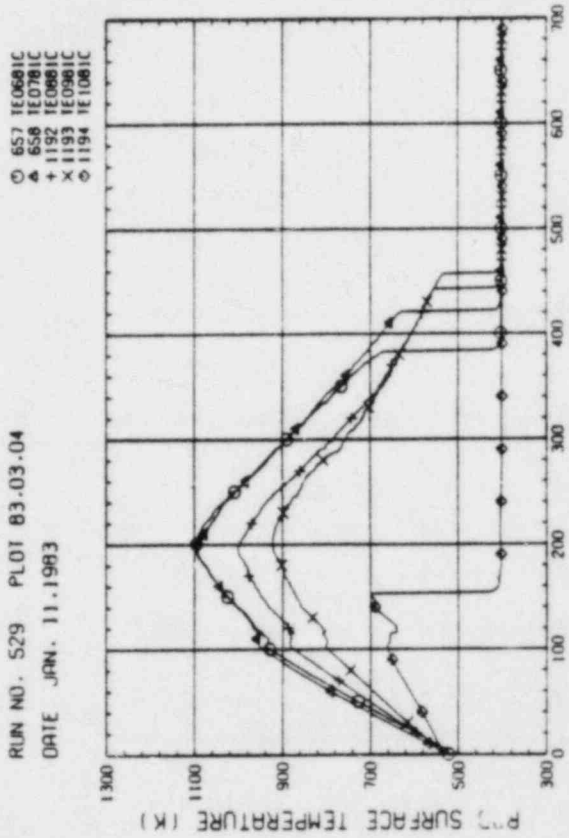

Fig. C-16 HEATER ROD TEMPERATURE (BUNDLE 8-IC, UPPER HALF)

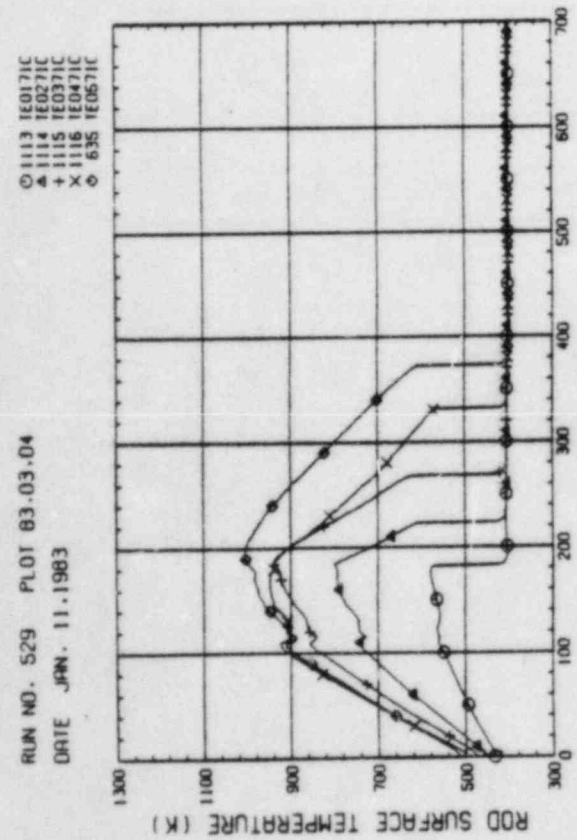

Fig. C-13 HEATER ROD TEMPERATURE (BUNDLE 7-IC, LOWER HALF)

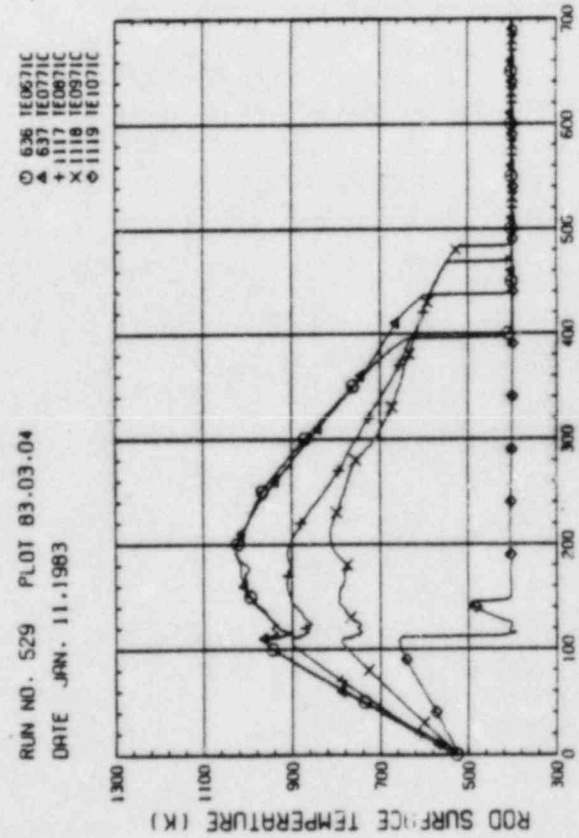

Fig. C-14 HEATER ROD TEMPERATURE (BUNDLE 7-IC, UPPER HALF)

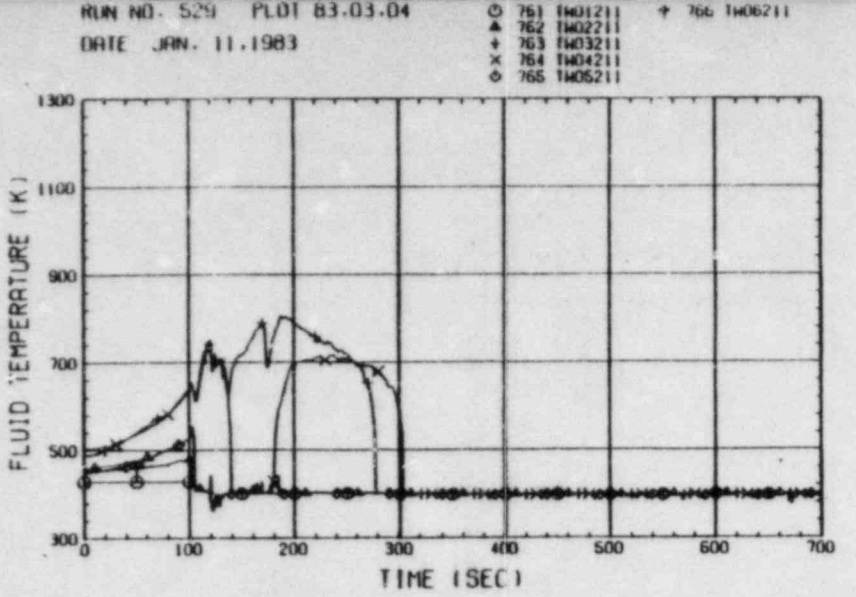

Fig. C-17 FLUID TEMPERATURE IN CORE (BUNDLE 2-1)

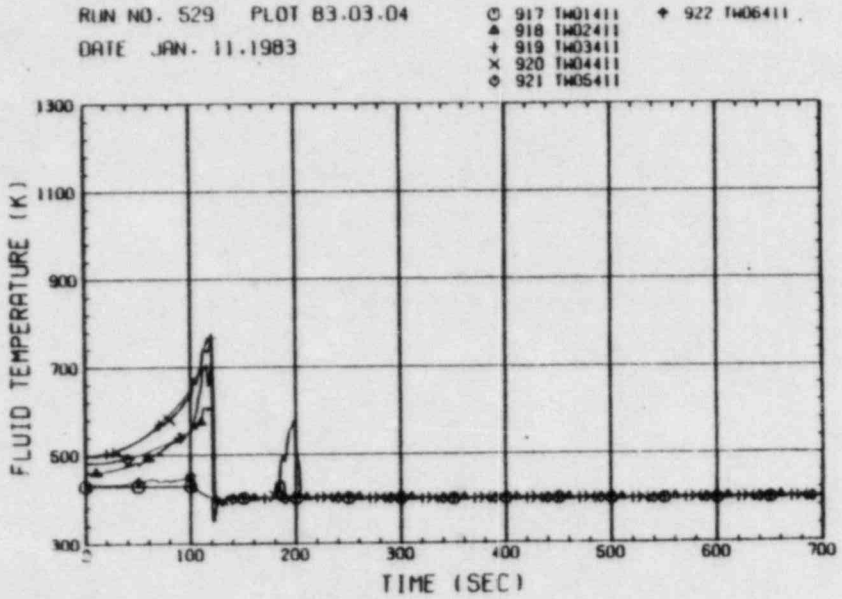

Fig. C-18 FLUID TEMPERATURE IN CORE (BUNDLE 4-1)

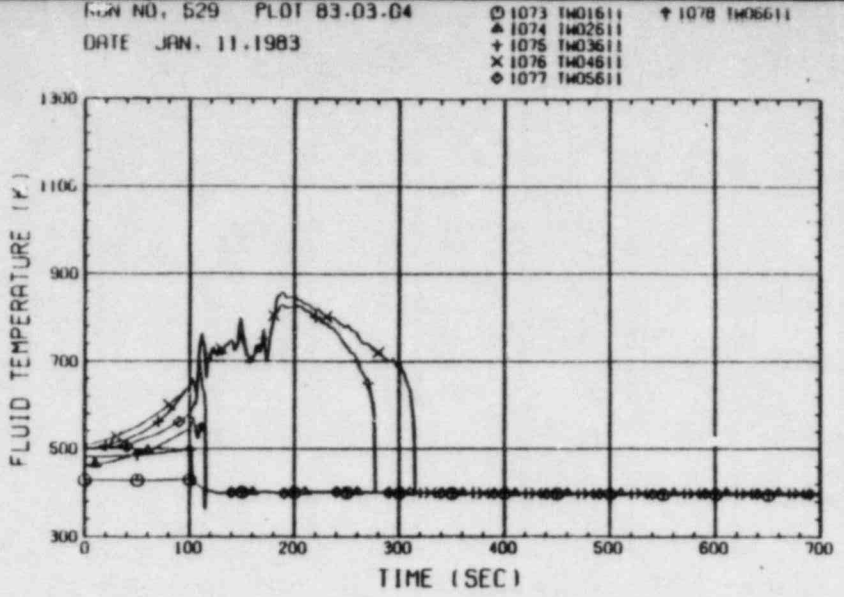

Fig. C-19 FLUID TEMPERATURE IN CORE (BUNDLE 6-1)

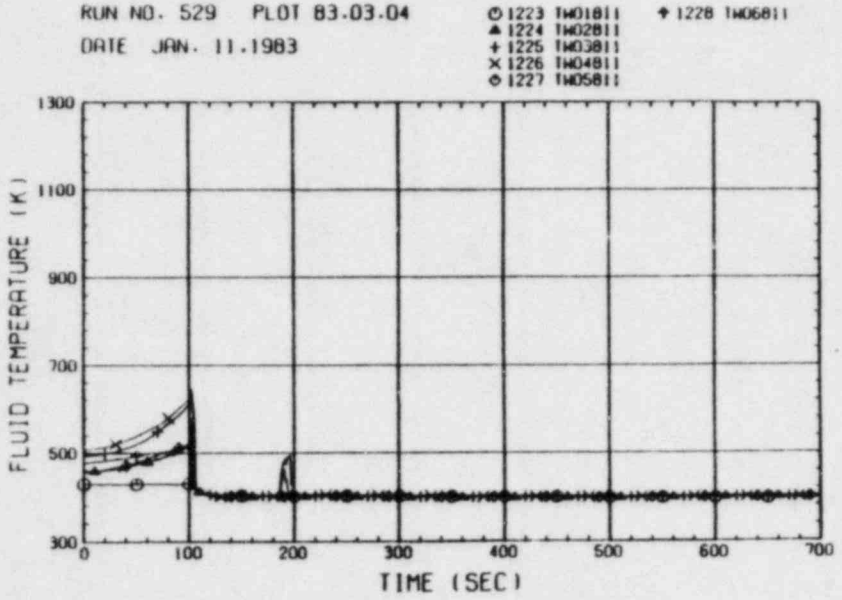

Fig. C-20 FLUID TEMPERATURE IN CORE (BUNDLE 8-1)

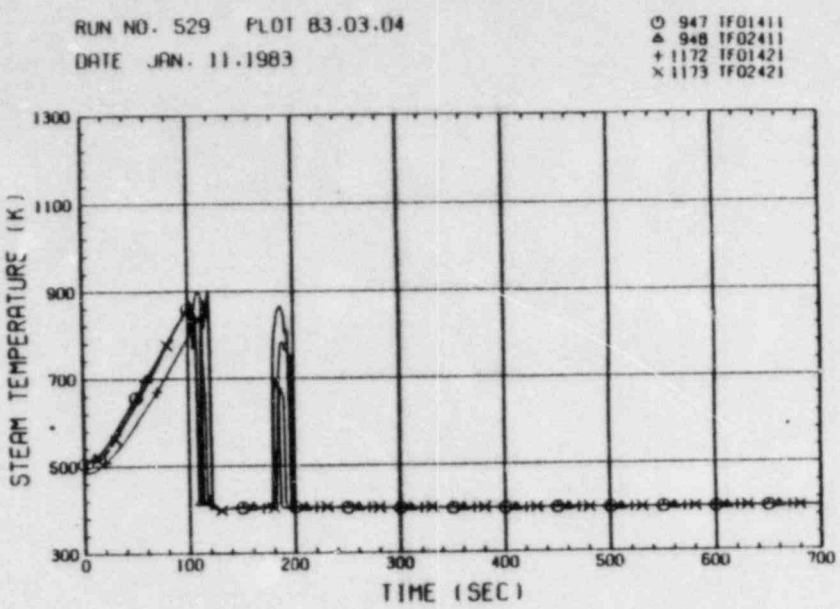

Fig. C-21 STEAM TEMPERATURE IN CORE, BUNDLE 4
(01411-1.735M, 02411-1.875M, 01421-1.38M, 02421-1.915M)

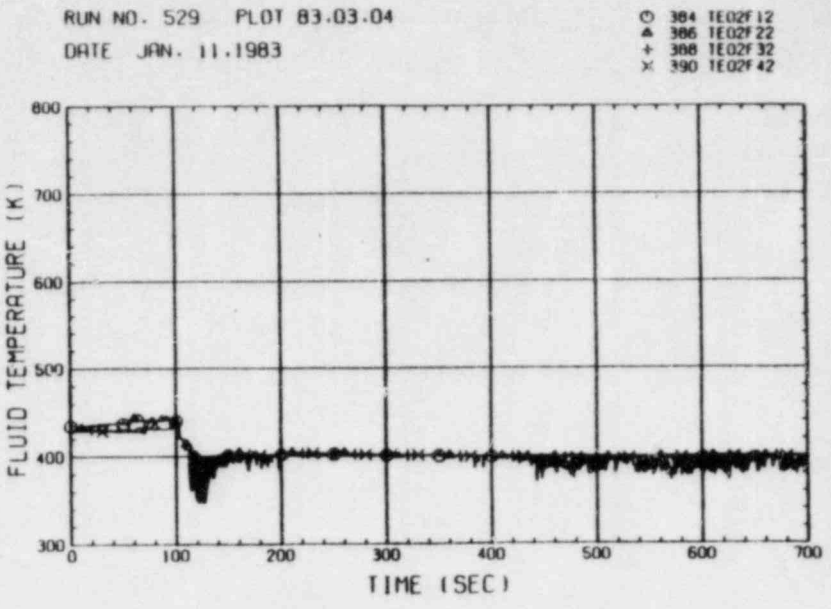

Fig. C-23 FLUID TEMPERATURE JUST ABOVE END BOX
(BUNDLE 1.2.3.4, COLD LEG SIDE)

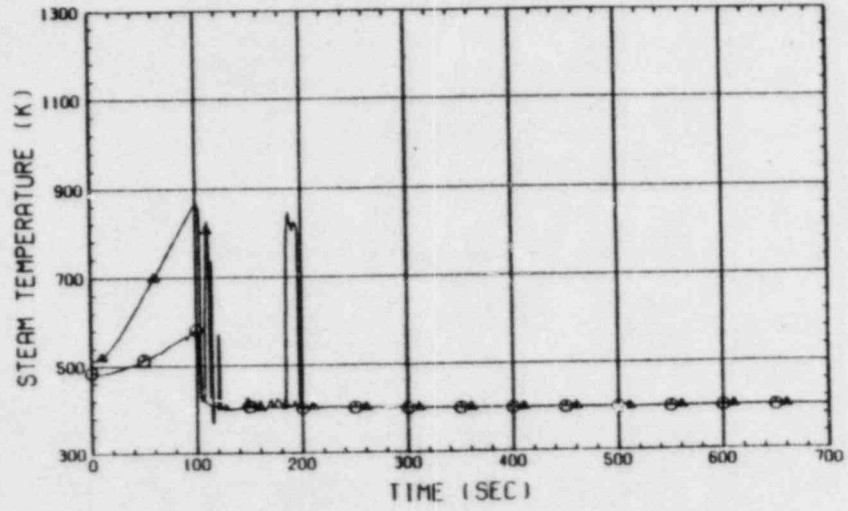

Fig. C-22 STEAM TEMPERATURE IN CORE, BUNDLE 6
(01611-3.62M, 01621-1.915M)

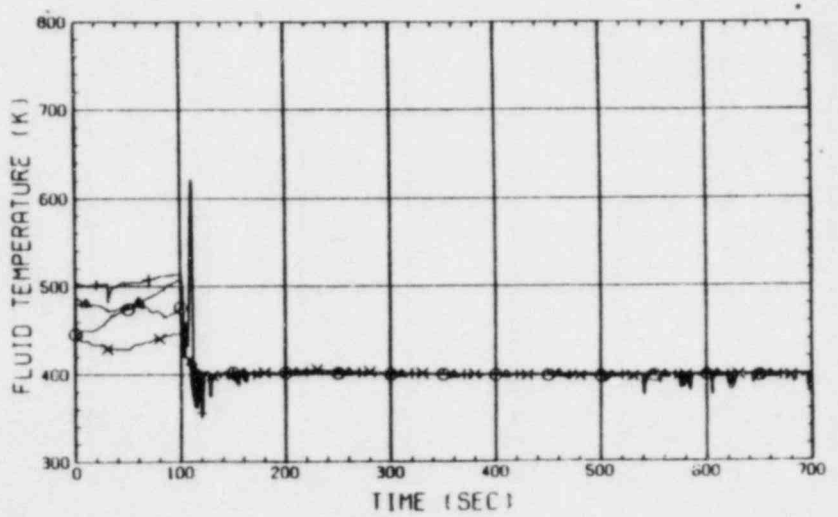

Fig. C-24 FLUID TEMPERATURE JUST ABOVE END BOX
(BUNDLE 5.6.7.8, COLD LEG SIDE)

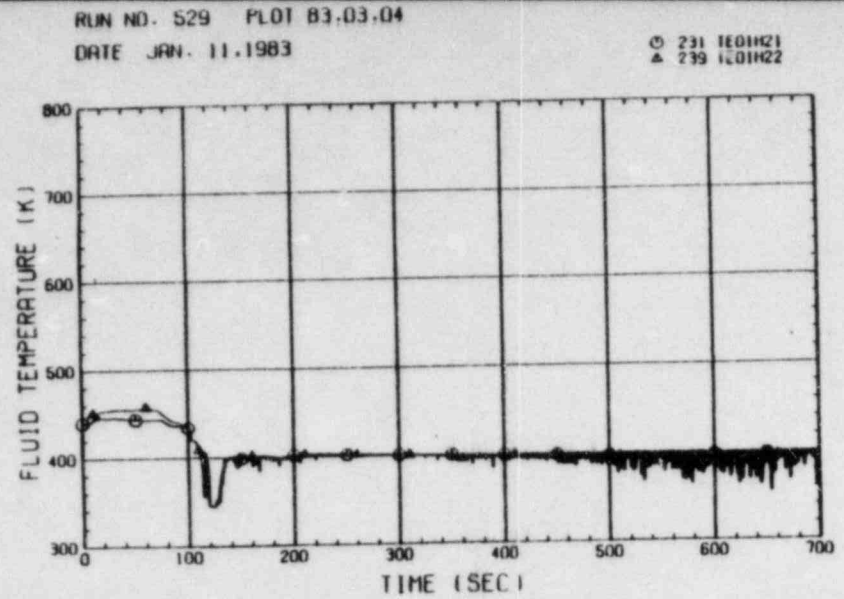

Fig. C-25 FLUID TEMPERATURE IN UCSP HOLE (BUNDLE 2. H21 - PERIPHERY. H22 - CENTER)

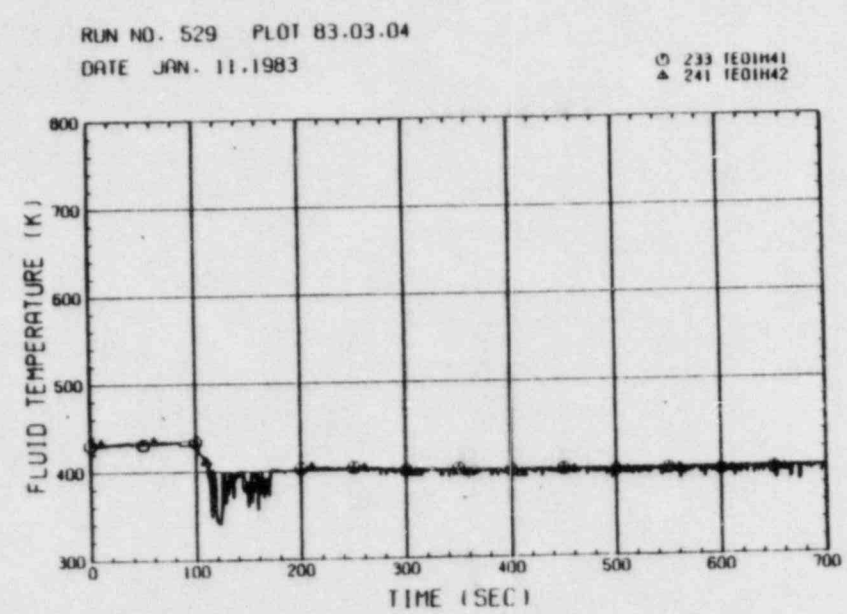

Fig. C-26 FLUID TEMPERATURE IN UCSP HOLE (BUNDLE 4. H41 - PERIPHERY. H42 - CENTER)

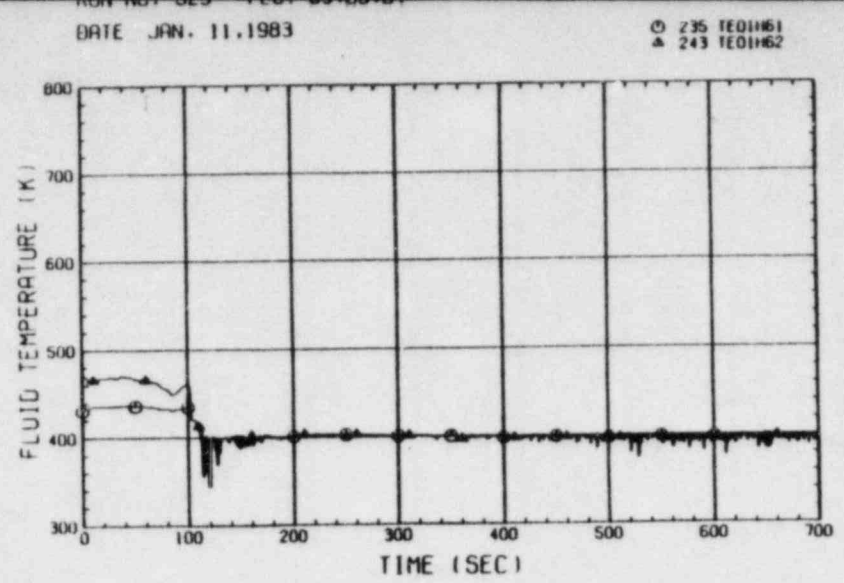

Fig. C-27 FLUID TEMPERATURE IN UCSP HOLE (BUNDLE 6. H61 - PERIPHERY. H62 - CENTER)

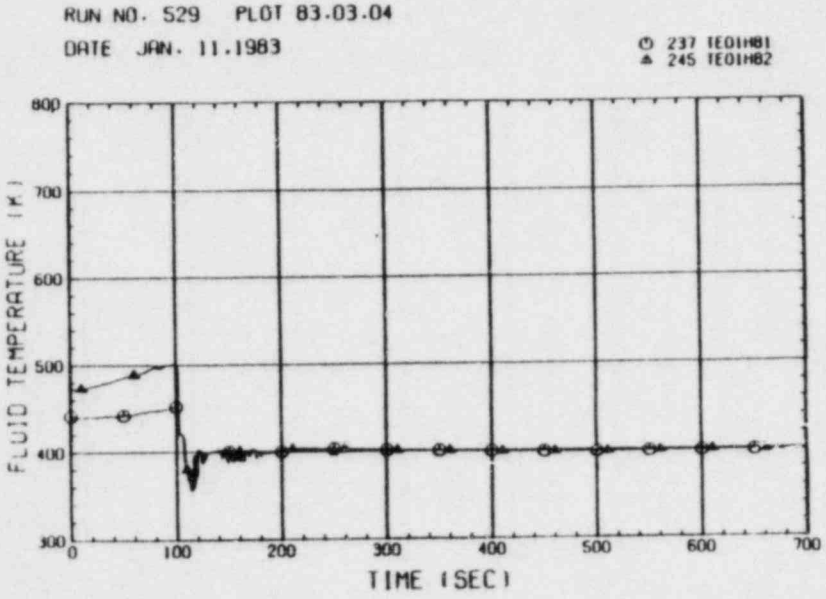

Fig. C-28 FLUID TEMPERATURE IN UCSP HOLE (BUNDLE 8. H81 - PERIPHERY. H82 - CENTER)

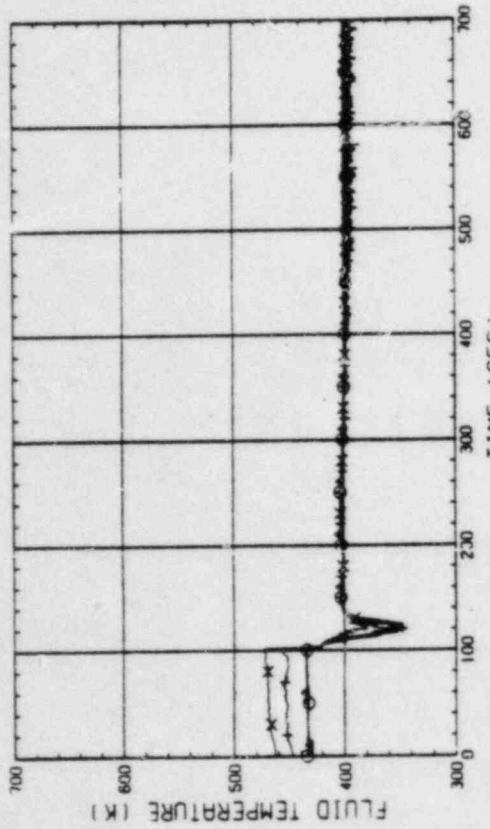

Fig. C-31 FLUID TEMPERATURE ABOVE UCSP (BUNDLE 2.4.6.8. 250MM ABOVE UCSP)

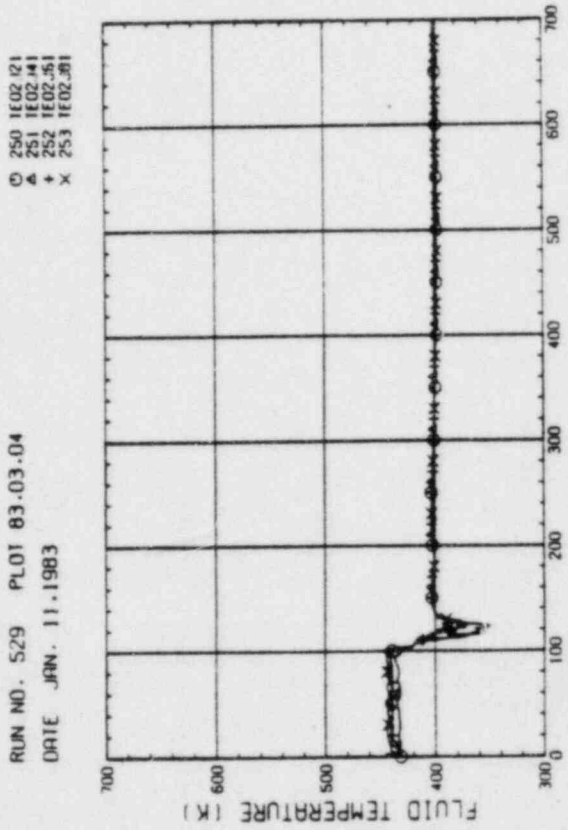

Fig. C-32 FLUID TEMPERATURE ABOVE UCSP (BUNDLE 2.4.6.8. 100MM ABOVE UCSP)

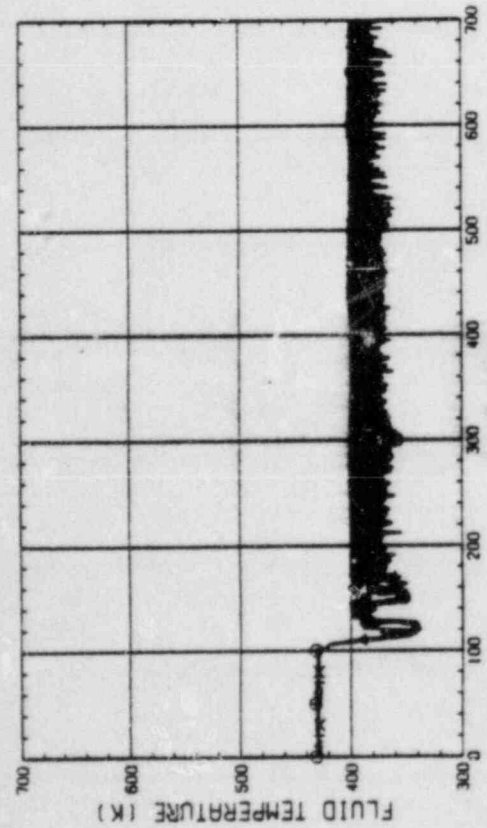

Fig. C-29 FLUID TEMPERATURE ON UCSP SURFACE (BUNDLE 1.2.3.4)

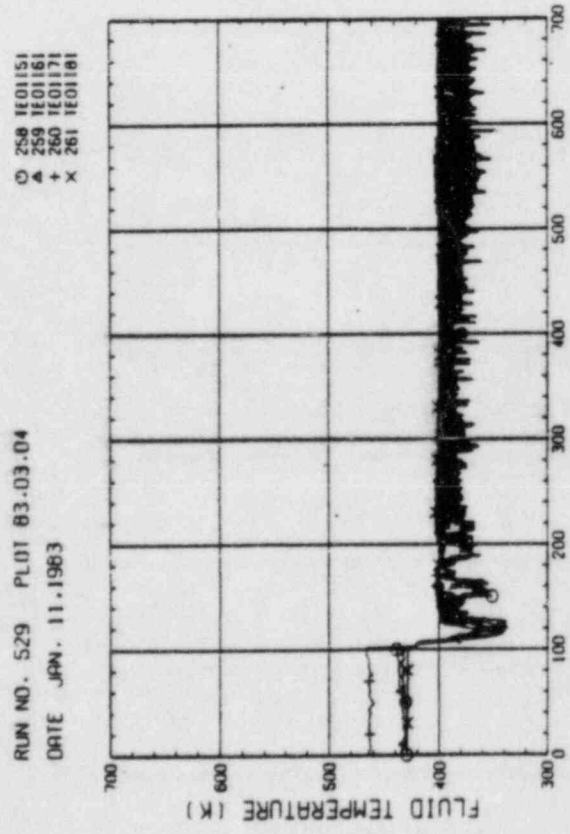

Fig. C-30 FLUID TEMPERATURE ON UCSP SURFACE (BUNDLE 5.6.7.8)

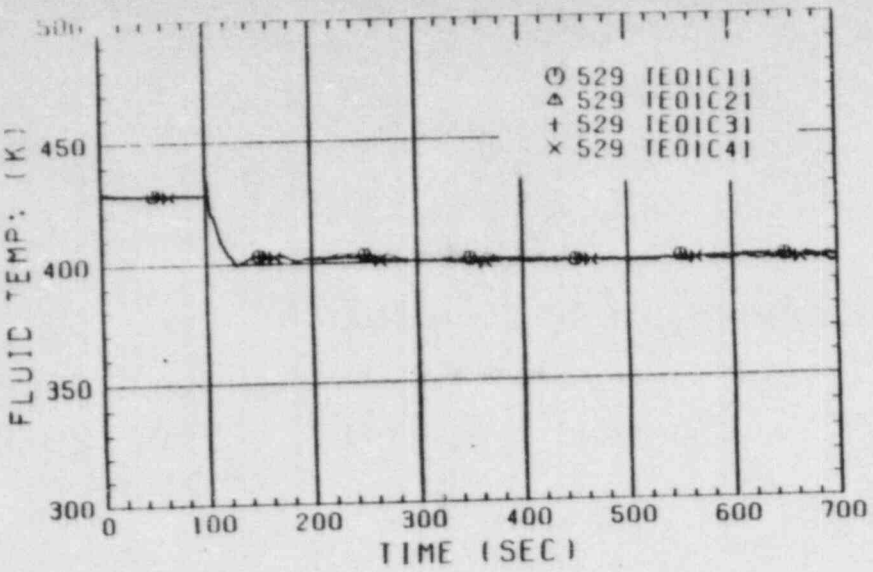

Fig. C-33 FLUID TEMPERATURE AT CORE INLET

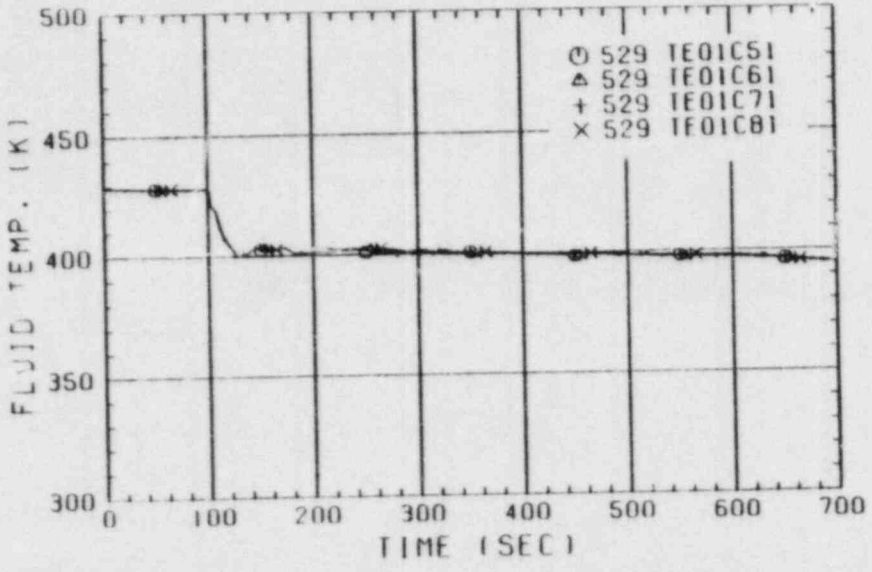

Fig. C-34 FLUID TEMPERATURE AT CORE INLET

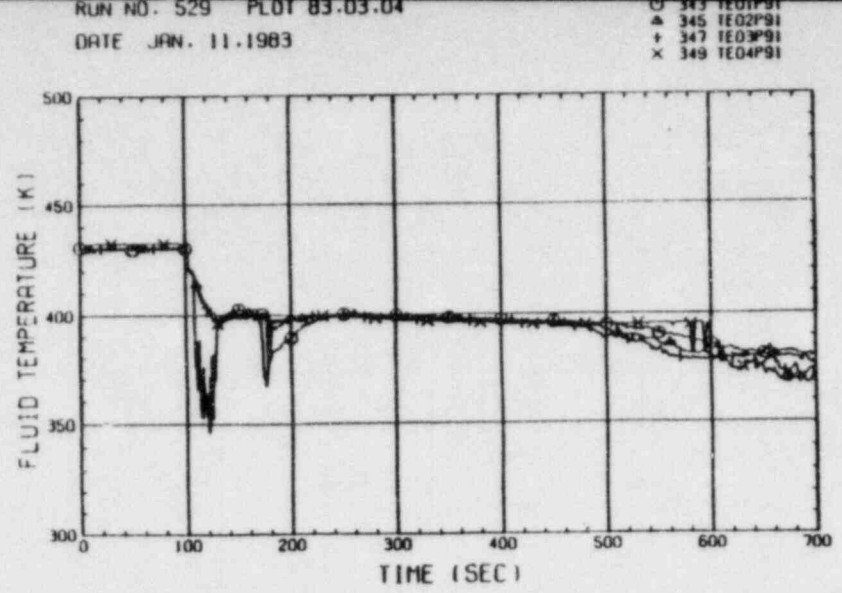

Fig. C-35 FLUID TEMPERATURE IN DOWNCOMER (BELOW INTACT COLD LEG)

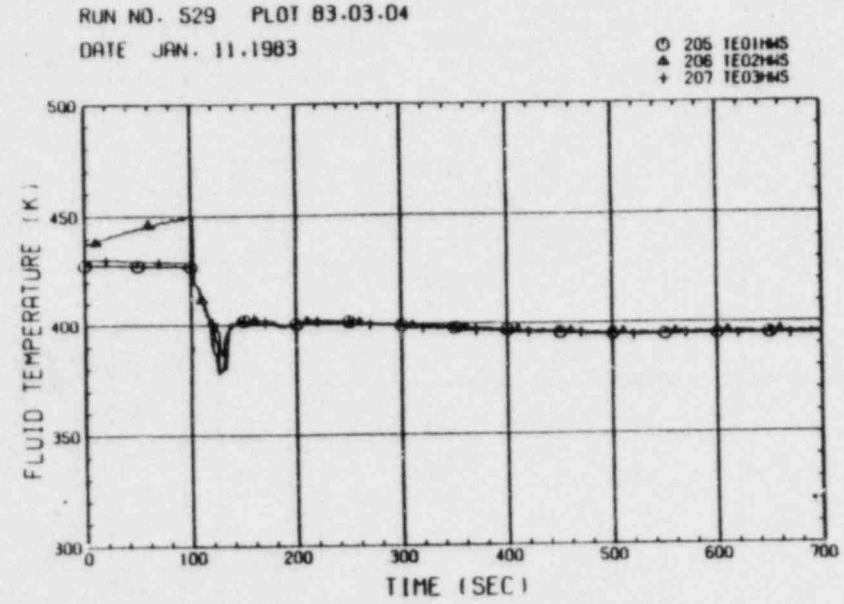

Fig. C-36 FLUID TEMPERATURE IN HOT LEG (01.02.03 - FROM PV TO STEAM/WATER SEPARATOR)

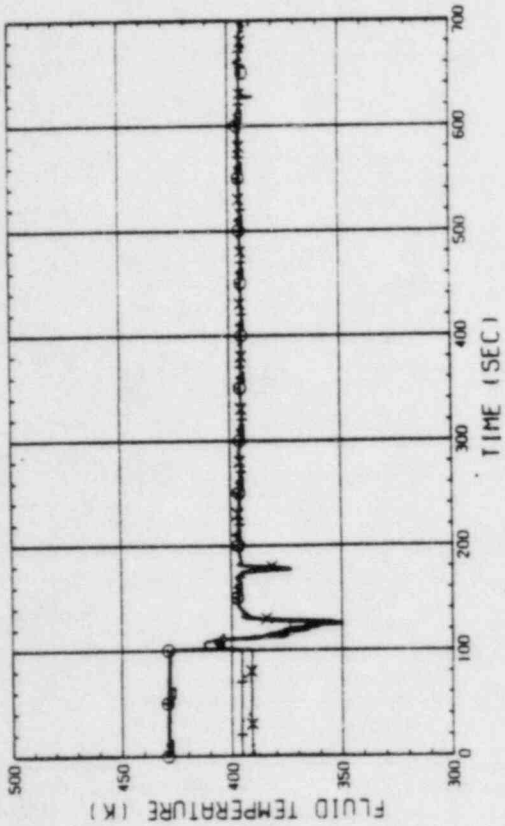

Fig. C-39 FLUID TEMPERATURE IN BROKEN COLD LEG - PV SIDE
101.02.03.04 - FROM PV TO CONTAINMENT TANK 11

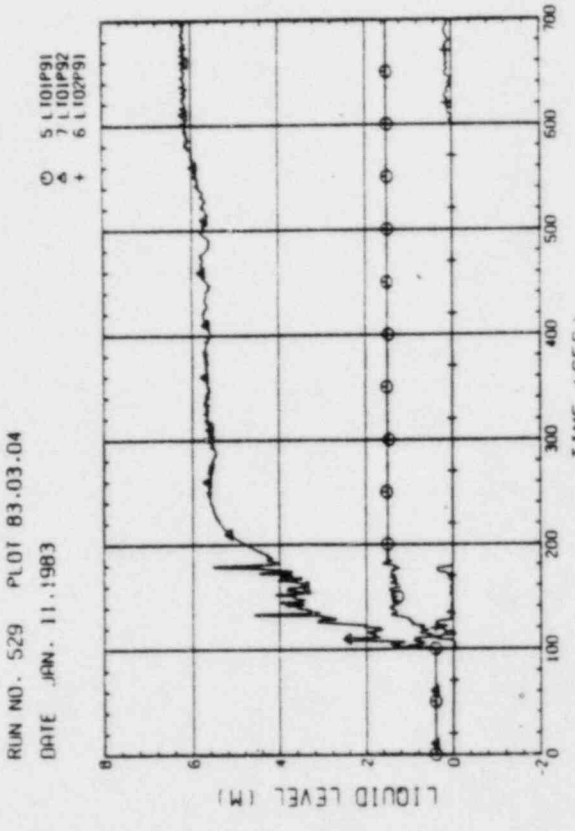

Fig. C-40 LIQUID LEVEL IN DOWNCOMER (01P91 BELOW CORE INLET,
01P92-BOTTOM TO COLD LEG, 02P91-COLD LEG TO TOP OF PV)

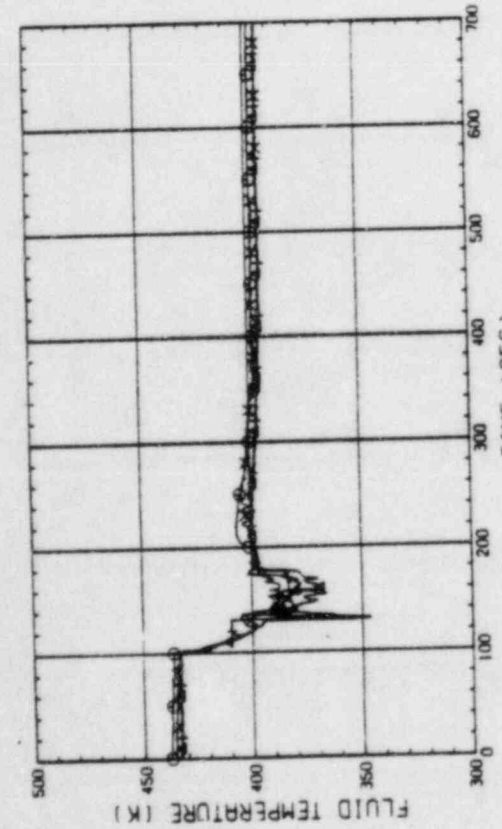

Fig. C-37 FLUID TEMPERATURE IN INTACT COLD LEG (01-BETWEEN PUMP
SIMULATOR AND S/W SEPARATOR, 02.03.04-INSIDE PUMP)

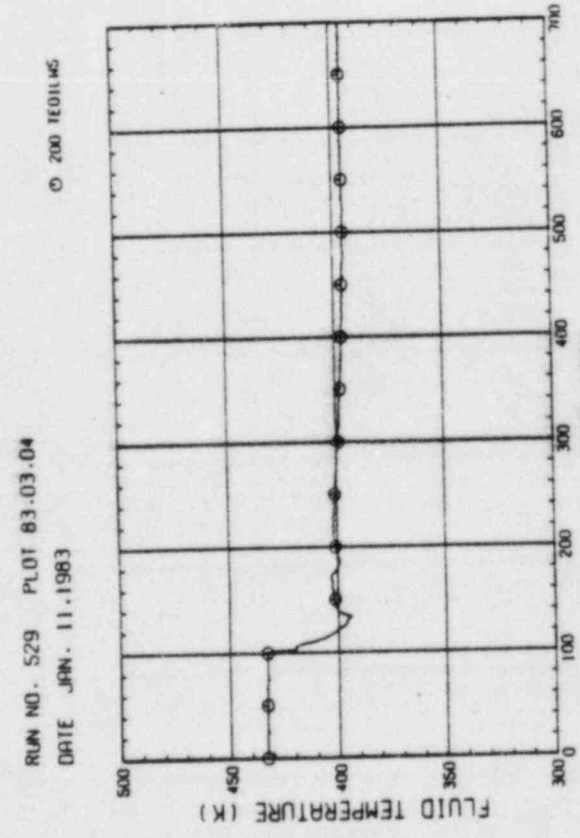

Fig. C-38 FLUID TEMPERATURE IN BROKEN COLD LEG - STEAM/WATER
SEPARATOR SIDE

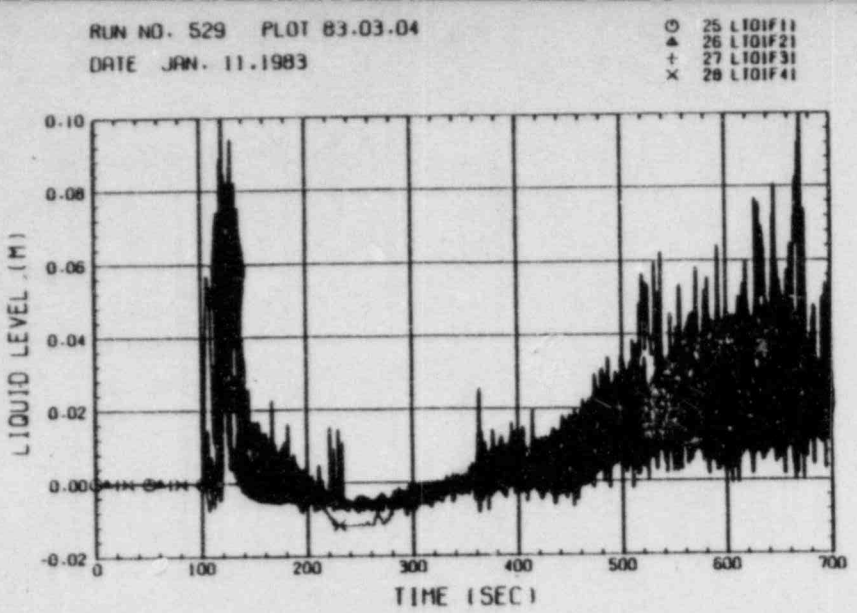

Fig. C-41 LIQUID LEVEL ABOVE END BOX TIE PLATE (BUNDLE 1.2.3.4)

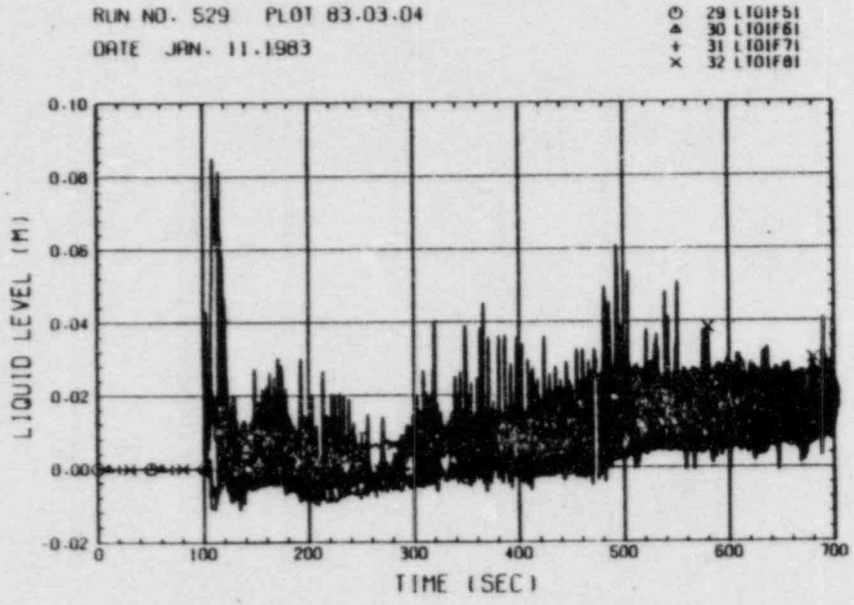

Fig. C-42 LIQUID LEVEL ABOVE END BOX TIE PLATE (BUNDLE 5.6.7.8)

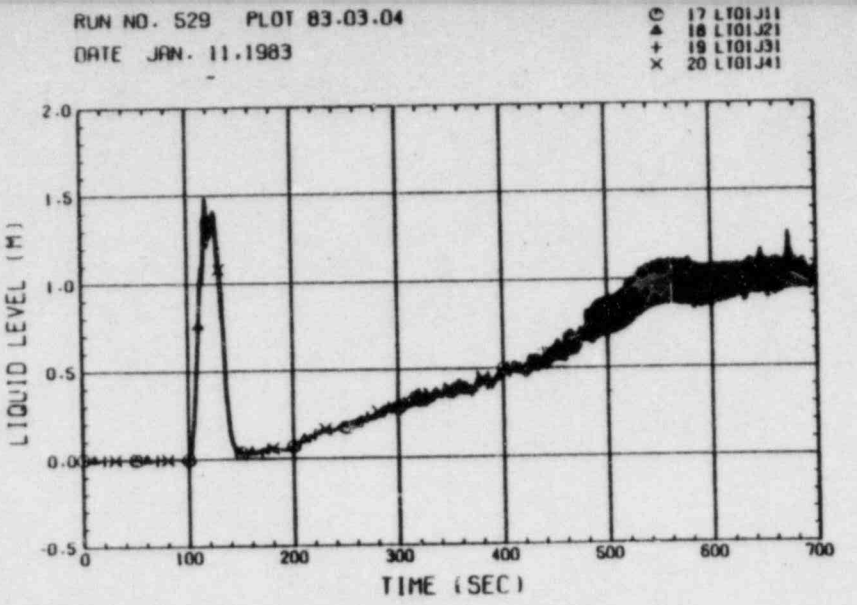

Fig. C-43 LIQUID LEVEL ABOVE UCSP (BUNDLE 1.2.3.4)

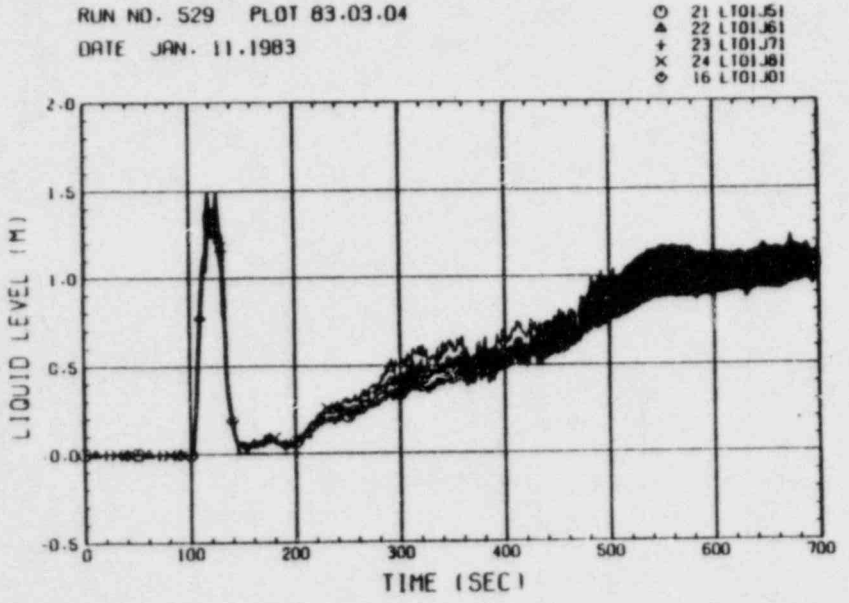

Fig. C-44 LIQUID LEVEL ABOVE UCSP (BUNDLE 5.6.7.8 AND CORE BAFFLE)

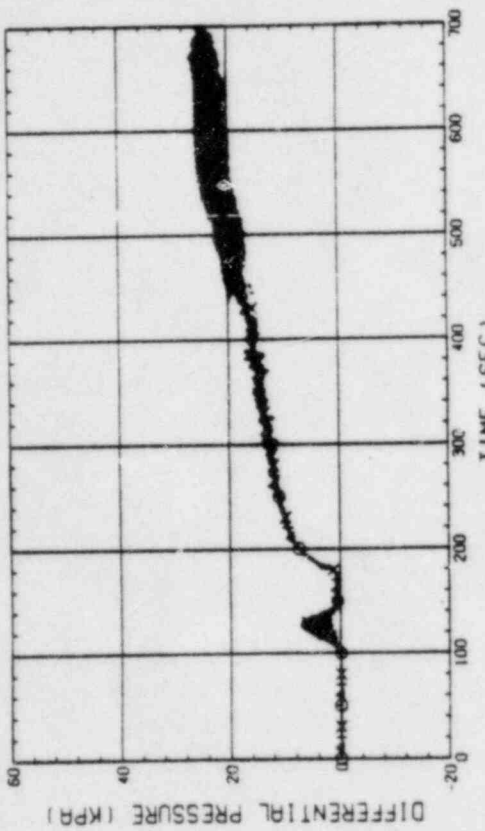

Fig. C-47 DIFFERENTIAL PRESSURE OF CORE FULL HEIGHT (BUNDLE 1.2.3.4)

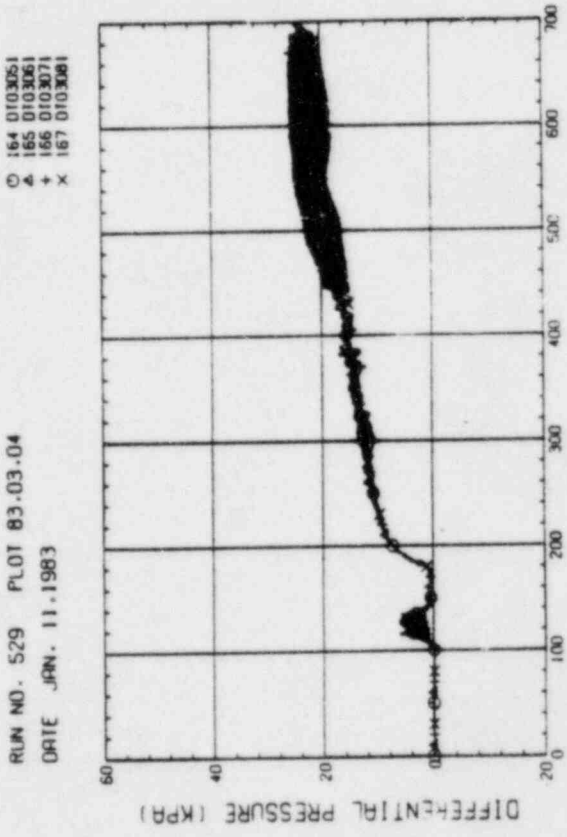

Fig. C-48 DIFFERENTIAL PRESSURE OF CORE FULL HEIGHT (BUNDLE 5.6.7.8)

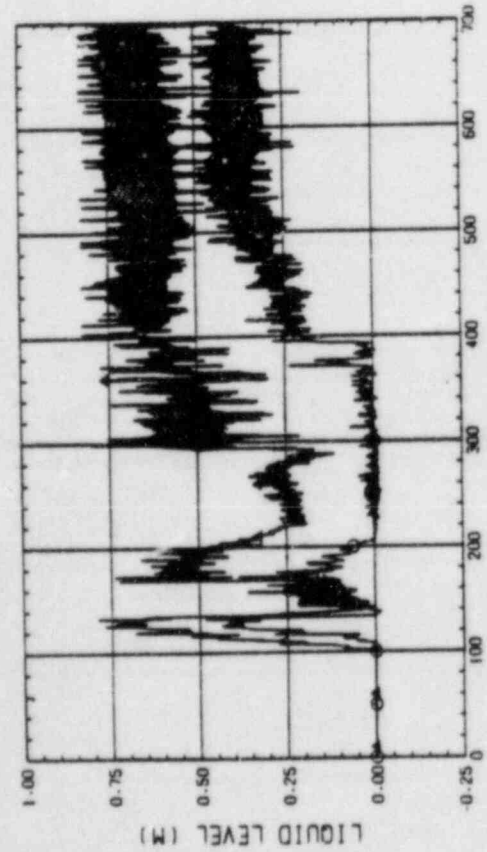

Fig. C-45 LIQUID LEVEL IN HOT LEG (10HS - PV SIDE, 02HS - STEAM/WATER SEPARATOR SIDE)

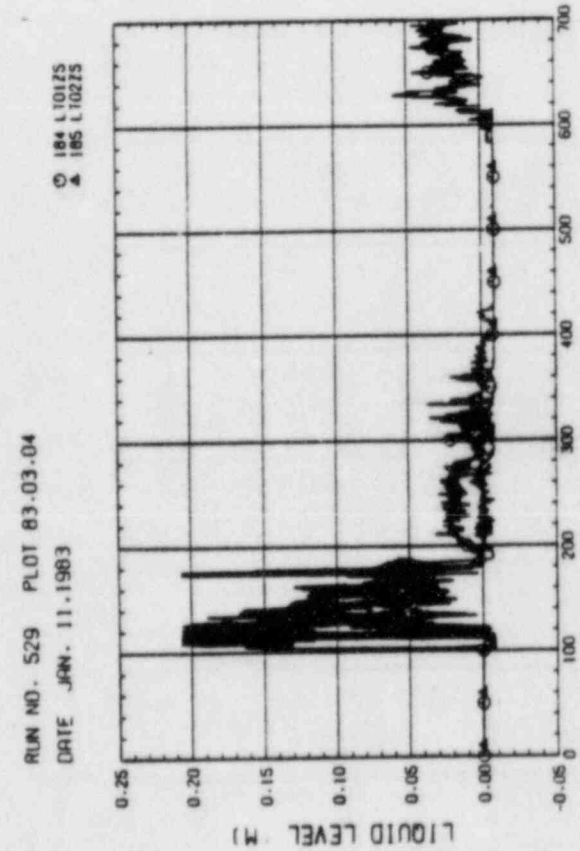

Fig. C-46 LIQUID LEVEL IN BROKEN COLD LEG - PV SIDE (01 - DOWNCOMER SIDE, 02 - CONTAINMENT TANK-1 SIDE)

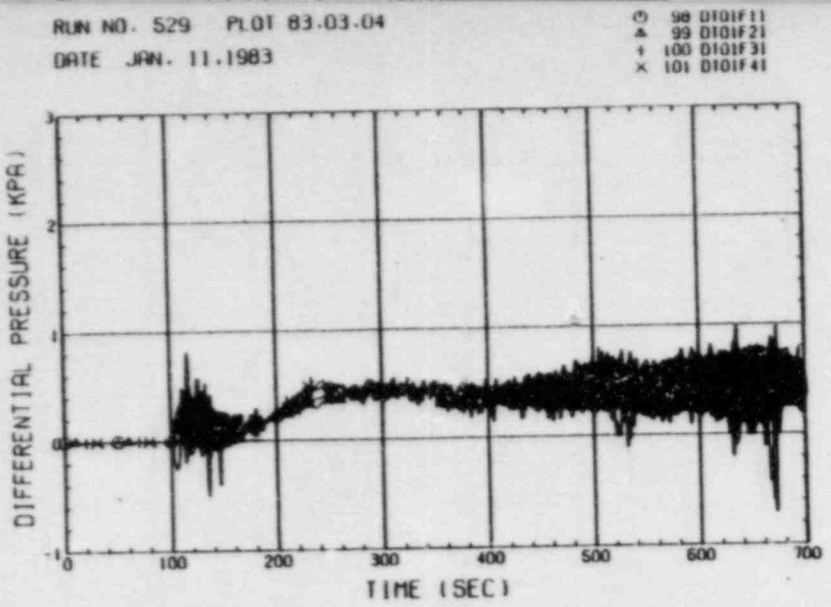

Fig. C-49 DIFFERENTIAL PRESSURE ACROSS END BOX TIE PLATE (BUNDLE 1.2.3.4)

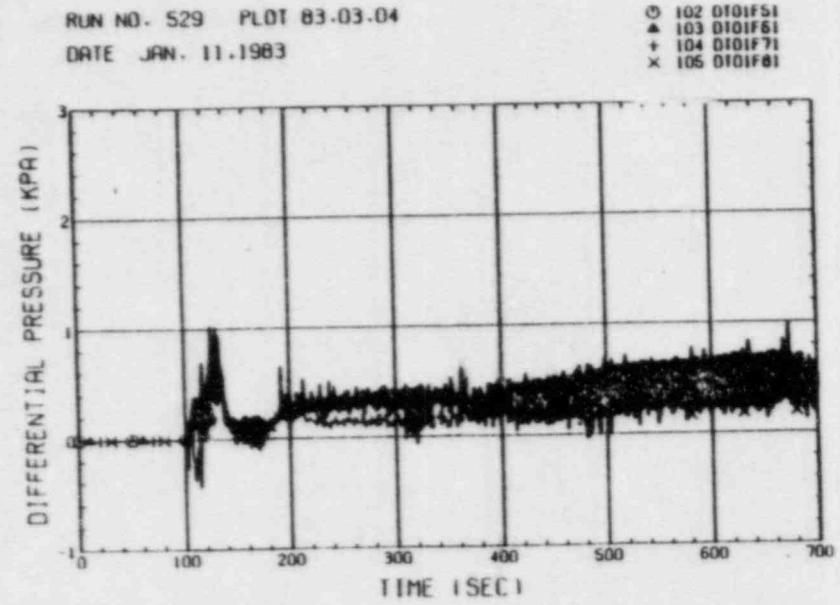

Fig. C-50 DIFFERENTIAL PRESSURE ACROSS END BOX TIE PLATE (BUNDLE 5.6.7.8)

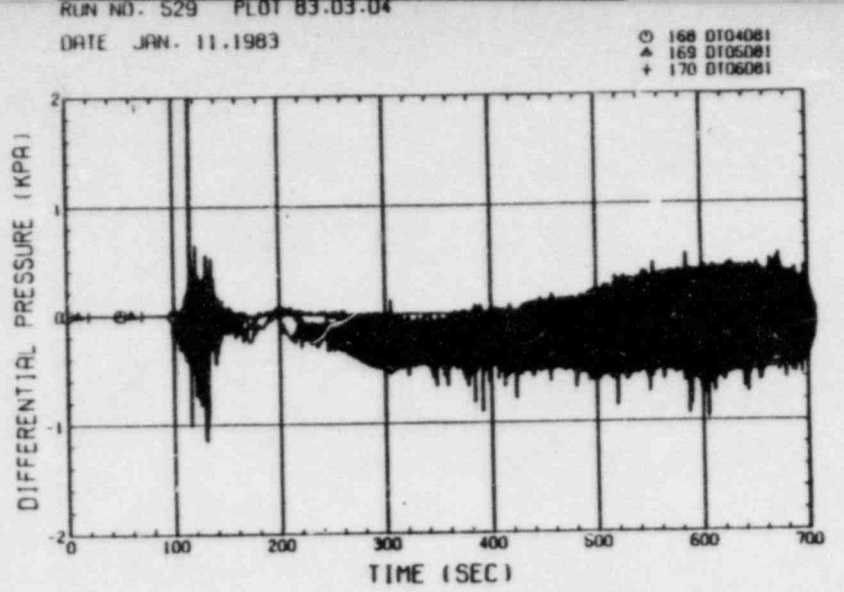

Fig. C-51 DIFFERENTIAL PRESSURE, HORIZONTAL, BUNDLE 5-8, (04-BELOW SPACER 4, 05-BELOW SPACER 6, 06-BELOW END BOX)

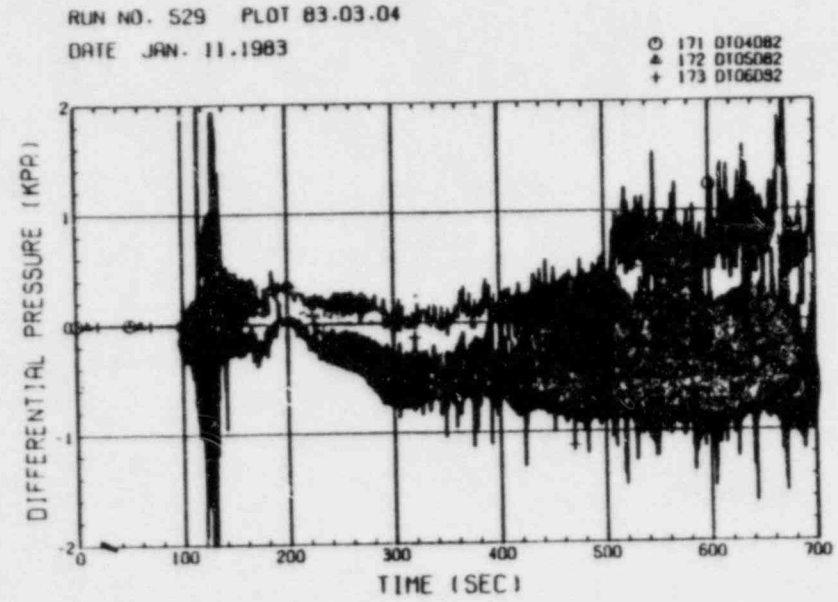

Fig. C-52 DIFFERENTIAL PRESSURE, HORIZONTAL, BUNDLE 1-8 (04-BELOW SPACER 4, 05-BELOW SPACER 6, 06-BELOW END BOX)

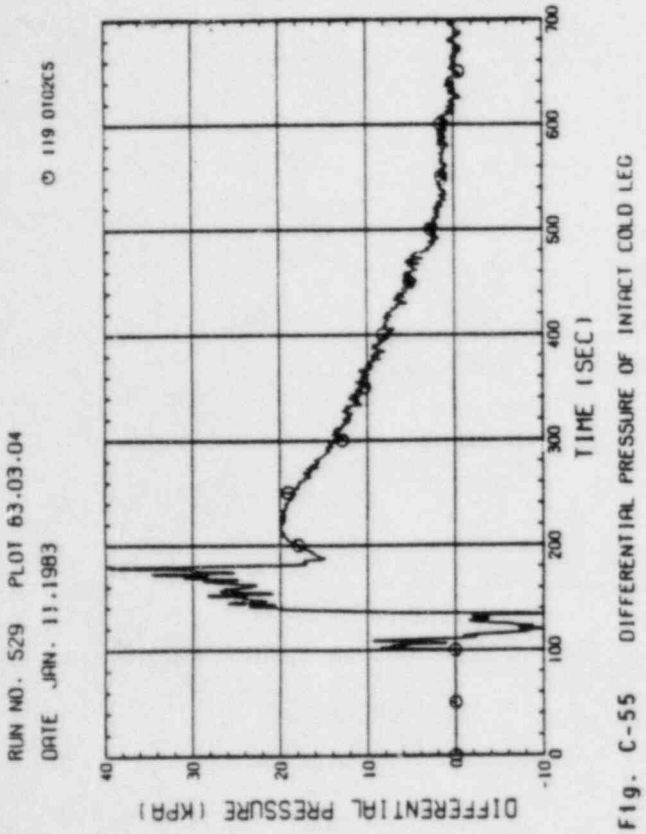

Fig. C-55 DIFFERENTIAL PRESSURE OF INTACT COLD LEG

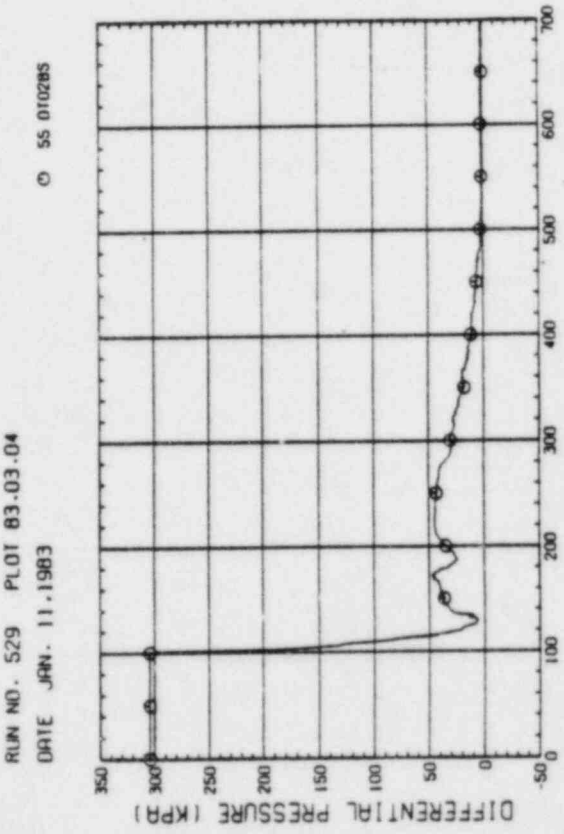

Fig. C-56 DIFFERENTIAL PRESSURE, STEAM/WATER SEPARATOR CONTAINMENT TANK-II

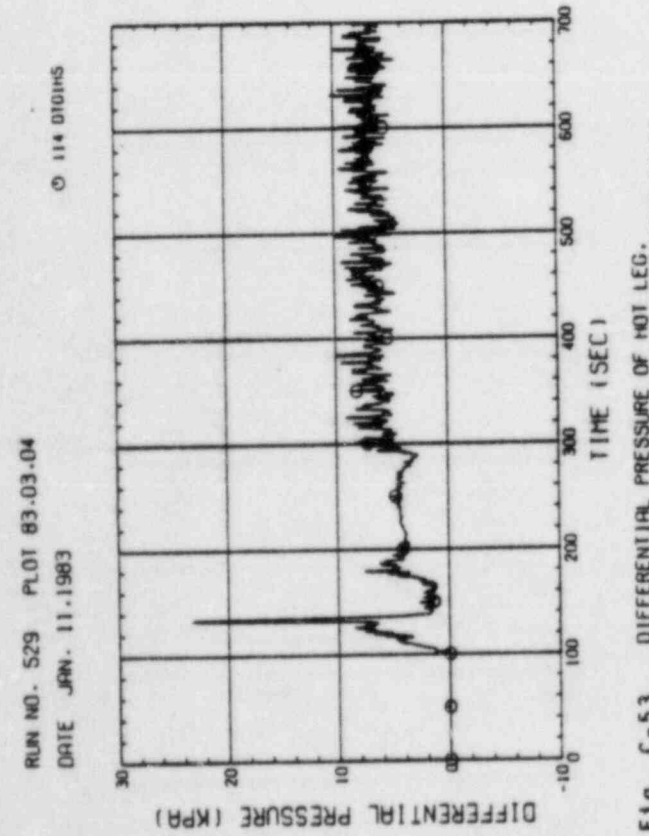

Fig. C-53 DIFFERENTIAL PRESSURE OF HOT LEG. HOT LEG INLET - STEAM/WATER SEPARATOR INLET

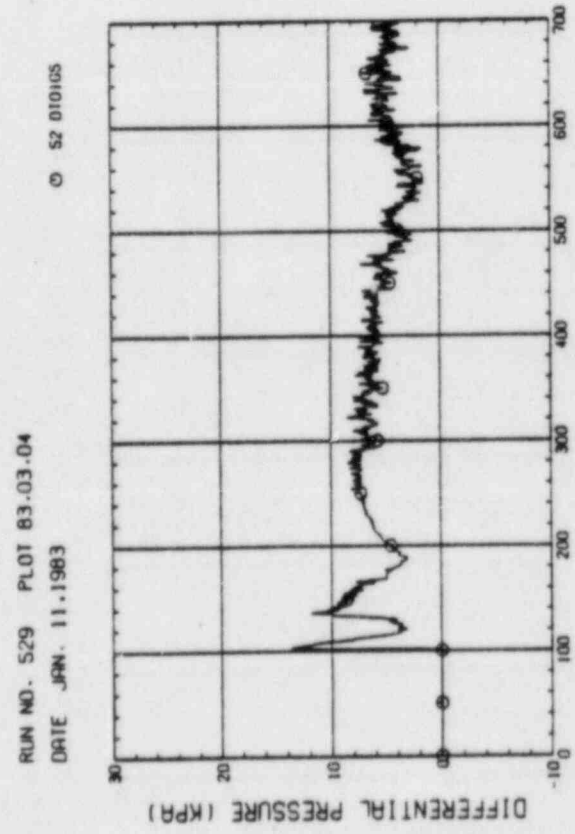

Fig. C-54 DIFFERENTIAL PRESSURE, STEAM/WATER SEPARATOR INLET - BROKEN COLD LEG - S/W SEPARATOR SIDE NOZZLE

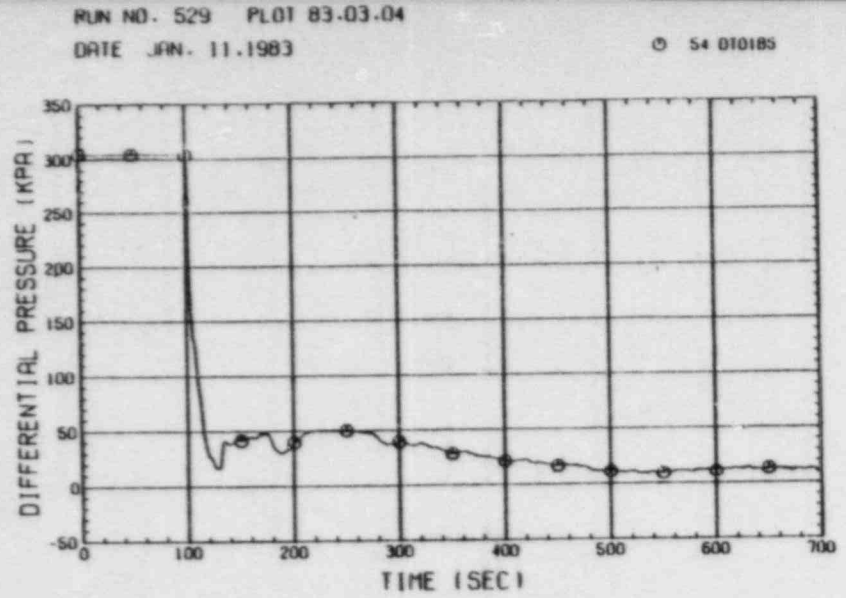

Fig. C-57 DIFFERENTIAL PRESSURE, TOP OF UPPER PLENUM - CONTAINMENT TANK-II

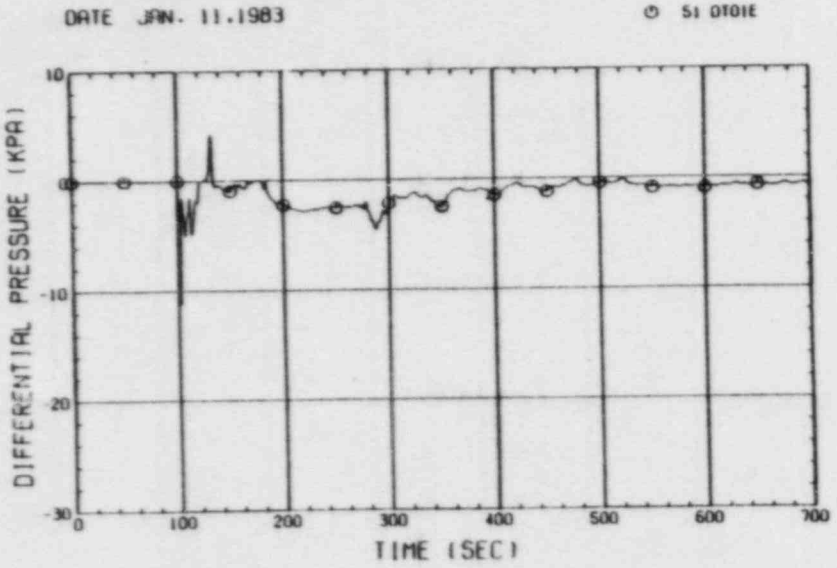

Fig. C-58 DIFFERENTIAL PRESSURE, CONTAINMENT TANK-II - CONTAINMENT TANK-I

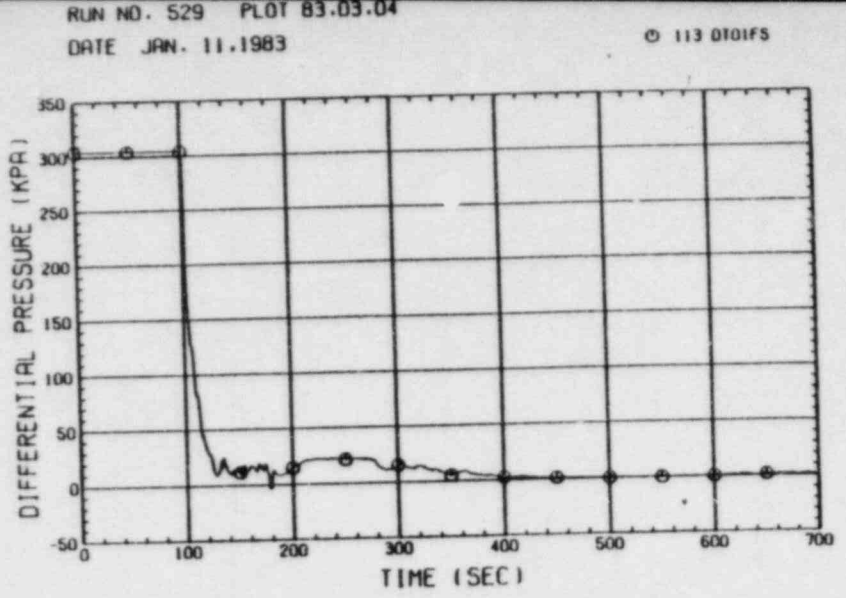

Fig. C-59 DIFFERENTIAL PRESSURE OF BROKEN COLD LEG - PV SIDE, DOWNCOMER - CONTAINMENT TANK-I

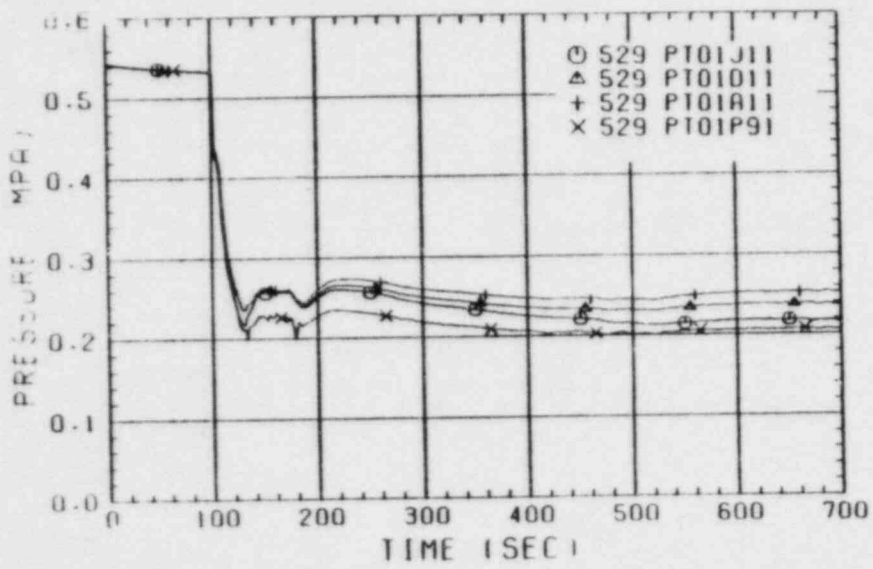

Fig. C-60 PRESSURE IN PV

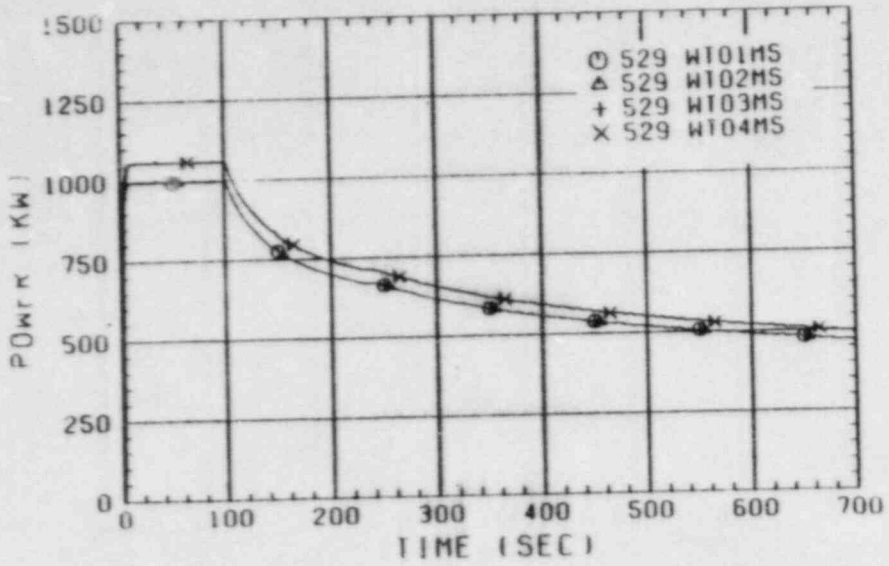

Fig. C-61 BUNDLE POWER , BUNDLE 1.2.3.4

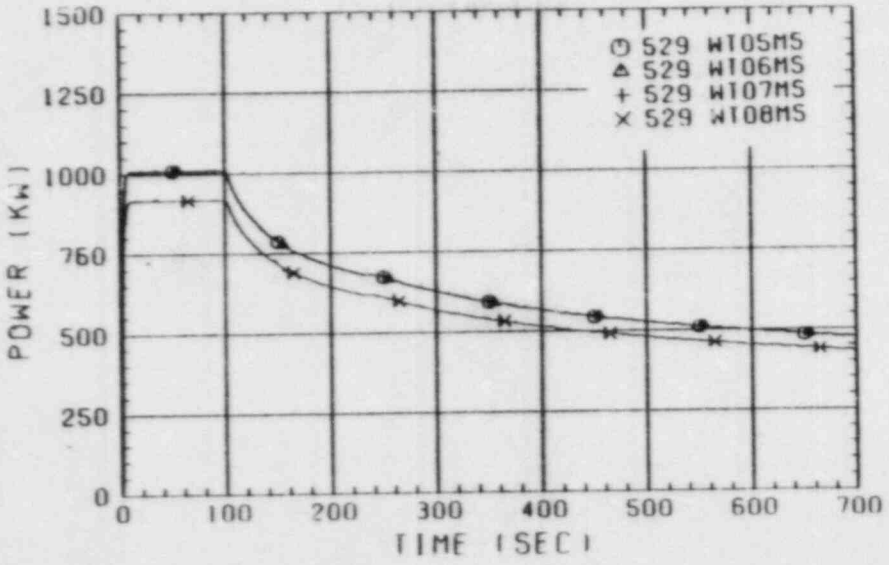

Fig. C-62 BUNDLE POWER , BUNDLE 5.6.7.8

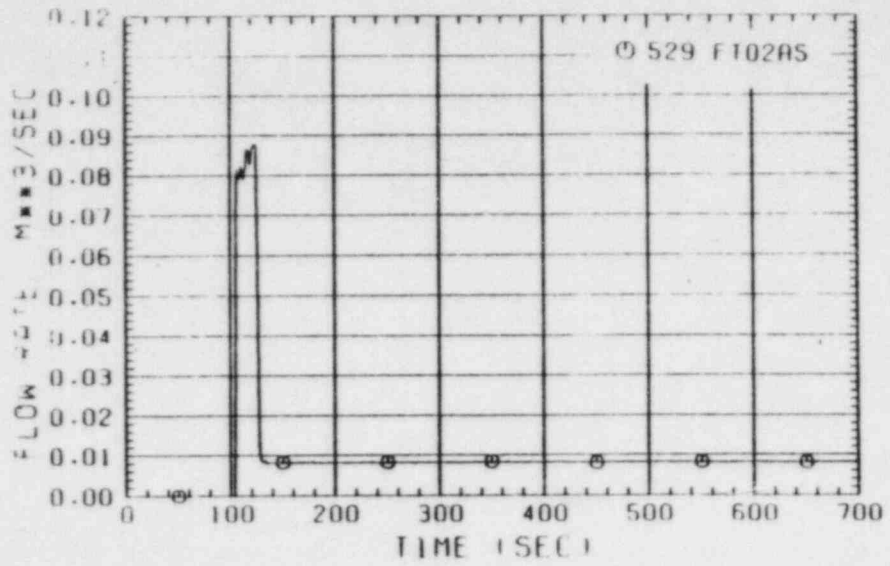

Fig. C-63 ECC INJECTION RATE INTO INIACI COLD LEG

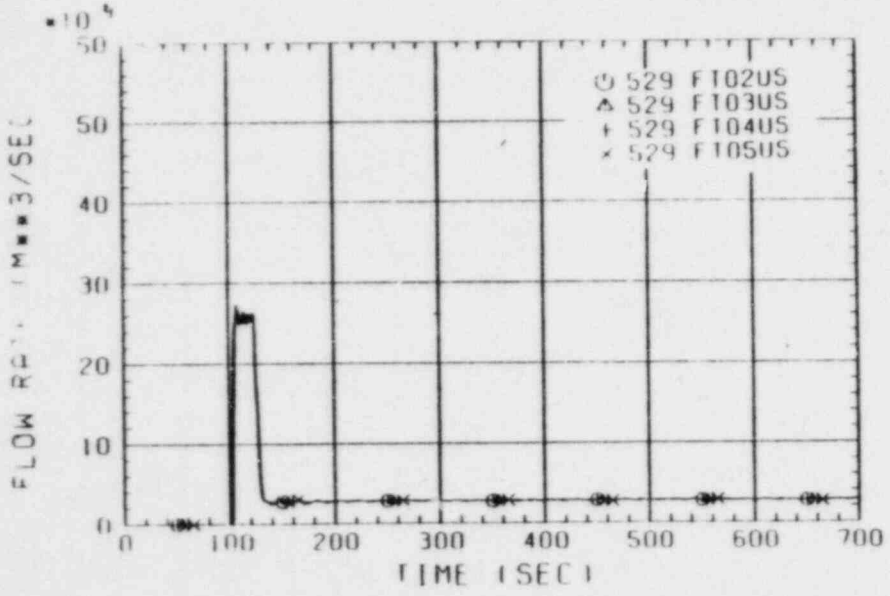

Fig. C-64 ECC INJECTION RATE INTO UPPER PLENUM

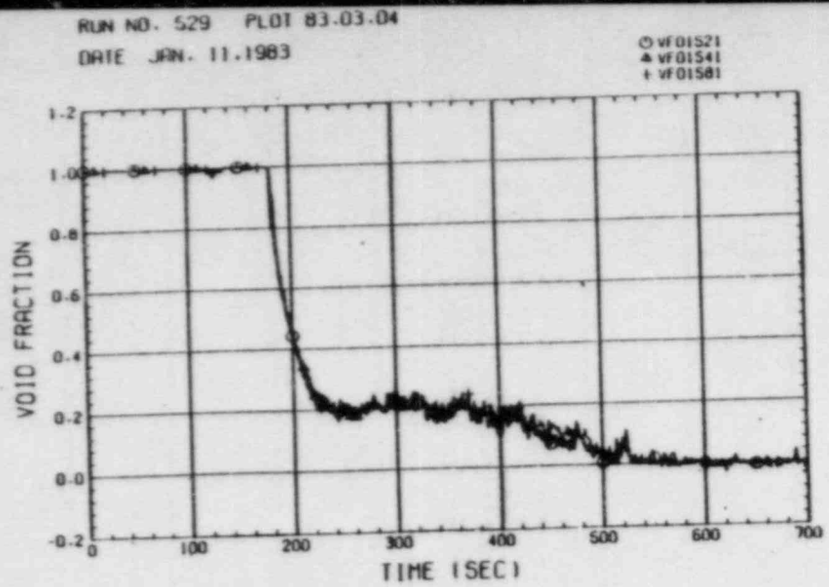

Fig. C-65 VOID FRACTION IN CORE. BUNDLE 2.4.8 (BETWEEN CORE SPACER 1 AND 2)

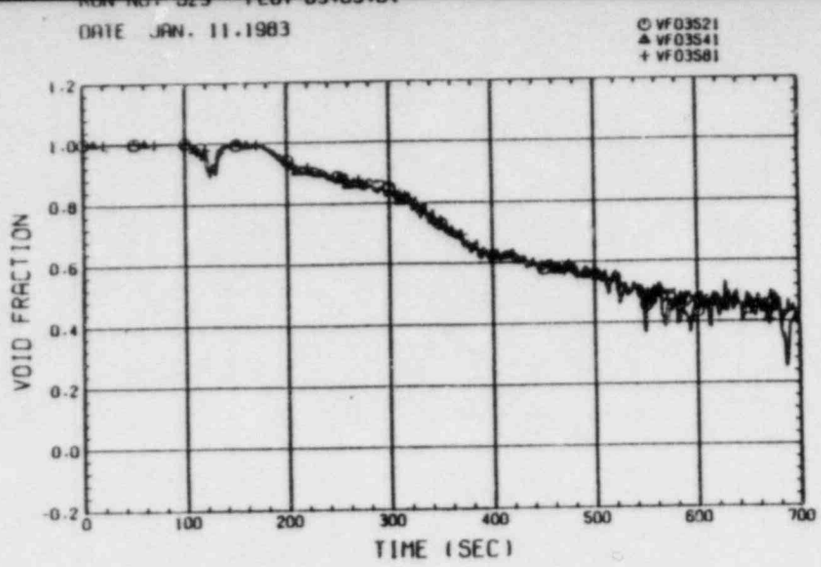

Fig. C-67 VOID FRACTION IN CORE. BUNDLE 2.4.8 (BETWEEN CORE SPACER 3 AND 4)

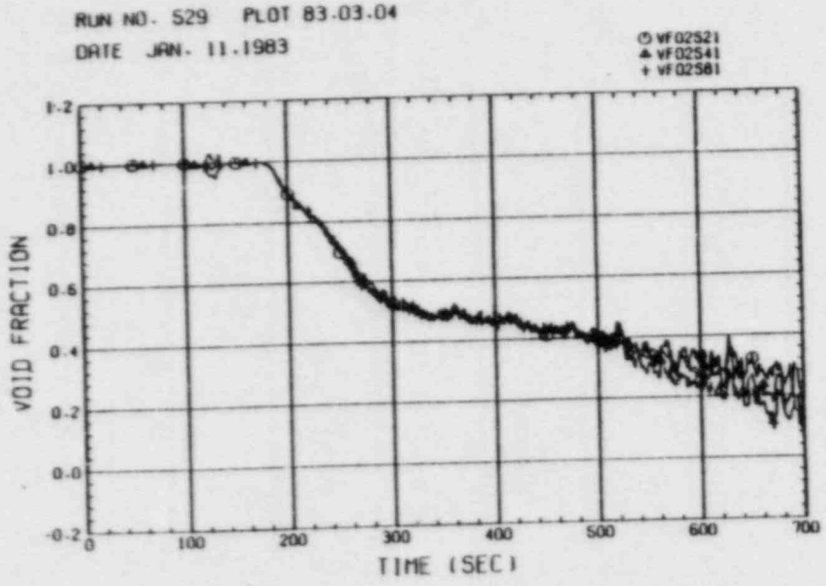

Fig. C-66 VOID FRACTION IN CORE. BUNDLE 2.4.8 (BETWEEN CORE SPACER 2 AND 3)

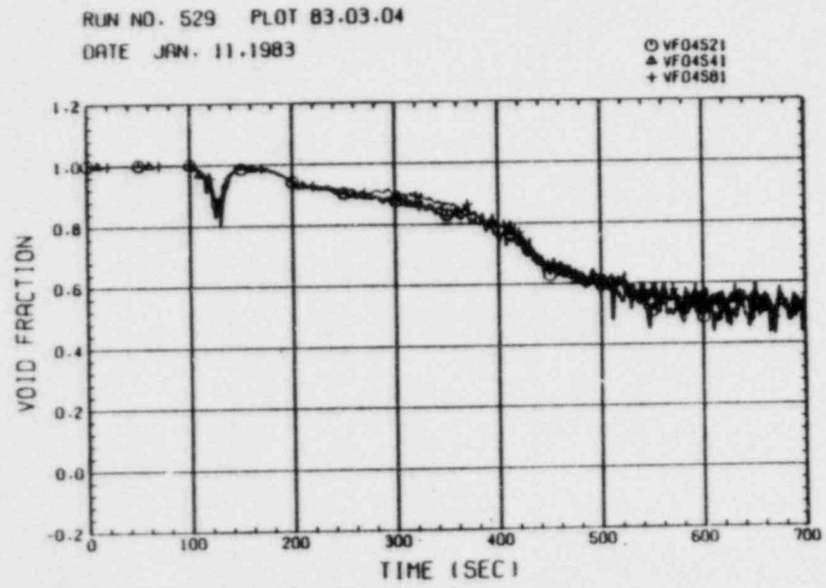

Fig. C-68 VOID FRACTION IN CORE. BUNDLE 2.4.8 (BETWEEN CORE SPACER 4 AND 5)

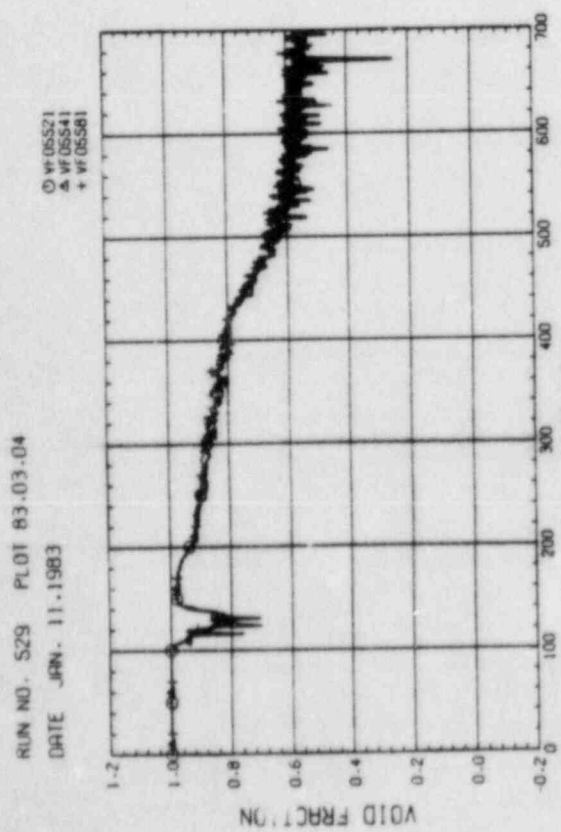

Fig. C-69 VOID FRACTION IN CORE, BUNDLE 2.4.8 (BETWEEN CORE SPACER 5 AND 6)

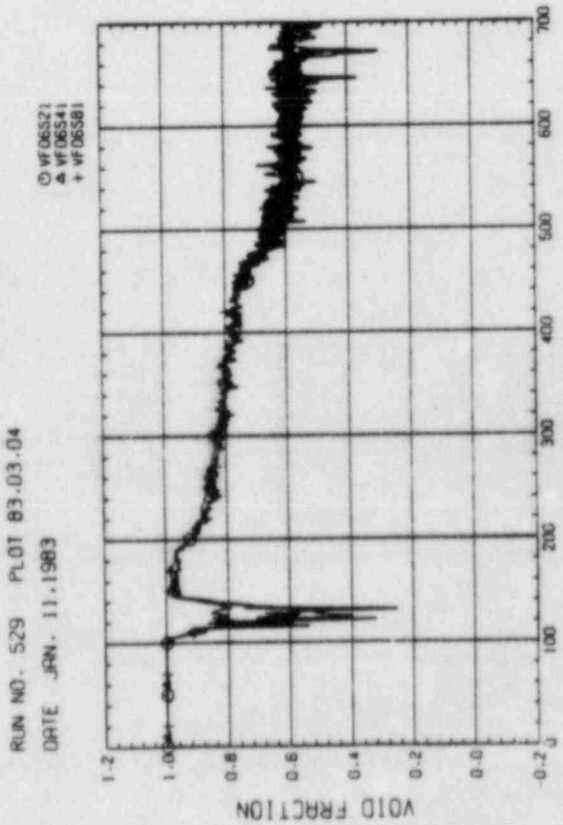

Fig. C-70 VOID FRACTION IN CORE, BUNDLE 2.4.8 (BETWEEN CORE SPACER 6 AND 7)